Investigations on the synthesis and reactivity of $\sigma^3\lambda^3$-oxaphosphirane complexes with fluorinated *C*-substituents

Dissertation

zur Erlangung des Doktorgrades (Dr. rer. nat.)
der
Mathematisch-Naturwissenschaftlichen Fakultät
der
Rheinischen Friedrich-Wilhelms-Universität Bonn

vorgelegt von

Cristina Murcia García

aus

Murcia, Spanien

Bonn, 2016

Angefertigt mit Genehmigung der Mathematisch-Naturwissenschaftlichen Fakultät
der Rheinischen Friedrich-Wilhelms-Universität Bonn.

1. Gutachter Prof. Dr. R. Streubel
2. Gutachter Prof. Dr. R. Glaum
3. Gutachter Prof. Dr. B. Kirchner
4. Gutachter Prof. Dr. C. Müller

Eingereicht am: 31.10.2016

Tag der Promotion: 20.12.2016

Erscheinungsjahr: 2017

TO MY PARENTS

AND TO MY HUSBAND

“One should not be afraid to say ‘I don’t know’ or ‘I don’t understand’. To continue even when things appear to be impossible; to stand alone or to be different; and not to be afraid to make and admit mistakes, for only those who dare to fail greatly can ever achieve greatly."

Margaret Hamilton

Software developer of the *Apollo Space Program*
(or the woman who put the men on the Moon)

Hiermit versichere ich, dass ich diese Arbeit selbst verfasst und keine anderen als die angegebenen Quellen und Hilfsmittel verwendet habe.

Bonn, den 29.10.2016

Some of the results of this PhD Thesis have been previously published:

1. "Study on the acid-Induced ring-expansion of an oxaphosphirane complex with an electron-withdrawing C-substituent", C. Murcia García, G. Schnakenburg, R. Streubel, *Aust. J. Chem.* **2017,** DOI: 10.1071/CH16609

2. "Ambiguous reactivity of Li/Cl phosphinidenoid complexes under redox conditions - a novel dichotomy in phosphorus chemistry", C. Murcia García, A. Bauzá, G. Schnakenburg, A. Frontera, R. Streubel, *Chem. Comm.* **2017**, *53*, 933-936.

3. "CPh_3 as a functional group in P-heterocyclic chemistry: elimination of $HCPh_3$ in the reaction of P-CPh_3 substituted Li/Cl phosphinidenoid complexes with Ph_2CO", C. Murcia García, A. E. Ferao, G. Schnakenburg, R. Streubel, *Dalton Trans*. **2016**, *45*, 2378–2385.

4. "Surprising behaviour of M–CO(lone pair)···π(arene) interactions in the solid state of fluorinated oxaphosphirane complexes", C. Murcia García, A. Bauzá, G. Schnakenburg, A. Frontera, R. Streubel, *CrystEngComm* **2015**, *17*, 1769–1772.

5. "On the nature of ε–CO(lone pair)··· π(arene) interactions in the solid state of fluorinated oxaphosphirane complexes", C. Murcia García, A. Bauzá, A. Frontera, R. Streubel, *CrystEngComm* **2015**,*17*, 6736–6743.

6. "Evidence for Terminal Phosphinidene Oxide Complexes in O,P,C-Cage Complex Formation: Rearrangement of Oxaphosphirane Complexes", R. Streubel, C. Murcia García, G. Schnakenburg, A. Espinosa Ferao, *Organometallics* **2015**, *34*, 2676–2682.

Conferences and workshops

1. C. Murcia García, A. Espinosa, A. Frontera, R. Streubel, 14th International Symposium on Inorganic Ring Systems, Regensburg, Germany, July 26th -31th **2015** *"Fluorinated oxaphosphirane complexes: synthesis, redox potentials and novel reactions"* (poster contribution).

2. C. Murcia García, R. Streubel, SFB 813 Women in Science@Spin Centers, Eisenach/Germany, May 18-20, **2015**: *"Synthesis, redox potentials and novel reactions of fluorinated oxaphosphirane complexes"* (oral contribution).

3. C. Murcia García, A. Espinosa, R. Streubel, SFB 813 International Symposium – Chemistry at Spin Centers II, Bad Honnef/Germany, September 24-26, **2014**: *"Fluorinated oxaphosphirane ligands: synthesis, redox potentials and reactions"* (poster contribution).

4. C. Murcia García, Rainer Streubel. ICPC (International Confere on Phosphorus Chemistry). Dublin/Ireland. June 28th -July 2nd **2014** "*Synthesis and acid-induced ring expansion of fluorinated oxaphosphirane complexes*" (poster contribution).

5. C. Murcia García, R. Streubel, Colloquia of the Institute for Inorganic Chemistry, Bonn/Germany, May 22nd , **2014** *"Fluorinated oxaphosphirane ligands –What to expect?"* (oral contribution).

6. C. Murcia, R. Streubel, MHC-6 PhD Workshop, Bonn/Germany, April 5-7, **2013**: *"Synthesis and ring expansion reactions of new oxaphosphirane complexes"* (oral contribution).

7. C. Murcia, M. Klein, R. Streubel, 10th European Workshop on Phosphorus Chemistry, Regensburg/Germany, March 18.-20., **2013** *"Synthesis, deoxygenation and ring-opening reactions of oxaphosphirane complexes"* (poster contribution).

8. C. Murcia, R. Streubel, The 14th International Seminar of PhD Students on Organometallic and Coordination Chemistry, Admont/Austria, September 9-13. **2012**: *"Synthesis and reactions of P-triphenylmethyl substituted oxaphosphirane complexes"* (oral contribution).

9. C. Murcia, J. M. Villalba Franco, V. Nesterov, R. Streubel, 9th European Workshop on Phosphorus Chemistry, Rennes/France, March 22.-24. **2012**: *"P-Functional azaphosphiridine and oxaphosphirane complexes"* (poster contribution).

10. C. Murcia García, R. Streubel, 5. Deutsch-Österreichischer Mitarbeiter-Workshop, Graz/Österreich, September 23.-25. **2011** *"Synthesis and reactions of oxaphosphirane complexes containing new ligands at phosphorus"* (oral contribution).

11. C. Murcia, M. Bode, R. Streubel, 8th European Workshop on Phosphorus Chemistry, Münster/Germany, March 28.-29. **2011**: *"New O,P,C-cage complexes: synthesis and reactions"* (poster contribution).

Acknowledgements

I would like to thank my supervisor Prof. Dr. Rainer Streubel and to express my special appreciation to him for being a tremendous mentor for me. I would like to thank him for encouraging my research and for allowing me to grow as a scientist. His advice on both research as well as on my career have been priceless.

I would also like to thank Prof. Dr. Robert Glaum for the nice work atmosphere on the first floor of the Inorganic Chemistry building and for taking the role as second referee of my thesis, as well as Prof. Dr. Barbara Kirchner and Prof. Dr. Christa Müller for their willingness to become members of this committee.

I want to express my acknowledgement to Prof. Arturo Espinosa Ferao, Prof. Antonio Frontera Beccaria and Prof. Takahiro Sasamori for the big support with theoretical calculations to my experimental work and for their brilliant comments and suggestions.

Many thanks as well to Prof. Dr. Olav Schiemann and to Dr. Hideto Matsuoka for the number of EPR measurements performed and the help with the interpretation.

The analytics and technics teams of our institute deserve my big appreciation for their high quality service and their willing to help. I will never forget the cooperativeness of Mrs. Prochnicki, Dr. Schnakenburg and Mrs. Rödde.

Thanks to former and present members of the Streubel research group, mainly to Dr. Vitaly Nesterov, Dr. José Manuel Villalba Franco, Tobias Heurich and Andreas Kyri, for the great atmosphere and the nice “barbecues” as well as for the helpful scientific discussions.

I acknowledge my friends for incentiving me to strive towards my goal.

Finally I thank my family in Spain and Germany and my husband Florian. Words cannot express how grateful I am to them for all their support during my writing.

Table of Contents

1. Introduction

Phosphorus, named after the Greek word “φωσφόρος” (light bearer) is one of the most important p-block elements of the periodic table and plays an outstanding role in biochemistry, organic synthesis, coordination chemistry, material science, etc. This non-metal element was first discovered in 1669 by the German chemist Hennig Brand, considered the last of the alchemists. Brand obtained phosphorus from human urine as an impure mixture of $Na(NH_4)HPO_4$ and carbon-based compounds, which after distillation yielded elemental white phosphorus (P_4).[1]

Nearly 95 percent of the modern chemical literature is devoted to carbon compounds. As a result, heteroatom chemistry simulating the chemistry of carbon has attracted very much attention since the second part of the 20th century. Phosphorus, as summarized in the book by Mathey, Nixon and Dillon: *Phosphorus: The Carbon Copy*,[2] presents noteworthy similarities to carbon although one might argue that the structures, bonding and reactivity of their respective compounds would be quite different.[3] However, an exceptional parallel chemistry has developed around the fact that, in low coordination numbers, phosphorus strongly resembles carbon. Electronegativity is a very useful concept in chemistry and has numerous applications, which include rationalization of bond energies and the types of reactions that substances undergo. Indeed, carbon and phosphorus show a diagonal relation by virtue of their similar electronegativity value (2.5 and 2.2 for C and P, respectively) which governs their ability to attract electrons to themselves in a molecule.[4]

A high reactivity means electrons in high-lying orbitals and/or accessible, low-lying, empty orbitals. In organic chemistry, such electronic distributions are normally associated with π-bonds, aromatic systems and strained rings. Thus being the diagonal carbon-phosphorus analogy well expressed in these areas.[5]

A theoretical study of isolated π-bonds was performed for ethylene, imine ($H_2C{=}NH$) and phosphaethylene, the later only known in the gas phase. ($H_2C{=}PH$; **Figure 1**). The results of calculations[6] have revealed that, in imine the HOMO (-10.62 eV) corresponds to the lone pair and the π-bond lies much lower in energy (-12.49 eV), while in phosphaethylene the π-bond is the HOMO (-10.30 eV) being the phosphorus lone pair slightly lower in energy (-10.70 eV). This suggests that, like in ethylene, most

reactions of phosphaethylene will occur at the π-bond, although the small energy difference of the orbitals, also makes reactions at phosphorus lone pair possible.

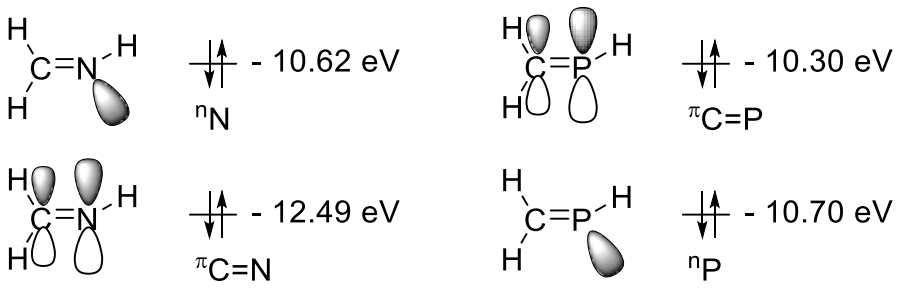

Figure 1. Highest occupied molecular orbitals of imine and phosphaethylene.[6]

Important reactions of olefins such as the 1,2-additions of polar molecules (*i.e.* HX) across the C=C bond are also observed with phosphaalkenes.[7] Even catalytic hydrogenations using rhodium phosphine catalyst are known for P=C bonds in phosphaalkenes **I**, however, the lone pair must be first protected through coordination to transition-metal complexing groups such as $[W(CO)_5]$ (**Scheme 1**).[8]

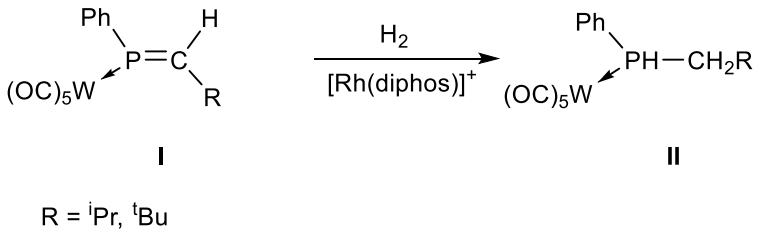

Scheme 1. Hydrogenation of phosphaethylene complexes using rhodium phosphine.[8]

As a result, phosphorus is considered "the carbon copy" and thus establishing an emergent field between organic and inorganic chemistry.[2]

1.1 P-Heterocycles

Ring systems, especially the ones substituted with heteroatoms, play a crucial role in organic chemistry. In fact, two thirds of organic compounds are heterocyclic compounds.[9]

Although the first known phosphorus heterocycle, the $\sigma^3\lambda^3$-1-phenylphosphinane **IV** (where σ is the coordination number and stands for the number of atoms directly attached to phosphorus or the number of σ bonds and λ represents the total number of bonds, including π bonds, which stands for the valence of phosphorus) was discovered in 1915 by Grüttner and Wiernik,[10] the domain really began to develop in

1953 with the discovery of the McCormack reaction between halophosphanes **V** and conjugated dienes like butadiene (**Scheme 2**).[11] Recently phosphorus heterocycles have received considerable interest because of their unique biological activities, their wide-ranging applications in organic synthesis as precursors for inorganic polymers and their use as sources of functional inorganic materials such as semiconductors and ceramics.[12]

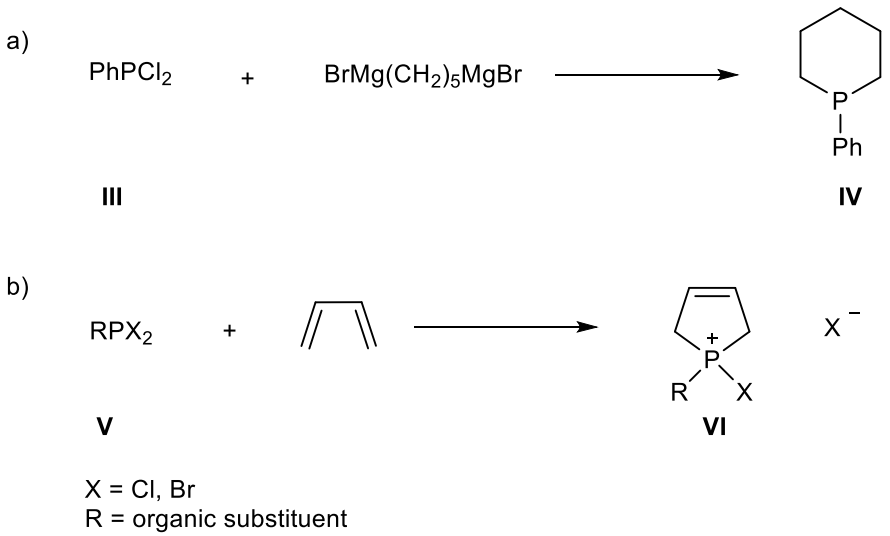

Scheme 2. (a) Synthesis of 1-phenylphosphinane;[10] (b) McCormack reaction.[11]

There are a number of other phosphorus-containing heterocycles. However, in this introductory part, an overview of selected P-heterocycles containing one phosphorus atom and two oxygen atoms (dioxaphosphinanes and dioxaphospholanes) or one phosphorus and one oxygen atom (oxaphosphetanes and oxaphosphiranes) will be presented.

1.2 Six-membered heterocycles with one phosphorus and two oxygen atoms

Dioxaphosphinanes, also named dioxaphosphorinanes, are six-membered phosphorus heterocycles containing two oxygen atoms (**VI-XI**; **Scheme 3**). They are of great importance as they have demonstrated biological activity as antibacterial and antiviral substances,[13] as well as, insecticidal properties,[14] being thus often used in agriculture.

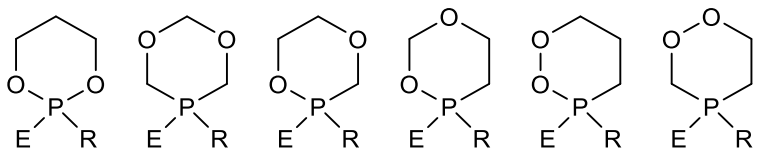

VII **VIII** **IX** **X** **XI** **XII**

Scheme 3. Dioxaphosphorinanes **VII - XII** (R: organic substituent, halogen, hydrogen or hydroxy; E: free electron pair or double bond to oxygen).

The synthesis of 1,3,2-dioxaphosphinanes **VII** (R = Cl) involves essentially reactions of a 1,3-propanediol and an electrophilic $\sigma^3\lambda^3$-phosphorus reagent like PCl_3 (**Scheme 4a**).[15] One of the most versatile methodologies for the formation of 1,3,5-dioxaphosphinanes **VIII** was first described by Epstein and Buckler via acid-catalyzed reaction of phenyl phosphine with benzaldehyde.[16] The derivatives of **IX** have been mainly produced by transesterification using a variety of bases as well as intramolecular nucleophilic displacement,[17] although there is also a report of this ring system being formed through a formal cycloaddition.[18] In 1994 Müller *et al.* succeeded in the synthesis of 1,5,2-dioxaphosphinanes **X** (R = ^{t}Bu) through the reaction of the *C*-amino substituted phosphaalkene **XIII** with hexafluoroacetone (**Scheme 4b**).[19] In contrast, derivatives of type **XI** and **XII** are still unknown.

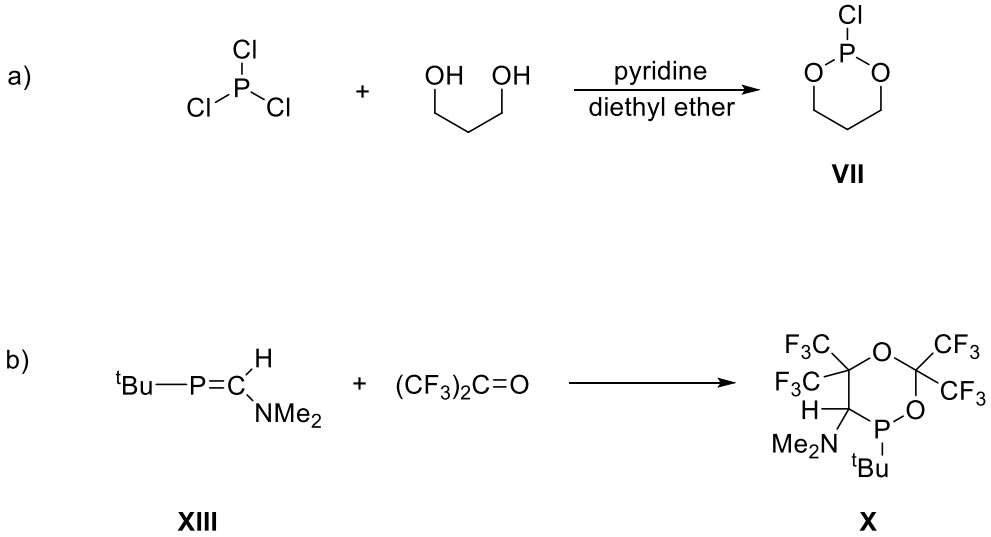

VII

XIII **X**

Scheme 4. Selected examples for the synthesis of dioxaphosphinanes of type **VII** (a) with a $\sigma^3\lambda^3$-phosphorus reagent[15] and of type **X** (b) through reaction of phosphaalkenes with hexafluoroacetone.[19]

1.3 Five-membered heterocycles with one phosphorus and two oxygen atoms

Dioxaphospholanes are five-membered heterocycles bearing one phosphorus and two oxygen atoms (**Scheme 5**). These, and specially 1,3,2-dioxaphospholanes **XIV,** are key compounds in the synthesis of phosphorus containing polymers and agrochemicals and have been exploited as indispensable tools in biochemistry and molecular biology of nucleic acids.[20]

XIV **XV** **XVI** **XVII**

Scheme 5. Dioxaphospholanes **XIV** - **XVII** (R: organic substituent, halogen, hydrogen or -OH; E: free electron pair, double bond to oxygen or metal complex).

As the criticism to the use of organohalogens became lately more prominent around the world because of their environment damaging effects,[21] dioxaphospholanes of the type **XIV** have attracted much more attention because of their ability to substitute organohalogens, act as initiators for polymerizations and also are being used as environment-friendly flame retardants.[22] By now only a few methods have been developed for P^{III} and P^{V} derivatives thus, of the type **XIV** by reaction of diols with dichlorophosphane **III** (**Scheme 6a**)[23] and of the type **XV** through cyclization of organophosphanes **XVIII** with aldehydes[24] or via thermolysis *P*-Cp*-substituted 2*H*-azaphosphirene complexes **XIX** in the presence of aldehydes (**Scheme 6b,c**).[25] In contrast, derivatives of 1,2,3-dioxaphospholanes **XVI** and 1,2,4-dioxaphospholanes **XVII** are still unknown.

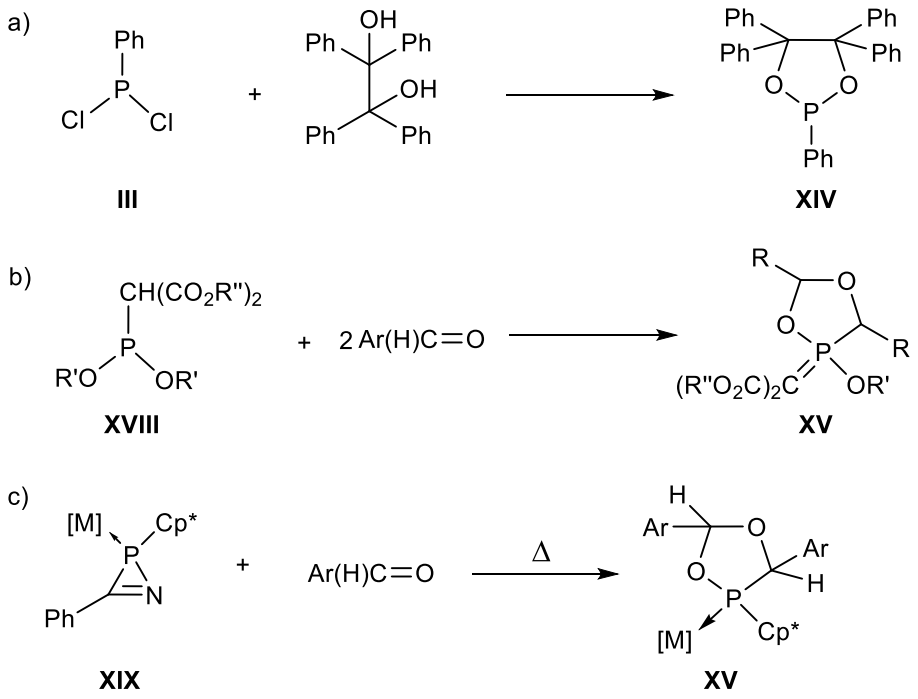

Scheme 6. Selected examples for the synthesis of dioxaphospholanes of type **XIV** (a) and of type **XV** (b, c).

1.4 Four-membered heterocycles with one phosphorus and one oxygen atom

Oxaphosphetanes, four-membered heterocycles containing one phosphorus and one oxygen atom (**XX**, **XXI**; **Scheme 7**) and, particularly 1,2-oxaphosphetanes **XX,** came to the fore as (potential) intermediates of the Wittig reaction. The latter allows the preparation of an alkene by the reaction of an aldehyde (or ketone) with the ylide generated from a phosphonium salt (**Scheme 8a**).[26]

XX **XXI**

Scheme 7. Oxaphosphetanes **XX** and **XXI** (R: organic substituent, halogen, hydrogen or -OH; E: free electron pair, double bond to oxygen or metal complex or two substituents).

The discovery of the Wittig reaction was a milestone in organophosphorus chemistry as well as a revolution for the chemical industry because of its application in the synthesis of vitamin A and β-carotenes.[27] Different P^V derivatives of **XX** have been described and structurally characterized along the years.[28] However, the generation of P^{III} analogues remained unexplored. Recently, Kyri *et al.* succeeded in the synthesis

of the first derivatives of $\sigma^3\lambda^3$–1,2-oxaphosphetane complexes by reaction of phosphinidenoid complexes **XXII** with different epoxides (**Scheme 8b**).[29] To date only a few derivatives of 1,3-oxaphosphetanes **XXI** have been selectively obtained, *i.e.* either through an intramolecular Mitsunobu reaction of bis(hydroxyalkyl)phosphinic acids with a mixture of triphenylphosphine (PPh_3) and diisopropylazodicarboxylate (DIAD, **Scheme 8c**).[30]

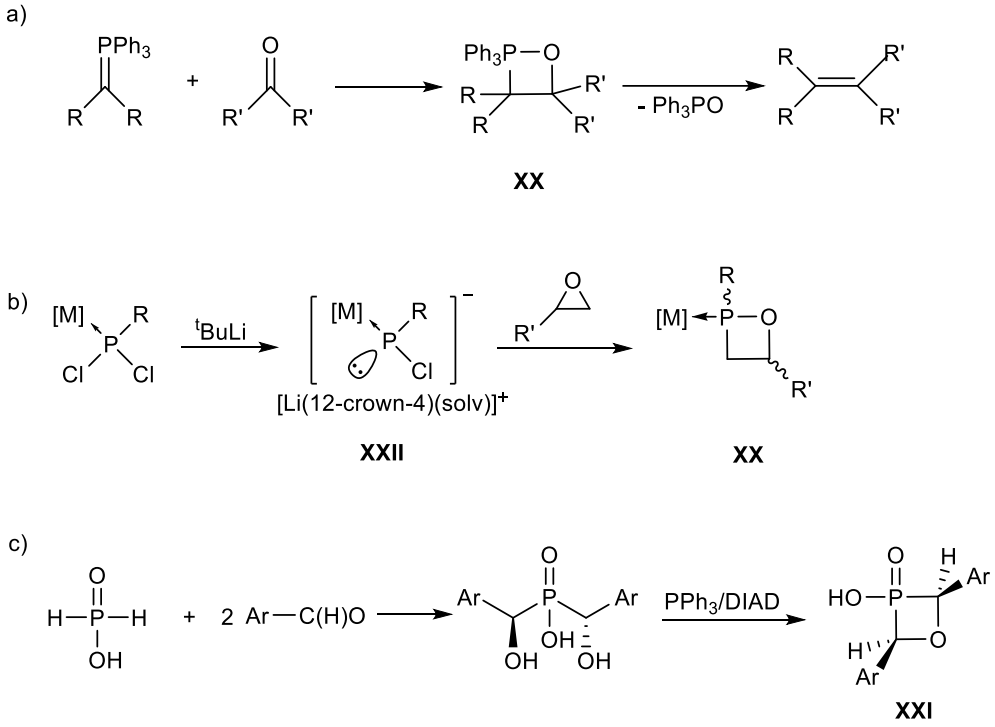

Scheme 8. Selected examples for the synthesis of oxaphosphetanes of the type **XX** (a[26]; b[29]) and of the type **XXI** (c).[30]

Up to here of the introduction it has been shown that phosphorus heterocycles containing oxygen are compounds of high importance and have many applications in industry as well as in medical sciences. Numerous derivatives of six, five and four-membered rings could be synthesized thus leading to a rapid increase and spread of knowledge. Furthermore, it has inspired continuous search of more use of phosphorus and oxygen containing rings for their successfully incorporation in chemical processes.

1.5 Three-membered heterocycles with one phosphorus and one oxygen atom

Three-membered rings belong to the most reactive classes of compounds in organic chemistry. As such, they are playing a role of ever increasing importance as intermediates in reactions including polymerizations.[31] One of the most important three-membered rings in chemistry is ethylene oxide, **XXIII**, also called oxirane (one oxygen and two carbon atoms). It is a vital raw material with a huge number of applications including the manufacture of products like polysorbate 20 and polyethyleneglycol (PEG). Ethylene oxide is a major industrial chemical and is consistently ranked among the top 25 highest production volume chemicals produced in the world.[32] The chemical behavior of oxiranes is governed by two factors: ring strain[33] and the basicity of the oxygen ring atom.[31]

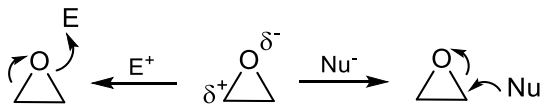

XXIII

Scheme 9. Ring-opening of oxiranes **XXIII** induced by electrophilic or nucleophilic attack.[34]

At this point, one may think that a three-membered heterocycle containing phosphorus, oxygen and carbon would present similar reactivity as ethylene oxide and possibly lead to new and useful properties. But the phosphorus analogues of oxiranes, the so-called $\sigma^3\lambda^3$-oxaphosphiranes, are experimentally still unknown to date, but they have been claimed as reactive intermediates.[35]

To have more information on this issue, Schöller performed *ab-initio* calculations and predicted the existence of free oxaphosphiranes in equilibrium with their open form.[36] He calculated heats of reactions of symmetric systems and determined that, in case of X = X' and carbon or silicon, the closed form **XXV** will be favored. But in presence of a free electron pair at X and X' atoms like oxygen, nitrogen or sulfur, this equilibrium will be displaced to the open form **XXIV** (**Scheme 10**).

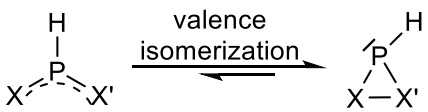

XXIV **XXV**

Scheme 10. Valence isomerization of symmetrically substituted phosphorus heterocycles.[36]

Table 1. Calculated heats of reaction for ring closure of bis(ylene)phosphoranes. (SCF/CEPA-1-Level).[36]

X/X'	CH_2	SiH_2	NH	S	O
ΔE [kcal/mol]	-46.8	-42.2	19.7	9.0	79.6

Although these systems are symmetrical, it is reasonable that the free oxaphosphirane would also follow this tendency and presents a similar equilibrium. It is possible to estimate the heat of reaction of a mixed system by calculating the average value of the energy data for X = carbon (-46.8 kcal/mol) and X' = oxygen (79.6 kcal/mol), resulting that this equilibrium, in the case of oxaphosphiranes, displaced to the open form **XXIV (Scheme 11)**

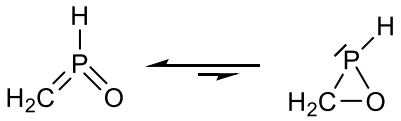

XXIV **XXV**

$\Delta E(CH_2/O) = (-46.8 + 79.6)/2 = 16.4$ kcal/mol

Scheme 11. Predicted heat of reaction between the closed (**XXIV)** and the open form (**XXV)** of a $\sigma^3\lambda^3$- oxaphosphirane using the data of Schöller.

A preliminary study of Espinosa[37] especially designed for oxaphosphirane systems bring more information on this equilibrium by calculating heats of reaction of unsymmetrical systems (**Table 2**).

Table 2. Calculated heats of reaction for ring closure of bis(ylene)phosphoranes. (SCF/CEPA-1-Level).[37]

X' (X = O)	CH_2	$C(NMe_2)_2$	$C(CF_3)_2$	$C(C_6F_5)$
ΔE [kcal/mol]	-10.1	-7.1	-4	-8.7

This table shows that the presence of electron-withdrawing atoms/groups would favor the closed form, *i.e.* the oxaphosphirane ring.

Nevertheless, the effects of substituents at the phosphorus atom may also have a significant influence on this equilibrium, and even promote the closed form **XXV**. However, such theoretical predictions are still not available.

Nevertheless, the first oxaphosphirane with phosphorus in high oxidation state, the $\sigma^4\lambda^5$-oxaphosphirane **XXVIII**, was achieved in 1978 by Röschenthaler *et al.* by reaction of Niecke's iminophosphane **XXVII** with hexafluoroacetone (**Scheme 12**).[38]

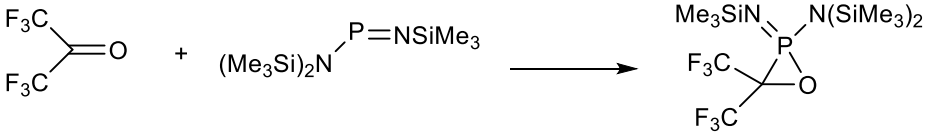

XXVI **XXVII** **XXVIII**

Scheme 12. Synthesis of the first oxaphosphirane derivative **XXVIII**.[38]

This type of [2+1] cycloaddition reactions with hexafluoroacetone were previously known with transition metals such as Ni or Rh, but not for main group elements. In 1985 Niecke *et al.* performed more investigations on this reaction and discovered that substituents at the nitrogen atom have a considerable effect in the reaction course, thus leading either to a [2+1] cycloaddition to give oxaphosphiranes or to a [2+2] reaction thus yielding oxazaphosphetidines.[39]

The pathway towards P^{III} derivatives was opened by Mathey who, in 1990, developed the synthesis of the first $\sigma^3\lambda^3$-oxaphosphirane complexes (**XXX**) via epoxidation of phosphaakene complexes (**XXIX**) with meta-chloroperbenzoic acid (*m*-CPBA) (**Scheme 13a**).[40,41] As oxidation of unligated phosphaalkenes occurs preferentially at the phosphorus atom, it was necessary to block the lone pair at phosphorus via ligation to a metal complex and, therefore, promote the formation of the ring ligand.

a)

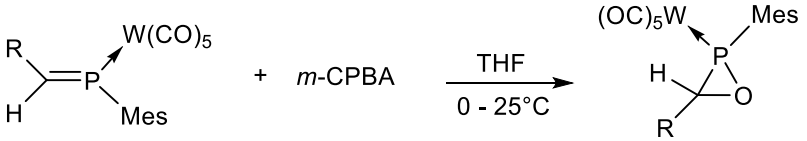

XXIX **XXX**

R = Me, ^{i}Pr

b)

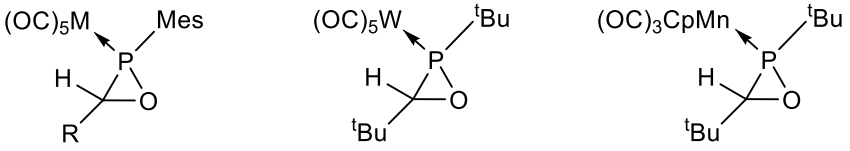

Scheme 13 a) Synthesis of oxaphosphirane complexes via epoxidation of phosphaalkene complexes; b) new derivatives synthetized by Schröder *et al.*[41,42]

This method permitted the formation and characterization of new oxaphosphirane complexes, not only having tungsten as transition metal attached to the phosphorus atom, but also having chromium and manganese (**Scheme 13b**) as Schröder demonstrated in his PhD thesis. They also pointed out the necessity of having a sterically demanding substituent at phosphorus to stabilize the oxaphosphirane ring.[42]

The work under such harsh conditions, *i.e.* with *m*-CPBA and the difficulties to obtain the corresponding phosphaalkene complexes, hindered the number of oxaphosphirane complexes to be achieved with this method. Most of the targeted oxaphosphirane complexes decomposed in an acid medium and/or were only stable at low temperature.

A new synthetic route came to the fore in 1994 when Streubel and co-workers reported on a thermally induced ring-cleavage of the 2*H*-azaphosphirene complex **XXXI** (**Scheme 14**) in presence of benzaldehyde[43] or benzophenone.[44] The selective formation of the desired oxaphosphirane complex **XXXIII**, was selectively achieved in the case of benzaldehyde by reaction with the transiently generated phosphinidene complex **XXXII**. By using benzophenone, a side-reaction to a benzo[c]-1,2-oxaphospholane complex occurred leading to a mixture of the corresponding oxaphosphirane complex **XXXIII** and the oxaphospholane complex **XXXIV**.

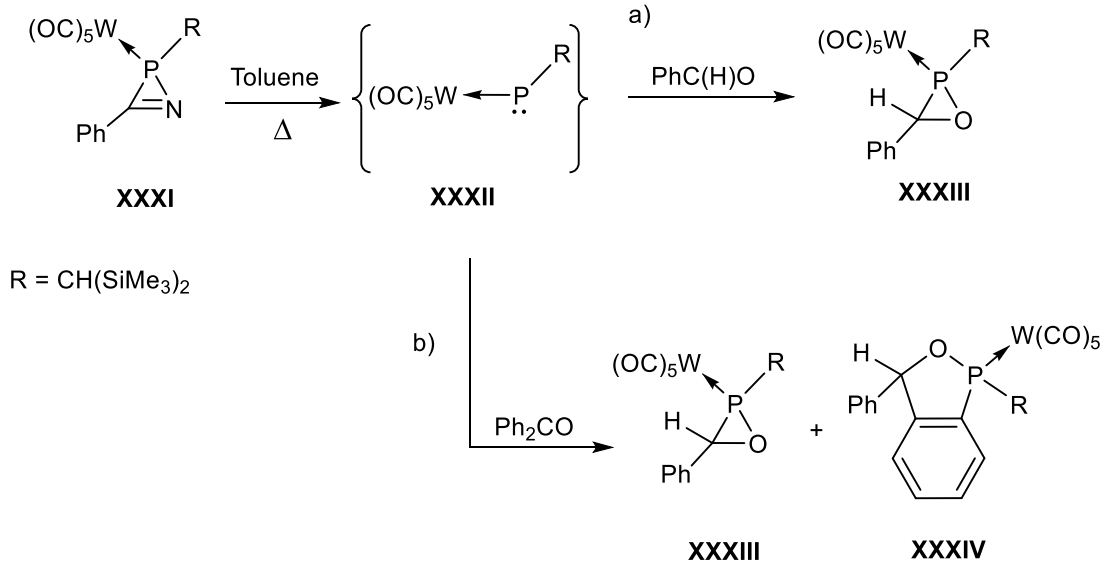

Scheme 14. Synthesis of $\sigma^3\lambda^3$-oxaphosphirane complexes by thermolysis of *2H*-azaphosphirene complexes: a) with benzaldehyde; b) with benzophenone. [43,44]

Due to the multistep synthetic process to obtain 2*H*-azaphosphirene complexes, and the difficulties to apply this method to the synthesis of oxaphosphirane complexes

using other aldehydes or ketones than benzaldehyde and benzophenone, this route – as well as the other – is unsuitable as standard pathway.

In 2007 an important breakthrough in the chemistry of oxaphosphirane complex chemistry arose thanks to the work of Özbolat-Schön, a co-worker of Streubel. She developed a facile procedure based on the generation of Li/Cl phosphinidenoid complexes (**XXXVII**) by treatment of chloro- or dichloro(organo)phosphanes **XXXV**, **XXXVI** with lithium bases in presence of 12-crown-4 at low temperature and subsequent treatment with aldehydes or ketones (**Scheme 15**).[45,46]

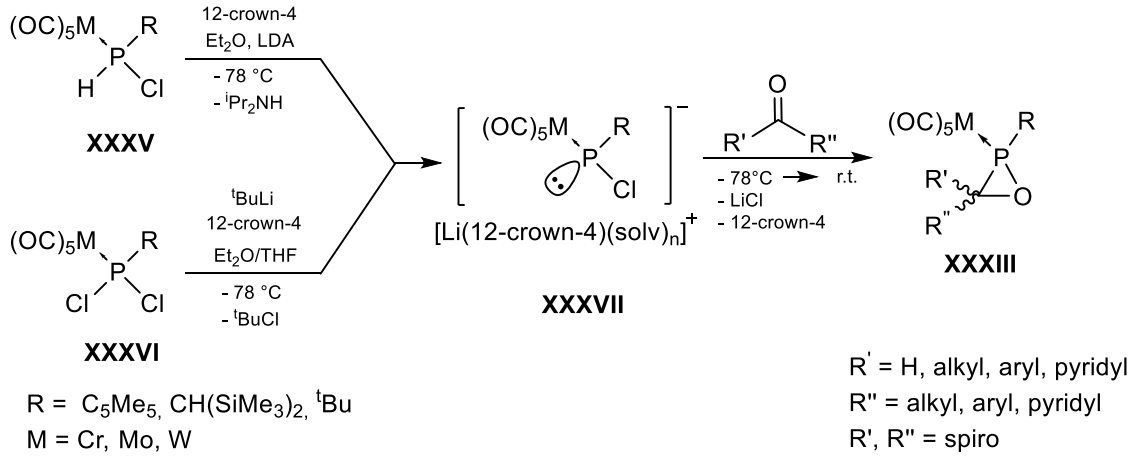

Scheme 15 Systhesis of $\sigma^3\lambda^3$-oxaphosphirane complexes via formation of a phosphinidenoid complex.[45,46]

Herewith, $\sigma^3\lambda^3$-oxaphosphirane complexes **XXXIII** were obtained in excellent yields with different substituents at the phosphorus atom such as the bis(trimethylsilyl)-methyl group ($CH(SiMe_3)_2$), the pentamethylcyclopentadienyl-group ($Cp^* = C_5Me_5$) and. More recently, with the *tert* butyl group ($^tBu = C_4H_9$), as well as with different alkyl or aryl substituents at the carbon atom of the ring. Moreover, different transition metals were able to be incorporated at phosphorus. It is noteworthy, that the easy accessibility to the starting materials combined with the mild conditions of the reaction course even allowed the introduction of functional groups such as alkenyl substituents,[47] donor-groups (pyridyl-groups),[48] and the spiro function into the carbon atom of the heterocycle.[49] In summary, the "phosphinidenoid route" is a method that permits, for the first time, the systematic synthesis of a wide variety of $\sigma^3\lambda^3$-oxaphosphirane complexes.

1.6 The triphenylmethyl group in organophosphorus chemistry

Triphenylmethane is an aromatic hydrocarbon in which phenyl groups replace three hydrogen atoms of methane. It is known for its steric and electronic abilities to form anions, radicals, and cations of considerable stability, because it allows an effective delocalization of charge/electrons over its three phenyl rings. The triphenylmethyl radical, also called “trityl”, was discovered in 1900 by Gomberg as the first trivalent carbon compound.[50] The radical **XXXVIII** is stable for weeks under inert atmosphere at room temperature and forms a chemical equilibrium with the quinoid type dimer **XXXIX** (**Scheme 16**).

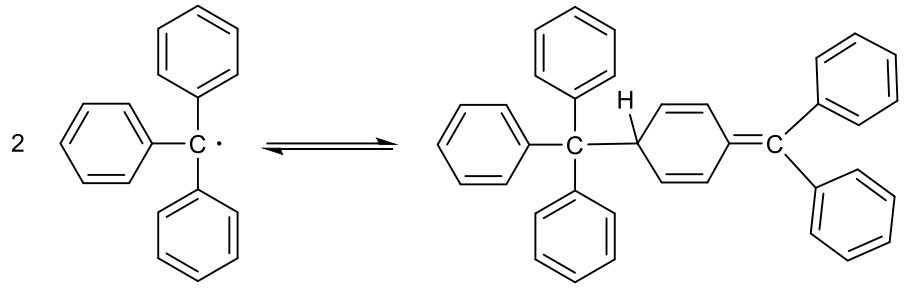

XXXVIII **XXXIX**

Scheme 16. Equilibrium between triphenylmethyl radical and its dimer.

Triphenylmethyl substituent was introduced in organophosphorus chemistry thanks to the work of Schmutzler and co-workers, which permitted the access to a wide variety of very reactive and/or unstable compounds, such as acyclic diphospha-urea derivatives, 1,3-diphosphetane-2,4-dione[51] and acyl(chloro)organophosphanes.[52] Recently, Streubel and co-workers characterized the first room temperature stable phosphinidenoid complex (**Scheme 15**, compound **XXXVII**) by incorporating the triphenylmethyl moiety into the phosphorus atom.[53] There are only two more examples of phosphinidenoid complexes reported so far (R = $CH(SiMe_3)_2$ and C_5Me_5), but they decompose around −45 °C.

The stability of the triphenylmethyl radical is not based only in electronic nature but also due to steric demand as the central carbon-carbon bond of the dimer possesses a strength of only 46 kJ/mol (**Scheme 16**).[54]

Under normal circumstances, phosphorus-carbon σ-bonds are of low reactivity,[55,56] and only a few examples are known in which, under forcing conditions, P-C bond cleavage is observed.[57] The reason for this is the strength of the σ-bond between

phosphorus and carbon, but also the inability of nearly all simple hydrocarbon substituents to work as leaving groups, and a good leaving group has to be stable under the reaction conditions. This may be achieved by steric and/or electronic (mesomeric, inductive) effects. As aforementioned, Schmutzler used such effects to selectively cleave P-C bonds in P^{III} triphenylmethyldichlorophosphine to benefit from triphenylmethyl as leaving group.[58]

Lately, an innovative computational study by Espinosa and Streubel[59] has provided first insights into the intrinsic strength of the exocyclic bonds to phosphorus in oxaphosphirane κP-pentacarbonylmetal(0) complexes, using a set of differently substituted derivatives (a = Me, b = ^{t}Bu, c = CPh_3; **Scheme 17**). This theoretical investigation analyzed the reactivity of oxaphosphirane complexes towards oxidative and reductive single electron transfer reactions (SET), and hence, offers valuable explanations to the problem of P-functionalization of oxaphosphiranes. In case of chromium(0) complexes homolytic bond cleavage of the exocyclic P-R bond was found to be always unfavorable (**Scheme 17** orange), the heterolytic cleavage leading to a carbocation and the oxaphosphiranide complex **XL**$^-$ was found to be the lowest energy process (**Scheme 17** black), especially if the R group is bulky and able to stabilize the positive charge efficiently, as is the case for the trityl substituent (**XLc**).[59]

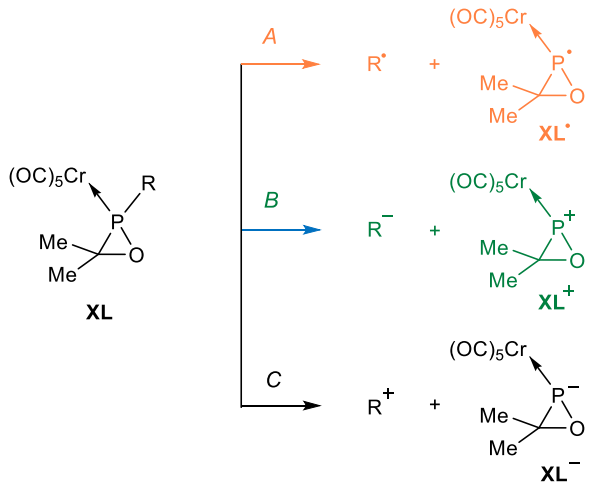

	R•/XL•	R−/XL+	R+/XL−
XLa	70.8	139.6	112.9
XLb	58.5	143.3	44.1
XLc	31.1	91.1	18.3

Scheme 17. Fundamental bond-cleavage processes (A–C) of the P−R bond and computed energetics (kcal/mol) for the dissociation and redox processes of compounds **1a-c**. ($COSMO_{THF}$/B3LYP-D/def2-TZVP).

The results of the study by Espinosa and Streubel for oxaphosphirane complexes are in agreement with the experimental results that Schmutzler and Plack obtained for phosphines[58], phosphonium salts[60] and phosphoranes,[61] in which the formation of

Ph_3C^+ becomes favorable when the phosphorus atom is substituted by groups that are strongly electron-withdrawing, and able to form stable anions (*e.g.* F, Cl, Br). To summarize here: the trityl group may play a major role in determining the reactivity of three-membered phosphorus heterocycles.

To date, only preliminary reports on the synthesis of a *P*-trityl substituted oxaphosphirane complex are available, and reactivity studies haven't been performed, yet.[60,62]

2. Aim of the thesis

The objective of this PhD work was to synthesize new oxaphosphirane complexes having the triphenylmethyl group bound to phosphorus. These derivatives may possess a higher lability of the P-C exocyclic bond than other derivatives, thus acting as a functional group, which should be studied in detail.

A further major objective was a comparative study of the effects of electron-withdrawing groups at the ring carbon atom on the reactivity using derivatives bearing three different bulky substitutents at phosphorus: triphenylmethyl, pentamethyl-cyclopentadienyl (C_5Me_5) and bis(trimethylsilyl)methyl ($CH(SiMe_3)_2$).

In particular, the reactivity of these novel oxaphosphirane complexes was to be investigated towards strong σ-donors *i.e.* N-heterocyclic carbenes, ring-opening reactions with Brønsted acids as well as SET (single electron transfer) and multiple electron reductions.

3. Synthesis of $\sigma^3\lambda^3$-oxaphosphirane complexes via Li/Cl phosphinidenoid complexes

3.1 Synthesis of dichloro(triphenylmethyl)phosphane complexes

To achieve the synthesis of *P*-triphenylmethyl substituted oxaphosphirane complexes, the critical step is the formation of the corresponding dichlorophosphane complexes. As the tungsten derivative **2c** was recently obtained in the group of Streubel, using selective reaction of dichlorophosphane **1** with acetonitrile(pentacarbonyl)-tungsten(0).[53] This procedure provided a conversion of approximately 75% of the starting phosphane. Attempts to improve this failed as this could not be increased neither by changing the reaction conditions, nor by variation of the stoichiometry. Complex **2c** was obtained in 65% yield after column chromatography at low temperature.

Therefore, another method was applied for the synthesis of dichloro(triphenylmethyl)phosphane complexes **2a-c**. First, the metal hexacarbonyles $M(CO)_6$ (M = Cr, Mo, W) were converted into the corresponding $[M(CO)_5(thf)]$ complexes by photolysis in THF and lately reacted with triphenylmethyl-dichlorophosphane (**Scheme 18**). This allowed, in the cases of tungsten and chromium, complete conversion of **1** into phosphane complexes **2a,c**. In case of molybdenum, only 30% of the phosphane **1** was converted into the corresponding phosphane complex **2b**. This result could not be improved neither by changing the method, nor by modification of the reaction conditions.

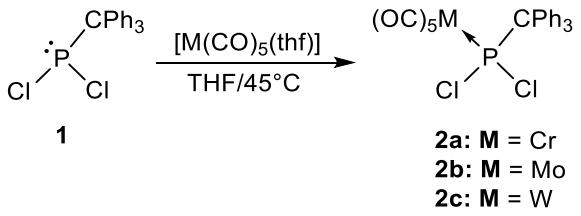

1

2a: M = Cr
2b: M = Mo
2c: M = W

Scheme 18. Synthesis of dichloro(triphenylmethyl)phosphane complexes **2a-c**.

The isolation of the phosphane complexes **2a-c** was performed by low temperature column chromatography using neutral aluminum oxide as solid phase. Complexes **2a,c** were obtained in excellent yields (92% and 86%, respectively), while only 25% of complex **2b** was obtained after eluation. Selected NMR data of the complexes are given in **Table 3**.

Table 3 Selected $^{31}P\{^1H\}$ and $^{13}C\{^1H\}$ NMR resonances [ppm], $^1J_{P,W}$ and $^2J_{P,C}$ [Hz] of complexes **2a-c** in THF-*d8* (**a** = Cr, **b** = Mo, **c** = W).

Compound	$\delta^{31}P\{^1H\}$ ($^1J_{P,W}$)	$\delta^{13}C\{^1H\}$ ($^2J_{P,C}$)		
		$\underline{C}Ph_3$	*cis*-CO	*trans*-CO
2a	234.2	77.7 (16.2)	213.7 (12.2)	220.1 (1.9)
2b	201.0	74.1 (17.6)	202.4 (9.0)	208.8 (48.9)
2c	166.2 (319.7)	75.5 (10.7)	195.9 (7.1)	198.9 (48.0)

The phosphorus chemical shift is extremely sensitive to the electronic, steric and geometric environment of the ^{31}P nucleus, thus the nature of the transition metal has an influence on the $^{31}P\{^1H\}$ chemical shifts of complexes **2a-c**. The resonances were observed between 235 ppm and 166 ppm and decrease in the order Cr > Mo > W. The so-called $\Delta\delta$ values, *i.e.,* the differences between the phosphorus resonances of transition metal complexes bearing the same ligand, are a common feature of metal-coordinated trivalent phosphorus compounds.[63–65]

The $^{13}C\{^1H\}$ chemical shifts of the carbonyl carbon atoms follow also the same tendency. The spectrum exhibits two carbonyl doublets due to the carbonyl groups, *cis* and *trans* oriented to phosphorus. For molybdenum **2b** and tungsten **2c** complexes, the phosphorus-carbon coupling constants show $|^2J_{P,C}(cis)| < |^2J_{P,C}(trans)|$, while in the case of the chromium complex **2a**, the *trans*-CO carbon atom has a smaller P−C coupling constant magnitude compared to the carbon nuclei in the *cis*-CO groups. This observation is also a common feature of pentacarbonyl phosphane chromium complexes.[63]

From concentrated solutions of **2a,b** in *n*-pentane, crystals were obtained and their molecular structures are represented in **Figure 2**. Both derivatives crystallize in the monoclinic system and space group $P2_1/n$ for chromium and $P2_1/c$ for molybdenum.

The triphenylmethyl moiety in dichlorophosphane complexes **2a-c** caused an enlargement of the P−C(1) bond having a value for **2c** of 1.955(2) Å (the sum of covalent radii of P and C atoms is 1.87 Å),[66] as observed by Streubel *et. al,*[53] which is significantly longer compared with that of the unligated phosphane **1**

(1.9333(14) Å).[67] The chromium analogue **2a** also follows this tendency presenting a value of its P−C bond length of 1.956(5) Å, while the molybdenum derivative **2b** shows a value of 1.938(16) Å (very similar to **1**). By comparison to the tungsten[53] and chromium analogues, the molybdenum derivative presents also the shortest distances for the P−Cl bonds. However, **2b** displays the largest P−M bond length, thus having a value of 2.489 Å.

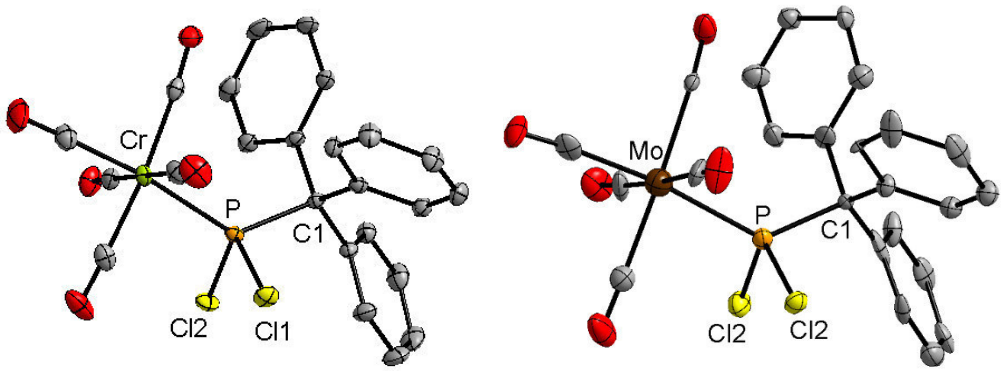

Figure 2. Molecular structures of oxaphosphirane complexes **2a** and **2b** (thermal ellipsoids are shown with 50% probability level); all hydrogen atoms are omitted for clarity; selected bond lengths (Å) and angles (°): **2a**: P-Cr 2.3327(5), P-C(1) 1.9557(15), P-Cl(1) 2.0534(5), P-Cl(2) 2.0592(5), Cr-P-C(1) 127.91(5), C(1)-P-Cl(1) 102.52(5), Cl(1)-P-Cl(2) 98.54(2). **2b**: P-Mo 2.489(5), P-C(1) 1.938(16), P-Cl(1) 2.049(6), P-Cl(2) 2.023(8), Mo-P-C(1) 130.5(7), C(1)-P-Cl(1) 101.6(5), Cl(1)-P-Cl(2) 100.8(3).

3.2 Synthesis of *C*-aryl, *P*-triphenylmethyl substituted oxaphosphirane complexes

As described in the introduction, the synthesis of *C*-phenyl, *P*-triphenylmethyl oxaphosphirane complex **4c** was recently published,[53] but its chromium (**4a**) and molybdenum (**4b**) analogues were still unknown as well as the respective Li/Cl phosphinidenoid complexes needed as starting material. In this chapter, the synthesis and characterization of the above mentioned compounds are described.

Li/Cl phosphinidenoid chromium and molybdenum complexes **3a,b** were quantitatively formed by a one-pot reaction of the corresponding dichlorophosphane complexes **2a**,**b** with *tert*-butyl lithium in the presence of 12-crown-4 in THF at -78°C (**Scheme 19**).[55]

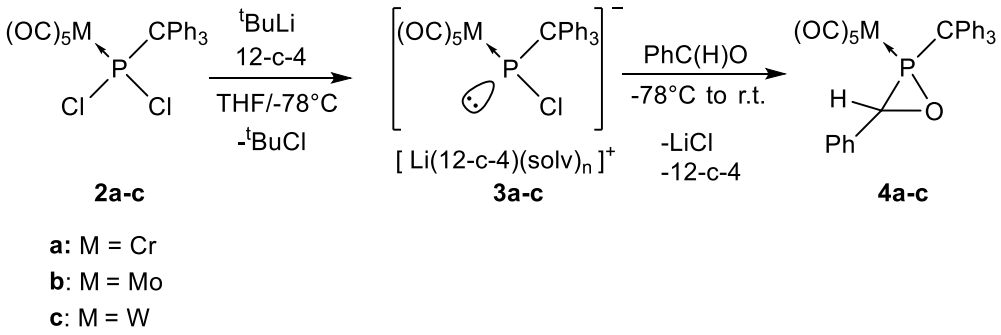

Scheme 19. Synthesis of oxaphosphirane complexes **4a-c** via Li/Cl phosphinidenoid complexes **3a-c**.

In the $^{31}P\{^{1}H\}$ NMR spectrum, complexes **3a,b** display signals at 310.4 and 280.4 ppm respectively. Both display a shoulder on the high-field side (ratio of ca. 3:1) that corresponds to the ^{37}Cl isotopomer of **3a,b**, a phenomenon which was first observed by Özbolat and which is one of the characteristic NMR features for the class of Li/Cl phosphinidenoid complexes.[45,68] Complexes **3a,b** were NMR spectroscopically characterized at -60°C in THF-*d8*. A NMR-monitoring from -60°C to room temperature, to determine their thermal stability, was carried out for both derivatives. While the molybdenum derivative starts to unselectively decompose at -20°C, the chromium analogue was stable over several days at room temperature under argon atmosphere. After six days, complex **2a** started to decompose slowly.

Having access to complexes **2a,b**, oxaphosphirane complexes **4a,b** were then synthesized through the reaction of *in situ* generated Li/Cl phosphinidenoid complexes **3a,b** with benzaldehyde at -78°C and warming up to room temperature (**Scheme 19**). The $^{31}P\{^{1}H\}$ NMR spectrum of **4a,b** showed phosphorus resonances significantly high-field shifted compared to those of analogous *P*-bis(trimethylsilyl)methyl (91.0 and 65.4 ppm for Cr and Mo, respectively) and *P*-Cp* (75.7 and 52.7 ppm for Cr and Mo, respectively) oxaphosphirane complexes (**Table 4**). The $^{13}C\{^{1}H\}$ NMR shifts, corresponding to the quaternary carbon atom of the $\underline{C}Ph_3$ group, appear in oxaphosphiranes and phosphinidenoid complexes high field-shifted in comparison to the dichlorophosphane complexes **2a-c**.

Table 4. Selected $^{31}P\{^{1}H\}$ and $^{13}C\{^{1}H\}$ NMR resonances [ppm], $^{1}J_{P,W}$ and $^{2}J_{P,C}$ [Hz] of complexes **3a,b** and **4a,b** in THF-*d8*.

Compound	$\delta^{31}P\{^{1}H\}$	$\delta^{13}C\{^{1}H\}$ ($^{2}J_{P,C}$)			
		CPh$_3$	P**C**O	***cis*-CO**	***trans*-CO**
3a	310.4	66.9 (22.8)	-	220.6 (6.9)	221.6 (20.1)
3b	280.4	67.1 (22.1)	-	208.8 (8.0)	216.2 (24.5)
4a	58.6	67.5 (14.1)	59.1 (20.6)	211.6 (14.5)	214.3 (37.6)
4b	33.4	66.2 (13.7)	51.2 (20.2)	202.3 (9.5)	208.5 (46.1)

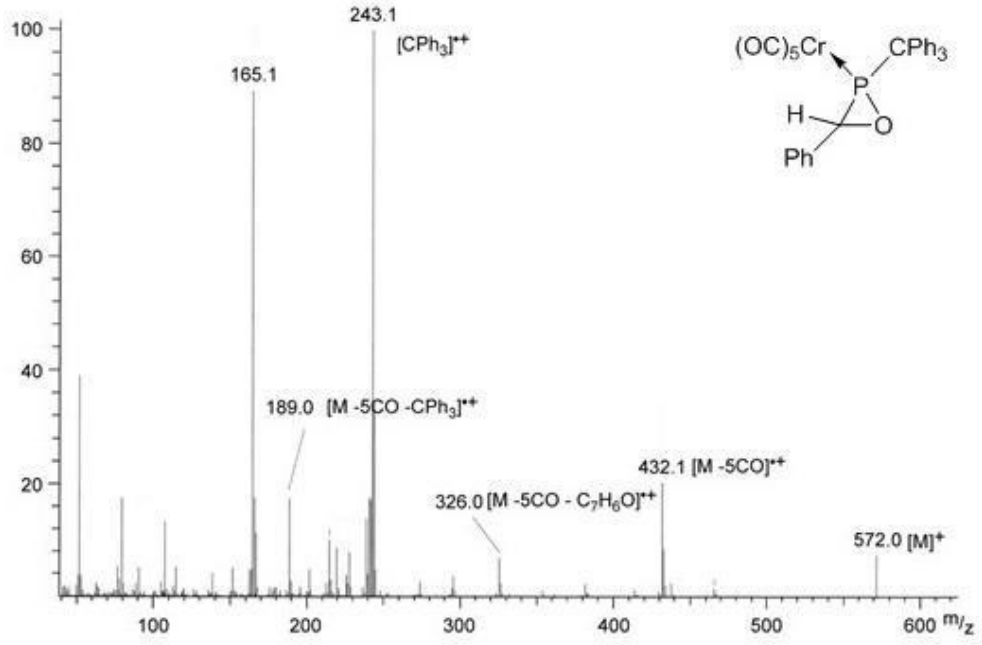

Figure 3. Mass spectrum (EI, 70eV) of oxaphosphirane complex **4a**.

Mass spectrometric investigations (EI, 70eV) for complexes **4a,b** were performed and showed similar results and, exemplarily, the mass spectrum of complex **4a** will be discussed (**Figure 3**). It shows the preference of the molecule radical cation m/z 572.0 ($[M]^{\bullet+}$) to extrude five unities of CO m/z 432.1 ($[M\text{-}5CO]^{+}$) followed by the loss of the triphenylmethyl moiety m/z 189.0 $[M\text{-}5CO\text{-}CPh_3]^{+}$ as the corresponding base peak indicates ($[CPh_3]^{+}$ m/z 243.1). However, another fragmentation pathway was observed, combining the extrusion of five CO units and the loss of the aldehyde moiety m/z 326.0 ($[M\text{-}5CO\text{-}C_7H_6O]^{+}$).

Light green and light yellow crystals of complexes **4a** and **4b**, respectively, were obtained from concentrated *n*-pentane solutions (**Figure 4**). X-ray diffraction analysis unveiled that **4b** crystallized in the triclinic crystal system, space group P-1, while complex **4a** showed an orthorhombic system and a P21 space group. Both phosphorus stereogenic centers present different configurations, thus possessing the phosphorus atom of the molybdenum derivative **4b** in an *S* configuration, while the chromium analogue **4a** shows an *R* configuration for its phosphorus atom. The phenyl substituent at the carbon atom of the ring is placed in a *cis* position to the pentacarbonylmetal(0) moiety.

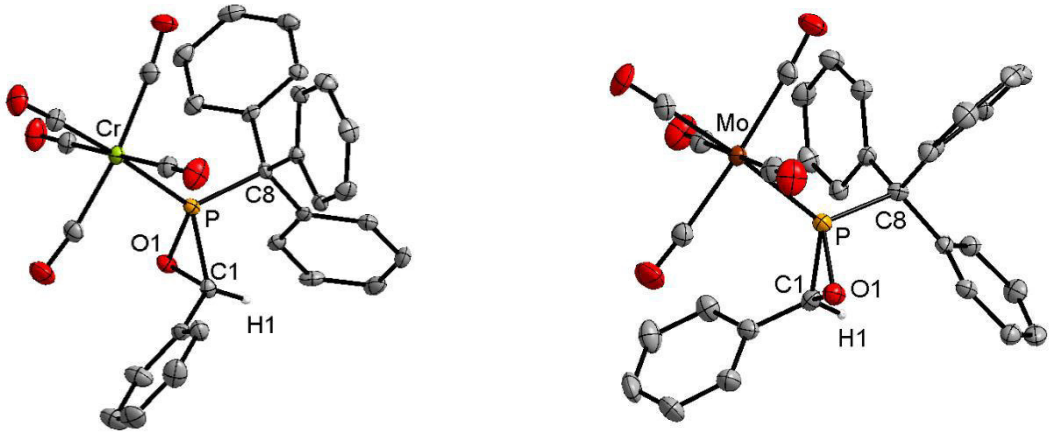

Figure 4. Molecular structures of oxaphosphirane complexes **4a** and **4b** (thermal ellipsoids are shown with 50% probability level); all hydrogen atoms (except H1), are omitted for clarity; selected bond lengths (Å) and angles (°): **4a**: P-Cr 2.3328(9), P-C(1) 1.785(3), P-C(8) 1.895(3), P-O(1) 1.663(2), O(1)-P-C(1) 50.88(11), C(1)-O(1)-P 68.83(14), O(1)-C(1)-P 60.30(13); **4b**: P-Mo 2.4864(10), P-C(1) 1.781(3), P-C(8) 1.892(4), P-O(1) 1.668(2), O(1)-P-C(1) 50.16(14), C(1)-O(1)-P 68.93(16), O(1)-C(1)-P 60.92(17).

Analysis of the single-crystal structures revealed that the P−C(8) bond in *P*-trityl oxaphosphirane complexes **4a,b** (1.895(3) Å and 1.892(4) Å) keeps some elongation but is significantly shorter than in the *P*-trityl dichlorophosphane complexes **2a,b,** although still longer than P−C bonds in related P-bis(trimethylsilyl)methyl and P-Cp* oxaphosphirane derivatives (1.794(6) Å and 1.855(3) Å). The largest P−M bond distance is observed in the molybdenum derivative, while the largest P−C exocyclic bond length was observed in tungsten derivative **4c**.[53] All other bond lengths and bond angles present similar values for the three metal complexes.

3.3 Synthesis of *C*-alkyl, *P*-triphenylmethyl substituted oxaphosphirane complexes

The syntheses of *C*-alkyl substituted oxaphosphirane complexes have been investigated for derivatives bearing pentamethylcyclopentadienyl (C_5Me_5) or bis(trimethylsilyl)methyl ($(CHSiMe_3)_2$) at the phosphorus atom. In most cases, they could not be isolated in good yields, partly due to rapid decomposition, and only a few derivatives could be confirmed by means of single-crystal X-ray analysis.[69,70]

In the following, attempts to synthesize new *C*-alkyl *P*-triphenylmethyl substituted oxaphosphirane derivatives are described using dichlorophosphane complex **2c**, thus taking advantage of the additional information obtained from the tungsten-phosphorus coupling constant.

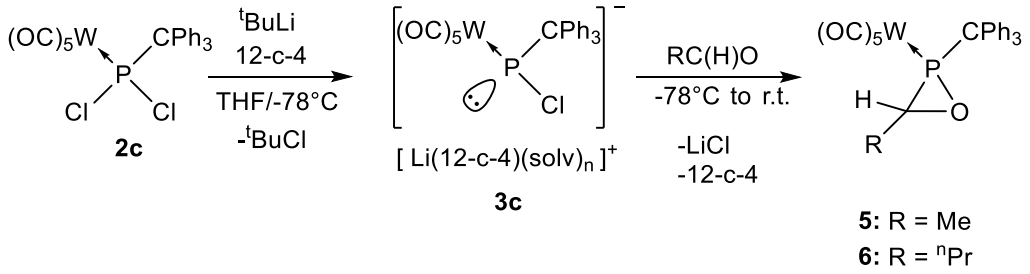

Scheme 20. Synthesis of oxaphosphirane complexes **5** and **6** through reaction of transiently formed Li/Cl phosphinidenoid complex **3c** and alkyl aldehydes.

The formation of oxaphosphirane complexes was selectively achieved for derivatives **5** (R = Me) and **6** (R = ^{n}Pr), following the established reaction protocol (**Scheme 20**). In the reaction of **2c** with pivalylaldehyde (^{t}BuC(H)O), the $^{31}P\{^1H\}$ NMR analysis of the reaction solution revealed a mixture of two compounds. The resonance of the minor product (30%) at 0.6 ppm could be assigned to the expected oxaphosphirane derivative **7** due to the observed coupling constant magnitude of $^1J_{P,W}$ = 303.5 Hz. The major resonance at 12.3 ppm (70%) shows a $^1J_{P,W}$ value of 231.7 Hz and a $^1J_{P,H}$ value of 342.5 Hz and could be assigned to the compound **8** which was already characterized in the group of Streubel (**Scheme 21**, **Table 5**).[71]

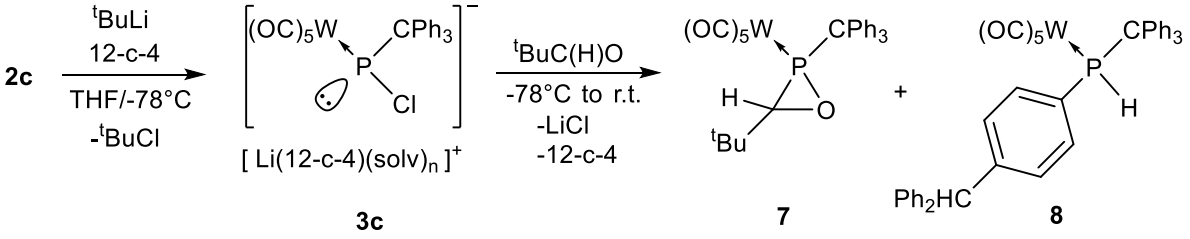

Scheme 21. Reaction of Li/Cl phosphinidenoid complex **2c** with pivalyl aldehyde.

Table 5. Selected $^{31}P\{^1H\}$ NMR resonances [ppm] and $^1J_{P,W}$ and $^1J_{P,H}$ [Hz] of complexes **5-8** in THF-*d8*.

Compound	$\delta^{31}P\{^1H\}$	$^1J_{P,W}$	$^1J_{P,H}$
5	8.3	301.7	-
6	8.7	303.3	-
7	9.2	303.9	-
8	12.3	231.7	342.5

Compounds **5** and **7** were found to decompose rapidly in solution, whereas compounds **6** and **8** are stable at room temperature. Oxaphosphirane complex **6** (R = ^{n}Pr) was successfully isolated by means of low temperature column chromatography and fully characterized.

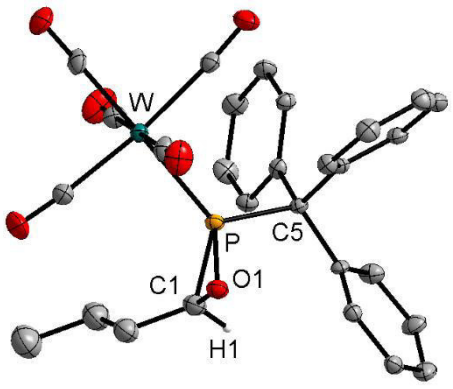

Figure 5. Molecular structure of oxaphosphirane complex **6** (thermal ellipsoids are shown with 50% probability level); all hydrogen atoms (except H1), are omitted for clarity; selected bond lengths (Å) and angles (°): P-Cr 2.3328(9), P-C(1) 1.785(3), P-C(8) 1.895(3), P-O(1) 1.663(2), O(1)-P-C(1) 50.88(11), C(1)-O(1)-P 68.83(14), O(1)-C(1)-P 60.30(13).

3.4 Study on the synthesis of *C*-disubstituted *P*-triphenylmethyl substituted oxaphosphirane complexes

3.4.1 Reaction of Li/Cl phosphinidenoid complexes 3a-c with benzophenone

As described in chapter 3.2, reaction of Li/Cl phosphinidenoid complexes **3a-c** with benzaldehyde led to the straightforward formation of oxaphosphirane derivatives **4a-c** (**Scheme 22**).

In order to investigate the effect of the expected increase of the ring strain energy of the oxaphosphirane ring imposed by two phenyl substituents on the heterocycle and the *P*-CPh_3 group, compounds **3a-c** were reacted with benzophenone.

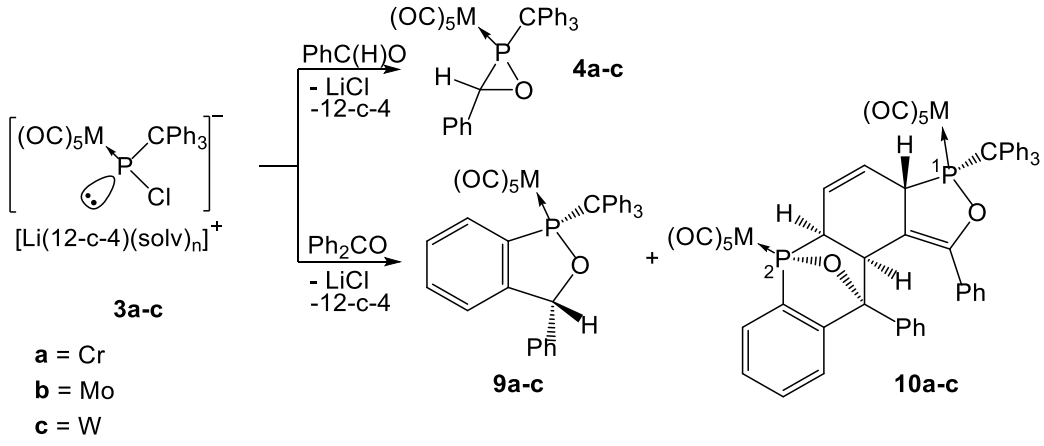

Scheme 22. Synthesis of oxaphosphirane complexes **4a-c** and complexes **9a-c** and **10a-c**.

The $^{31}P\{^{1}H\}$ NMR spectra of the reaction solution showed no oxaphosphirane complexes even at low temperature, but two unexpected resonances: singlets for complexes **9a-c**, whereas AB-type spin systems appeared for the distinctly different phosphorus nuclei of **10a-c**, all signals appeared as doublets with a $^{5}J_{P,P}$ coupling of 3.8 Hz (**Table 6**).

Table 6. $^{31}P\{^{1}H\}$ NMR resonances [ppm] and $^{5}J_{P,P}$ [Hz] of **4a-c**, **9a-c**, **10a-c** and **9**:**10** ratios in THF solution.

Metal	4a-c	9a-c	10a-c (P^1/P^2)	$^{5}J_{P1,P2}$	Ratio 9:10
Cr	58.7	190.3	210.5/165.6	3.8	5:1
Mo	33.4	167.4	186.3/138.2	3.8	5:3
W	16.0[8d]	145.1	164.4/112.3	3.8	5:1

The tungsten derivative **9c** was chosen to attempt separation from the mixture with **10c** by low temperature column chromatography, which was successful (68% yield). The constitution of **9c** was finally confirmed by X-ray crystallography (**Figure 6**), revealing the presence of a bicyclic 1,2-oxaphospholane ligand.[55]

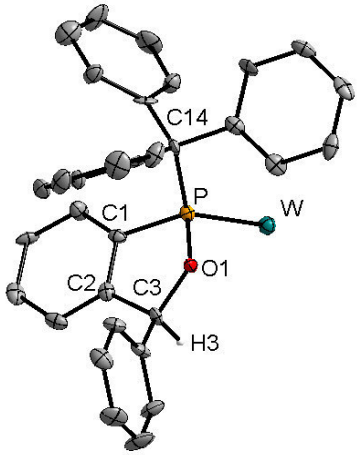

Figure 6. Reduced molecular structure of complex **9c** (thermal ellipsoids are shown with 50% probability level); all hydrogen atoms (except H3), as well as carbonyl groups at the metal are omitted for clarity; selected bond lengths (Å) and angles (°): P-W 2.5101(3), P-C(14) 2.9161(2), P-O(7) 1.6423(2), C(1)-C(2) 1.4083(2), P-O(1)-C(3) 112.748(8), P(1)-C(1)-C(2) 107.616(9), C(1)-C(2)-C(3) 113.966(8), C(2)-C(3)-O(1) 104.406(8).

Although several attempts to separate **10b** from **9b** via column chromatography were unsuccessful, a better ratio of **10b**:**9b** (cf. **Table 6**) enabled to get single crystals of the latter from diethylether at -30 °C. The X-ray structure of the pentacyclic complex **10b** (**Figure 7**) surprisingly showed (formally) two units of Ph_2CO, but only one belonging to a complete (opened) oxaphosphirane unit.[55] In the other P-containing part, only a partial oxaphosphirane complex can be (formally) identified, but without a $HCPh_3$ moiety. All bond lengths and angles in **10b** are in the expected range except, *e.g.* P(1)-Mo(1) (2.4258 Å), which is significantly shorter than P(2)-Mo(2) (2.5259 Å). The five-membered ring containing P(2) is roughly planar (distance of O(7) to the P(2)-C(14)-C(15)-C(25) mean plane, 0.108 Å) due to the double bond between C(15) and C(25) (**Figure 7**).

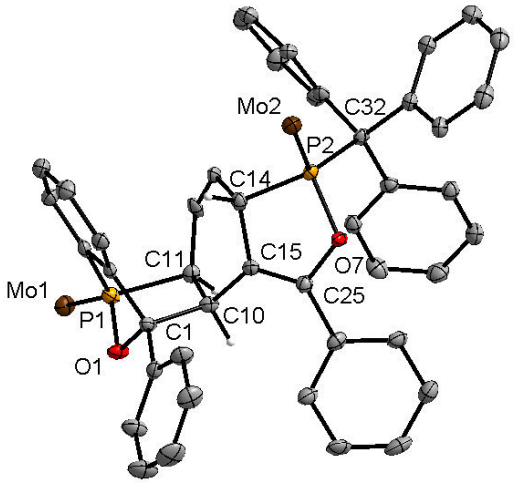

Figure 7. Reduced molecular structure of complex **10b** (thermal ellipsoids are shown with 50% probability level); all hydrogen atoms (except H10A, H11A and H14A), and carbonyl groups at the metals are omitted for clarity; selected bond lengths (Å) and angles (°): P(1)-Mo(1) 2.4258(1), P(1)-O(1) 1.6456, P(2)-Mo(2) 2.5259(2), P(2)-C(32) 1.9597(7), C(15)-C(25) 1.3667(5), C(14)-C(15) 1.5256(6), C(10)-C(11) 1.5457(6), P(1)-O(1)-C(1) 102.597(3), O(1)-C(1)-C(10) 100.224(4), C(1)-C(10)-C(11) 105.523(3), C(10)-C(11)-P(1) 102.424(3), P(2)-O(7)-C(25) 113.674(5), O(7)-C(25)-C(15) 116.226(4), C(25)-C(15)-C(14) 113.486(3), C(15)-C(14)-P(2) 102.959(1).

Quantum chemical calculations, performed by Espinosa Ferao,[56] were used to study the formation of products of type **9** and **10** in the reaction of *P*-trityl substituted Li/Cl phosphinidenoid complexes **3a-c** with benzophenone.

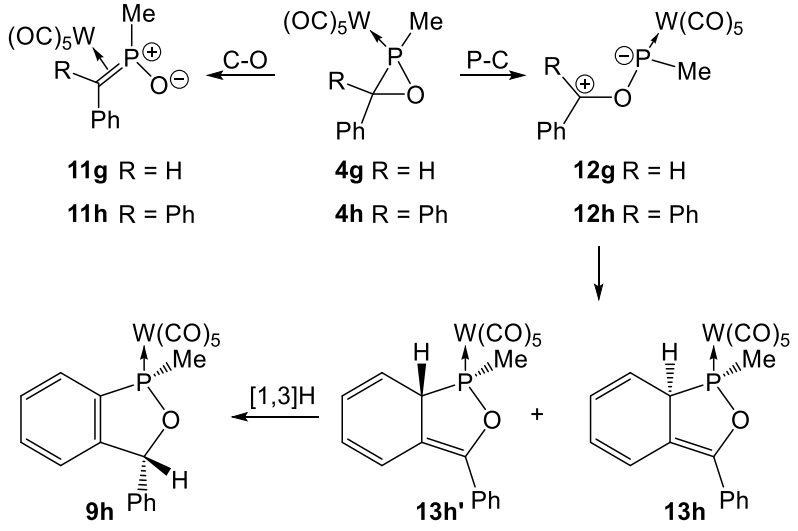

Scheme 23. Mechanistic proposal for the formation of **9h** indicating ring opening pathways from a primary formed oxaphosphirane complex.

For the sake of computational efficiency the first part of the mechanistic search was performed starting from *P*-Me model complexes **4g,h** (**Scheme 23**) at the highest

computational level (level A: B3LYP functional[72] together with the def2-TZVP basis set[73] in case of model complexes (*P*-methyl substituted)).

Tungsten complexes were used as models to enable comparison with previous reports[74,75] and in agreement with them, formation of the corresponding oxaphosphirane complex was assumed as first product in the reaction of Li/Cl phosphinidenoid complexes with carbonyl compounds, although simple substitution of Cl by O at P could also be envisaged (*vide infra*). According to the above mentioned report, mono-aryl substituted oxaphosphirane complex **4g** preferentially undergoes exergonic (-6.57 kcal/mol) C-O bond cleavage with a moderate energy barrier 28.91 kcal/mol), leading to the *side-on* phosphaalkene *P*-oxide complex **11g**. In contrast, a higher barrier for the P-C bond cleavage path (37.72 kcal/mol), being rather endergonic (+28.90 kcal/mol), affords **12g**. In case of the diphenyl model system **4h**, both processes have a lower barrier (**Figure 8**), the P-C bond cleavage product **12h** being comparatively stabilized with respect to **12g** due to extensive delocalization of the positive charge. In stark contrast, the C-O cleavage product **11h** is destabilized presumably due to steric reasons.

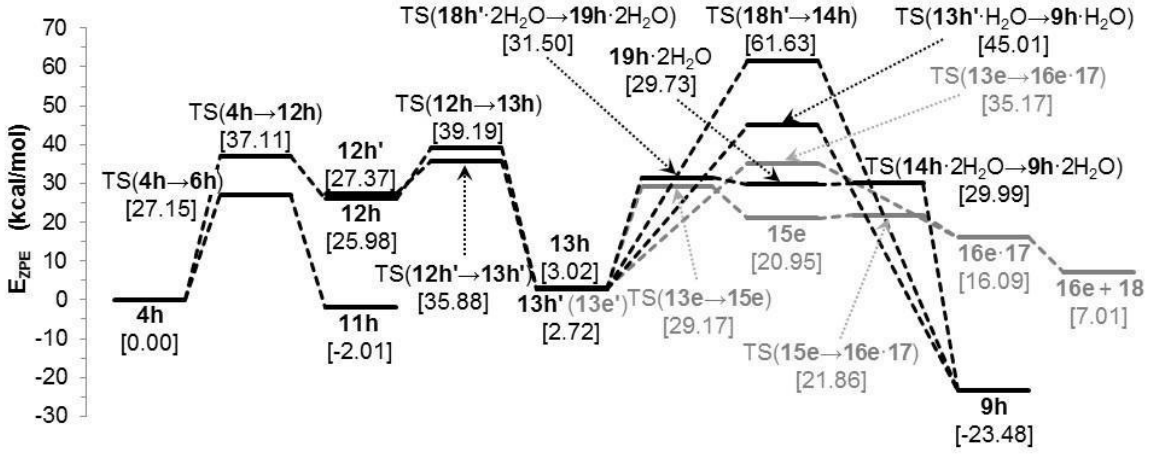

Figure 8. Computed ZPE-corrected energy profile for the conversion of complexes **4** into **9** and **16**. In grey the relative energies for full *P*-trityl substituted complexes (relative energy of **13e'** is set to the same value than **13h'**).

Therefore, the C-O bond cleavage equilibrium for **4h** is expected to be shifted to the rather reactive (more slowly formed) P-C bond cleavage product **12h** which readily undergoes cyclization by attack of the nucleophilic P atom at the closest phenyl *ortho* position, thus giving rise to bicyclic derivative **13h**. Complex **12h** exists as two conformers, differing in the helical orientation of the Ph_2C^+ moiety, the most unstable of which (**12h'**) cyclizes to the most stable diastereomer of the bicyclic complex **13h'**,

whereas the other helical isomer **12h** gives rise to less stable diastereomer **13h**. Worth mentioning is that oxaphosphirane complex **4** might not be formed in real systems due to steric congestion and, alternatively, ylide complex **12** could directly result upon reaction of phosphinidenoid complex **3** with benzophenone and evolve towards the five-membered derivative **13**.

Formation of the final (model) complex **9h**, whose comparative stability arises from the gain of aromatic character in the benzo-fused ring, could be explained through *supra* [1,3]H shift to the benzylic position in diastereomer **13h'**. According to Woodward-Hoffmann orbital symmetry rules[76] this process is thermally forbidden and displays a high energy barrier. In order to explain the formation of **9** through a lower energy process, the assistance of a molecule having hydrogen bond (HB) donor and acceptor sites might be assumed, therefore acting as a catalyst for the H-shift **13h'**→**9h** rearrangement. A water molecule has been used as model for such a catalytic species (*vide infra*),[77] although any other proton carrier species present in the reaction medium could similarly account for the catalyzed proton transfer. Thus **13h'**·H_2O was found to isomerize to **14h**·H_2O (**Scheme 24**) through a much lower yet significantly high pericyclic transition state ($\Delta\Delta E_{ZPE}$ = 42.30 kcal/mol; **Figure 8**) with thermal symmetry-allowed nature. The occurrence of two water molecules involved in the H transfer process further decreases the energy barrier of the rate-limiting first step ($\Delta\Delta E_{ZPE}$ = 28.79 kcal/mol) which leads to a dihydrated zwitterion **14h**·2H_2O (**Scheme 24**), whose almost barrierless (water-mediated) O-to-C [1,2]H shift affords the final model product **9h**·2H_2O.

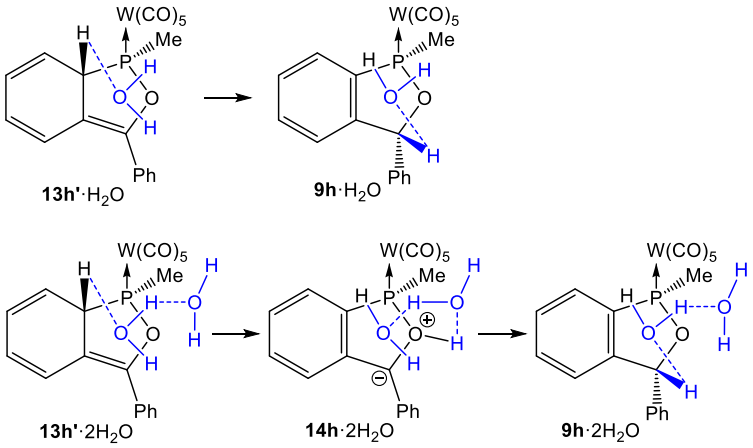

Scheme 24. Mechanistic proposals for the water-catalyzed isomerization of **13h'** into **9h.**

Elimination of the *P*-trityl substituent in complex **13** (studied at a somewhat lower computational level B (def2-SVP basis set[78] for full P-trityl substituted complexes) for the molybdenum complex requires relative *cis* orientation of the H atom and the trityl group in **13e** This in turn enables a pericyclic phospha-ene reaction affording diphenylmethylidenecyclohexadiene **17** as by-product (**Scheme 25**). The latter can then isomerize to the more stable triphenylmethane **18** (ΔE_{ZPE} = -26.58 or -27.20 kcal/mol at A or B levels, respectively). The below **17**→**18** transformation is again thermally forbidden as a concerted (pericyclic) process, but could alternatively take place in a water-catalyzed manner (not studied), as the previously described **13h'**·nH_2O→**9h**·nH_2O transformation, or when coupled to the **13h'**→**9h** rearrangement, therefore **17** acting as the required simultaneous HB donor and acceptor species (*vide supra*), although in a non-catalytic fashion.

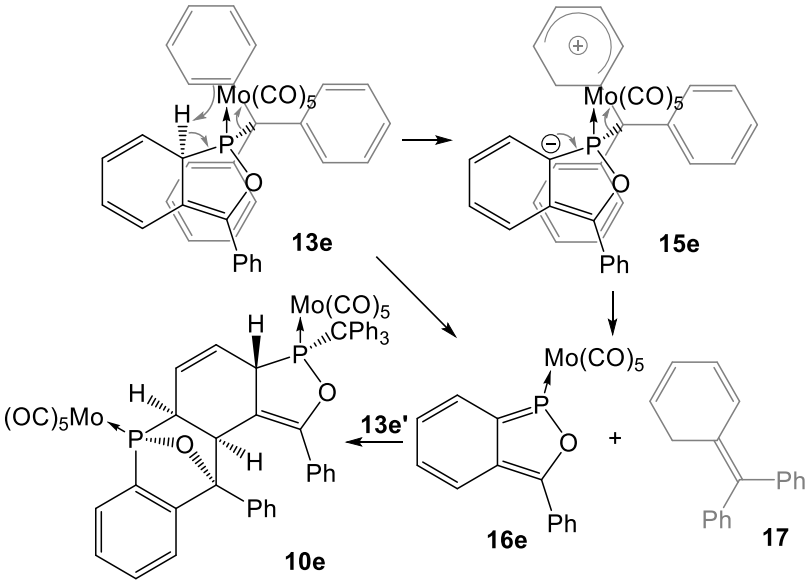

Scheme 25. Proposal for the formation of **10** according to Espinosa Ferao.

The alternative two-step proton transfer through zwitterionic complex **15e** followed by P-group detachment constitutes a lower energy sequence to **16e**. The resulting non-aromatic (*i.e.* reactive) bicyclic 2-phosphafurane complex intermediate[79] **16e** features a cyclic, conformationally *s-cis* locked phosphadiene character and, therefore, can be expected to behave as 4π-component and undergo a phospha-Diels-Alder[80] reaction. The 2π component is the central double bond of the triene moiety in **13e'**, the diastereomer which cannot undergo trityl group elimination due to its relative *trans* orientation of the H atom at the ring junction. The regioselectivity of the [4+2]

cycloaddition reaction might tentatively arise from i) π-stacking between the two phenyl rings that not only guides the approach of the two components but also stabilizes the final adduct and ii) the steric demand of the metal fragment in **16e** hampering the approach to the phenyl substituent side in **13e'**.

These reactions demonstrated that reactions of *P*-trityl substituted Li/Cl phosphinidenoid complexes with carbonyl derivatives are very sensitive towards steric overcrowded substrates.

3.4.2 Reaction of Li/Cl phosphinidenoid complex 3c with alkyl ketones

The chemistry of oxaphosphirane complexes was mostly developed for derivatives bearing bis(trimethylsilyl)methyl ($CH(SiMe_3)_2$)[69] or pentamethylcyclopentadienyl (C_5Me_5)[65] as organic substituents at phosphorus. A large number of oxaphosphirane complexes could be synthesized thanks to this methodology, however, the synthesis of *C*-disubstituted oxaphosphirane complexes is still nowadays a challenge. This may be due to an increase of the ring strain, thus promoting unexpected rearrangements such as ring opening reactions.[81,82] To date, only three derivatives could be confirmed by X-ray crystallography.[69,75]

Hereafter, reactions of Li/Cl phosphinidenoid complex **3c** with different alkyl ketones aiming the synthesis of *C*-disubstituted oxaphosphirane complexes will be discussed (**Scheme 26**).

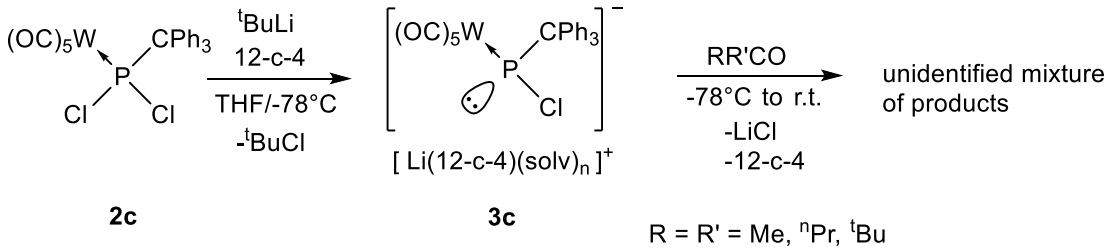

Scheme 26. Attempts to the synthesis of *C*-disubstituted oxaphosphirane complexes.

Despite several attempts, the reaction of **3c** with different alkyl ketones (acetone, dipropyl ketone and di-*tert*-butyl ketone) was unsuccesful. Even by $^{31}P\{^1H\}$ NMR low temperature monitoring, it was not possible to detect intermediately formed oxaphosphirane complexes. While reactions of **3c** with sterically low demanding ketones (R = R' = Me, ^{n}Pr) led always to unidentified mixtures of products, the reaction

of **3c** with di-*tert*-butyl ketone, led to a main product showing a phosphorus resonance, not in the expected range for oxaphosphirane complexes, with two different tungsten satellites. Unfortunately, all attempts to isolate the compounds were not successful due to their poor stability in solution.

4. Synthesis of the first fluorinated oxaphosphirane complexes

4.1 Synthesis of *C*-aryl^F substituted oxaphosphirane complexes

In order to study the effects of strong electron withdrawing groups at the carbon atom of the ring in *P*-triphenylmethyl substituted oxaphosphirane complexes, aldehydes with different degree of fluorination were reacted with Li/Cl phosphinidenoid complex **3c**; various *C*-pyridyl substituted oxaphosphirane complexes have been reported.[81,83]

Oxaphosphirane complexes **20-22** were readily synthesized reacting complex **2c** with *tert*-butyl lithium in presence of 12-crown-4, yielding the respective Li/Cl phosphinidenoid complex **3c.**[53] Subsequently, **3c** was treated with aldehydes having a different degree of fluorination of the phenyl group to give the novel oxaphosphirane complexes **20-22** in good to very good isolated yields (**20**: 74%; **21**: 81%; **22**: 87%).[84]

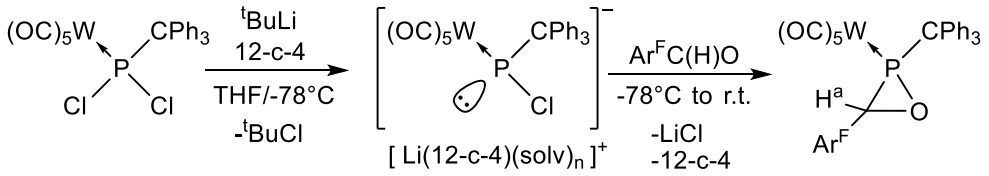

2c **3c** **20-22**

20: Ar^F = 2,6-difluorophenyl
21: Ar^F = 2,4,6-trifluorophenyl
22: Ar^F = perfluorophenyl

Scheme 27. Synthesis of fluorinated oxaphosphirane complexes **20-22**.

The $^{31}P\{^1H\}$ NMR chemical shifts of complexes **20-22** are ~8 ppm shifted to higher field in comparison to the resonance of the phenyl derivative **4c**[53] (δ = 16; **Table 7**), which is a counterintuitive effect. It was expected that the electron-withdrawing character of the fluoro-substituted phenyl rings should lead to a deshielding of the phosphorus nucleus, thus resulting in $^{31}P\{^1H\}$ NMR resonances of the oxaphosphirane complexes appearing downfield to **4c**. The degree of fluorination is nicely reflected in the $^1J_{P,W}$ coupling constants, *i.e.,* as the number of fluorine atoms at the aromatic ring increases,

the coupling constant increases in going from the phenyl derivative **4c**[53] ($^1J_{P,W}$ = 311 Hz) to the pentafluorophenyl derivative **22** ($^1J_{P,W}$ = 320 Hz).

Table 7. $^{31}P\{^1H\}$ NMR chemical shifts [ppm] and $^1J_{P,W}$ coupling constants [Hz] of complexes **4c**[53] and **20-22**.

Compound	#F atoms	$^{31}P\{^1H\}$ NMR	$^1J_{P,W}$
4c[53]	0	16.0	311
20	2	8.9	314
21	3	8.5	316
22	5	7.5	320

The ^1H NMR chemical shift of the hydrogen atom at the three-membered ring-carbon atom (H^a in **Scheme 27**), is especially influenced by the degree of fluorination and shows a clear trend (**Table 8**) In case of **25**, the effect onto the proton H^a is very strong and it may appear in the aromatic area, so its signal is overlapped by the signals of the trityl substituent*, i.e.,* its resonance should be between δ = 6-7.

Table 8. Selected ^1H and $^{13}C\{^1H\}$ NMR chemical shifts [ppm] and $^2J_{P,C}$ coupling constants [Hz] of compounds **4c**[53] and **20-22**.

Compound	^1H NMR	$^{13}C\{^1H\}$ NMR ($^2J_{P,C}$)			
	C<u>H</u>P	<u>C</u>HP	<u>C</u>Ph$_3$	***cis*-CO**	***trans*-CO**
4c[53]	4.14	60.4 (23.6)	67.7 (8.1)	194.6 (8.2)	196.3 (40.9)
20	4.95	54.0 (25.6)	67.3 (6.7)	193.8 (8.1)	195.8 (41.6)
21	5.75	53.4 (25.7)	67.4 (6.3)	193.9 (7.9)	195.6 (41.6)
22	(*)	53.3 (24.7)	67.6 (6.6)	193.7 (8.1)	195.1 (41.8)

(*): signal overlapped by trityl resonances

The $^{13}C\{^1H\}$ NMR shifts of compounds **20-22** differ only slightly from each other as well as from the non-fluorinated derivative **4c**[53] and lie in the expected range, as **Table 8** reveals. Only the resonance of the carbon atom of the oxaphosphirane heterocycle (<u>C</u>HP) in **20-22**, which is directly bonded to the fluorinated aromatic ring, shows a resonance shifted by ~7 ppm to higher field compared to the non-fluorinated compound **4c**[53].

IR measurements were performed for **20-22** to give evidence of the electronic situation of the oxaphosphirane ring, in particular to get insight into the π-acidity/basicity of the oxaphosphirane ligand. In general, hexacoordinated complexes with pentacarbonylmetal fragments can serve as good systems to study the ligand bonding properties of the sixth ligand.[85] As it was shown before, the oxaphosphirane ligand is known,[43,75,86] but the effect of electron-withdrawing groups at the ring carbon center was not investigated. It is a widely accepted model that the IR absorption due to the A_1 mode of the *trans*-CO depends on the electron density on the metal delivered to the CO ligand *via* π-backbonding.[87] If the electron density on the metal centre increases, an enhanced π-backbonding to the CO ligand results in a shift of the IR absorption frequency to smaller wavenumbers (blueshift).

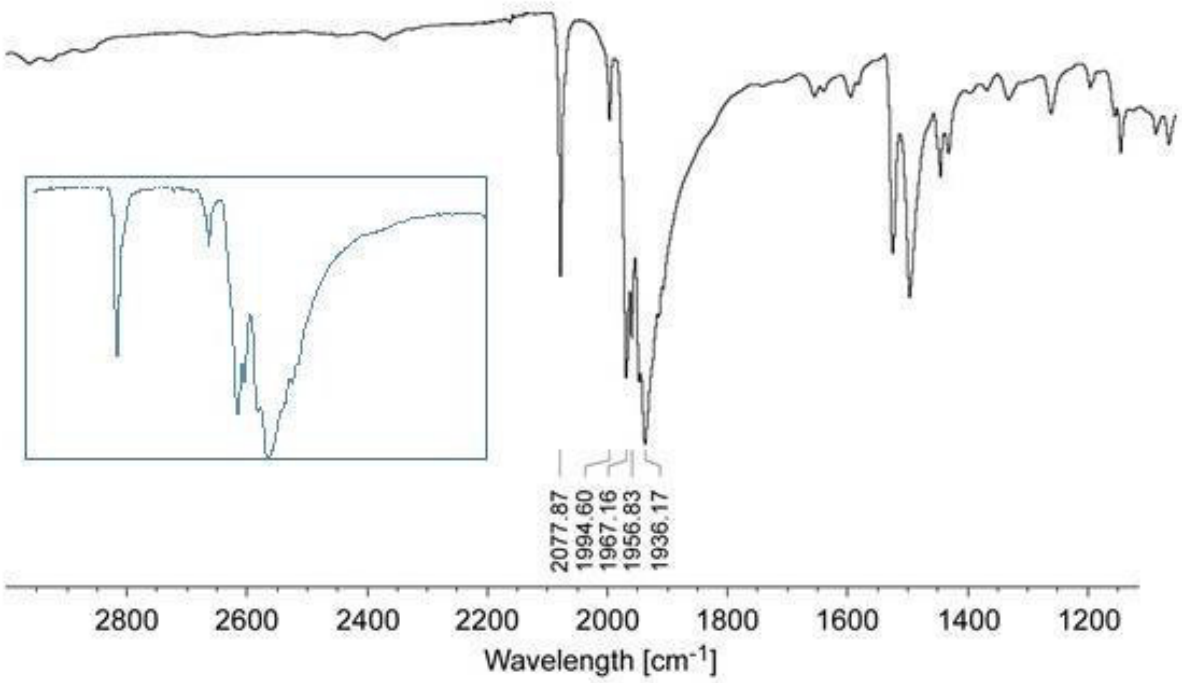

Figure 9. IR spectrum of complex **22**.

In case of complexes of the type $M(CO)_5L$ (local C_{4v} symmetry) three IR bands were expected for complexes **20-22**. The corresponding $A_1^{(1)}$, $A_1^{(2)}$ and E bands were observed at ν = 2077, 1994 and 1936 cm^{-1} respectively. Additionally, two extra IR bands were observed at ν = 1967, 1956 cm^{-1} (**Figure 9**). This can be interpreted as the degenerated A_{1g} and B_{1g} modes, which may be caused by a reduction of the C_{4v} symmetry to only C_1.[87]

The molecular structure of complexes **20-22** could be confirmed by X-ray diffraction studies as **Figure 10** shows; selected bond lengths and angles are shown in **Table 9.** Complexes **20** and **21** crystallize in the triclinic space group P-1, while complex **22**, having the highest degree of fluorination, crystallizes in monoclinic space group C2/c.

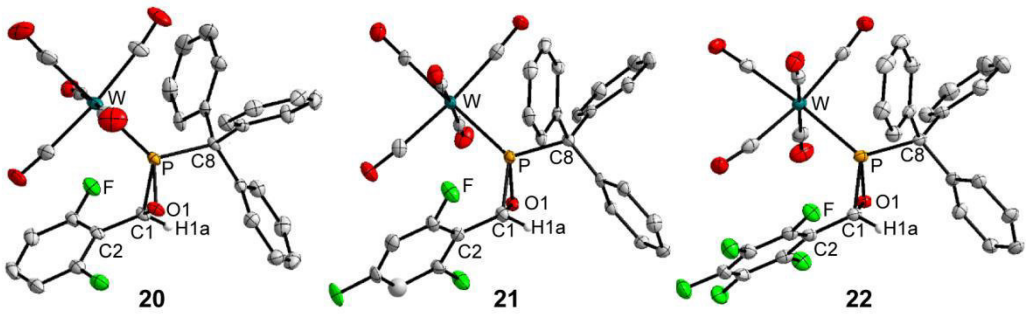

Figure 10. Molecular structures of complexes **20-22** (Diamond 3.0, ellipsoids represent 50% probability level). Except H1a, all hydrogen atoms are omitted for clarity.

In all cases the metal complex fragment is *cis*-orientated to the fluorinated aromatic ring as in other *P*-triphenylmethyl substituted oxaphosphosphirane complexes. In the particular case of complexes **20**-**22**, bearing electron-withdrawing substituents, this orientation will enable and/or promote intramolecular interactions never observed before in oxaphosphirane complex chemistry and, will be discussed later on. The influence of the electronegative atoms in the bond lengths of oxaphosphirane complexes is shown in **Table 9.** The P–C(8) distance becomes shorter as the degree of fluorination increases, and the same trend is seen for the P–W bond length. In contrast, the bond distance between the phosphorus atom and C(1) increases with the number of fluorine atoms. The P–O(1) distance does not present remarkable differences and remains almost constant for the four compounds.

Table 9. Selected bond lengths of oxaphosphirane complexes **4c**[53] and **20-22**.

Selected	**Selected bond lengths (Å) of**			
Bonds	**4c**[53]	**20**	**21**	**22**
P – C(1)	1.788(2)	1.783(3)	1.786(5)	1.793(4)
P – O(1)	1.6692(16)	1.663(2)	1.663(3)	1.669(3)
P – C(8)	1.896(2)	1.902(3)	1.892(4)	1.881(4)
P – W	2.4820(6)	2.4783(8)	2.4656(13)	2.4630(11)

Inspection of the molecular structures of complexes **4c**[53] and **20-22** revealed that the

rigid oxaphosphirane ring with the arene ring attached to the carbon atom is an ideal system to analyse the M–CO···π interaction due to the spatial arrangement of the arene and the interacting CO ligand. In fact, the X-ray structures of **4c**[53] and **20-22** clearly show the close M–CO···π contacts from 3.001 to 3.243 Å.

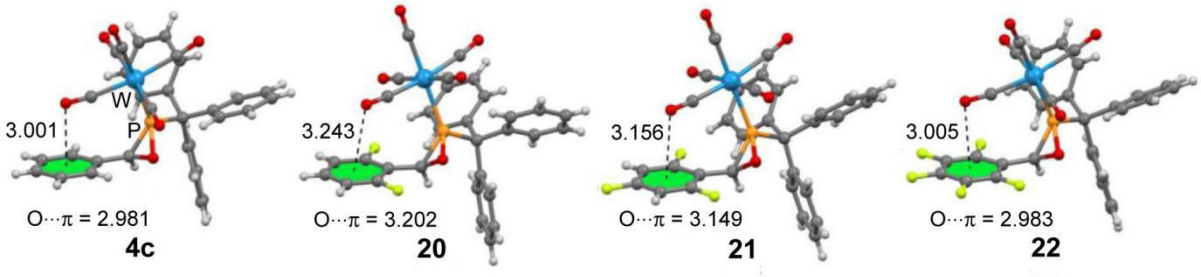

Figure 11. X-ray structures of **4c**[53] and **20-22** showing the intramolecular interaction (distances in Å). O···π distance stands for the oxygen atom to the ring mean plane distance.

This surprising feature of the X-ray structures prompted us to further inspect this situation. Apart from this, interactions involving aromatic rings are enormously significant in supramolecular chemistry. They play a crucial role in chemistry and biology, in particular drug–receptor interactions, crystal engineering, enzyme inhibition and protein folding.[88] In particular, lone pair-π interaction, which takes place between lone-pair bearing electronegative atoms of the neutral molecules and π-acidic aromatic systems, is a counterintuitive intermolecular force in supramolecular chemistry.[89] Recently, it has been demonstrated that M–CO(lone pair)···π(arene) interactions are relevant in the structures of a number of transition organometallic carbonyl derivatives.[90] In spite of their inherent weak nature, M-CO(lone pair)···π(arene) interactions do provide a measure of stability to their crystal structures and lead to well-defined supramolecular architectures. As a matter of fact, such interactions are needed in order to have a complete understanding of the way this type of organometallic molecules associate in the solid state.

As expected, the (lone pair)···π plane distance progressively increases as the number of fluorine substituents decreases from **4c**[53] to **22.** In this series the electronic nature of the ring progressively changes from π-acidic to π-basic. However, the close (lone pair)···π contact in complex **4c**[53] is totally unexpected. It exhibits the shortest distance of the series and this experimental result is in striking contrast to the expectation taking into consideration the π-electron rich nature of the phenyl ring.

4.1.1 Theoretical analysis

In order to provide an explanation to these counterintuitive results, observed in the NMR and IR spectroscopic data as well as in the molecular structures, intensive theoretical calculations were carried out by Frontera,[84] which will be reported hereafter.

4.1.1.1 Theoretical methods

The geometries of the complexes included in this study were computed at the BP86-D3/def2-TZVP level of theory using the crystallographic coordinates within the TURBOMOLE program.[91] This level of theory that includes the latest available dispersion correction (D3) is adequate for studying non-covalent interactions dominated by dispersion effects like π-stacking.[92] The basis set superposition error for the calculation of interaction energies has been corrected using the counterpoise method.[93] The "atoms-in-molecules" (AIM) analysis of the electron density has been performed at the same level of theory using the AIMAll program.[94]

4.1.1.2 Discussion of results

The optimized complexes exhibit similar M–CO···π distances and the expected behaviour, which is a progressive decrease in the distance as the fluorine substitution increases. In spite of this disagreement between theory and experiment, the optimized distance in complex **4c**[53] is quite short (3.116 Å) which is an indication of favourable M–CO···π interaction. Obviously, small experimental differences in the M–CO···π distances observed in the complexes can be also due to packing effects that are not considered in the calculations. The energy necessary for the dissociation of the interacting CO ligand for each complex was computed at the BP86-D3/def2-TZVPD level of theory (**Scheme 10**). The dissociation energy (ΔE) is similar in all complexes and the small differences of 2 kcal/mol from **4c**[53] to **22** may be attributed to a stronger contribution of the M–CO···π interaction in **22**.

Table 10. Ligand dissociation energy (ΔE, kcal/mol) and experimental and theoretical distances M–CO···π distances (Re, Å) for **4c**[53] and **20-22**.

Complex	ΔE	Re (Theor.)	Re (Exp.)
4c[53]	52	3.116	2.981
20	53	3.095	3.202
21	53	3.063	3.149
22	54	3.027	2.983

In order to further analyse the (lone pair)···π interaction in these complexes, a molecular orbital study and the Bader's "atom-in-molecules" characterization of the complexes were carried out.[94] In particular, all molecular orbitals of complexes **4c**[53] and **22** were obtained to find some differences that could explain the strange behavior of **4c**[53]. Interestingly, in some of the typical aromatic molecular orbitals of the arene, a small contribution of the atomic orbitals of the interacting CO was found. Surprisingly, this small but noteworthy contribution is different in both complexes (**Figure 12**).

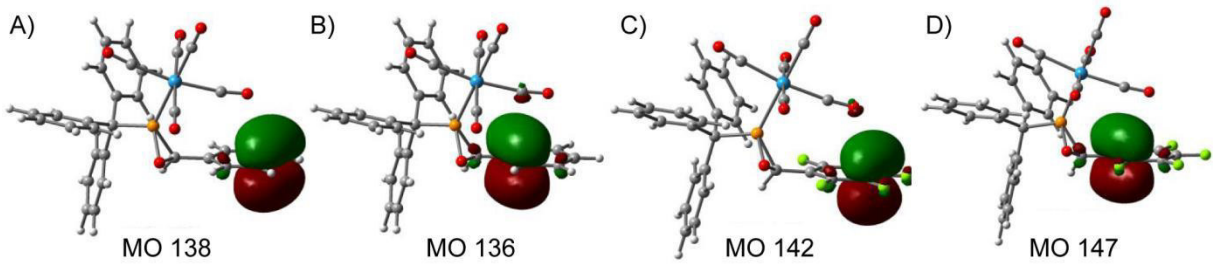

Figure 12. Representation of some molecular orbitals (MO) in complexes **4c**[53] (A, B) and **22** (C, D).

The π-bonding orbital MO 138 in **4c**[53] does not have any atomic contribution of the CO ligand **Figure 12A**) and, conversely, the equivalent orbital in complex **22** shows a small contribution of the p atomic orbital of the oxygen atom **Figure 12C**). Moreover, the π-bonding orbital MO 136 in **4c**[53] **Figure 12B**) exhibits an atomic contribution of the p atomic orbital of the close carbon atom of the CO and no contribution is found in the equivalent orbital (MO 147, **Figure 12D**). Therefore, the interaction can be roughly described as an (lone pair)···π interaction in complex **22** and as a π–π stacking interaction in **4c**[53]. The "atoms-in-molecules" distribution of bond critical points in complexes **4c**[53] and **20-22** were also calculated. The representations are shown in **Figure 13** for complexes **4c**[53] and **22**.[95]

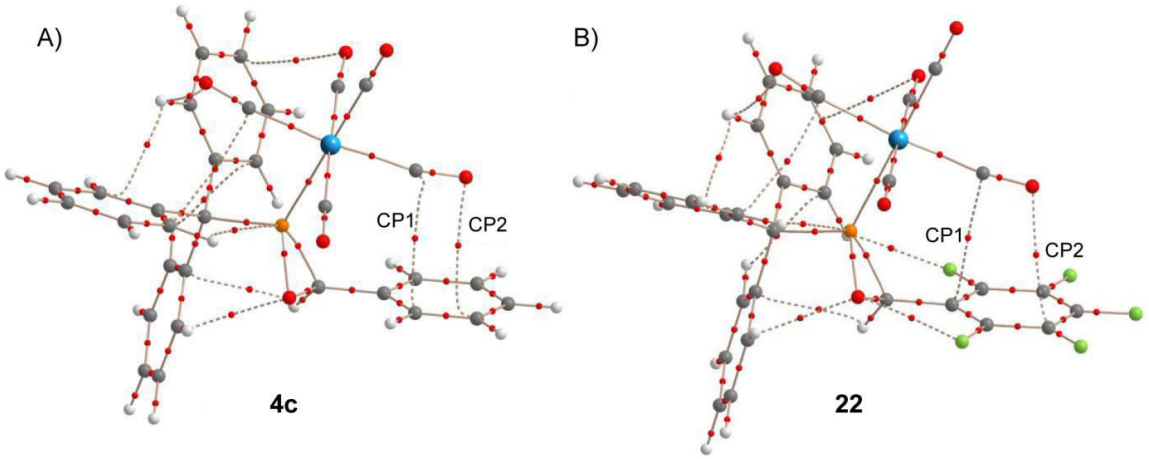

Figure 13. Distribution of bond critical points (CP, small red spheres) in complexes **4c**[53] and **22**.

Remarkably, the CO···π interaction in all complexes is characterized by at least two bond critical points that connect both atoms of the CO ligand to two (or three in **21**) carbon atoms of the ring. This distribution of critical points indicates that the M-CO···π interaction can be also understood as a π–π stacking interaction with the participation of the π-system of the CO ligand. It is interesting to discuss the different values of the charge density computed at the bond critical points that characterize the CO···π interaction, which are summarized in **Table 11**. The value of ρ(r) at the bond critical point can be used as a measure of bond order in non-covalent interactions.[94] In complex **4c**[53] (electron rich arene) the value of ρ(r) at CP1 is higher than in CP2 and is the highest of the series. Therefore, the C end of the CO is interacting more strongly than the O end (positive part of the CO dipole). This behavior is also observed for complexes **20** and **21**. However they exhibit smaller ρ(r) values in both CP1 and CP2, indicating a weaker interaction compared to **4c**[53] which is in agreement with the experimental distance. Remarkably, in complex **22** (electron poor arene), the charge density is higher in CP2 than in CP1 and it is the highest of the series, thus the oxygen atom of the CO is interacting more strongly than the carbon atom (negative part of the CO dipole). Consequently, the nature of the interaction changes depending on the electronic nature of the arene. This dual behavior of the CO ligand is in sharp agreement with the orbital analysis represented in **Figure 12**, where a small atomic contribution of the C atom was observed in **4c**[53] (MO 138) and, conversely, a small atomic contribution of the O atom was observed in **22** (MO 142).

Table 11. Electron charge density (102 × ρ(r), a.u.) computed at the CP1 and CP2 bond critical points.

Complex	**4c**[53]	**20**	**21**	**22**
CP1	0.69	0.66	0.68	0.64
CP2	0.57	0.48	0.52	0.66

4.1.2 Influence of additional interactions

The experimental W–CO···π distances observed in the solid state structures of compounds **4c**[53] and **20-22** (**Figure 11**) can be influenced by other interactions. Therefore, the crystal packing of complexes **4c**[53] and **22** was analyzed in order to investigate if the CO and aryl groups participate in other non-covalent interactions, which could shorten the W–CO···π distance. A partial view of their crystal packing was represented, paying attention to the short contacts involving the CO and arene groups (**Figure 14**). In this exploration, the default criterion, *i.e.,* a short contact between two atoms exists if they are separated by a distance that is less or equal to the sum of the van der Walls radii, was used. In compound **4c**[53] the CO does not participate in any contact apart from the already described W–CO···π interaction, therefore the W–CO···π distance is not influenced by other effects. Only the C_6F_5 ring establishes an antiparallel CF···CF interaction that does not affect the W–CO···π interaction. In complex **22** the CO group is close to one carbon atom of the phenyl ring of the neighbour molecule (black dashed line in **Figure 14**) that participates in the W–CO···π interaction. However, the directionality of this interaction clearly indicates that it does not contribute to shorten the W–CO···π distance observed in complex **22**. These results evidence that the short W–CO···π contacts observed in **4c**[53] and **22** are not due to crystal packing effects.

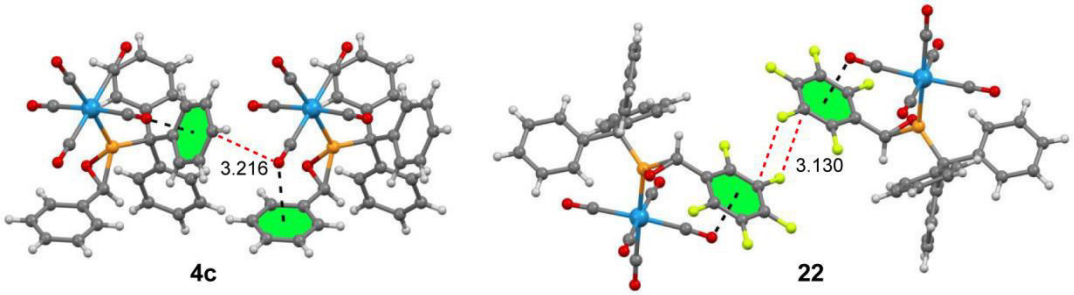

Figure 14. Partial view of the crystal packing of **4c**[53] and **22**, distances in Å (black dashed lines: W-CO···π contacts; red dashed lines: CO/arene interactions).

4.1.2.1 Crystal packing and strong intermolecular interactions

The intermolecular interactions that govern the crystal packing in compounds **4c**[53] and **20-22** were also evaluated. In the case of compound **22** the packing is basically governed by intermolecular W–CO···π and W–CO···H–C interactions. Infinite zig-zag 1D columns (**Figure 16A**) are formed in the solid state stabilized by two different W–CO···π interactions, one involving the trityl group and the other one the phenyl substituent of the oxaphosphirane ring. The 1D column is further stabilized by W–CO···H–C hydrogen bonds that involve the H atom of the oxaphosphirane and the coordinated CO (**Figure 16A**) These 1D columns interact to each other by means of additional W–CO···π and W–CO···H–C hydrogen bonds generating 2D layers. The interaction energy of a dimer as a representative model was evaluated, as well. The interaction energy is large and negative due to the contribution of the three interactions. Interestingly the distance of W–CO···π interaction that implies the phenyl substituent (3.21 Å, **Figure 15A** is very similar to the theoretical one (**Figure 15B**). The binding energy of the self-assembled dimer, which is dominated by non-covalent interactions, was calculated to be ΔE = -13.7 kcal/mol (**Figure 15B**).

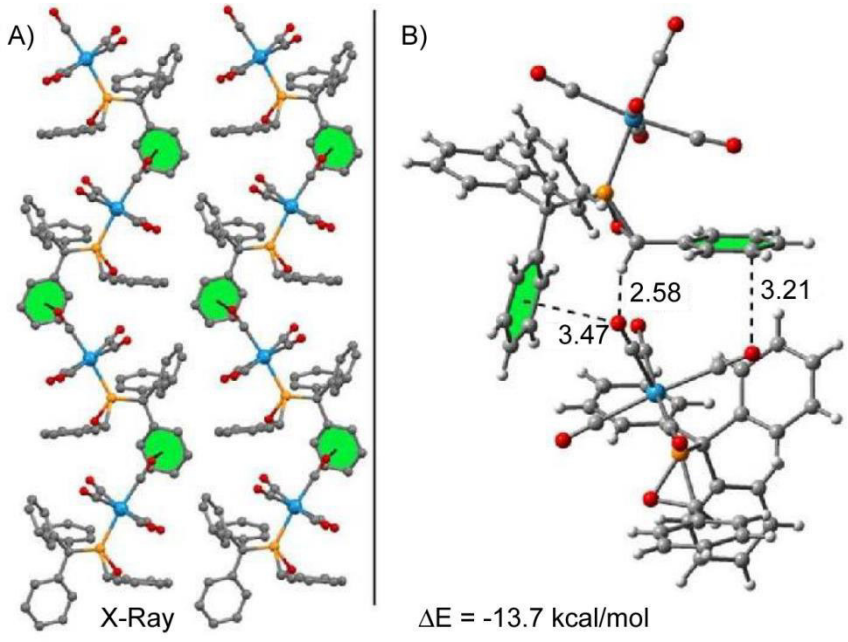

Figure 15. (A) Partial view of the crystal packing in **4c**[53]; H atoms are omitted for clarity. (B) Theoretical model based on the X-ray geometry used to evaluate the non-covalent interactions (distances in Å).

A representative fragment of the crystal packing of compound **20** is shown in **Figure 16** where the disordered solvent molecule has been omitted. Two important self-assembled dimers are observed in the solid state. One of both is dominated by two

equivalent W–CO···H–C hydrogen bonds (**Figure 16B**) and the other is characterized by the presence of two symmetrically equivalent T-shaped stacking interactions (or C–H/π interactions, **Figure 16C**). The binding energies of both self-assembled dimers, which are ΔE = -5.2 kcal/mol and ΔE = –8.6 kcal/mol for the H-bonded and T-shape stacked dimers, respectively were evaluated. Unexpectedly, the H-bond interaction is less favourable than the T-shape stacking likely due to the low basicity of the oxygen atom of the coordinated CO.

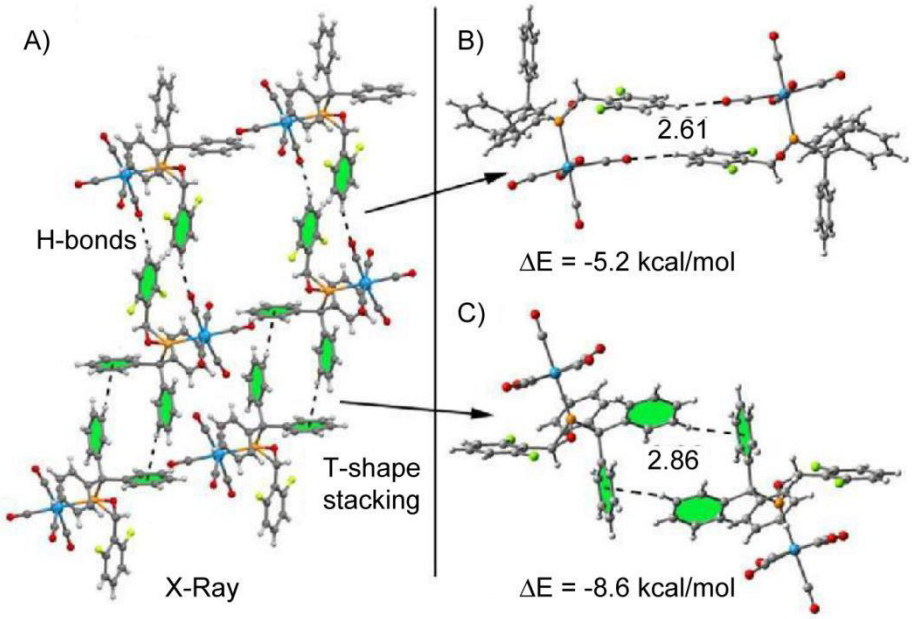

Figure 16. (A) Partial view of the crystal packing in **20**. (B and C) Theoretical models of the self-assembled dimers based on the X-ray geometry used to evaluate the noncovalent interactions (distances in Å).

For compound **21**, the exploration of the crystal packing reveals the existence of two important dimers. One dimer is formed by means of two by two equivalent W–CO···H–C hydrogen bonds (**Figure 17A**). This self-assembled dimer interacts with another one by means of an antiparallel stacking interaction involving the trifluorophenyl rings. Both interactions (**Figure 17B** and **C**) were evaluated energetically. The binding energy of the stacking interaction is ΔE = –8.1 kcal/mol, which is stronger than expected due to the contribution of an ancillary C–F···H– C hydrogen bond (2.77 Å, **Figure 17B**). The interaction energy of the self-assembled dimer that is dominated by the H-bonds was calculated to be ΔE = -6.4 kcal/mol. This interaction energy is larger in absolute value than the one computed for the same interaction (W–CO···H–C hydrogen bond) in compound **20** (ΔE = –5.9 kcal/mol see **Figure 14B**), likely due to the different directionality. In compound **21** the C≡O···H angle that characterizes the H-bond is 85º.

Therefore, the positive H atom is interacting with the negative belt of the oxygen atom, giving rise to a stronger interaction compared to compound **20** showing an angle of 178º.

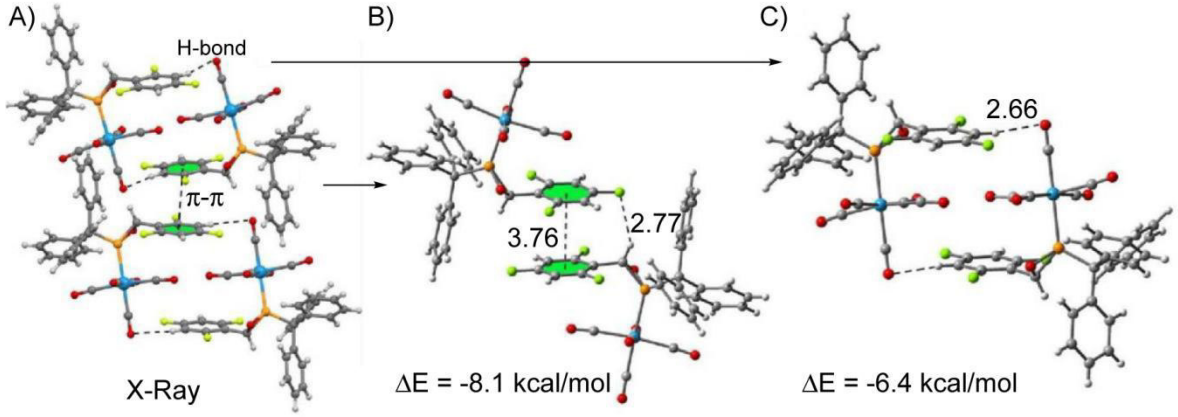

Figure 17. (A) Partial view of the crystal packing in **21**. (B and C) Theoretical models of the self-assembled dimers based on the X-ray geometrie used to evaluate the noncovalent interaction (distances in Å).

Finally, a representative fragment of the crystal packing of compound **22** is shown in **Figure 18**. The solid state structure is basically dominated by two interactions: (i) an antiparallel C– F···C–F described above (**Figure 18A** and intermolecular W–CO···π interactions (**Figure 15A**) involving the pentafluorophenyl ring. Therefore the electron deficient pentrafluorophenyl moiety establishes an intramolecular (lone pair)···π interaction by one side of the ring and an intermolecular (lone pair)···π interaction by the opposite side of the ring. Both interactions were evaluated theoretically and the energetic results are also included in **Figure 18**. It can be observed that the antiparallel C–F···C–F interaction is ΔE = –3.0 kcal/mol, confirming the importance of this interaction in the solid state. Moreover, the other intermolecular complex under consideration that combines W–CO···π and H-bond interactions (**Figure 18C**) exhibits a large and negative interaction energy (ΔE = -15.5 kcal/mol). Interestingly, all compounds **4c**[53] and **20-22** exhibit W-CO···H–C hydrogen bonds in the solid state that influence the crystal packing. Moreover, compounds **4c**[53] and **22** also present intermolecular W–CO···π interactions which are in good agreement with the interaction energies summarized in **Figure 18** and the short intramolecular distances observed for both the π-acidic and π-basic rings. In compound **20** and **21**, W–CO···π interactions are not observed. Instead π–π and T-shape stacking interactions are present influencing the final architecture of both compounds in the solid state.

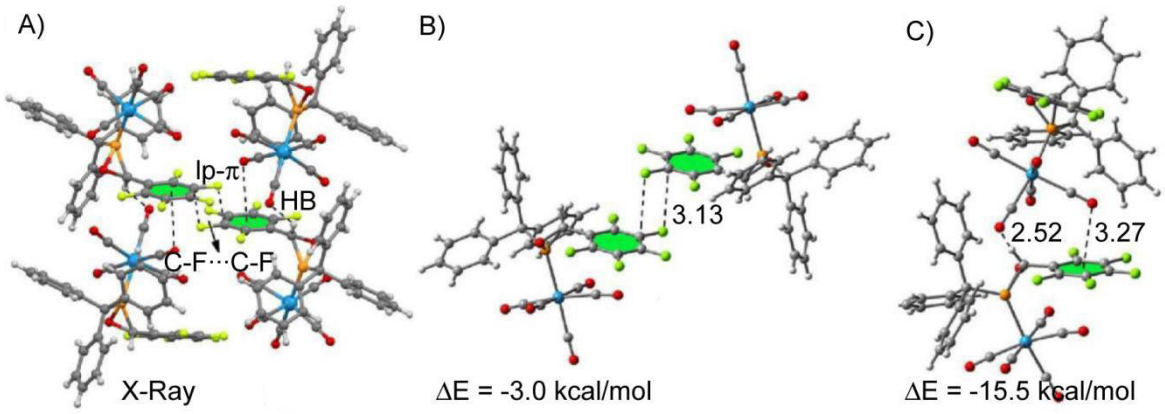

Figure 18. (A) Partial view of the crystal packing in **22**. (B and C) Theoretical models of the self-assembled dimers based on the X-ray geometrie used to evaluate the noncovalent interaction (distances in Å).

4.1.3 ^{31}P NMR chemical shifts

In this work, it is proposed that W–CO···π contact in complexes **4c**[53] and **20-22** can be defined as π–π stacking interaction to rationalize the fact that both the π–electron poor pentafluorophenyl and π–electron rich phenyl substituted oxaphosphirane complexes (**4c**[53] and **22**) present the shortest W–CO···π distances. It is also suggested that the negative end of the metal-coordinated CO is dominant in the π-acidic arene (**4c**)[53] and the positive part is dominant in the π-basic arene (**22**). This explanation was supported by DFT calculations, including "atoms-in-molecules" and NBO analyses.

The degree of fluorination of the arene has also an influence onto the ^{31}P{^{1}H} NMR chemical shifts observed in compounds **4c**[53] and **20-22**, which are summarized in **Table 12**. The experimental ^{31}P–NMR chemical shift of a model oxaphosphirane compound has also been included in **Table 12** for comparison. In this model, the arene has been replaced by an alkyl chain (propyl) and, consequently, the W–CO···π contact is not present. Interestingly, it can be observed that compound **22** presents a ^{31}P{^{1}H} NMR resonance shifted to higher field than those of the model compound, which is a counterintuitive result taking into account the electron withdrawing character of the pentafluorophenyl ring. Strikingly, the contrary is found in compound **4c**[53] that exhibits ^{31}P{^{1}H} NMR chemical shift displaced to lower field, compared to the model complex. In complex **22**, the charge transfer from the CO group to the π-acidic C_6F_5 ring causes a concomitant induction effect through the σ-bonds that decreases the ^{31}P{^{1}H} NMR

chemical shift. Since in compound **4c**[53] the charge transfer is from the π-basic ring to the CO group, the contrary induction effect increases the $^{31}P\{^{1}H\}$ NMR chemical shift. In the other rings (compounds **21** and **22**) the differences in $^{31}P\{^{1}H\}$ NMR chemical shifts with respect to the model compounds are smaller, being (formally) correlated with the weaker W–CO···π interaction.

Table 12. $^{31}P\{^{1}H\}$ NMR chemical shifts [ppm] and $^{1}J_{P,W}$ coupling constants [Hz] of compounds **4c**[53] and **20-22** and a model oxaphosphirane having a propyl chain instead of an arene ring (without W–CO···π contacts).

Compound	$^{31}P\{^{1}H\}$	$^{1}J_{P,W}$
4c[53]	16.0	311
20	8.9	314
21	8.5	316
22	7.5	320
Model	10.1	303

4.2 Synthesis of *C*-aryl^{F} *P*-Triphenylmethyl substituted fluorinated oxaphosphirane chromium and molybdenum complexes

As in the case of *C*-aryl substituted oxaphosphirane complexes, **chapter 3.2**, the influence of the transition metal is also analysed for the perfluoro derivatives and the corresponding analogues of chromium **23** and molybdenum **24** were synthesized (**Scheme 28**).

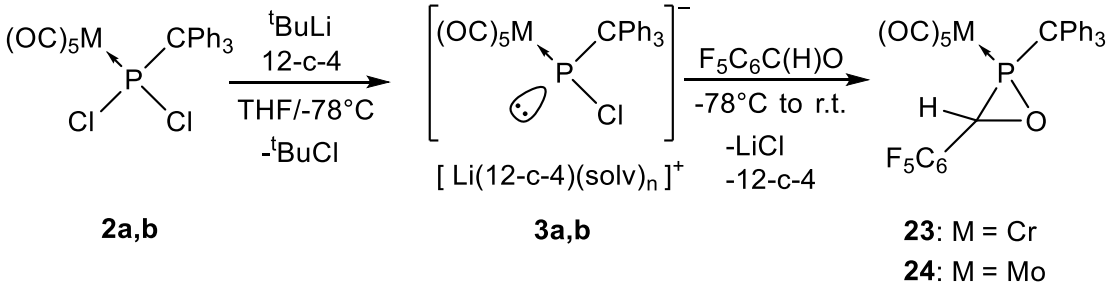

Scheme 28. Synthesis of fluorinated oxaphosphirane complexes **23** and **24**.

Dichlorophosphane complexes **2a,b** were treated with *tert*-butyl lithium in presence of 12-crown-4 at low temperature to yield the corresponding Li/Cl phosphinidenoid complexes **3a,b**. Subsequently, pentafluorobenzaldehyde was added to selectively

give oxaphosphirane complexes **23** and **24** in very good isolated yields (96% for **23** and 88% for **24**).

Table 13. $^{31}P\{^{1}H\}$ NMR and selected $^{13}C\{^{1}H\}$ chemical shifts [ppm] as well as $^{1}J_{P,W}$ coupling constants [Hz] of complexes **22-24**.

Compound	$\delta^{31}P\{^{1}H\}$	$\delta^{13}C\{^{1}H\}$ ($^{2}J_{P,C}$)			
		P<u>C</u>O	<u>C</u>Ph$_3$	***cis*-CO**	***trans*-CO**
22^{W}	7.5	53.3 (24.7)	67.6 (6.6)	193.7 (8.1)	195.1 (41.8)
23Mo	27.4	51.2 (19.5)	66.2 (13.4)	201.6 (10.2)	205.6 (42.5)
24^{Cr}	53.6	51.1 (21.8)	67.8 (13.1)	212.3 (14.2)	214.2 (23.6)

The $^{31}P\{^{1}H\}$ NMR resonances of complexes **22**-**24** present, again, a significant dependence from the metal ($\Delta\delta$ = 16 – 20 between homologues)[96], while the $^{13}C\{^{1}H\}$ chemical shifts of complexes **23** and **24** are much less affected by the substitution pattern and presents similar values for the three derivatives. It should be pointed out that the resonance of the *trans*-CO carbon atom of the chromium metal complex **23** has a smaller phosphorus-carbon coupling constant magnitude than the *cis*-CO groups, which is also a common feature of pentacarbonyl phosphane chromium complexes.[63,96] The effect of the electron-withdrawing substituent is very remarkable for the carbon atom of the heterocycle (P<u>C</u>O in **Table 11**) leading to higher P−C coupling constants in comparison to the ones of the carbon atom of the trityl substituent.

The molecular structures of **23** and **24** were confirmed for the solid state by X-ray crystallography and are depicted in **Figure 19**.

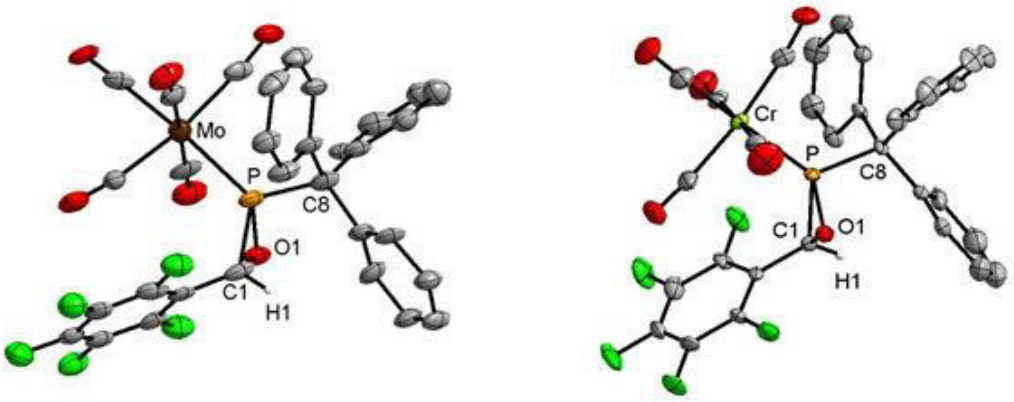

Figure 19. Molecular structures of oxaphosphirane complexes **23** (left) and **24** (right; thermal ellipsoids are shown with 50% probability level); all hydrogen atoms (except H1), are omitted for clarity; selected bond lengths (Å) and angles (°) for **23**: P-Cr 2.3328(9), P-C(1) 1.785(3), P-C(8) 1.895(3), P-O(1) 1.663(2), O(1)-P-C(1) 50.88(11), C(1)-O(1)-P 68.83(14), O(1)-C(1)-P 60.30(13). Selected bond lengths (Å) and angles (°) of complex **24**: P-Mo 2.4864(10), P-C(1) 1.781(3), P-C(8) 1.892(4), P-O(1) 1.668(2), O(1)-P-C(1) 50.16(14), C(1)-O(1)-P 68.93(16), O(1)-C(1)-P 60.92(17).

Here, as in the case for the chromium and molybdenum phenyl derivatives, the two phosphorus stereogenic centers present a different configuration for each metal, thus possessing the phosphorus atom of the chromium derivative **23** a S configuration, while the molybdenum derivative **24** has a phosphorus with R configuration. In **chapter 3.2** it was shown, that the chromium analogue **4a** has an *R* configuration and the molybdenum **4b** a *S* configuration.

The P–C bond in both derivatives is maintaining the enlargement due to the triphenylmethyl substituent and has values of 1.889(10) and 1.912(8) Å for **24** and **23**, respectively. In both cases, as well as in all oxaphosphirane complexes described so far, the metal center is *cis*-oriented to the aromatic substituent at the heterocycle. Intramolecular interactions of the type W–CO···π were also observed for **23** and **24** and were determined by calculating the centroid of the fluorinated ring and measuring the distance from this centroid to the nearest oxygen atom of the metal complex using Mercury 3.8.

The close M–CO···π contacts have a magnitude of 3.025 Å for molybdenum **24** and 3.081 Å for the chromium derivative **23**. These values are slightly higher than the values found for **22** bearing tungsten as transition metal. This shows, that the O···π interactions in fluorinated oxaphosphirane complexes are independent from the transition metal used, but highly influenced by the fluorinated C-substituent.

4.3 Synthesis of *C*-aryl^F oxaphosphirane complexes with other substituents at phosphorus

This work has started studying the properties of different *P*-triphenylmethyl oxaphosphirane complexes in which the carbon atom of the heterocycle was bonded to a phenyl ring. After that, the effects of electron-withdrawing groups at the same atom were analysed and showed intramolecular interactions in the solid state. This section focuses on the synthesis and analysis of *C*-aryl^F substituted oxaphosphirane complexes with different organic substituents at the phosphorus atom thus, bis(trimethylsilyl)methyl ($CH(SiMe_3)_2$) and pentamethylcyclopentadienyl (C_5Me_5), commonly represented as Cp*.

4.3.1 Synthesis of a *C*-aryl^F *P*-pentamethylcyclopentadienyl oxaphosphirane complex

Dichloro(pentamethylcyclopentadienyl)phosphane complex **25**[86,97] was reacted with *tert*-butyl lithium at low temperature in presence of 12-crown-4 and yielded Li/Cl phosphinidenoid complex **26**[86], which by subsequently addition of pentafluorobenzaldehyde generated selectively (isolated yield = 90%) the fluorinated *P*-pentamethylcyclopendienyl oxaphosphirane complex **27** (**Scheme 29**).

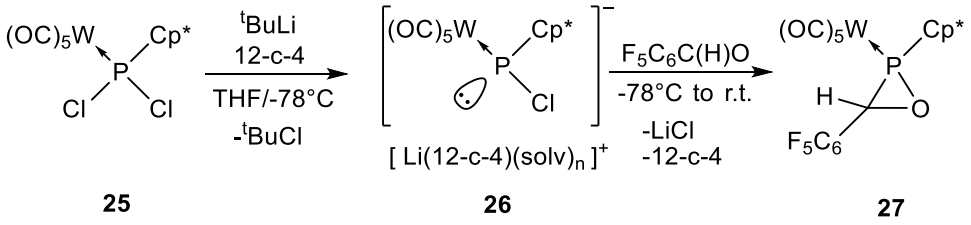

Scheme 29. Synthesis of fluorinated *P*-pentamethylcyclopentadienyl oxaphosphirane complex **27**.

Complex **27** was isolated by extraction and washing the residue with *n*-pentane at low temperature. It was fully characterised by NMR spectroscopy, mass spectrometry and X-ray crystallography.

Table 14. $^{31}P\{^{1}H\}$ NMR and selected $^{13}C\{^{1}H\}$ chemical shifts [ppm] as well as $^{1}J_{P,W}$ coupling constants [Hz] of complexes **22, 27** and the *C*-phenyl derivative **28**.[86]

Compound	$\delta^{31}P\{^{1}H\}$ ($^{1}J_{P,W}$)	$\delta^{13}C\{^{1}H\}$ ($^{2}J_{P,C}$)			
		PCO	CPh$_3$/Cp*	cis-CO	Trans-CO
22	7.5 (320.1)	53.3 (24.7)	67.6 (6.6)	193.7 (8.1)	195.1 (41.8)
27	24.6 (314.5)	49.1 (17.2)	62.9 (9.6)	192.4 (8.2)	193.4 (38.1)
28[86]	31.6 (309.0)	55.5 (17.5)	63.0 (10.0)	194.8 (8.4)	197.3 (37.5)

Table 14 compares NMR data of the fluorinated *P*-pentamethylcyclopentadienyl substituted complex **27** with its *P*-triphenylmethyl substituted analogue **22** and its *C*-phenyl substituted derivative **28**.[86] As mentioned beforehand, the perfluorophenyl substituent has a remarkable influence on the $^{31}P\{^{1}H\}$ NMR chemical shift of **28** being displaced to higher field, which is a counterintuitive result taking into account the electron withdrawing character of the pentafluorophenyl ring, and follow the same tendency as the *P*-triphenylmethyl derivative **22**. The rest of the NMR resonances do not present any significant changes and are in the expected range.

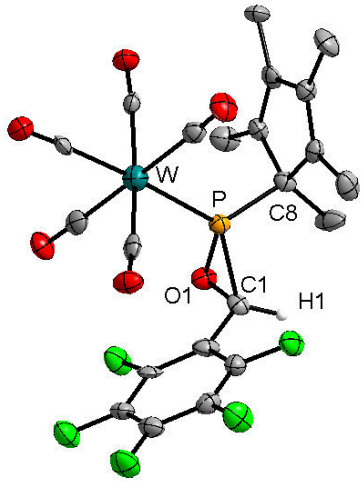

Figure 20. Molecular structure of oxaphosphirane comeplex **27** (thermal ellipsoids are shown with 50% probability level); all hydrogen atoms (except H1), are omitted for clarity; selected bond lengths (Å) and angles (°) for **27**: P-W 2.467(2), P-C(1) 1.815(8), P-C(8) 1.852(9), P-O(1) 1.668(6), O(1)-P-C(1) 49.1(3), C(1)-O(1)-P 70.7(4), O(1)-C(1)-P 60.1(4).

The molecular structure of **27** was confirmed for the solid state by X-ray crystallography and is depicted in **Figure 20**. Complex **27** crystallises in a monoclinic system and a space group Pn. Bond lengths and bond angles are very similar to the ones observed

for its *P*-triphenylmethyl analog **22** except for the P–C(1) bond, which is in **27** enlarged by 2.5 pm and for the P–C(8), which is in **27** shortened by 3 pm.

Also for **27**, intramolecular interactions of the type W–CO···π were observed and determined by calculating the centroid of the fluorinated ring and measuring the distance from this centroid to the nearest oxygen atom of the metal complex; this measurement was performed using Mercury 3.8. The fluorinated complex **27** shows considerable close M–CO···π contacts of a magnitude of 3.054 Å. The *C*-phenyl-*P*-pentamethylcyclopentadienyl derivative **28**[86] was also analysed using the above mentioned methodology but in contrast to the results observed for *C*-phenyl-*P*-triphenylmethyl **4c**, **28**[86] shows the largest W–CO···π distance 3.450 Å, much larger than in the case of **4c** (**Figure 21**).

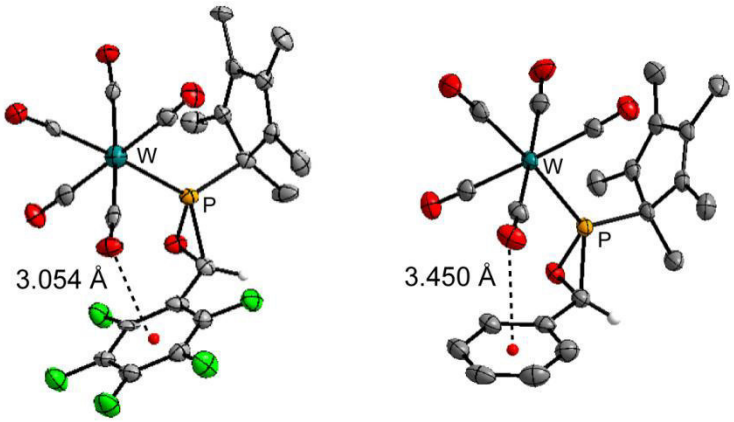

27 **28**

Figure 21. Mercury representations of **27** and **28**[86] showing the centroid of the fluorinated or phenyl ring and its distance to the nearest oxygen atom of the metal complex.

4.3.2 Synthesis of a *C*-aryl^F *P*-bis(trimethylsilyl)methyl oxaphosphirane complex

The same Li/Cl exchange methodology [45] was followed for the synthesis of a *C*-aryl^F *P*-bis(trimethylsilyl)methyl oxaphosphirane complex.

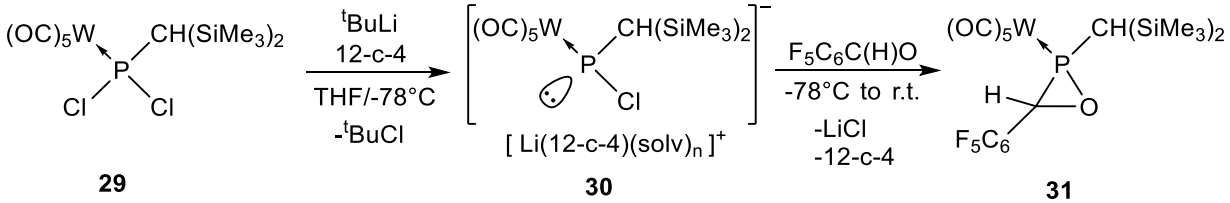

29 **30** **31**

Scheme 30. Synthesis of fluorinated *P*- bis(trimethylsilyl)methyl oxaphosphirane complex **31**.

Attempts to isolate the complex **31** at low temperature or/and by changing the solvent or the method were unsuccessful due to the rapid decomposition of **31** in solution. Nevertheless, the formation of complex **31** was observed and its characterisation was carried out, instantly, after addition of the highly reactive aldehyde to the reaction solution by means of multinuclear NMR analysis.

Table 15. $^{31}P\{^1H\}$, $^{29}Si\{^1H\}$ and selected $^{13}C\{^1H\}$ NMR chemical shifts [ppm] as well as $^1J_{P,W}$ coupling constants [Hz] of complexes **31** and the *C*-phenyl derivative **32**.[70]

Compound	$\delta^{31}P\{^1H\}$ ($^1J_{P,W}$)	$\delta^{13}C\{^1H\}$ ($^2J_{P,C}$)		$\delta^{29}Si\{^1H\}$ ($^2J_{P,Si}$)
		P<u>C</u>O	<u>C</u>H(SiMe$_3$)$_2$	
31	32.9 (311.8)	51.4 (21.2)	30.9 (18.9)	-0.05 (5.1) 1.4 (8.2)
32[70]	40.4 (308.2)	59.7 (27.3)	32.5 (18.9)	0.2 (5.6) 1.5 (8.0)

The counterintuitive effect of the fluorinated substituent is displayed in **Table 15**, causing this shift of the resonances of the different nuclei to higher field.

It was not possible to obtain a crystal structure of the fluorinated oxaphosphirane complex **31** and therefore the intramolecular interactions of the type W–CO···π could not be analysed for this system. Nevertheless, the phenyl derivative was examined using Mercury 3.8 and the result was the absence of any considerable W–CO···π interaction. **Figure 22** shows the distances to the calculated centroid of the two nearest CO groups which have values of 4.294 and 3.907 Å, thus revealing that such π··· π intramolecular interactions are not a phenomenon present in every solid state structure of oxaphosphirane complexes, but a special electronic situation that fluorinated derivatives can induce.

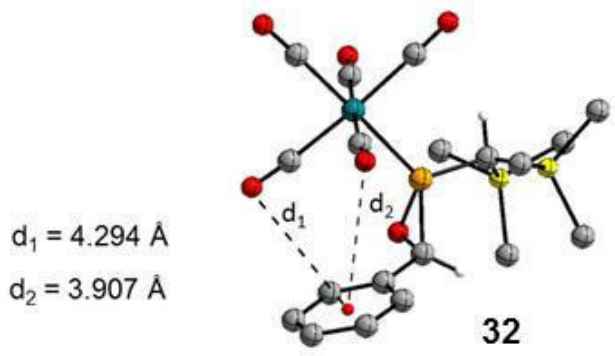

Figure 22. Mercury representations of **32** the centroid of the phenyl ring and its distance to the two nearest oxygen atoms of the metal complex.

4.4 Attempts to synthesize *C*-disubstituted, fluorinated oxaphosphirane complexes

As shown in chapter **4.1**, first derivatives of *C*-aryl^F substituted oxaphosphirane tungsten(0) complexes were successfully prepared, isolated and characterized. Moreover, the influence of the fluorinated aromatic ring was studied, thus revealing intramolecular W–CO(lone pair)$\cdots\pi$(arene) interactions. In this new chapter, the reactivity of the Li/Cl phosphinidenoid complexes **3c, 26** and **30** towards different fluorinated ketones will be described.

4.4.1 Reaction of phosphinidenoid complexes 3c, 26 and 30 with hexafluoroacetone

The synthesis of the first oxaphosphirane, a $\sigma^4\lambda^5$-derivative was performed by Röschenthaler using Niecke's iminophosphane and hexafluoroacetone (see introduction).[38] Therefore, it deemed interesting to prove if the reaction of Li/Cl phosphinidenoid complexes with hexafluoroacetone leads as well to the expected oxaphosphirane complexes.

In the next sections the reactivity of Li/Cl phosphinidenoid complexes towards hexafluoroacetone is described focusing on the effects of different substituents at phosphorus.

The reaction of in *situ* generated Li/Cl phosphinidenoid complexes **3c,**[53] **26,**[86] and **30**,[45] via chlorine/lithium exchange in the corresponding dichlorophosphane complex (see **Scheme 31**), with hexafluoroacetone proceeded readily at low temperature, but with a different outcome. In case of **3c** and **26** (R = CPh_3, C_5Me_5) a fluoride substitution occurred quantitatively leading to complexes **33, 34**, which were isolated via column chromatography and single crystals obtained for both (**Figure 23**). In case of **30** the result was very different: complex **35** was obtained as major product (~ 70%) along with two other minor products (~ 30% by $^{31}P\{^1H\}$ NMR spectroscopy) which could not be separated, but a few single-crystals of **35** were obtained and, hence, the proposed structure of **35** could be confirmed.

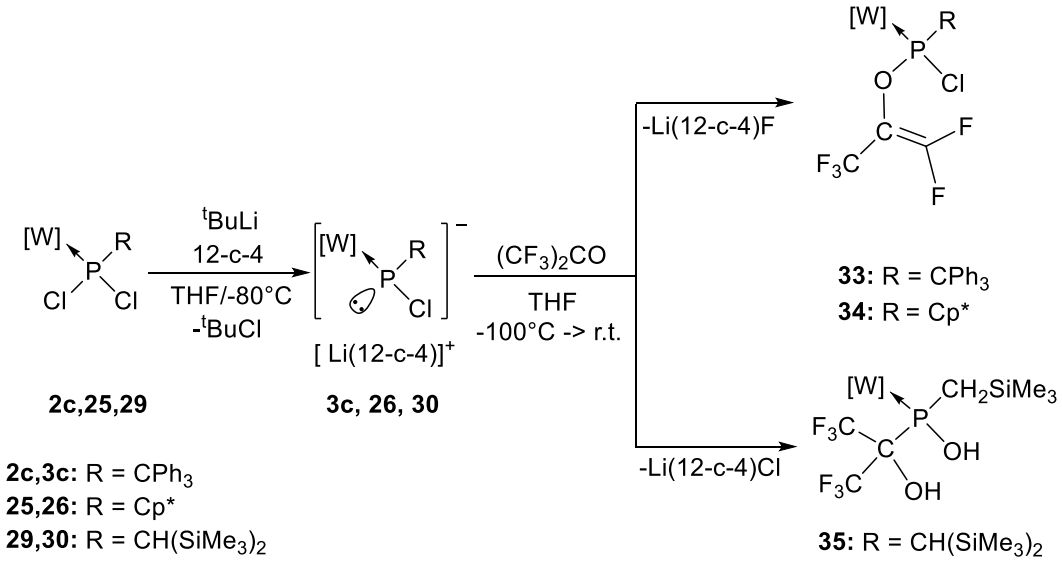

Scheme 31. Reaction of phosphinidenoid complexes **3c, 26** and **30** with hexafluoro-acetone.

Complexes **33-35** display characteristic multinuclear NMR data (**Table 16**) which reveal the strong electron-withdrawing effect of the unusual O-bound and C-bound perfluorinated substituents derived from hexafluoroacetone.

Table 16. $^{31}P\{^1H\}$, $^{19}F\{^1H\}$ NMR chemical shifts [ppm] as well as $^1J_{P,W}$ and $^nJ_{P,F}$ coupling constants [Hz] of complexes **33-35**.

Compound	$^{31}P\{^1H\}$	$^1J_{P,W}$	$^{19}F\{^1H\}$		$^nJ_{P,F}$
			CF_3	CF_2	
33	200.6	336.5	-63.2	-77.2/-92.5	6.0[a]
34	193.2	344.4	-65.3	-76.6/-88.9	7.2[a]
35	247.6	277.8	-67.1/-67.5	-	[a]

[a] The coupling from phosphorus the CF_3 unit could not be resolved.

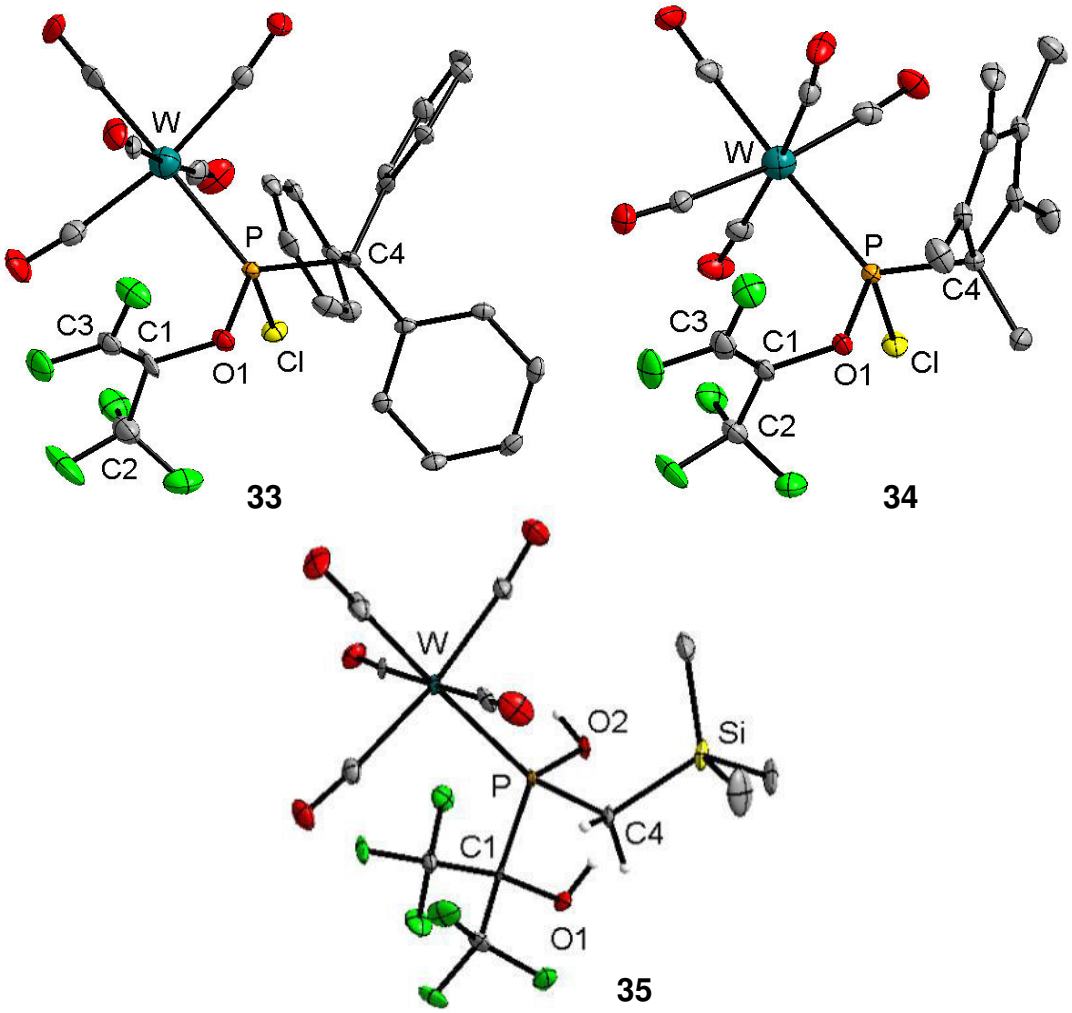

Figure 23. Molecular structure of chlorophosphane complex **33-35** (thermal ellipsoids are shown with 50% probability level); all hydrogen atoms (except H1), are omitted for clarity; selected bond lengths (Å) and angles (°) for **33**: P-W 2.4696(12), P-C(4) 1.925(5), P-O(1) 1.645(3), P-Cl 2.0596(16), C(1)-O(1) 1.392(5), C(1)-C(3) 1.304(7), C(1)-C(2) 1.501(7), O(1)-P-Cl 99.74(13), C(4)-P-Cl 102.22(15), W-P-C(4) 126.08(15); **34**: P-W 2.4795(6), P-C(4) 1.832(2), P-O(1) 1.6568(17), P-Cl 2.0749(8), C(1)-O(1) 1.377(3), C(1)-C(3) 1.310(4), C(1)-C(2) 1.502(3), O(1)-P-Cl 98.90(7), C(4)-P-Cl 100.94(8), W-P-C(4) 125.25(7); **35**: P-W 2.4761(4), P-C(4) 1.7944(6), P-O(2) 1.6249(11), P-C(1) 1.9442(8), C(1)-O(1) 1.4155(3), C(4)-Si 1.9070(2).

As the oxidation of Li/Cl phosphinidenoid complexes using hexafluoroacetone yields different products depending on the organic substituent at phosphorous, this interesting behavior was rationalized using DFT calculations at the BP86-D3/def2-TZVP level of theory, done by Frontera,[98] and taking into consideration solvent effects (THF).

4.4.1.1 Theoretical methods

The mechanism proposed for the *P*-trityl and *P*-Cp* derivatives is shown in **Scheme 32**; the calculations have been performed for CPh_3 as the exemplifying case. It involves an initial noncovalent complex **36** (P···C electrostatic interaction,[99] see **Figure 24a**) followed by a single electron transfer (SET) that generates a solvent-caged radical pair **37**. The radical coupling yields the intermediate **38**. The final product is easily generated by an E_1cB_I elimination mechanism[100] mediated by the lithium cation which facilitates the elimination of fluorine with the concomitant formation of the double bond.

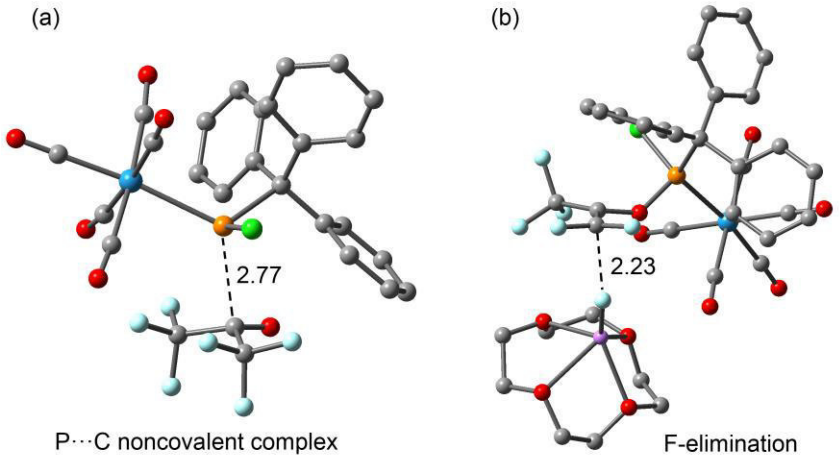

Figure 24. (a) Noncovalent π-hole complex between the phosphinidenoid anion and perfluoroacetone. (b) Resulting product of the E_1cB_I elimination promoted by Li^+@12-c-4.

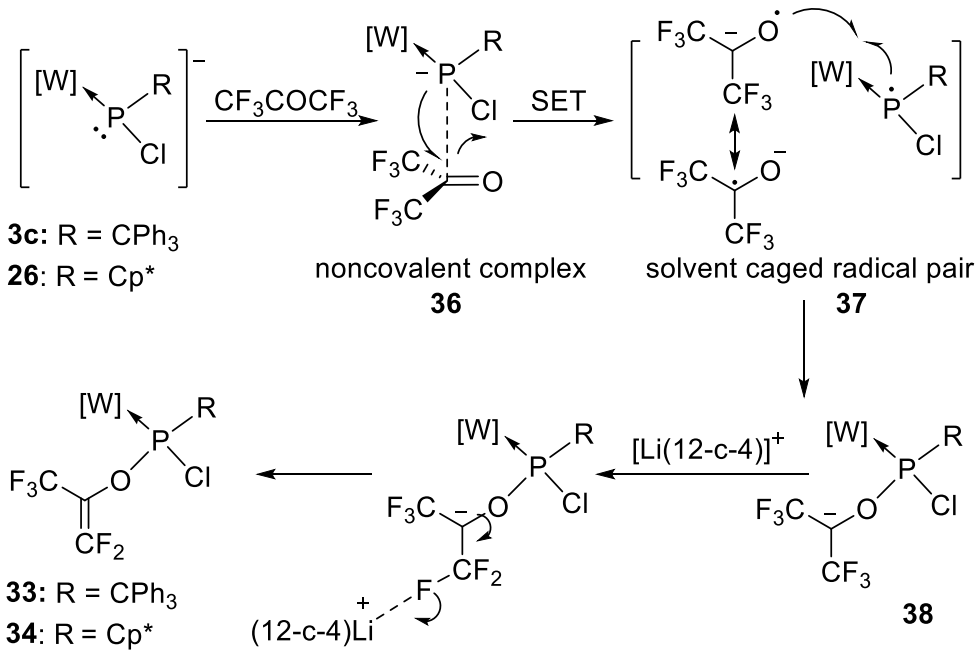

Scheme 32. Proposed SET mechanism for phosphinidenoid complexes **3c** and **26.**

The SET oxidation mechanism is feasible taking the frontier orbital energies of the fluorinated ketone and the anion into consideration (**Figure 25a**). Here, the HOMO of the phosphinidenoid complex corresponds to a lone pair atomic orbital of the P atom and it is 1.5 eV higher in energy than the LUMO of the perfluoroacetone, *i.e.,* antibonding π^* C=O orbital. Interestingly, the spin density plot of perfluoroacetone radical anion clearly reflects that the unpaired electron is equally distributed between both C and O atoms (**Figure 25b**). The O···P (instead of C···P) radical coupling within the solvent caged radical pair is thermodynamically favored.

The closed-shell mechanism where a nucleophilic attack of the phosphinidenoid complex anion to the C atom of the ketone takes place as first mechanistic step was also explored. Unexpectedly, the stationary point that corresponds to the product where the new P–C bond is formed (addition to the C=O bond) was not found. Instead the stationary point corresponds to a noncovalent complex where simply a P···C interaction is established (**Figure 24**) where the SET likely occurs.

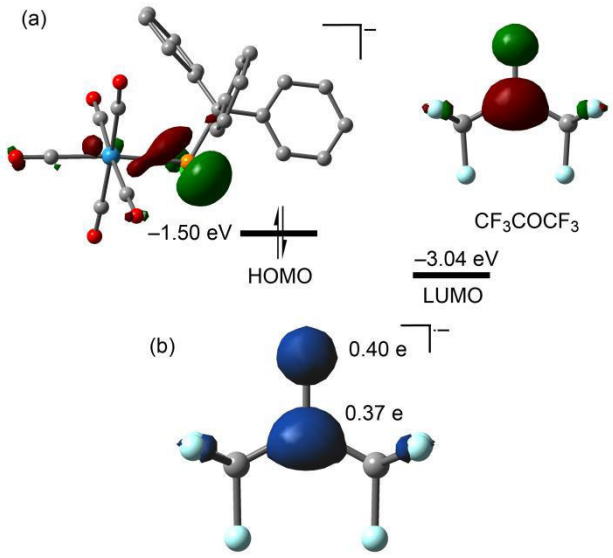

Figure 25. (a) Plots of the HOMO (anion) and LUMO (hexafluoroacetone). (b) The spin density plot of the radical anion $[CF_3COCF_3]^{\cdot-}$ is represented. The values of spin density at selected atoms are also given.

The different stationary points and energetic profile (**Figure 26**) of the suggested mechanism (**Scheme 32**) have been computed. The solvent cage radical pair (**37**) lies 8.4 kcal/mol higher in energy than the starting products and the recombination of radicals yields to the intermediate (**38**) that is 16.2 kcal/mol lower in energy than the starting products. Approach of the complex Li^+@12-c-4 to the F atom provokes the

elimination of the fluoride without any energy cost. The final products are 43.6 kcal/mol more stable than the starting material.

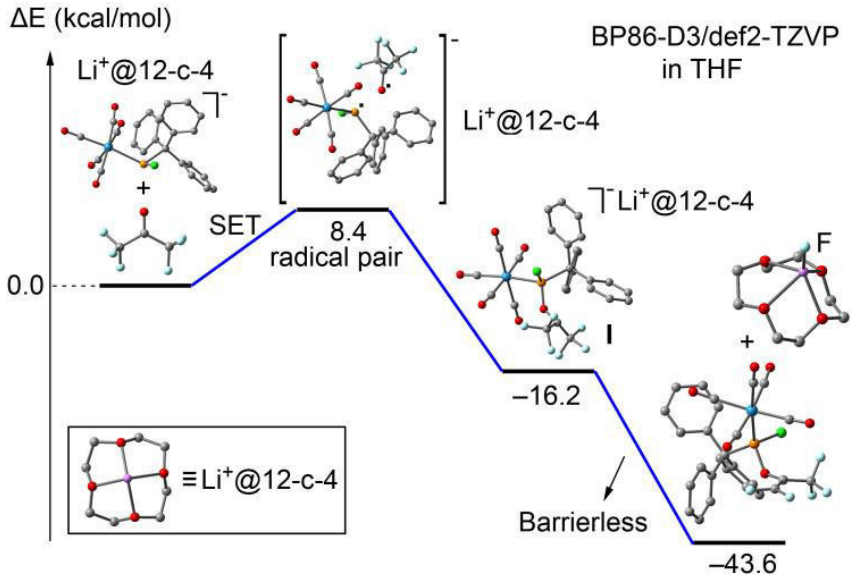

Figure 26. Reaction profile for the reaction of the *P*-trityl phosphinidenoid complex with hexafluoroacetone. The hydrogen atoms have been omitted in the representation of the optimized compounds.

Experimentally, a totally different product was obtained in case of the *P*-$CH(SiMe_3)_2$ derivative **30**. Here, a different mechanism (closed-shell instead of radical) is proposed, because computationally it is shown that the nucleophilic attack of the ketone is favored energetically (*vide infra*). The mechanism is shown in **Scheme 33** and starts with the nucleophilic attack of the P center to the C=O carbon and, consequently, the formation of the inter-mediate **39** that is stabilized by a strong tetrel bonding inter-action.[101] This first intermediate is transformed into a second intermediate **40** where a Si–O bond and a carbanion (in alpha with respect to the $SiMe_3$ group) are formed. The elimination of the chloride is promoted by the complex Li^+@12-c-4 yielding the final product (trimethylsilylmethylene)phosphane complex. Obviously, this product can easily be transformed via hydrolysis into the experimentally observed final product.

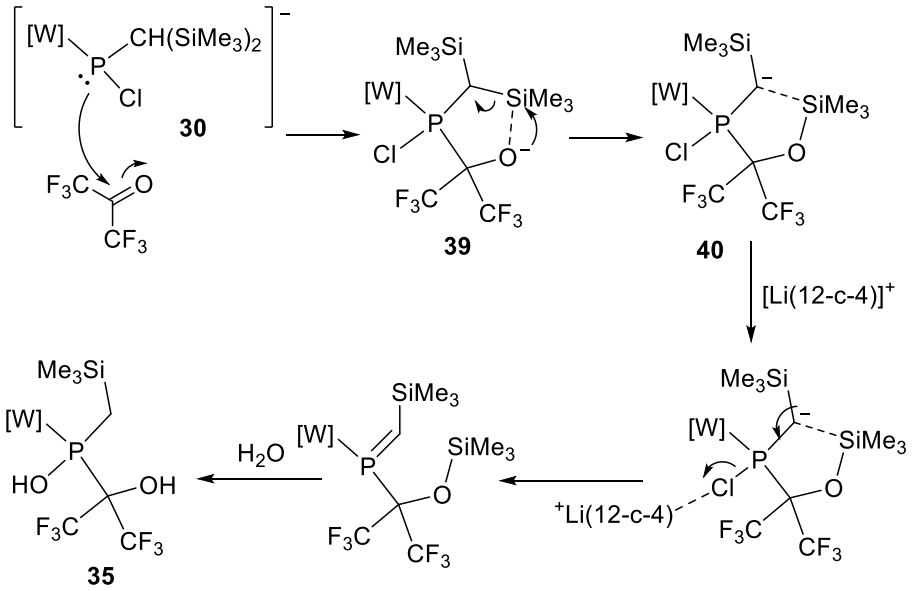

Scheme 33. Proposed mechanism for the *P*–CH(SiMe3)2 substituted phosphini denoid complex **30**.

The energetic profile of the mechanism is shown in **Figure 27**. The first step is barrierless and yields the intermediate **39** that is 22.8 kcal/mol lower in energy than the starting products. This intermediate is stabilized by a strong Si···O interaction (2.87 Å) that likely explains the totally different mechanism found for this compound compared to the *P*-trityl or *P*-Cp* substituted phosphinidenoid complexes that do not have the possibility to form this strong interaction. This first intermediate is easily transformed into the second intermediate **40** (barrier 3.8 kcal/mol) that is 6.2 kcal/mol more stable than the former. This carbanionic intermediate is also stabilized by a tetrel bonding interaction (C···Si, 3.62 Å). Moreover, in this intermediate the P–Cl bond is elongated (2.26 Å) and approach of the complex Li^+@12-c-4 to this Cl atom causes chloride elimination without energy cost, yielding the product shown in **Figure 28** where the P=C double bond is formed and the Cl atom is bound to Li. The final products are –39.8 kcal/mol more stable than the starting ma-terial. This product should be easily hydrolysable in contact with water, yielding the X-ray characterized product.

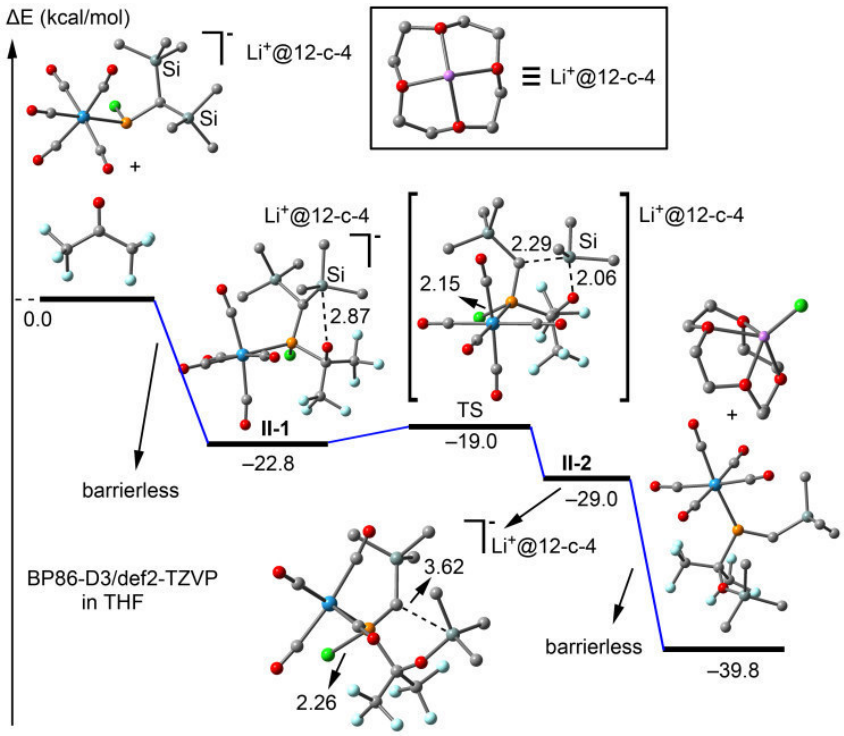

Figure 27. Reaction profile for the reaction of *P*–CH(SiMe$_3$)$_2$ Li/Cl phosphi-nidenoid complex with hexafluoroacetone. The hydrogen atoms have been omitted in the representation of the optimized compounds (distances in Å).

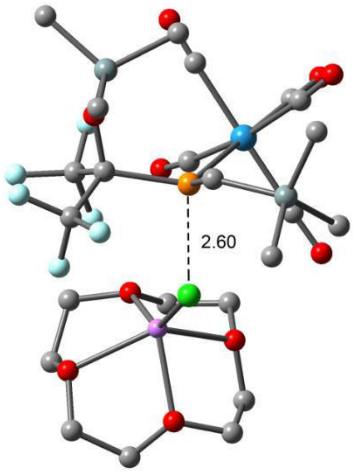

Figure 28. Resulting product of the Cl elimination promoted by Li$^+$@12-c-4. Distance in Å. H-atoms omitted for clarity.

4.4.2 Reaction of phosphinidenoid complexes 3c, 26 and 30 with perfluorobenzophenone

As discussed beforehand, the reaction of phosphinidenoid complexes with hexafluoroacetone leads to an unprecedented ambiguous reactivity that for the *P*-trityl and *P*-Cp* derivatives disclose a SET pathway involving a transient phosphanyl complex hexafluoroacetonyl radical (See part **4.4.1**)

In *situ* generated Li/Cl phosphinidenoid complexes **3c,**[53] **26,**[86] and **30**,[45] via chlorine/lithium exchange in the corresponding dichlorophosphane complex (see **Scheme 34**), were treated with perfluorobenzophenone at low temperature.

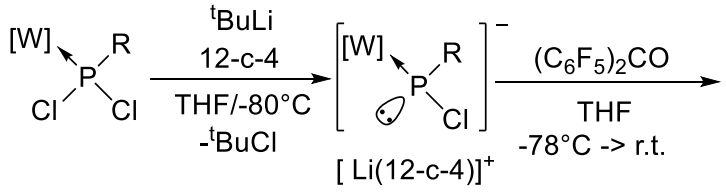

2c,25,29 **3c, 26, 30**

2c,3c: R = CPh_3
25,26: R = Cp*
29,30: R = $CH(SiMe_3)_2$

Scheme 34. Reaction of phosphinidenoid complexes **3c**, **26** and **30** with perfluorobenzophenone.

The $^{31}P\{^1H\}$ NMR measurement of the reaction of the trityl derivative **3c** resulted in an "empty" spectrum, *i.e.,* no signals were obtained. This could be, presumably, due to the presence of radicals located on or near the phosphorus atom. To have more information about this reaction, EPR measurements were performed by the group of Schiemann (Bonn). If perfluorobenzophenone induces the formation of ketyl radicals as in the reaction of phosphinidenoid complexes **3c**, **26** and **30** with hexafluoroacetone, it would be easy to detect them by EPR measurements, since this reactions are slower than the previous. However, the literature[102] says that it is difficult to detect the perfluorobenzophenone anion radical by EPR spectroscopy, due to nucleophillic degradation. Instead of the anion radical, only partially fluorinated species were observed in most publications in which the para fluorine atom had been replaced and, in addition, solvents seem to react with the anion radical in many cases.

First measurements revealed a spectrum that was reasonably interpreted by the EPR parameters reported for the triphenylmethyl radical as depicted in **Figure 29**.

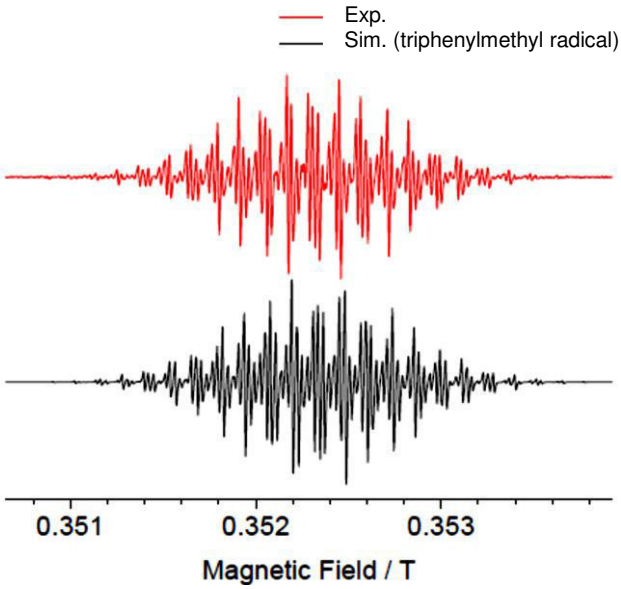

Figure 29. EPR measurement of the reaction solution of **3c** with perfluorobenzophenone (red) and simulated spectrum of the triphenylmethyl radical (black).

But other radicals were also found. If a higher modulation amplitude and higher microwave power are used (represented as hard conditions and with blue lines in **Figure 30 top**), it is possible to detect some additional signals in the lower and higher field regions, as shown in **Figure 30 top** on an expanded scale. The additional peaks cannot be interpreted as the ones of the triphenylmethyl radical as shown in **Figure 30 bottom** (simulations of perfluorobenzophenone anion radical and triphenylmethylradical). Perfluorobenzophenone anion radicals may also exist in the solution, but it cannot be analyzed because the signals of the triphenylmethyl radical mask them. Since the unwanted radical (triphenylmethyl radical) is produced in the solution, the additional peaks may also be due to another unwanted radical.

The high-resolution EPR spectrum (red lines in the figures of this chapter) could be observed under a smaller modulation amplitude and lower microwave power (soft experimental conditions). If hard conditions are used in the measurement, the signal-to-noise ratio can be increased (weaker signals can be seen), but also results in a broadening, as shown by blue lines **Figure 30**. It should be noted again that both red and blue lines **Figure 30** are the EPR spectra from the same sample, in which only the measurement conditions are different.

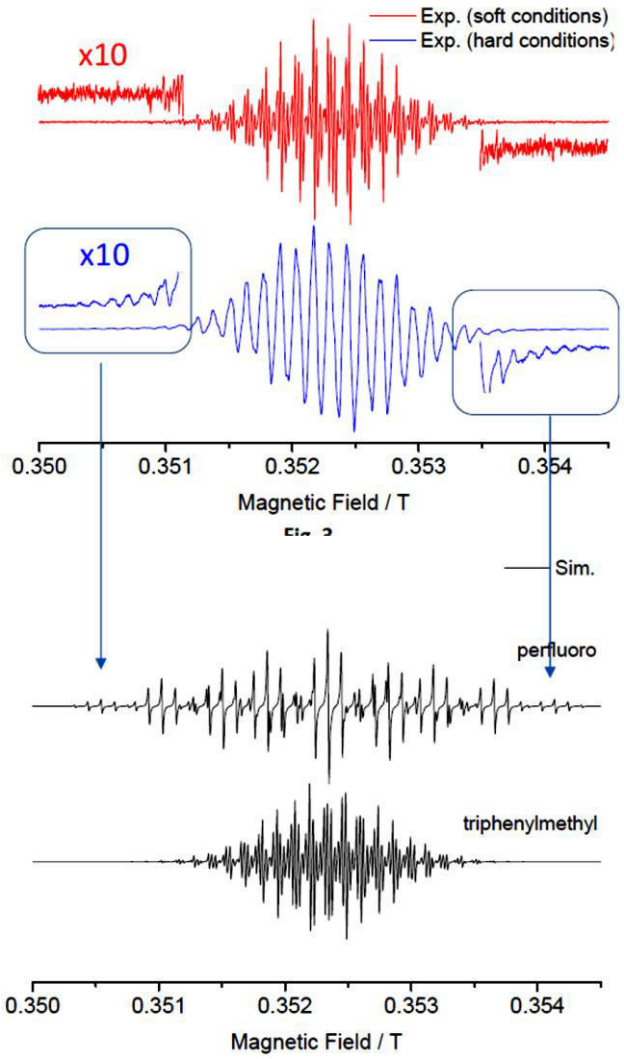

Figure 30. Results of the EPR measurement under soft conditions (red) and hard conditions (blue) and comparison with simulated spectra for perfluorophenone radical and triphenylmethyl radical.

Another broad peak was also observed, as shown in **Figure 31**. Since the signal intensity was very weak, the assignment (analysis) was impossible. But from the peak position, it is expected to be a metal complex.

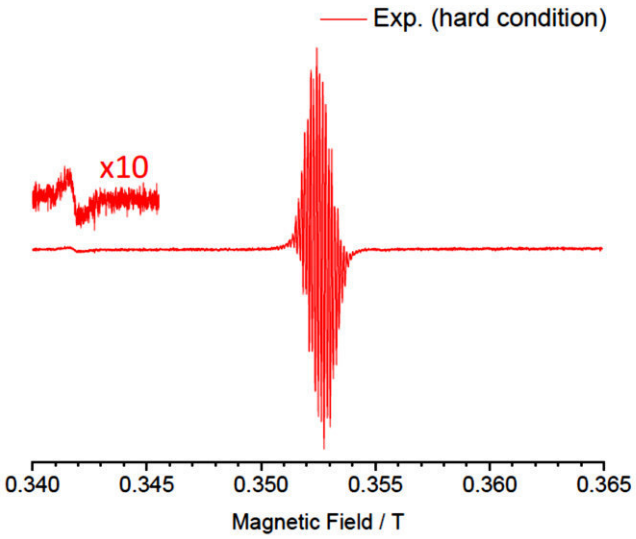

Figure 31. EPR spectroscopic measurement (under hard conditions) of the reaction solution of **3c** with perfluorobenzophenone.

The reaction the Cp* derivative **26** with perfluorobenzophenone generated radicals as well but could not be completely identified. **Figure 32** shows the experimental result (black line) and a simulation (red line). The simulation was done by assuming a radical containing 10 inequivalent nuclei with $I = 1/2$ that could be proton or fluorine.

There is a possibility that the radical is located at the fluorinated benzophenone, but the splitting is smaller than expected.

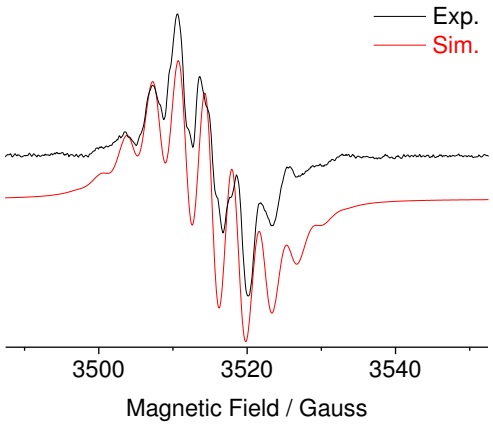

Figure 32. EPR spectrum of the reaction solution of **26** with perfluorobenzophenoe (black) and simulation of the perfluorobenzophenone radical cation (red).

Although the signal to noise ratio of the $^{31}P\{^{1}H\}$ NMR spectrum of the reaction of **26** with perfluorobenzophenone is very bad, a resonance at 183.7 ppm could be detected, showing a direct coupling to one fluorine atom with a magnitude of 866 Hz.

The reaction of the *P*-CH(SiMe$_3$)$_2$ substituted derivative **30,** displayed a $^{31}P\{^1H\}$ NMR sprectrum with a much better signal to noise ratio. The main resonance (60%) at 172.2 ppm ($^1J_{P,W}$ = 309 Hz, $^1J_{P,F}$ = 864 Hz) showed a direct coupling to one fluorine atom. In addition to this resonance, several signals were also observed between -10 and -115 ppm (40%), all of them showing a direct coupling to a hydrogen atom of a magnitude > 300Hz.

The EPR spectral analysis of this reaction was also performed and a radical was detected. This radical may correspond to a different, partially fluorinated benzophenone radical (**Figure 33**) because the spectral width was wider in this case than that of the anion radical of fully protonated benzophenone and narrower than that of the anion radical of fully fluorinated benzophenone.

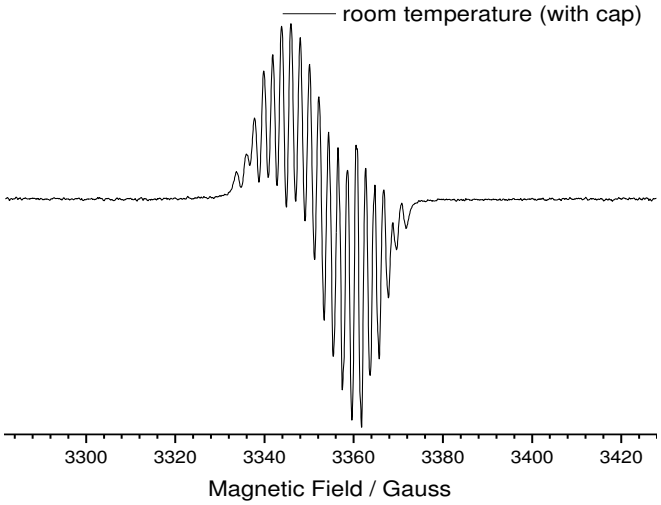

Figure 33. EPR spectrum of the reaction solution of **30** with perfluorobenzophenone.

Nevertheless, preliminary computational investigations by Frontera for this reaction revealed that, in case of using perfluorobenzophenone, a stable radical anion is formed easily as the LUMO energy picture (**Figure 34a**) shows. The spin density plot shown in **Figure 34b** indicates that the spin density is highly delocalized on the aromatic ring carbons. Moreover, the spin density value at the O atom is only 0.27 e and, consequently, the radical coupling to form the P–O bond is not favored. Therefore, the unstable phosphinidenoid radical likely reacts with any source of H$^{\cdot}$ (X = solvent or other species from the reaction mixture, see **Scheme 35**) as reavealed by the NMR analysis, generating a complicated mixture of radicals, confirmed by the different EPR spectra.

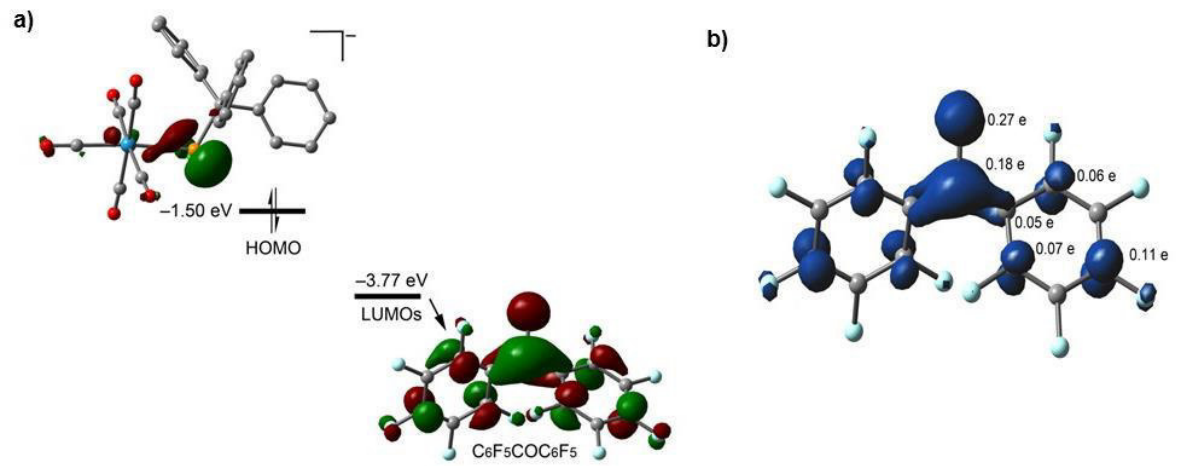

Figure 34. a) Plots of the HOMO (anion) and LUMO (perfluorobenzophenone) and b) the spin density distribution in the perfluorobenzophenone radical anion.

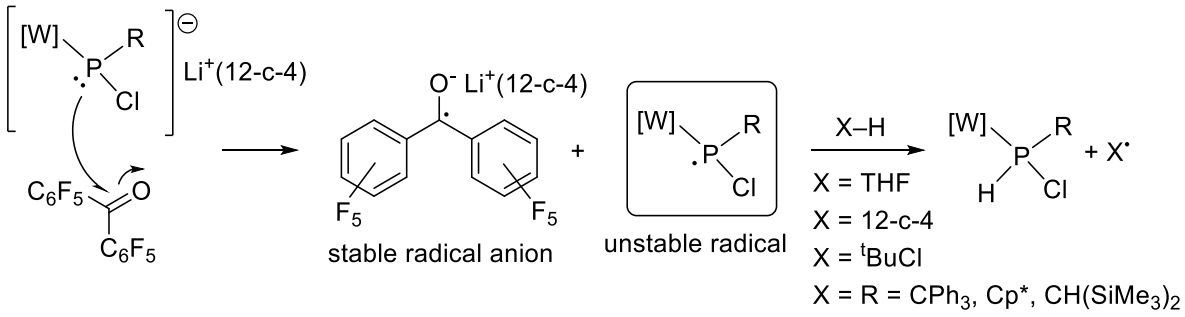

Scheme 35. Proposed mechanism for the reaction of X with perfluorobenzophenone.

4.4.3 Reaction of Li/Cl phosphinidenoid complexes 3c, 26 and 30 with 2,2,2-trifluoromethylbenzophenone

The reaction of in *situ* generated Li/Cl phosphinidenoid complexes **3c,**[53] **26,**[86] and **30**,[45] via chlorine/lithium exchange in the corresponding dichlorophosphane complex (**Scheme 36**), with 2,2,2-trifluoromethylbenzophenone at low temperature was analysed. While several attempts for the *P*-CPh_3 and *P*-$CH(SiMe_3)_2$ substituted Li/Cl phosphinidenoid complexes led always to very unselected reaction mixtures, the *P*-Cp* substituted derivative led selectively to the expected oxaphosphirane complex **41** (**Scheme 36**).

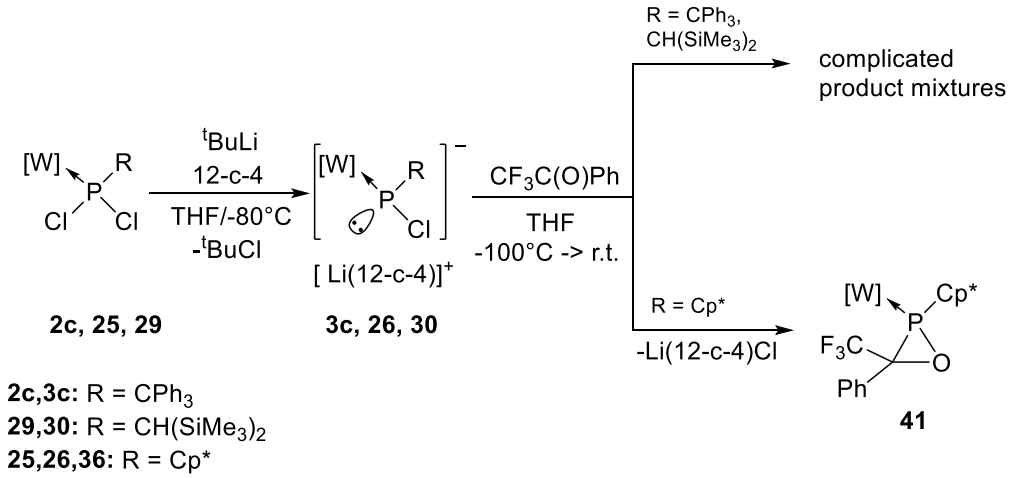

Scheme 36. Reaction of Li/Cl phosphinidenoid complexes **3c**, **26** and **30** with 2,2,2-trifluoromethylbenzophenone.

Complex **41** presents a $^{31}P\{^{1}H\}$ NMR resonance at 42 ppm with a phosphorus-tungsten coupling constant magnitude of 309 Hz which are in the typical range of oxaphosphirane complexes.

That the reaction was not succesful for the cases of the trityl and bis(trimethylsilyl)methyl substituted derivatives **3c** and **26** maybe due to the high steric hinderance of these P-substituents combined with the sterically demanding ketone, which hampers the ring closure and leads to the formation of primary and secondary phosphane-tungsten complexes among others as observed in the $^{31}P\{^{1}H\}$ NMR spectra.

Suitable crystals for X-ray diffractomeric studies of complex **41** were obtained from concentrated *n*-pentane solutions (**Figure 35**). All bond lengths and angles are in the normal range for oxaphosphirane but for the P-C(9) which is very enlongated and displays a value of 1.9102 Å, similar to the *P*-CPh_3 substituted oxaphosphirane complexes.

Table 17. $^{31}P\{^{1}H\}$ NMR data [ppm], $^{1}J_{P,W}$ [Hz] and selected bond lengths [Å] of oxaphosphirane complexes **27**, **28** and **41**.

Compound	R/R'-C_{ring}	$^{31}P\{^{1}H\}$	$^{1}J_{P,W}$	P-W	P-C_{exo}
27	H/C_6F_5	24.6	314.2	2.467(2)	1.852(9)
28	H/Ph	31.3	307.3	2.469(7)	1.821(3)
41	CF3/Ph	42.2	309.6	2.517(7)	1.911(4)

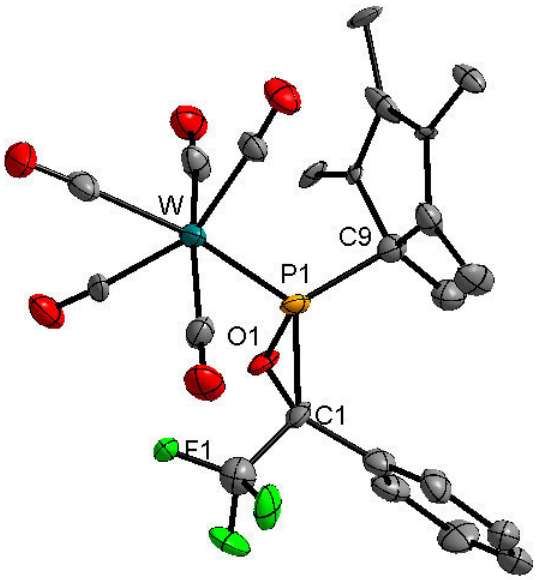

Figure 35. Molecular structure of oxaphosphirane complex **41** (thermal ellipsoids are shown with 50% probability level); all methyl hydrogen atoms are omitted for clarity; selected bond lengths (Å) for **41**: P-W 2.517(7), P-C(9) 1.9102(3), P-O(1) 1.6712(3), P-C(1) 1.7964(8), C(1)-O(1) 1.4550(3).

5. Investigations on the reactivity of *P*-CPh$_3$ substituted $\sigma^3\lambda^3$-oxaphosphirane complexes

5.1 Thermal reactions of *P*-CPh$_3$ substituted $\sigma^3\lambda^3$-oxaphosphirane complexes

Previous investigations of thermal reactions for non-fluorinated $\sigma^3\lambda^3$-oxaphosphirane complexes of the type **XLI** (**Scheme 37**) were performed for derivatives having different substituents at phosphorus such as bis(trimethylsilyl)methyl and pentamethylcyclopentadienyl (Cp*).

For the first case, Marinas Pérez had observed that the *C*-phenyl-*P*-bis(trimethylsilyl)methyl substituted derivative showed no reaction upon heating (gently) in toluene, and even upon addition of different (trapping) reagents such as DPPE no reaction was observed, even at temperatures at about 100°C.[103] Recently, donor and (weak) acceptor groups were incorporated as substituents at the ring carbon atom (R' in **Scheme 37**). The *C*-pyridyl-*P*-bis(trimethyl-silyl)methyl derivatives by Klein revealed that thermal reactions in *ortho*-dichlorobenzene led to the loss of one CO group of the pentacarbonyl tungsten moiety followed by the coordination of the nitrogen atom at the pyridyl group to tungsten to give complex **XLII** (**Scheme 37a**).[104]

The *P*-Cp* derivative (R' = Ph in **Scheme 37**) presents noteworthy differences due to the versatility of the pentamethylcyclopentadienyl moiety to perform rearrangements.[65,105] While thermal reactions in toluene resulted in complicated mixtures of products, Bode showed that the introduction of a trapping agent, *i.e.* an aldehyde led to the formation of O,P,C-cage complexes (**Scheme 37b**).[106]

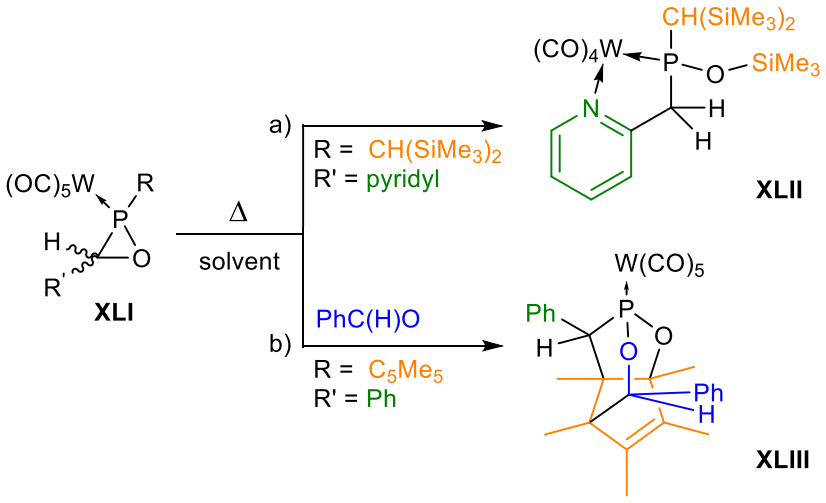

Scheme 37. Thermal reactions of: a) *P*-CH(SiMe$_3$)$_2$ and b) *P*-Cp* substituted oxaphosphirane complexes of the type **XLI**.[106]

In this section, thermal reactions of *P*-CPh_3 substituted oxaphosphirane complexes will be discussed. Furthermore, a comparative study on the use of fluorinated *P*-Cp* derivatives in thermal reactions in the presence of aldehydes will be described; a theoretical study explaining the mechanism of this latter reaction will be presented, too. Oxaphosphirane complexes **4c** and **22** were dissolved in toluene and a NMR monitoring was performed while gently warming from room temperature to 100°C (**Scheme 38**). While **4c** unselectively decomposed at about 70°C, leading to a complicated mixture of phosphorus-containing products, complex **22** showed a higher stability in solution and at 100°C experienced a selective conversion.

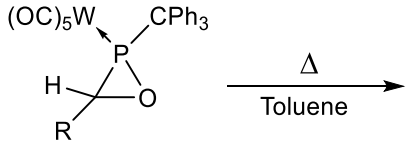

4c: R = Ph; M = W
22: R = C_6F_5; M = W
23: R = C_6F_5; M = Cr
24: R = C_6F_5; M = Mo

Scheme 38. Thermal reaction of oxaphosphirane complexes **4c** and **22-24** in toluene.

At 100°C, complex **22** was selectively transformed to give two phosphorus-containing compounds in a 3:1 ratio as **Figure 36** displays in which a tungsten-phosphorus coupling was absent; the reaction needed four hours to reach completion.

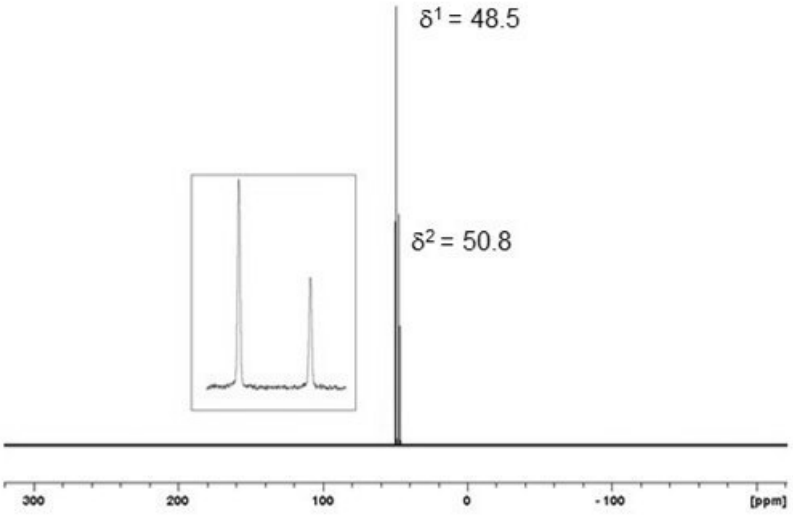

Figure 36. $^{31}P\{^1H\}$ NMR spectrum of the thermal reaction of **22** in toluene (100°C).

The same thermal protocol was followed using derivatives bearing other transition metals, *i.e.,* chromium (**23**) and molybdenum (**24**). Under the same conditions both derivatives present a comparable NMR pattern (**Figure 37**) and display a 2:1 ratio.

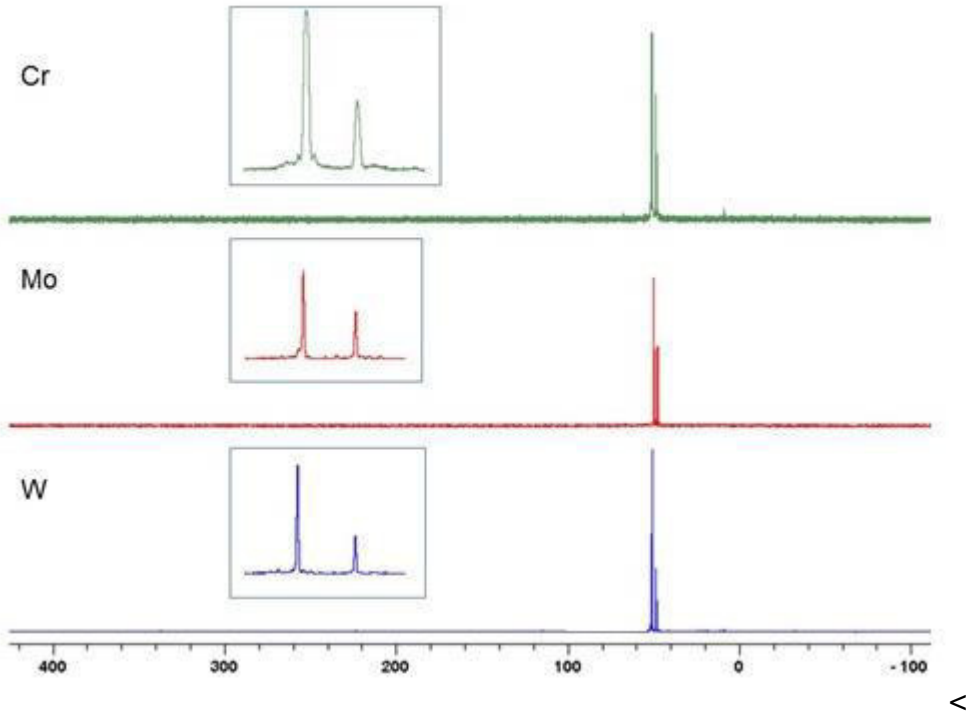

Figure 37. $^{31}P\{^{1}H\}$ NMR data of the reaction solutions in toluene at 100°C of complexes **22**-**24**.

With the information obtained from multinuclear NMR spectral analysis, the deduced constitution of the new products will be discussed. The $^{13}C\{^{1}H\}$ NMR data clearly revealed the absence of resonances corresponding to the carbonyls of the metal complex fragment. According to the information of two-dimensional NMR data, the triphenylmethyl group is still attached to phosphorus. The pentafluorophenyl moiety is also intact, and by analysis of the dept135 NMR, an unexpected resonance corresponding to a CH_2 group appears. This resonance emerges at 26.5 ppm as a broad doublet, presenting a $^{1}J_{P,C}$ of 82.3 Hz, from which it can be assumed that this carbon atom is directly attached to the phosphorus atom, the latter, most probably, being in a higher oxidation state. $^{19}F\{^{1}H\}$ NMR spectral analysis confirms the resonances for the *ortho*, *metha* and *para* fluorine atoms, thus corresponding to the intact C_6F_5 moiety.

^{1}H-NMR spectral data show the aromatic protons of the triphenylmethyl group within the expected area between 6.5 and 7.9 ppm and two additional resonances at 2.6 and 3.2 ppm (integration corresponds to one proton each), both displaying a doublet of doublets (dd). These two (new) proton resonances show a doublet in the $^{1}H\{^{31}P\}$ NMR, meaning these represent two diastereotopic protons in a geminal position, near to the

phosphorus atom. These observations are in agreement with the $^{13}C\{^1H\}$-NMR-based conclusions described before. Using this information, it can be suggested that, after loss of the pentacarbonyltungsten moiety, the oxaphosphirane **42** (**Scheme 39**) opens to form **43** and accepts a hydrogen atom, presumably from the solvent, thus leading to the formation of compound **44** that dimerizes to form the final product **45**.

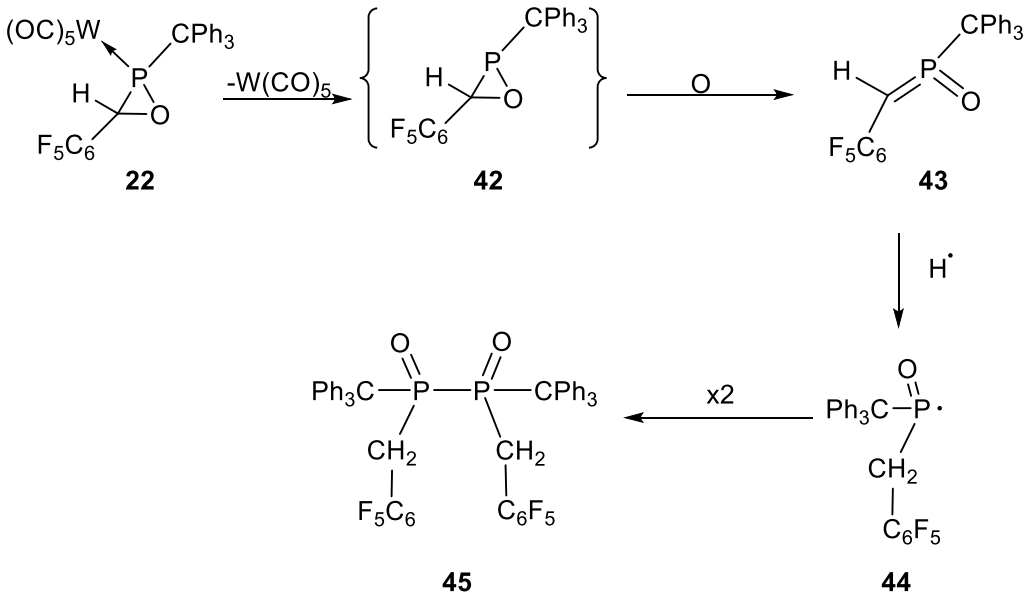

Scheme 39. Proposed mechanism for the thermal reaction of **22** in toluene.

Due to the symmetry of compound **45** only one phosphorus resonance can be expected, but there is the possibility of the formation of the *meso* and *rac* diastereomers that could explain the two phosphorus resonances observed in the NMR spectrum as displayed in **Figure 36** and **Figure 37**.

5.1.1 Thermal reactions of *C*-C_6F_5 *P*-Cp* substituted $\sigma^3\lambda^3$-oxaphosphirane complexes

Although the history of cage complexes containing phosphorus and oxygen is quite short, it is assumed that due to their properties they are promising compounds representing a very interesting area in the chemistry of polymers.[107] For example, polycyclic phosphites are well known class of O,P,C-cage compounds, which have the ability to act as good copolymerization reagents, and thus lead to interesting flame-retardants such as **XLIV** and **XLV** (**Scheme 40**).[108] Besides, they are used in catalysis and as model compounds in DNA and neurosteroids research.[109]

As mentioned at the beginning of this section, Bode showed that oxaphosphirane complexes bearing Cp* at phosphorus, lead easily to the formation of O,P,C-cage complexes through thermal reactions in presence of aldehydes.[106] This was a valuable discovery because the building of asymmetric cage structures represents, still today, a major synthetic challenge.

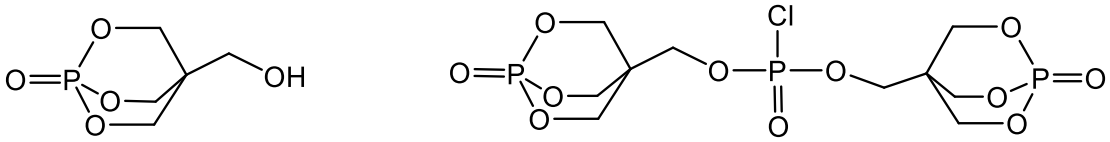

XLIV **XLV**

Scheme 40. Examples of known O,P,C cage compounds.[108]

To analyse the behaviour that electron-withdrawing groups *i.e.* pentafluorophenyl group at the ring carbon atom could induce in thermal reactions of *P*-Cp* substituted oxaphosphirane complexes. Complex **27** was subjected to thermal reactions with benzaldehyde and pentafluorobenzaldehyde in toluene. Surprisingly, no reaction was observed neither by gentle warming at 75°C during several hours nor under refluxing conditions. This shows a remarkable increase of the thermal stability of the oxaphosphirane complex due to the fluorinated moiety. Nevertheless, a solvent with a higher boiling point was chosen to perform the reaction, *i.e. ortho*-dichlorobenzene and by refluxing during 2 hours the reactions led selectively to the expected cage complex **46** if benzaldehyde was used for the cage formation (**Scheme 41**). If pentafluorobenzaldehyde was used, the reaction led to a complicated mixture of phosphorus-containing products and, finally, to decomposition. But it was possible to detect a phosphorus resonance at 144.0 ppm with a phosphorus-tungsten coupling

constant magnitude of 322.7 Hz, which could correspond to the targeted fluorinated cage complex **46^{F}**. In contrast, fluorinated O,P,C-cage complex **46** was isolated and characterised as result of a high diastereoselective reaction, and the connectivity of the ligand framework was confirmed by X-ray crystallography (**Figure 38**).

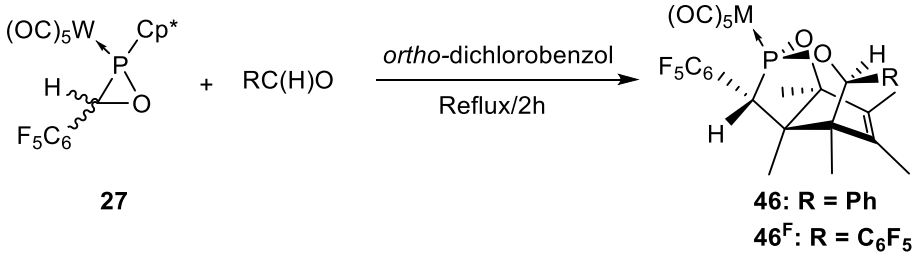

Scheme 41. Synthesis of fluorinated O,P,C-cage complexes **46** and **46^{F}**.

Table 18. Selected ^{31}P NMR resonances [ppm] and $^{1}J_{P,W}$ and $^{2}J_{P,H}$ [Hz] of complexes **28, 46-46^{F}** in THF-d8.

Complex	R	^{31}P{^{1}H}	$^{1}J_{P,W}$	$^{2}J_{P,H}$
28[106]	Ph	155.1	334.4	12.7
46	Ph	153.1	346.9	24.8
46^{F}	C_6F_5	161.8	348.3	27.3

These NMR data of the complexes **46-46^{F}** are closely related to those of the known O,P,C-cage tungsten(0) complexes synthesized by Bode,[106] except for the influence of the C_6F_5 second unity which remarkably shifts the phosphorus resonance to lower field. Whereas the ^{31}P{^{1}H} and ^{1}H NMR spectra of **28** clearly shows a $^{2}J_{P,H}$ coupling constant magnitude of about 13 Hz, complexes **46-46^{F}** possess much larger coupling constants of above 20 Hz.

Complex **46** crystallizes in a monoclinic lattice with space group $P2_1/n$. The selected data of the molecular structures of **46** and **28**[106] are displayed in **Table 19** and unambiguously confirm the ligand cage constitutions. Some structural differences between the cages of **46** and **28** are found within the particular cage moieties, but shall not be discussed further. The geometries at phosphorus are quite similar for cages in **46** and **28** and the P-O and P-C bond distances shown in **Table 19** are found to be similar to polycyclic phosphites and to previously reported tungsten(0) analogues.

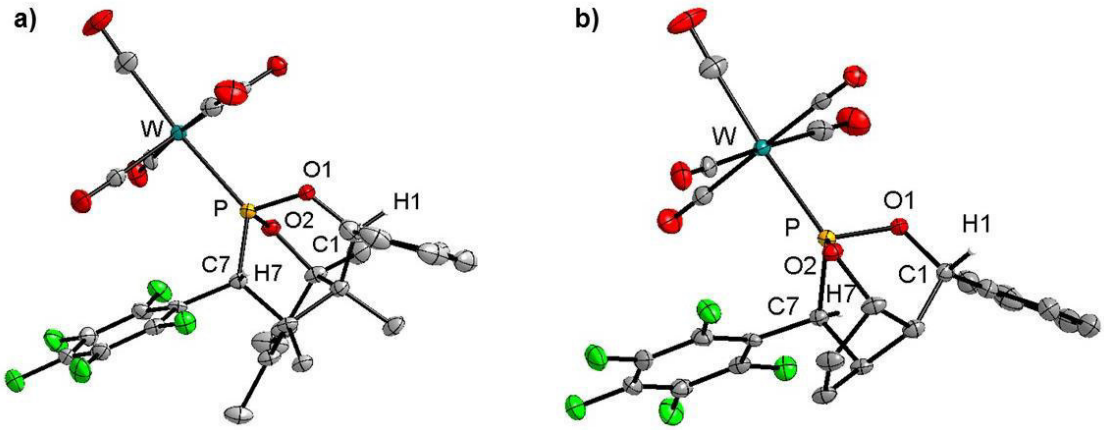

Figure 38. a) Molecular structure of complex **46** (Diamond 3.0, ellipsoids represent 50% probability level). Except C7−H7 and C1−H1, all hydrogen atoms are omitted for clarity. b) Reduced molecular structure of complex **46** (Diamond 3.0, ellipsoids represent 50% probability level). Except C7−H7 and C1− H1, all hydrogen atoms and Cp* methyl groups are omitted for clarity.

Table 19. Bond lengths and bond angles of complexes **31**[106] and **41.**

Bond lengths [Å]	28[106]	46	Bond angles [deg]	28	46
W-P	2.457(4)	2.4345(7)	O(1)-P-O(2)	107.5(4)	102.1(11)
P-O(1)	1.614(10)	1.613(2)	O(1)-P-C(7)	99.6(2)	96.7(11)
P-O(2)	1.609(11)	1.605(2)	O(2)-P-C(7)	95.1(18)	105.1(11)
P-C(7)	1.829(14)	1.855(3)	C(1)-O(1)-P	125.5(3)	117.1(11)
O(1)-C(1)	1.451(15)	1.459(3)	C(3)-O(2)-P	112.7(3)	117.1(17)

5.1.1.1 Theoretical studies on the O,P,C-cage ligand formation

To get further insight into mechanistic aspects, Espinosa performed quantum chemical calculations (see next page for the level of theory) on the complicated sequence leading to O,P,C-cage complexes. For the sake of simplicity only the potential energy surface (PES) for the reaction of chromium complex **47** (shown in **Scheme 42**) with acetaldehyde to lead the O,P,C-cage complex **48** was inspected.[74]

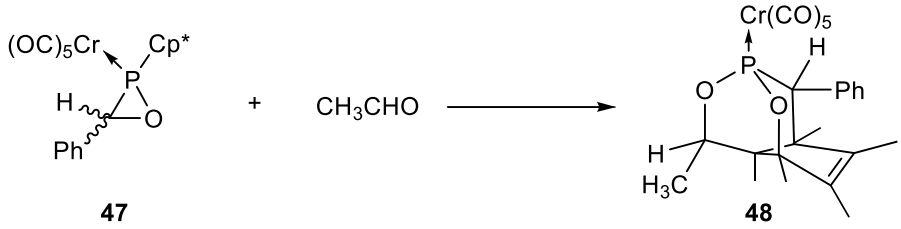

Scheme 42. Selective conversion of oxaphosphirane **47** to **48** used for the theoretical calculation of the cage ligand formation.

The first question to be solved was if the initial step is the cleavage of the endocyclic P-C or C-O bond. Noteworthy might be here to mention the recent report that related azaphosphiridine complexes undergo N,P,C-cage formation initiated by endocyclic P-C bond cleavage.[110] In a preliminary approach and for the sake of performing high-level calculations at a reasonable computational cost, uncomplexed model oxaphosphirane species were evaluated with regard to the cleavage of the two weakest endocyclic bonds. At the DLPNO-CCSD(T)/def2-QZVPP level of theory the C-O bond cleavage (i) is rather exergonic for the parent oxaphosphirane ring **XLVIa** (**Scheme 43**, **Table 20**). It also possesses a slightly lower energy barrier than the very endergonic endocyclic P-C bond cleavage (ii). The introduction of particular substituents able to stabilize an adjacent positive charge at the ring carbon atom, *i.e.* a CH_3 group in model derivatives **XLVIb,d**, and others, *i.e.* a SiH_3 group in **XLVIc,d**, able to stabilize a negative charge at phosphorus slightly favour both ring opening processes (**Table 20**), but keep the C-O bond cleavage as the (almost) preferred pathway.

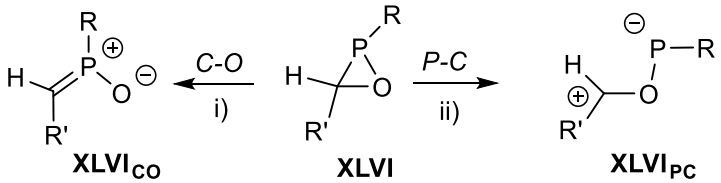

	R	R'
a	H	H
b	H	CH_3
c	SiH_3	H
d	SiH_3	CH_3

Scheme 43. Endocyclic bond cleavage processes i) and ii) in model oxaphosphiranes **XLVIa-d**.

Table 20. Computed (DLNPO-CCSD(T)/def2QZVPP) Relative energies (kcal/mol) for endocyclic bond cleavage processes (i) and (ii in model oxaphosphiranes **XLVI**).[110]

Entry	ΔE^{TS}_{CO}	ΔE_{CO}	ΔE^{TS}_{PC}	ΔE_{PC}
XLVIIa	41.57	-11.49	42.31	33.49
XLVIIb	39.71	-6.52	39.57	33.56
XLVIIc	38.78	-14.43	40.53	31.59
XLVIId	36.66	-19.18	37.23	30.14

It can be expected that the real system **47** (**Scheme 44**) behaves along this line as it bears a *C*-phenyl substituent which stabilizes the positive charge in both P-C and P-O endocyclic bond cleavage intermediates **49** and **50**, respectively **Scheme 44**. Consequently, it would favour both ring cleavage processes, whereas the presence of the metal fragment can additionally stabilize the negative charge developed at P after P-C bond cleavage and, hence, qualitatively favouring this latter pathway. This is further supported by the computed energetics for both processes in **51** (**Figure 39**).[23] In consequence, this rules out the P-C bond cleavage route, and points to a C-O cleavage as the rate determining step in the O,P,C-cage complex formation, at least in the formation of **52**.

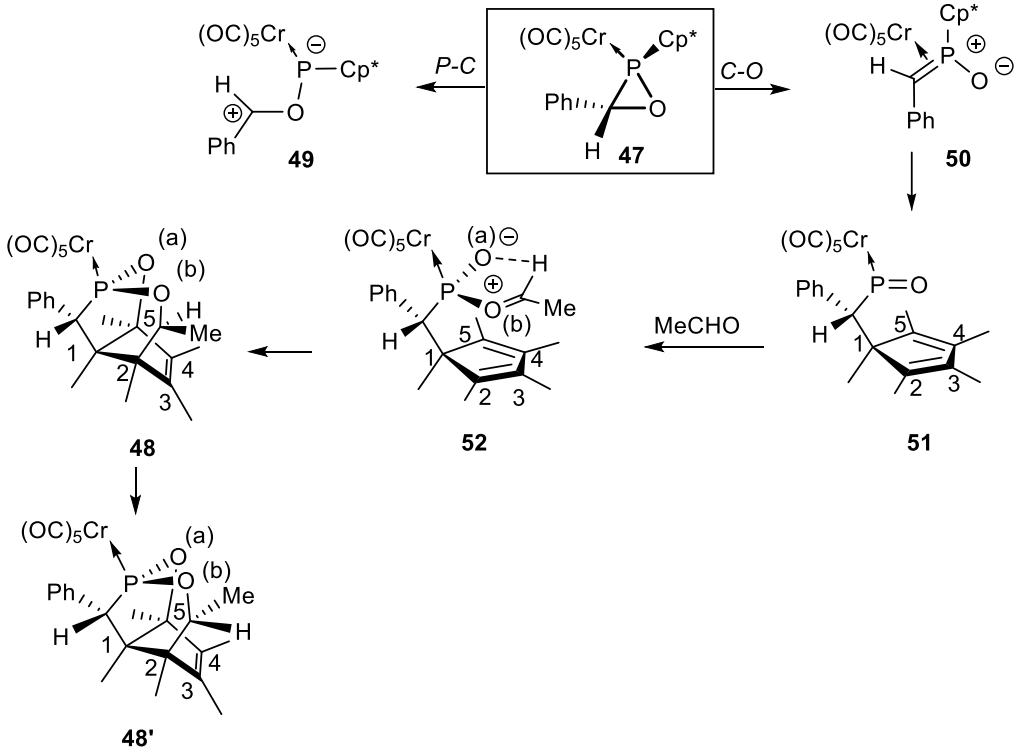

Scheme 44. Calculated mechanism for the formation of O,P,C-cage complex **48** as well as other minima on the PES starting from **47** and acetaldehyde.[110]

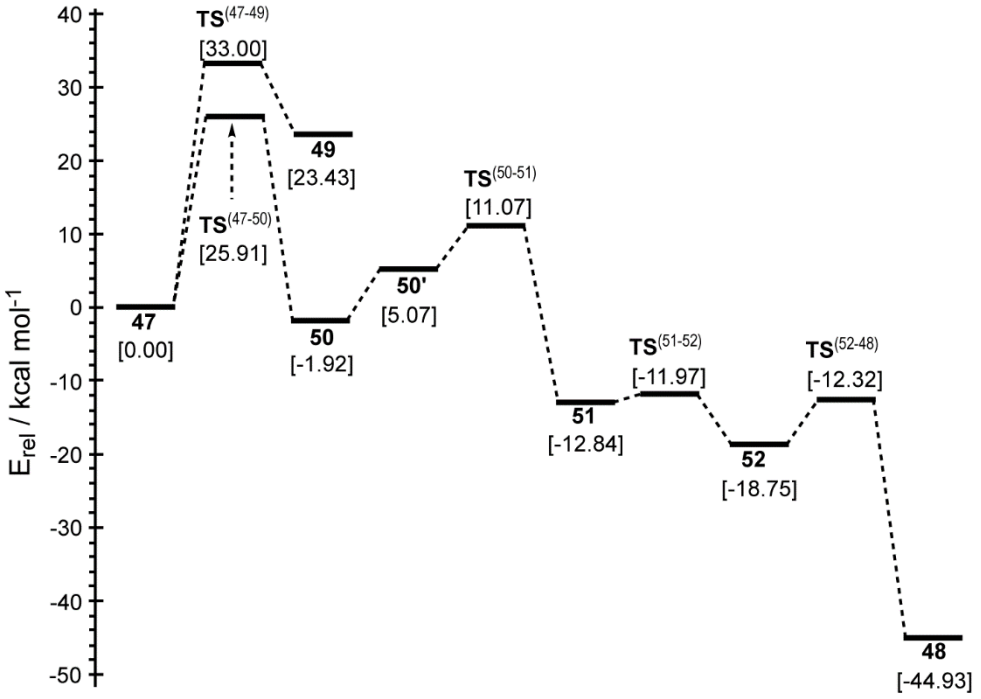

Figure 39. Calculated ($COSMO_{toluene}$/B3LYP-D3/def2-TZVPP//$COSMO_{toluene}$/B3LYP-D3/def2-TZVP) minimum energy profile for the conversion of **47** into **48**.[110]

Moreover, it can be assumed that the following reaction sequence starts with formation of a van der Waals complex between oxaphosphirane complex **47** and the aldehyde CH_3CHO. Generation of this **47**·$OHCCH_3$ complex entails a strengthening of the endocyclic C-P and P-O bonds whereas the C-O bond is weakened, as shown by the variation of bond strength descriptors (VBSD)[111,112] using several commonly used parameters such as the Wiberg bond index (WBI),[113] Löwdin bond order (LBO),[114] Mayer bond order (MBO)[115] or the electron density at bond critical points (ρ(r)) in the framework of Bader's atoms-in-molecules (AIM) theory[116] (**Table 21**). Furthermore, the initial van der Waals complex also increases the ring strain as shown by the increase in the Lagrange of the kinetic energy density at ring critical points, *G(r)*, which was recently reported to correlate with ring strain energies within related systems.[117] Worth mentioning is that complex **50** is the result of not only C-O bond cleavage in **47** but also of an additional migration of the $Cr(CO)_5$ metal fragment from P (*end-on* complex) to a *side-on* coordination at the C=P bond.

According to the calculations, complex **50** must undergo a P-Cp* bond rotation (**50'**) to allow for a [2,3] shift of the Cp* group from P to the adjacent C atom. This exergonic, low-barrier rearrangement is accompanied by a back-shift of the pentacarbonylmetal group to phosphorus resulting in an *end-on* coordination mode and leading to a terminal phosphinidene oxide complex **51** as the key intermediate. The expected

electrophilicity for phosphinidene complexes, in general, is partly reduced in this particular case due to *through-space* electron density donation from a neighboring C=C unit to a formally vacant 3*p* atomic orbital at P ($d_{P\cdots C2}$ = 2.724 Å; $\Sigma WBI_{P\text{-}C2/C3}$ = 0.151; LBO = 0.187; MBO = 0.218), which results in a relatively stable complex. Furthermore, using the Natural Bond Orbital (NBO) analysis[118] this corresponds to a $\pi_{(C2=C3)} \rightarrow p_P$ electron transfer with an associated stabilization of 18.82 kcal/mol in the second order perturbation theory (SOPT) analysis of the Fock matrix in NBO basis. The aldehyde reagent CH_3CHO interacts via its basic O atom with the electrophilic P atom in **51** affording adduct **52** (**Scheme 44**) in a slightly exergonic and almost barrierless process (**Figure 39**).

Table 21. Computed (B3LYP-D3/def2-TZVPP) bond-strength and ring strain related descriptors and their variation in complexes **47** and **47**·$OHCCH_3$.[110]

Entry		**47**	**47**·$OHCCH_3$	**Δ** (%)
	P-C	0.843	0.849	0.75
WBI	P-O	0.696	0.704	1.09
	C-O	0.947	0.940	-0.64
	P-C	1.047	1.053	0.63
LBO	P-O	1.318	1.331	0.98
	C-O	1.384	1.375	-0.69
	P-C	0.967	0.999	3.31
MBO	P-O	0.924	0.941	1.85
	C-O	0.912	0.892	-2.16
	P-C	0.1567	0.1604	2.37
ρ(r), e/a_o^3	P-O	0.1572	0.1588	1.01
	C-O	0.2425	0.2406	-0.79
G(r), au		0.1594	0.1653	3.67

Opposite to the case of **47**·$OHCCH_3$, the interaction in **52** cannot be considered as a van der Waals complex, as far as a moderately strong but genuinely covalent P-O$^{(b)}$ bond is formed ($d_{P\text{-}O}$ = 1.952 Å; WBI = 0.347; LBO = 0.696; MBO = 0.521; ρ(r) = 9.25 x $10^{-2} e/a_o^3$) (compare to the values for **47** in **Table 21**; $d_{P\text{-}O}$ = 1.673 Å). The high diastereoselectivity in the formation of the final O,P,C-cage complex **48** arises from the

selective orientation of the aldehyde in **52** by means of a second anchoring point between the H atom and $O^{(a)}$ atom attached to P ($d_{O\cdots H}$ = 2.299 Å; WBI = 0.007; ρ(r) = 1.66 x 10^{-2} e/a_o^3), in addition to a π-stacking (π-acceptor/donor) interaction between the carbonyl group and the Cp* mean plane (distance from the carbonyl C atom to Cp* mean plane: 2.784 Å; ΣWBI = 0.126; one BCP ρ(r) = 1.68 x 10^{-2} e/a_o^3, ε = 1.130). The above mentioned interactions are easily visualized by means of reduced electron density (RDG) isosurfaces using the NCIplot technique (**Figure 40**).[32,33] Such a docking fixes the acetaldehyde unit and enables an intramolecular 1,4-addition of the nucleophilic $O^{(b)}$ atom and the electrophilic carbonyl C atom across the Cp* diene moiety affording exergonically the stable O,P,C-cage complex **48**.[119]

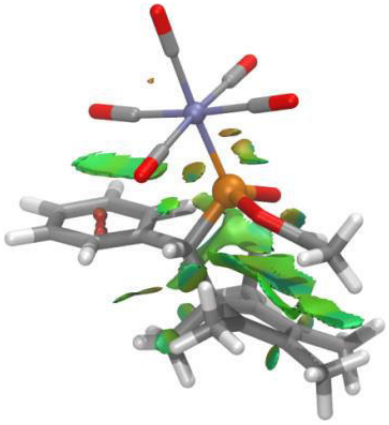

Figure 40. Computed ($COSMO_{toluene}$/B3LYP-D3/def2-TZVPP//$COSMO_{toluene}$/B3LYP-D3/def2-TZVP) most stable structure for **52** with NCIplot highlighting key stabilizing NCIs. The RDG s = 0.3 au isosurface is colored over the range -0.07 < sign(λ_2)·ρ< 0.07 au: blue denotes strong attraction, green stands for moderate interaction, and red indicates strong repulsion.[110]

It is worth mentioning that epimerization at the newly formed chiral center (the position arising from the carbonyl C atom) in **48** is a slightly exergonic process (relative energy E_{rel} = -46.42 kcal/mol for **48'**) because 1,4-diaxial interactions in the boat-shaped six-membered ring decrease, but requires to pass a very high energy barrier (ΔE^{TS} = 70.19 kcal/mol), which in practice is not affordable.

5.2 Acid-induced ring expansion reactions of *C*-pentafluorophenyl-*P*-triphenylmethyl oxaphosphirane complexes

Dioxaphospholanes are five-membered heterocycles bearing one phosphorus and two oxygen atoms. They are key compounds in the synthesis of phosphorus containing polymers and agrochemicals and have been exploited as indispensable tools in biochemistry and molecular biology of nucleic acids.[20] As described in the introductory part, until now only a few examples of 1,3,4-dioxaphospholane complexes **XV** are known (E = ML_n), and there is also not much literature about their P^V analogues.

XIV **XV** **XVI** **XVII**

Scheme 45. Dioxaphospholanes **XIV** - **XVII** (R: organic substituent, halogen, hydrogen or -OH; E: free electron pair, double bond to oxygen or metal complex).

The first 1,3,4$\sigma^3\lambda^3$-dioxaphospholane complexes were synthesized by Bode[120] through thermolysis of *P*-Cp* substituted 2*H*-azaphosphirene complex **XLVII** in the presence of aldehydes (**Scheme 46**).

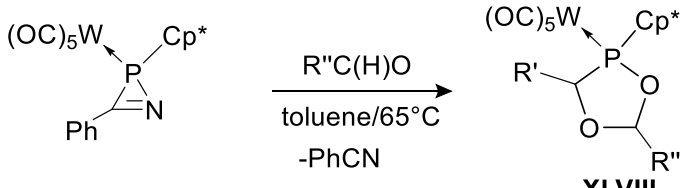

XLVII **XLVIII**

Scheme 46. Synthesis of 1,3,4-dioxaphospholane complexes **XLVIII**.[104]

Shortly afterwards, Pérez[121] developed a new methodology for the ring expansion reaction of oxaphosphirane complex **XLIX** (**Scheme 47**), being the first example of a Brønsted acid-induced ring expansion of a transition metal coordinated $\sigma^3\lambda^3$-oxaphosphirane to give 1,3,4-dioxaphospholane complexes **L**. This protocol is based on the selective insertion of the π-system of aldehydes into the P,O bond of oxaphosphiranes **XLIX** yielding diasteromeric mixtures of 1,3,4-dioxaphospholane complexes with C^2,C^5 unsymmetrical substituents which are difficult to synthesize under other conditions. This study revealed that the ring expansion of aryl-substituted oxaphosphirane complexes of the type **XLIX** using trifluoromethyl sulfonic acid (triflic acid) is demanding concerning precise reactions conditions, because protonation and

deprotonation processes needed to be executed within a very narrow temperature regime: below -30°C protonation was not effective as was deprotonation well above -30°C. The protonated five-membered ring ligand (TfOH-L, two isomers) decomposed to give a mixture of *side*-on *E,Z*-methylene phosphonium complexes **LI** (Scheme 2).[121]

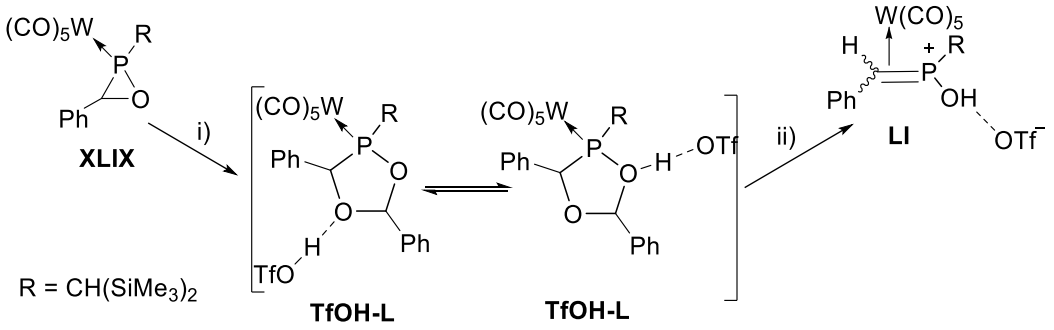

Scheme 47. Formation of methylene phosphonium complexes **LI:** i): PhC(H)O, TfOH, -30°C; ii): -20°C, -PhC(H)O.[105]

During the present work, fluoro-substituted phenyl aldehydes were successfully employed in the synthesis of oxaphosphirane complexes.[84] The electron withdrawing fluorophenyl substituents showed a significant influence on the electronic situation of this heterocycle and revealed interesting noncovalent M(CO)-π(aryl) interactions.[84]

Surprisingly, the *C*-pentafluorophenyl substituted oxaphosphirane complex **22** neither reacted at -30 C, as reported previously for the *C*-phenyl derivative **XLIX**,[121] nor at ambient temperature with aldehydes having different content of fluorine atoms. Therefore, complex **22** was treated in CH_2Cl_2 with TfOH in the presence of the aldehydes represented in **Scheme 48** under refluxing conditions for 2h. Upon addition of NEt_3 and subsequent work-up the 1,3,4-dioxaphospholane complexes **53-55** were obtained in high diastereomeric selectivity in good to excellent yields (**53**: 70%; **54**: 80%, **55**: 84%) after column chromatography.

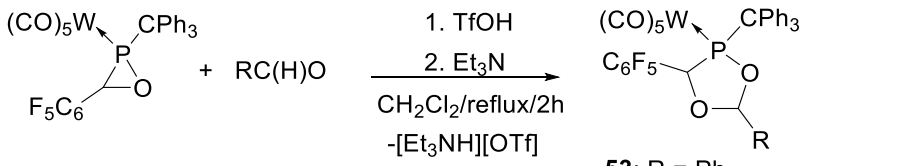

53: R = Ph
54: R = 2,6-difluorophenyl,
55: R = C_6F_5

Scheme 48. Ring expansion of **25** to yield 1,3,4-dioxaphospholane complexes **53-55**.

Table 22 displays $^{31}P\{^1H\}$ NMR chemical shifts and corresponding $^1J_{P,W}$ coupling constants of **53-55** compared with literature known compounds **Ld-f**.[121] The presence

of fluorinated *C*-substituents led to downfield-shifted resonances in the ^{31}P NMR spectra by about 30 ppm in the case of **55** compared to **Ld-f**, bearing alkyl and/or aryl substituents without fluorine atoms. Astonishingly, the chemical shifts of **53** and **55**, are comparable to those of **Ld-f** featuring the $CH(SiMe_3)_2$ substituent at phosphorus and aryl substituents at the ring carbon atoms. But the increase in the $^1J_{P,W}$ coupling constant of about 10 Hz was observed for all derivatives **53-55**.

Table 22. $^{31}P\{^1H\}$ NMR data of complexes **53-55** and **Ld-f.**

Compound	δ ^{31}P [ppm]	$^1J_{P,W}$ [Hz]
53	137.0	295.1
54	137.6	297.2
55	162.9	294.6
Ld[a)]	130.0/132.0[b)]	279.7/279.7[b)]
Le[a)]	131.5/129.0[b)]	281.0/279.7[b)]
Lf[a)]	130.6/130.8[b)]	281.0/281.0[b)]

[a)] See ref. [17]; [b)] data of both isomers; **d**: R' = Ph, R'' = Ph; **e**: R' = Ph, R'' = Me; **f**: R' = Ph, R'' = ^{i}Pr

Suitable crystals for X-ray diffractometry of complexes **53-55** were obtained from *n*-pentane at -30°C. The molecular structures are depicted in **Figure 41** and selected bond lengths and angles are given in **Table 23**. All observed bond lengths are in the typical range for the corresponding bonds in 1,3,4-dioxaphospholane ligands.

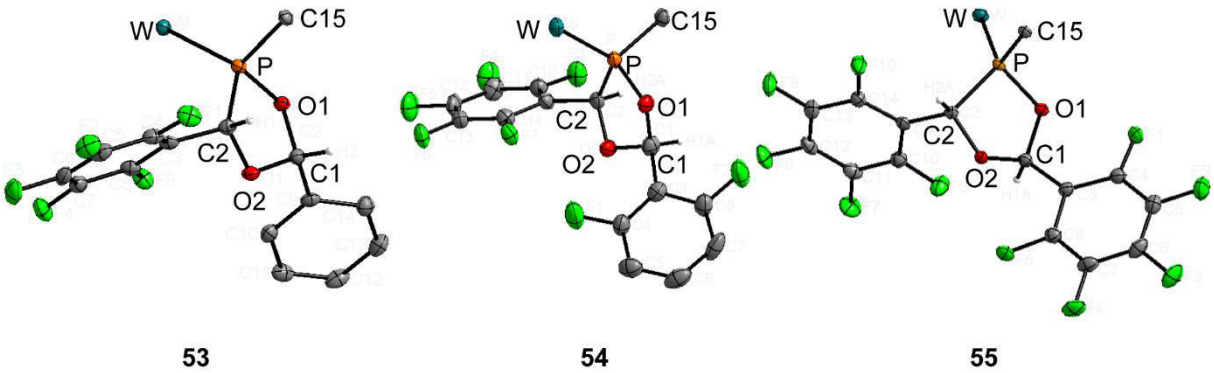

Figure 41. Diamond 3.0 X-ray structures of **53-55** (thermal ellipsoids are at 50 % probability level; carbonyl ligands at the metal atom and phenyls rings at C^{15} are omitted for clarity.

Table 23. Selected bond lengths [Å] and angles [°] of **53-55**.

Bond lengths [Å]	**53**	**54**	**55**
P-W	2.5230(7)	2.5271(14)	2.5090(8)
P-C15	1.949(3)	1.957(5)	1.944(3)
P-O1	1.632(2)	1.639(3)	1.639(2)
O1-C2	1.474(3)	1.454(6)	1.425(4)
C2-O2	1.404(3)	1.406(5)	1.421(4)
O2-C1	1.426(3)	1.437(5)	1.29(4)
C2-P	1.916(3)	1.903(5)	1.890(3)
Angles [°]			
C2-P-O1	90.65(11)	90.54(19)	91.38(13)
P-O1-C1	113.52(16)	112.8(3)	115.6(2)
O1-C1-O2	106.1(2)	107.0(4)	108.9(2)
C1-O2-C2	110.8(2)	108.2(3)	113.1(2)
O2-C2-P	103.19(17)	103.2(3)	103.8(2)
Torsion angle [°]			
C2-P-O1-C1	-9.99(18)	8.8(3)	0.9(1)

Complexes **53** and **54** crystallized in the monoclinic crystal system, while complex **55** has a triclinic system. The central O,P,C-heterocycles show an envelope conformation, and in all complexes **53-55** the oxygen atom O2 is in the *endo* position and stands out of the plane C4-P-O1-C2 plane by 0.357 Å. Besides, a slight enlargement of the P-W distance (**Table 23**) in **53-55** compared to **Ld-f** (**IIId**: 2.497(1) Å; **Le**: 2.502(2) Å; **Lf**: 2.5107(19) Å) can be noted.[121] Interestingly, the protons C1-H and C2-H show different relative orientations: in **53,54** C1-H and C2-H are *cis* orientated, while in **55** both hydrogen atoms are in a *trans* orientation.

Furthermore, the reactivity of the fluorinated Cp*-*P* substituted derivative towards triflic acid and aldehydes to give 1,3,4-dioxaphospholane complexes was also studied (**Scheme 49**).

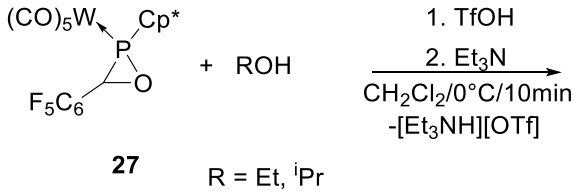

Scheme 49. Reaction of oxaphosphirane complex **27** towards acid-induced ring-expansion.

Since it is known, that the Cp* substituent is able to participate in ring expansion reactions[122], the reaction of Cp*-*P* substituted derivative **27** with triflic acid was investigated without an aldehyde. Following the procedure, explained above, a mixture of several unidentified compounds was obtained. The addition of the phosphophilic nucleophile EtOH as trapping reagent gave 1,3-oxaphospholane complex **60**. Comparable to a known mechanism for a reaction using HBF_4,[122] the addition of TfOH to the oxaphosphirane complex **27** can be explained from the mechanistic point of view as depicted in **Scheme 50**.

First, the protonation of the oxygen ring atom of **27** would give short-lived **56**, followed by the P–O bond cleavage which would result in the acyclic form **57**. Addition of the O-H functionality to the cyclopentadienyl substituent in **57** could furnish selectively the bicyclic 1,3-oxaphospholane complex **58** as proposed in **Scheme 50**.

Subsequent addition of EtOH to the highly electrophilic phosphenium center of **58** followed byelimination of TfOH could result in a selective formation of complex **60**.

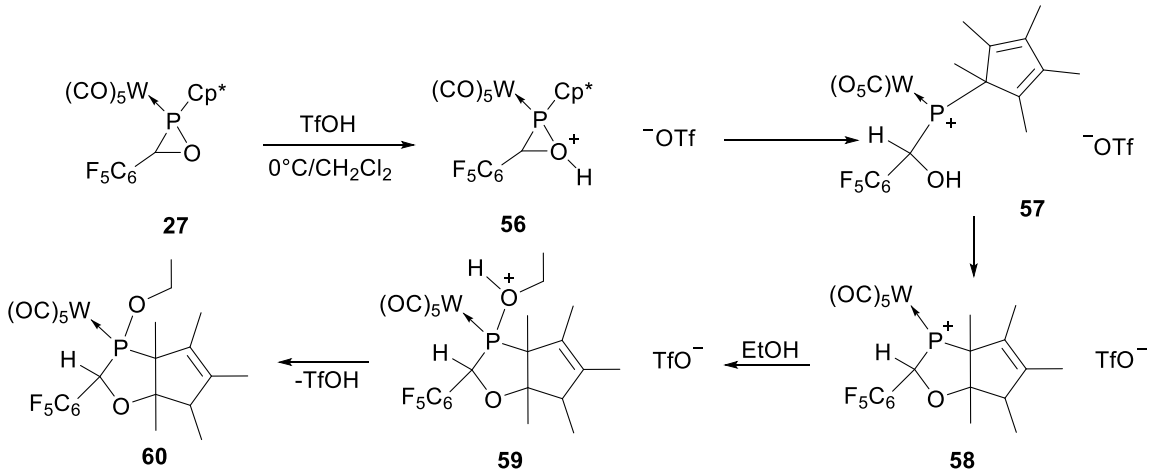

Scheme 50. Proposed mechanism for the reaction of **27** with TfOH in the presence of EtOH.

Complex **60** presents a chemical shift of 178.7 ppm ($^1J_{P,W}$ = 275.4 Hz), and was completely characterized by NMR spectroscopy; the connectivity of the ring ligand framework was confirmed by X-ray crystallography (**Figure 42**).

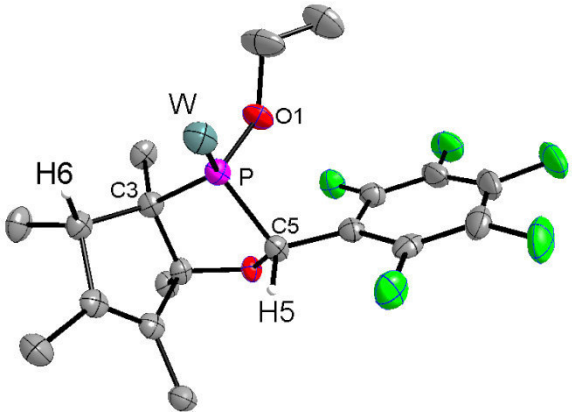

Figure 42. Diamond 3.0 X-ray structures of **60** (thermal ellipsoids are at 50 % probability level; carbonyl substituents of the metal atom and hydrogen atoms, except for H5 and H6, are omitted for clarity. Selected bond lengths (Å) for **60**: P-W 2.5150(13), P-C(5) 1.882(5), P-O(1) 1.610(3), P-C(3) 1.885(5), C(5)-O(2) 1.416(5).

All bond lengths are comparable to those reported by Albrecht for a *P*-F substituted 1,3-oxaphospholane complex[122] and are in the normal range for such bicyclic complexes, *e.g.* the P-W bond length is in **60** slightly enlongated by 0.07 Å compared to the *P*-F substituted complex (2.4431(6) Å). This might originate from the more electronegative fluorine atom than the oxygen atom in **60**, thus leading to a reduced electron density at the corresponding phosphorus atom and an increasing of the back donation from the tungsten atom to the phosphorus, thus resulting in a shorter P-W bond length.

5.3 Reactitivity of oxaphosphirane complexes towards *N*-heterocyclic carbenes

5.3.1 N-heterocyclic carbenes

Carbenes are defined as neutral compounds bearing a divalent carbon atom and six valence electrons. This carbon atom can exhibit a linear or bent geometry, depending on the hybridization of the carbon atom and they will be therefore classified as singlet or triplet carbenes. Singlet carbenes are spin-paired in their ground state and bear a vacant p_π-orbital ($\sigma^2p_\pi^0$, $^1\mathbf{A_1}$, **Figure 43**) and hence, due to their sp^2-hybridization, contain a bent geometry. In the ground state of a sp^2-hybridized triplet carbene ($\sigma^1p_\pi^1$, $^3\mathbf{B_1}$, **Figure 43**),[123] both the p_π and the σ-orbital of sp^2-type are occupied with one

electron of parallel orientation. Another example for carbenes, depicted in **Figure 43**, shows a linear geometry, which implies a sp-hybridization of the carbene center with two parallel orientated electrons in two non-bonding degenerated orbitals (p_x, p_y). These compounds are energetically disfavored compared to the bent carbenes and represent rare examples in carbene chemistry.[124]

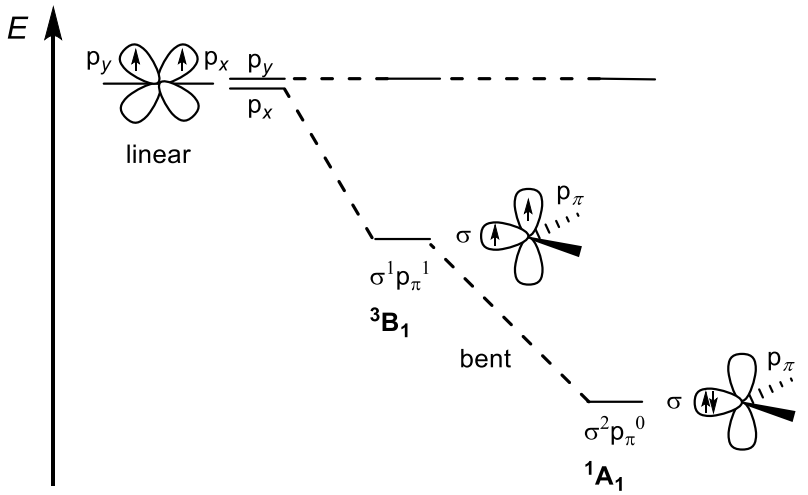

Figure 43. Illustration of the frontier orbitals and electron configuration of carbenes.[124]

The diaminocarbene **LIII** represented in **Scheme 51**, represents the first isolated and crystallographically characterized singlet carbene and was published by Arduengo *et al.* in 1991.[125] This group investigated the reaction of the sterically very demanding 1,3-diadamantylimidazolium chloride **LII**$^{(Ad/H)}$[Cl] with sodium hydride and catalytic amounts of dimethyl sulfoxide (DMSO) in THF. Isolation of the *N*-heterocyclic carbene **LIII**$^{(Ad/H)}$ was a breakthrough in the synthesis of stable and isolable carbenes.

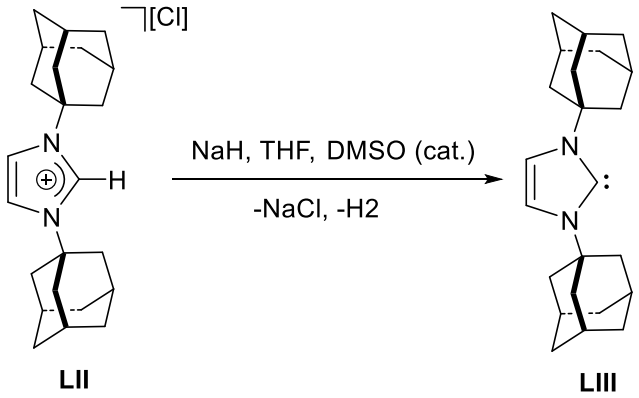

Scheme 51. *Synthesis of N*-heterocyclic carbene **LIII**

In the following 20 years a broad variety of stable NHC's and acyclic heteroatom substituted carbenes were synthesized. Due to their relative stability most of them were isolated and their chemistry was intensively investigated. Reasons why the NHC's are

relatively persistent are the combination of resonance stabilization and steric shielding. **Scheme 52** illustrates the electron-donating effect of the neighbouring group (X = NR in the case of an NHC) into the empty p_π-orbital of the carbene carbon atom. Hence the energy level of the p_π-orbital is raised and the difference of p_π-orbital and σ-orbital increases. Consequently, the singlet ground state is stabilized, rendering this type of carbenes very strong σ-donors.

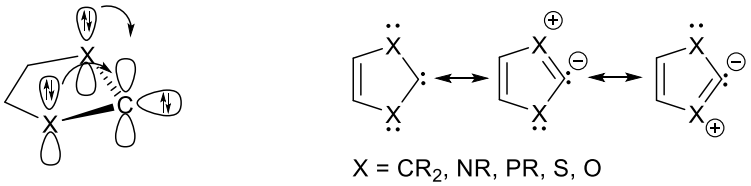

Scheme 52. Electronic configuration in a five membered heterocycle with electron donating substituents (X, left); selected resonance structures of the heterocycle (right).

In the sixties and seventies, among others, the groups of Lappert and Öfele intensively studied the chemistry of NHC transition metal complexes and investigated their reactivity in organometallic chemistry.[27] Besides their strong σ-donating properties, Herrmann *et al.* pointed out that NHC's serve as ligands with similar properties in transition metal chemistry as electron rich organophosphanes PR_3.[28]

Recently the group of Streubel used nucleophilic singlet *N*-heterocyclic carbenes as a strong organic base for the deprotonation of P–H functional phosphane complexes, thus stabilizing phosphinidenoid complexes through weakly coordinating cations.[126] Moreover, they developed a new route to *N*-heterocyclic carbene adducts of terminal phosphinidene complexes by transformation of an oxaphosphirane complex into zwitterion **LVI,**[127] presented in **Scheme 53**, which is a new example of a substitution of a formally *side*-on bound unit to phosphorus by an *end*-on bound unit, *i.e.,* an NHC. In total, this finding resembles transition metal coordination behavior, at least to some extent.

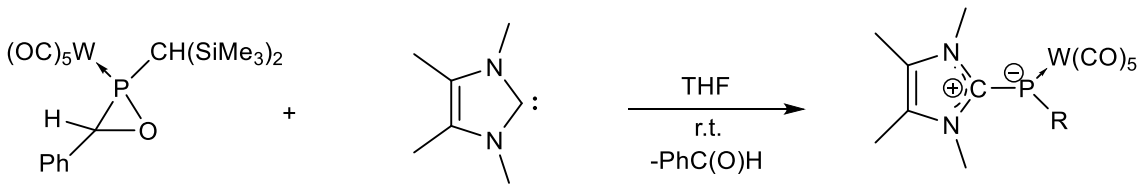

32 **57$^{Me/Me}$** **LVI**

Scheme 53. Reaction of oxaphosphirane complex **35** with an N-heterocyclic carbene.

5.3.2 Experimental results

In the following, the reactivity of *P*-CPh_3 substituted oxaphosphirane complexes towards various *N*-heterocyclic carbenes (NHCs) is discussed. Being strong σ-donors and good bases at the same time, it was of especial interest to examine whether a ring opening or a ligand exchange reaction could take place, either cleaving the P-W bond, thus leading to an unligated oxaphosphirane, or showing a deprotonation at the ring carbon atom. Therefore, N-heterocyclic carbenes with different steric demand (R' = Me, ^{i}Pr) were synthesized (according to established procedures[128]) and reacted with *P*-CPh_3 substituted oxaphosphirane complexes **4c** and **22 (Scheme 54)**.

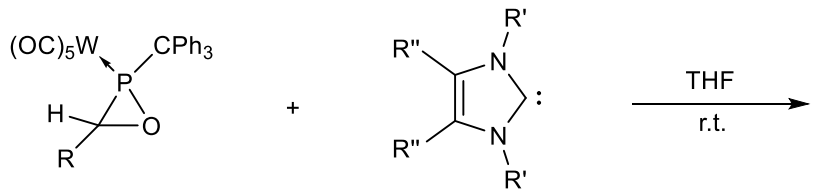

4c, 22 **$61^{R',R''}$**

4c: R = Ph
22: R = C_6F_5

R' R'' = Me
R' = ^{i}Pr, R'' = Me

Scheme 54. Reaction of *P*-CPh_3 substituted oxaphosphirane complexes with **$61^{R'/R''}$**.

5.3.2.1 Reactions of *P*-CPh_3 substituted oxaphosphirane complex 4c towards NHCs

A solution of the *P*-CPh_3 substituted oxaphosphirane complex **4c** in THF was reacted with 1.2 equivalents of the corresponding NHC **61** at room temperature (performed inside the glovebox) as it is depicted in **Scheme 55**.

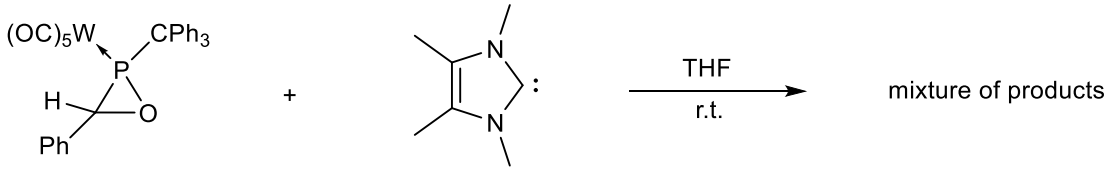

4c **$61^{Me,Me}$**

Scheme 55. Reaction of **4c** and **$61^{Me/Me}$**

The reaction led to a mixture of three main products A, B and C (**Figure 44** violet color-coded spectrum at the top) whose $^{31}P\{^{1}H\}$ NMR data are presented in **Table 25**.

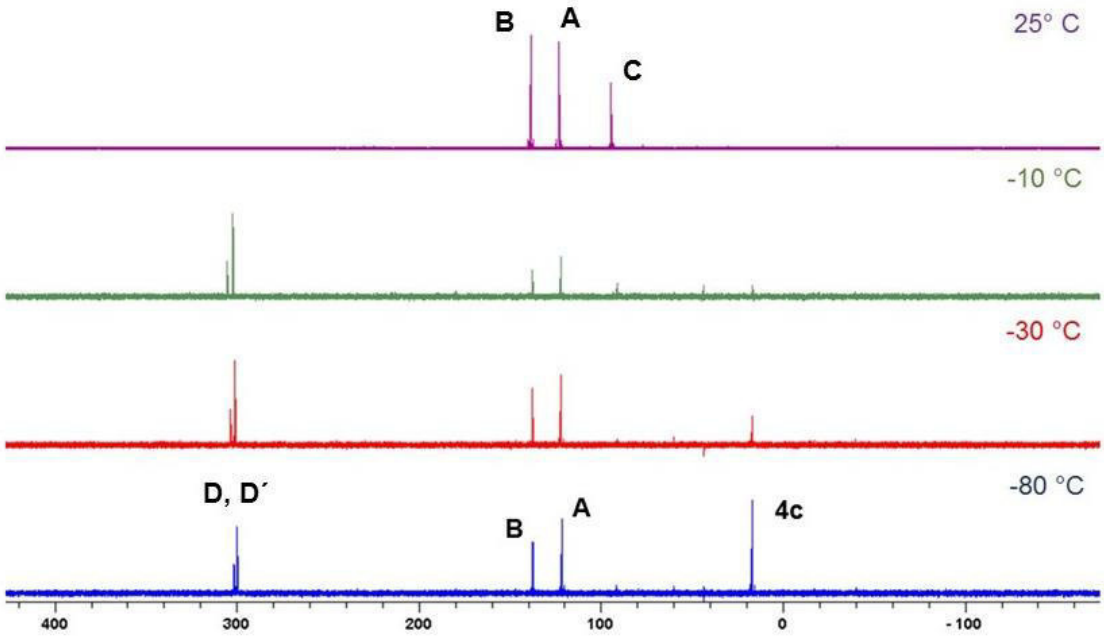

Figure 44. Low temperature $^{31}P\{^{1}H\}$-NMR monitoring of the reaction of **4c** with **61$^{Me/Me}$**

Table 24. $^{31}P\{^{1}H\}$ NMR data of reaction of **4c** with **61$^{Me/Me}$** (shifts in [ppm] and $^{1}J_{P,W}$ in [Hz]

Compound	$^{31}P\{^{1}H\}$	$^{1}J_{P,W}$
A	108.6	280.3
B	136.3	296.8
C	151.7	302.6
D/D´	299.8 / 301.4	99.1 / 100.2

The reaction mixture was analyzed via multinuclear NMR spectroscopy. From the ^{13}C and 2D ^{1}H - ^{31}P HMBC spectrum, it was possible to confirm that the trityl moiety is still attached to the phosphorus atom in all products. The ^{1}H NMR spectrum displays the resonances corresponding to the aromatic protons of the triphenylmethyl group as well as for the methyl protons of the N-heterocylic carbene. Besides, a new resonance appearing at 9.8 ppm was also observed, which may correspond to the C^{2}-H atom of the protonated NHC.[129] This suggests that the NHC reacts as base deprotonating the ring carbon atom of the oxaphosphirane complex, thus leading to the species 65 as shown in **Scheme 56**. All attempts to separate the products were unsuccessful because in THF they slowly decomposed at ambient temperatures to give a

complicated mixture of unidentified products, and a separation (at an early stage) via low temperature column chromatography was unsuccessful.

To get further insights, a low temperature $^{31}P\{^{1}H\}$ NMR monitoring from -80 °C to room temperature was performed revealing that the reaction already started at very low temperature, and resonances D and D' were observed (**Figure 44** blue spectrum at the bottom). These resonances, appearing at low field shift (299.8 ppm for D and 301.4 for D'), together with the small magnitude of their $^{1}J_{P,W}$ coupling constant (99.1 Hz for D and 100.2 Hz for D') may indicate the formation of zwitterionic phosphinidenoid complex 64.[45,62,86] A possible mechanism for this reaction is shown in **Scheme 56** and will be described hereafter. Initially, nucleophilic attack of the oxaphosphirane complex **4c** by **61$^{Me/Me}$** at the ring carbon atom leads to the zwitterionic short-lived phosphinidenoid complex **62** (via P-C bond cleavage) and/or in a competing reaction to the (not observed) oxaphosphiranido complex **63** via deprotonation; **61** may even decompose to yield also **63**. The latter could undergo P-O bond cleavage to form the phosphanido complex **64** which is stabilized due to the delocalization, *i.e.* the phospha-enolate complex **65**, the counter cation being the protonated NHC. Further calculations will help to understand the mechanism and bonding of the species involved.

According to the literature,[45,62,86] the formation of **62** is in agreement with the NMR data observed for D and D' and the complex **65** could be assigned to the resonances represented by A and B, as observed before for similar neutral complexes.[130] The complex C could result from another competing reaction pathway, but its constitution could not be clarified.

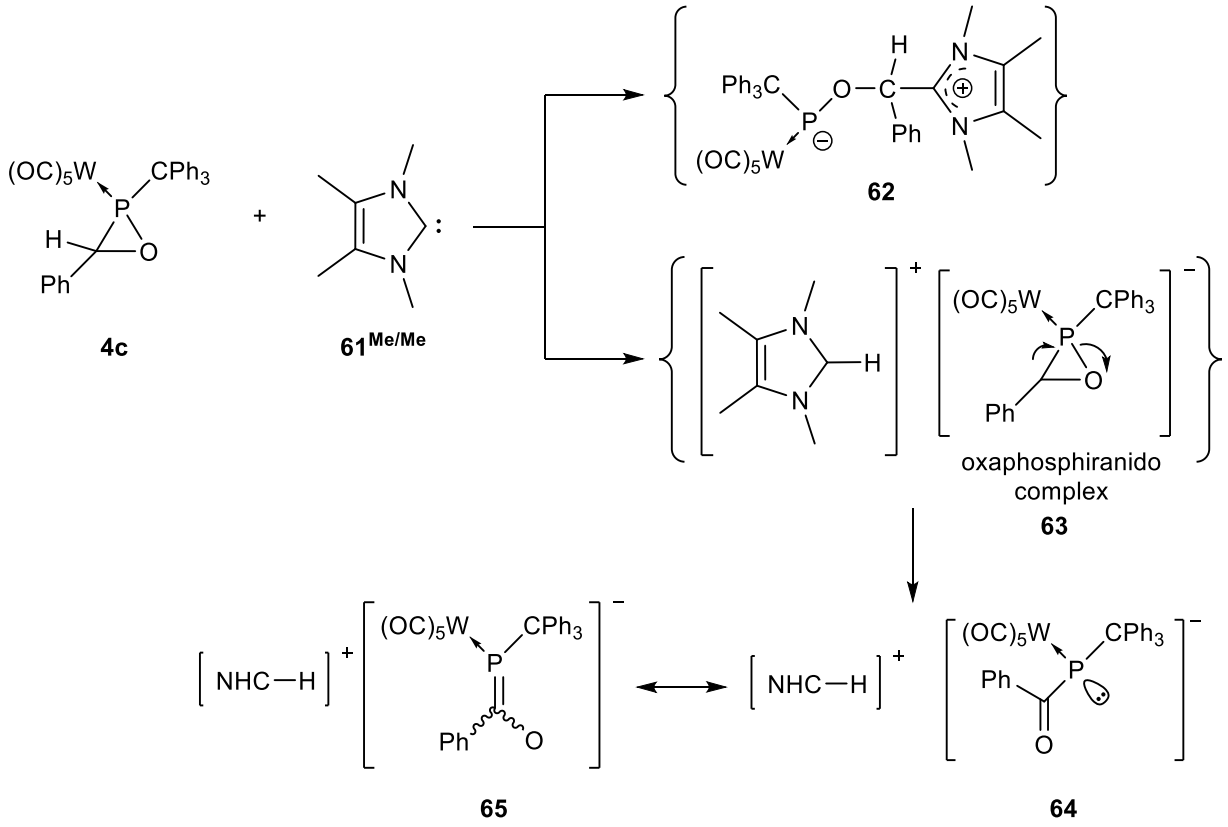

Scheme 56. Proposed reaction course orf the reaction of **4c** with **61$^{Me/Me}$**.

5.3.2.2 Reactions of *P*-CPh$_3$ substituted oxaphosphirane complex 22 towards NHCs

To investigate this reaction further, the fluorinated derivative **22** was employed and the same protocol applied (using a glovebox): **22** was reacted with 1.2 equivalents of the corresponding NHC with different steric demand **61$^{Me/Me}$** or **61$^{iPr/Me}$** at room temperature to selectively lead to tetramethylimidazolium fluorophosphinite complexes **66** and **67**.

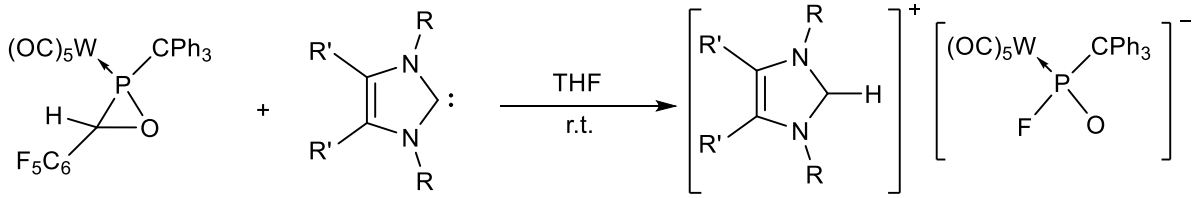

Scheme 57. Reaction of oxaphosphirane complex **22** with NHCs **61$^{R/R'}$**.

A $^{31}P\{^{1}H\}$ NMR spectroscopic measurement of the reaction mixture was performed 10 minutes right after the addition of the NHC to the solution of **22** and the result is shown in **Figure 45**.

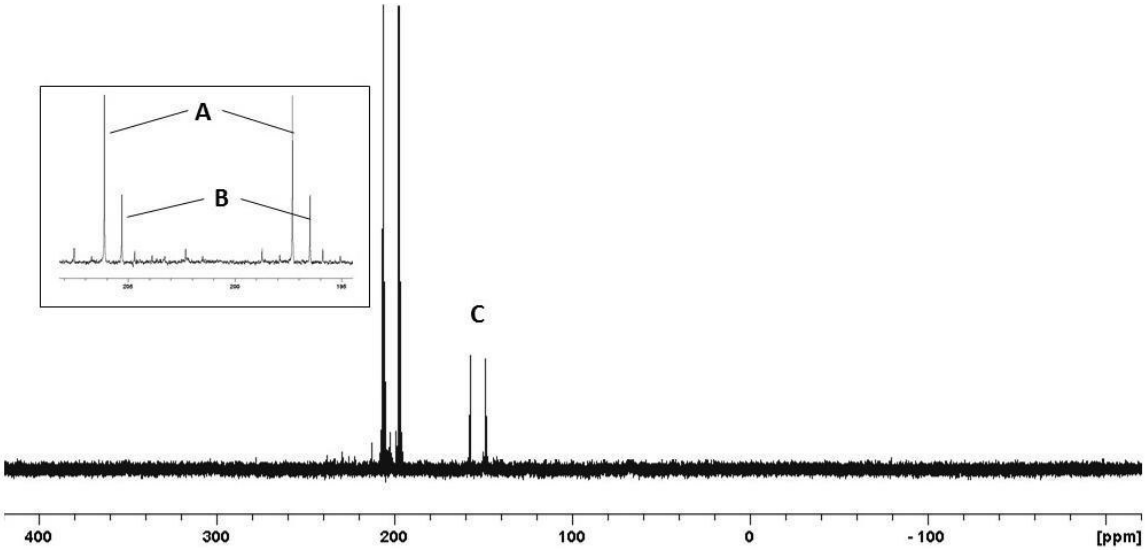

Figure 45. $^{31}P\{^{1}H\}$ NMR spectrum measured 10 min. of the addition of **61$^{Me/Me}$** to a solution of **22**.

The NMR spectrum depicted in **Figure 45** shows that the main phosphorus resonances display each a doublet with ^{183}W satellites; the NMR data of these signals are given in **Table 25**.

Table 25. Selected NMR data (shifts [ppm], ^{n}J[Hz]) of the reaction of **22** with **61$^{Me/Me}$.**

Resonance	^{31}P-NMR	^{19}F-NMR	$^{1}J_{P,W}$	$^{1}J_{P,F}$	$^{2}J_{F,W}$
A	201.7	-60.4	345.5	1070.7	[a]
B	200.9	-60.6	344.6	1071.4	[a]
C	152.7	-33.0	319.8	1032.7	30.3

[a] Not detected

New NMR measurements after hours and days of stirring revealed that resonances A and B decreased while C increased and remained as the resonance for the final product.

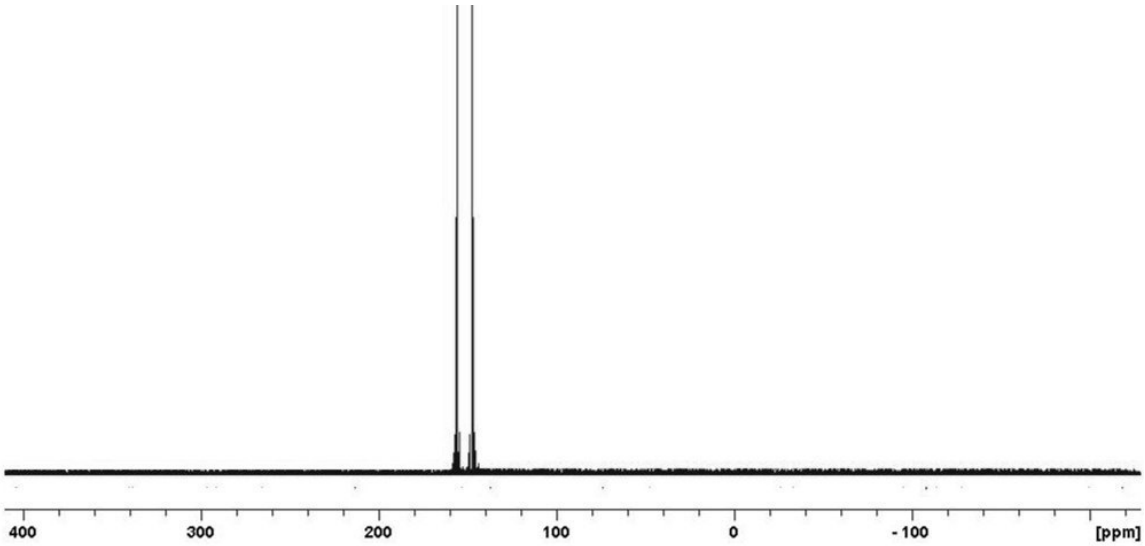

Figure 46. ^{31}P NMR spectrum of the reaction of **22** with **61$^{Me/Me}$** after one week at ambient temperature.

Further multinuclear NMR measurements unveiled that the trityl moiety is still attached to the phosphorus atom. Apart from the aromatic protons of the triphenylmethyl group, the methyl hydrogen atoms of **61$^{Me/Me}$** were also observed, as well as a resonance at 10.6 ppm (integration corresponding to one proton) which according to the literature[129] could correspond to the NHC-H imidazolium. $^{19}F\{^{1}H\}$ NMR analysis showing 4 different resonances at -138.4, -142.2, -143.7 and -162.3 ppm. In general, pentafluoro substituted aromatic rings show 3 resonances.[131] This may indicate the presence of a non-symmetrically substituted tetrafluorinated ring. The fifth fluorine atom should be the one coordinated to phosphorus, as the NMR analyses indicates (**Table 25**).

After purification, suitable crystals for X-ray analysis were obtained for **66** and **67** as **Figure 47** and **Figure 48** show.

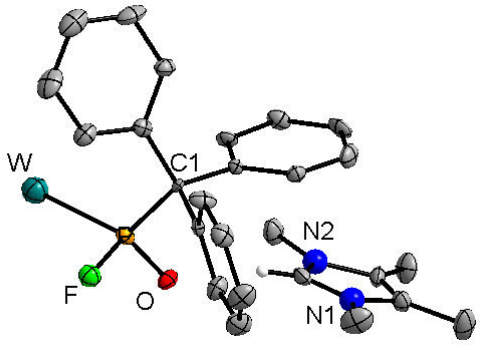

Figure 47. Diamond 3.0 X-ray molecular structure of **66** (thermal ellipsoids are at 50 % probability level; carbonyl ligands at the metal atom, hydrogen atoms, except for N-H, are omitted for clarity. Selected bond lengths (Å) for **66**: P-W 2.544(3), P-C(1) 1.937(9), P-O 1.492(8), P-F 1.633(7), O···H_{NHC} 2.1768(1).

A related lithium fluorophosphinite complex was obtained by Nesterov[132] as decomposition product of a *P*-nitroxyl phosphane complex from a reaction of an Li/F phosphinidenoid complex with a mixture of triphenylcarbenium tetrafluoroborate and TEMPO. This compound shows comparable NMR data and bond lengths and angles, meaning that the counter cation has a rather small influence on these parameters.

A similar result was obtained by reacting oxaphosphirane complex **22** with the N-heterocyclic carbene **61$^{iPr/Me}$**. The X-ray crystallography analysis confirmed the connectivity as displayed in **Figure 48**. And selected NMR data of **66** and **67** are represented in **Table 26**

Table 26. Selected NMR data; shifts in [ppm] and $^{1}J_{P,W}$ in [Hz] of **61** and **62**.

Compound	$^{31}P\{^{1}H\}$	$^{1}J_{P,W}$	$^{19}F\{^{1}H\}$	^{1}H-N
66	152.7	319.8	-33.0	10.6
67	148.5	319.7	-33.0	10.9

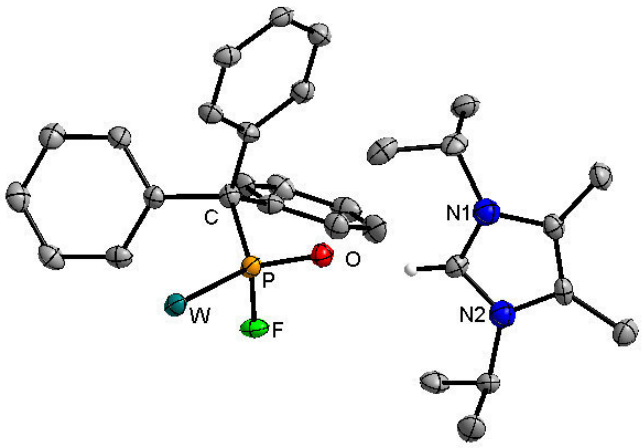

Figure 48. Diamond 3.0 X-ray structures of **67** (thermal ellipsoids are at 50 % probability level. All hydrogen atoms, except for N-H, are omitted for clarity. Selected bond lengths (Å) for **67**: P-W 2.5362(17), P-C 1.935(6), P-O 1.505(4), P-F 1.615(4), O···H_{NHC} 2.0758(1).

In order to get first insights into the pathway, a preliminary theoretical study was done by Sasamori analyzing the possible pathways at the B3PW91/6-311G level of theory.[133]

The first hypothesis to be analyzed was the deprotonation of the H-C proton of the oxaphosphirane ring **22** by **61$^{Me/Me}$**, as depicted in **Scheme 58**, to give the

deprotonated complex, the oxaphosphoranido complex **68**. But as this reaction is endergonic by +78 kcal/mol, it is unfavorable.

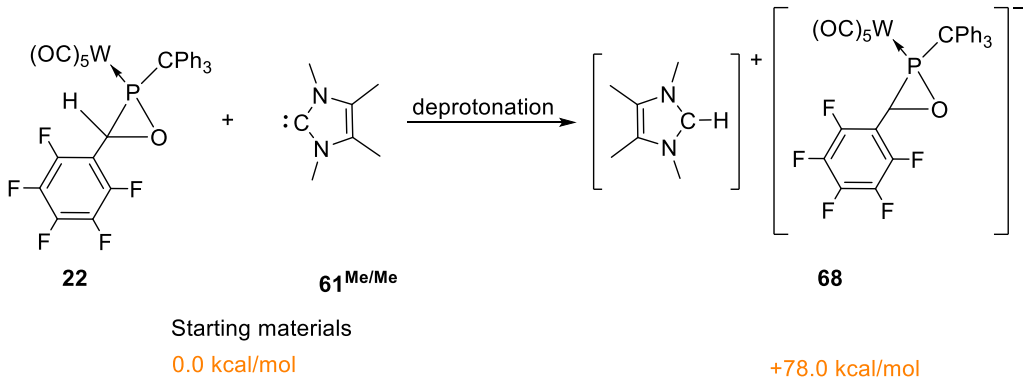

Scheme 58. Deprotonation of **22** by **57**$^{Me/Me}$.

According to earlier calculations of Frontera,[84] the LUMO of the oxaphosphirane complex **22** is largely localized at the *ortho* and *para* position of the C_6F_5 ring, the nucleophilic attack of the NHC at the *para* carbon position was the next to be considered. In this case, the migration of a fluoride anion towards a CO ligand of the $W(CO)_5$ group giving the product **69** could occur; **69** is slightly more stable than **22**/**61**$^{Me/Me}$ by -4.0 kcal/mol (**Scheme 59**).

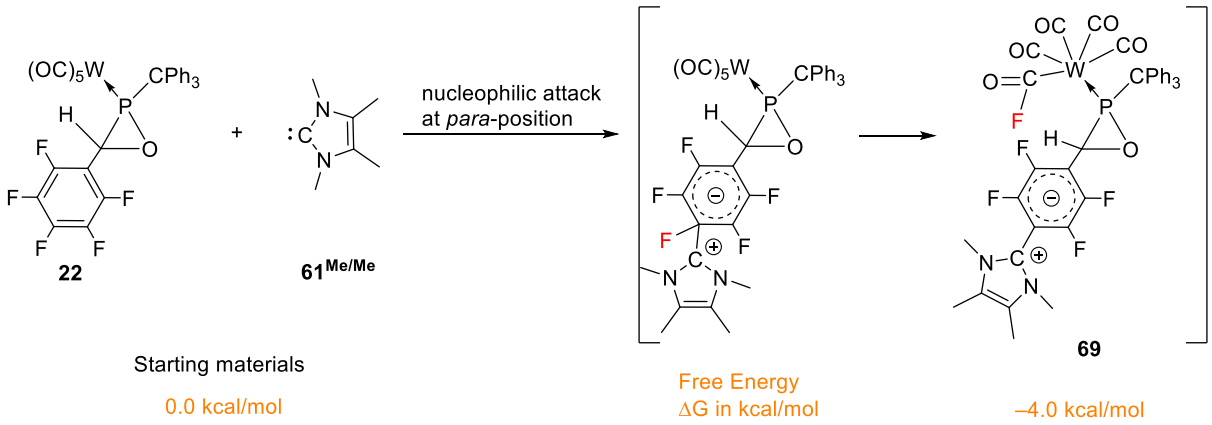

Scheme 59. Nucleophilic attack at the *para* position of the fluorinated ring in **22**.

In case the NHC is attacking the *ortho* position, a migration of a fluoride to the phosphorus atom to give **70** in an exergonic reaction (-19.3 kcal/mol; **Scheme 60**) could be favorably envisaged.

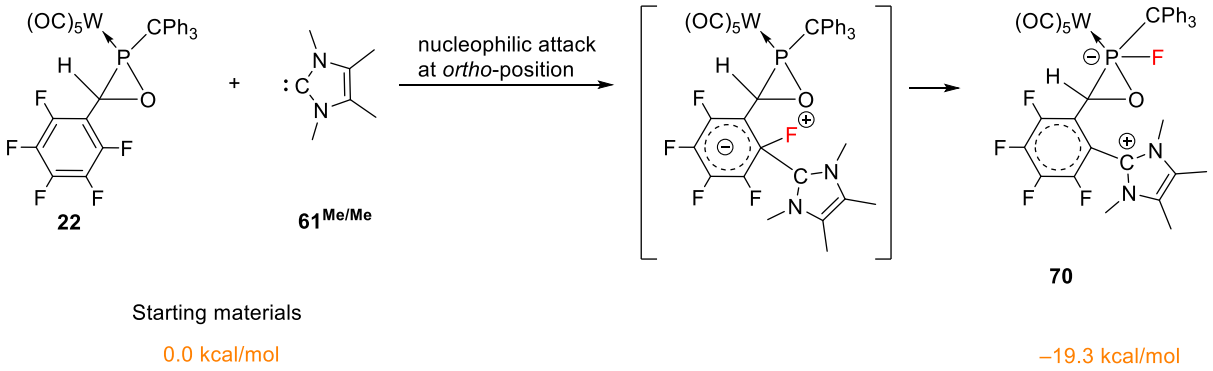

Scheme 60. Nucleophilic attack at the *ortho* position of the fluorinated ring in **22**.

For the subsequent reactions two different pathways were considered (**Scheme 61**). The first possibility (i) is the dissociation of the aldehyde moiety to give **71** (-1.8 kcal/mol) as the phosphorus atom in **70** (**Scheme 60**) is highly coordinated**.** The second possibility (ii) is the P-C endocyclic bond cleavage of **70** to give **72**, representing an exothermic process of 13.3 kcal/mol (**Scheme 61**).

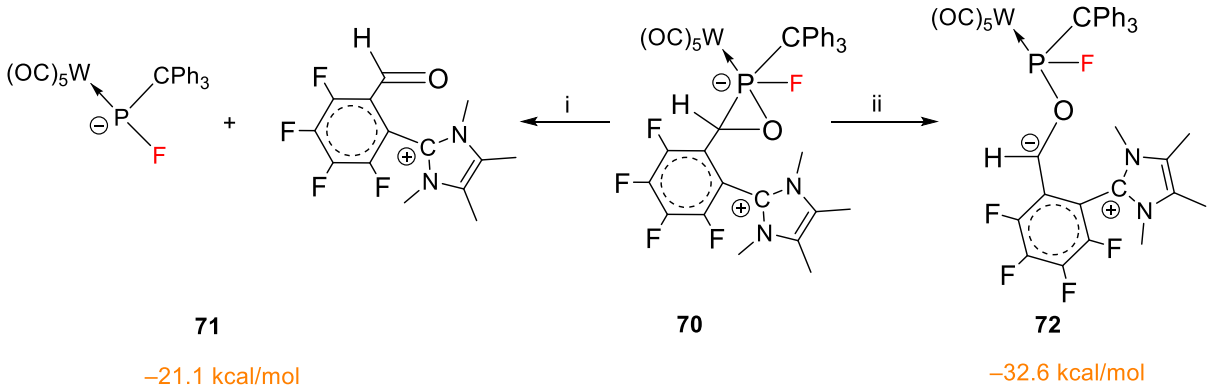

Scheme 61. Dissociation of the aldehyde moiety to **71** and endocyclic P-C bond cleavage to **72**.

To obtain the final product, as confirmed by the X-ray analysis, the presence of moisture seems to be necessary. The reaction of **72** with water leads to the elimination of the partially fluorinated aldehyde moiety and formation of the final product, salt **66** (**Scheme 62**). The partially fluorinated aldehyde was observed in the $^{19}F\{^{1}H\}$ NMR spectrum showing 4 different resonances at -138.4, -142.2, -143.7 and -162.3 ppm, whereas, in general, pentafluoro substituted phenyl rings show only 3 resonances.[131] This indicates the presence of a non-symmetrically tetrafluorinated phenyl ring, while the “fifth” fluorine atom should be the one bound to phosphorus of the final product.

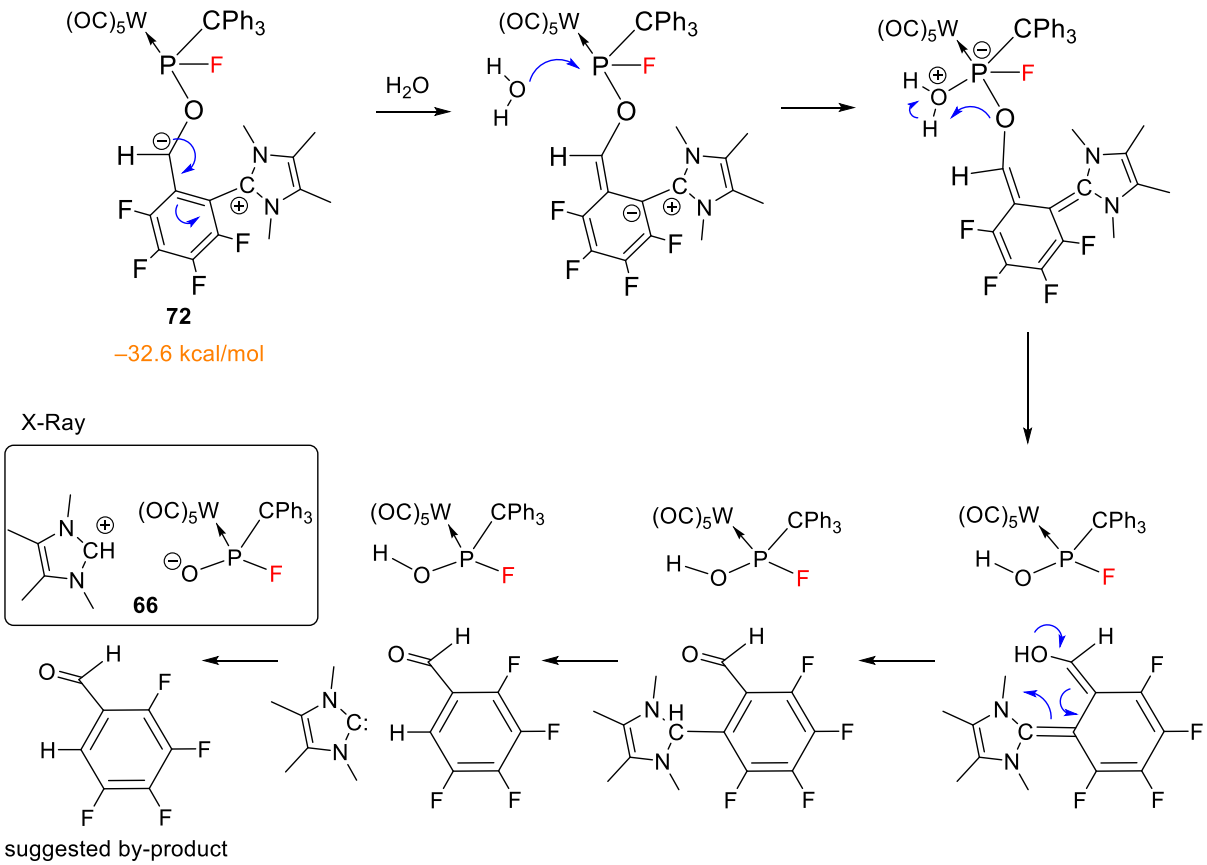

Scheme 62. Reaction of **72** with a water molecule and subsequently formation of **66**.

The reaction was also tested by using the fluorinated chromium complex **23** to examine if the nature of the transition metal could have any influence in the reaction process.

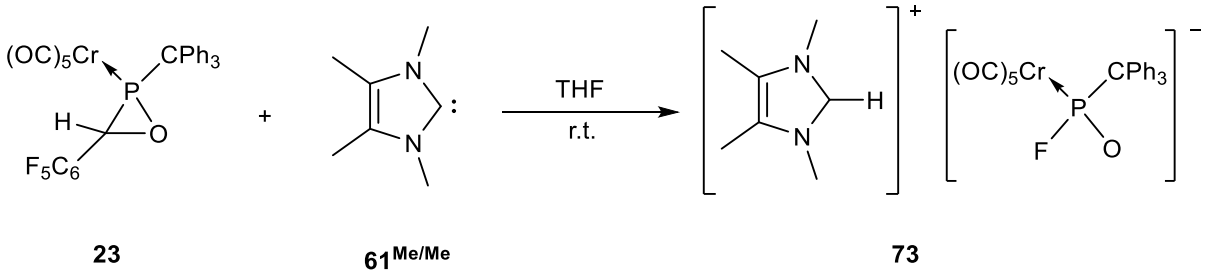

23 **61$^{Me/Me}$** **73**

Scheme 63. Reaction of oxaphosphirane complex **23** with **61$^{Me/Me}$**.

Although, the molecular structure of **73** could not be confirmed by X-ray analysis, the multinuclear NMR data reveal the formation of the tetramethylimidazolium fluoro-phosphinite complex **73**. A comparison of the data obtained for **66** and **73** is summerized in **Table 27**.

Table 27. Selected NMR data shifts in [ppm] and $^{1}J_{P,X}$ in [Hz] of **66** and **72.**

Compound	M	$^{31}P\{^{1}H\}$	$^{1}J_{P,W}$	$^{19}F\{^{1}H\}$	$^{1}J_{P,F}$
66	W	152.7	319.8	-33.0	1033.2
73	Cr	188.6	-	-33.0	1062.6

To examine if an intermolecular fluoride transfer is also feasible, it was then decided to react oxaphosphirane complex **22** with **61$^{Me/Me}$** in the presence of a fluoride donor such as TBAF (tetra-*n*-butylammonium fluoride). But this reaction led only to a complicated mixture of phosphorus compounds, all of them displaying a direct coupling to a fluorine atom.

But if the reaction of oxaphosphirane complexes **22, 23** with TBAF was performed in the absence of **61$^{Me/Me}$** the tetrabutylammonium fluorophosphinite complexes **74, 75** were selectively obtained (**Scheme 64**) which could be isolated and fully characterized.

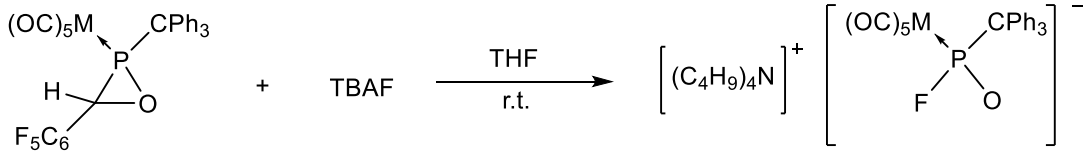

22: M = W
23: M = Cr

TBAF =
tetra-n-butylammonium fluoride

74: M = W
75: M = Cr

Scheme 64. Reaction of oxaphosphirane complexes **22** and **23** with TBAF.

It was possible to confirm the constitution of **75** by single-crystal X-ray analysis and the molecular structure is shown in **Figure 49**.

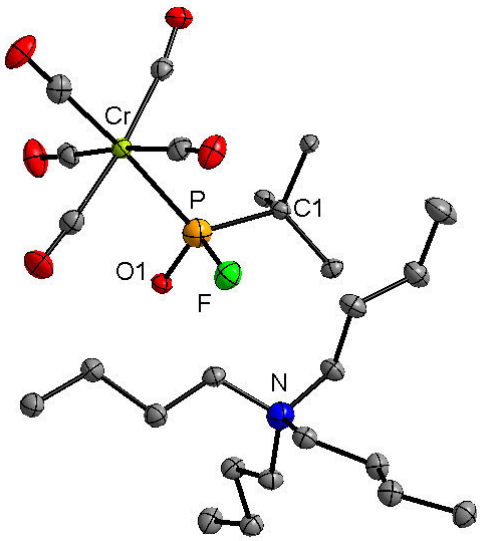

Figure 49. Diamond 3.0 X-ray structures of **75** (thermal ellipsoids are at 50 % probability level. All hydrogen atoms and, except for the *ipso* carbon, the phenyl rings of the trityl moiety are omitted for clarity.

5.4 Reduction reactions of *P*-CPh$_3$ substituted oxaphosphirane complexes

As described in the introductory part of this thesis, a study of Espinosa and Streubel provided first insights into the intrinsic strength of the exocyclic bonds to phosphorus in oxaphosphirane κP-pentacarbonylmetal(0) complexes towards reductive reaction conditions.[111] They demonstrated that the heterolytic bond cleavage leading to a carbocation and the oxaphosphiranido complex **XLI**$^-$ was found to be lowest in energy, especially if the R group is bulky and able to stabilize the positive charge efficiently as is the case for the trityl substituent (**XLIc**) in **Scheme 65**.[59]

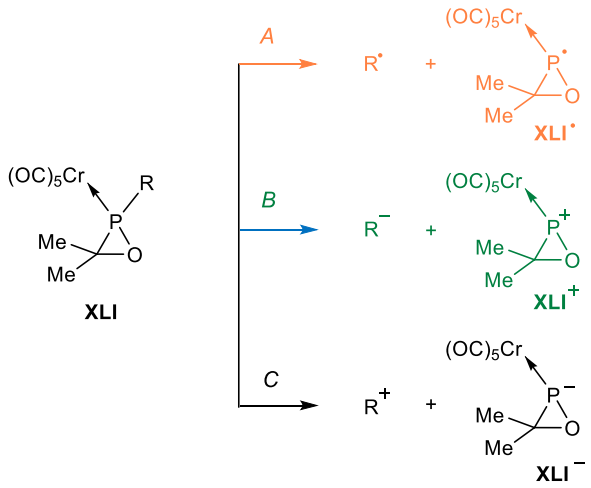

	R•/XLI−	R−/XLI+	R+/XLI−
XLIa	70.8	139.6	112.9
XLIb	58.5	143.3	44.1
XLIc	31.1	91.1	18.3

Scheme 65. Fundamental bond-cleavage processes A–C of the P–R bond and computed energetics (kcal/mol) for the dissociation and redox processes of compounds **XLIa-c** (COSMO$_{THF}$/B3LYP-D/def2-TZVP).[111]

Recently, a new theoretical study of redox potentials and on anion/cation radical formation from oxaphosphirane complexes, especially designed for **4c** and the fluorinated derivatives **20**-**22,** was performed by Frontera (**Figure 50**).

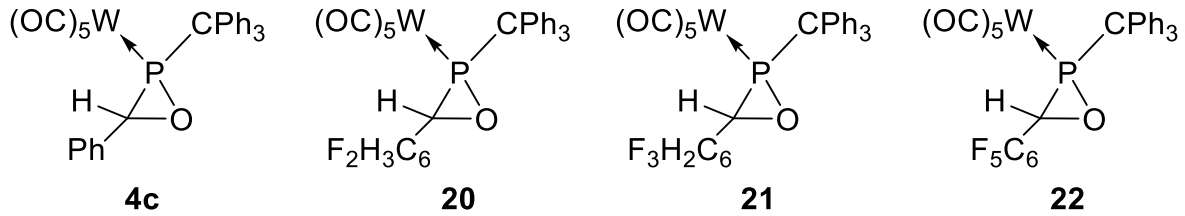

4c **20** **21** **22**

Figure 50. Oxaphophirane complexes **4c, 20-22** theoretically studied.[84]

The HOMO-LUMO energies and the reduction potentials of complexes **4c** and **20**-**22** are summarized in **Table 28** and **Table 29** (gas phase and THF respectively). The following, expected trend can be stated: the energy of the HOMO/LUMO decreases as the number of electron withdrawing fluorine substituents increases.

Table 28. HOMO-LUMO energies in eV (gas-phase) and theoretical redox potential in Volts for compounds **4c** and **20**-**22** at the BP86/def2-TZVP//BP86-D3/def2-TZVP level of theory

Complex	HOMO (eV)	LUMO (eV)	E_{red} (Volts)
4c	–5.65	–2.54	–1.84
20	–5.67	–2.55	–1.85
21	–5.73	–2.59	–1.81
22	–5.83	–2.80	–1.60

Table 29. HOMO-LUMO energies in eV (solvent: THF) and theoretical redox potential in Volts for compounds **4c** and **20**-**22** at the BP86/def2-TZVP//BP86-D3/def2-TZVP level of theory

Complex	HOMO (eV)	LUMO (eV)	E_{red} (Volts)
4c	–5.71	–2.62	–1.78
20	–5.77	–2.64	–1.76
21	–5.80	–2.66	–1.74
22	–5.83	–2.78	–1.62

The one electron reduced species of complexes **4c** and **20**-**22** (= anion radicals) were also computed. The optimized geometries together with the spin density plots are shown in **Figure 51**. The distances of the three membered rings are given in **Table 30** for the oxaphophirane complexes **4c, 20-22** and their corresponding anion radical especies. In the anion radical compounds **4c, 20-22**, the P–C distance increases considerably and the P–O distance increases moderately after one electron reduction and, in contrast, the C–O distance shortens. The significant enlargement of the P–C distance can be explained by examining the LUMOs that are half-filled upon the one electron reduction (**Figure 52** for the plot of the HOMO/LUMO of compounds **4c** and **25**) and the antibonding nature in the P–C bond is clearly appreciated. In fact, the spin density plots show that, in all complexes, the unpaired electron is basically localized at the P–C bond with some delocalization onto the aromatic ring (**Figure 51**). Another interesting bond that also enlarges is the exocyclic *P*–CPh_3 bond (approximately 0.05 Å in all complexes) that also agrees with the antibonding nature of this bond in the LUMO.

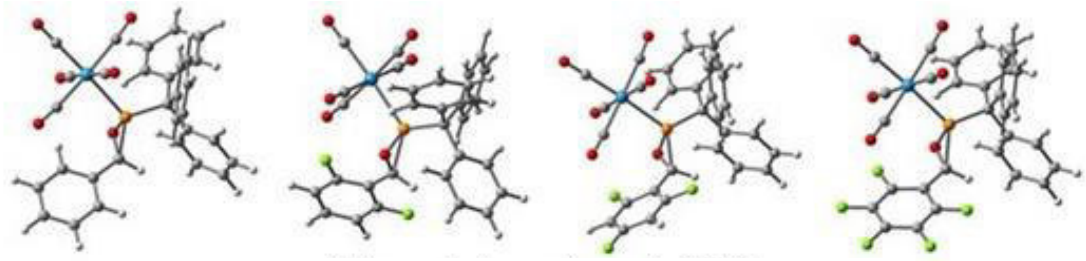

Anion radical complexes 4c, 20-22

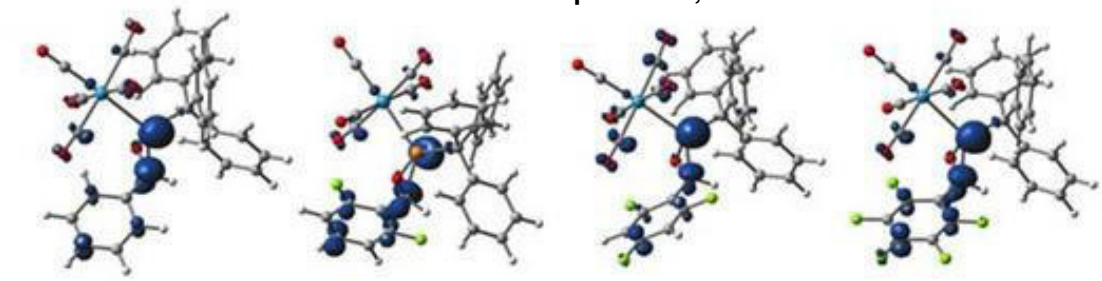

Spin density plots

Figure 51. Top: Optimized geometries of the anion-radicals of complexes **4c** and **20**-**22**. Bottom: Spin density plots of the anion radicals (isovalue = 0.004 e $Å^{-3}$).

Table 30. Three membered ring distances (Å) computed for neutral compounds **4c, 20-22** and their anion radical species at the BP86-D3/def2-TZVPD level of theory

Bond	4c	$[4c^{-}]^{\bullet}$	20	$[20^{-}]^{\bullet}$	21	$[21^{-}]^{\bullet}$	22	$[22^{-}]^{\bullet}$
P–C	1.809	1.944	1.800	1.970	1.801	1.880	1.811	1.944
P–O	1.686	1.707	1.682	1.706	1.682	1.708	1.687	1.709
C–O	1.465	1.442	1.471	1.435	1.469	1.445	1.455	1.436

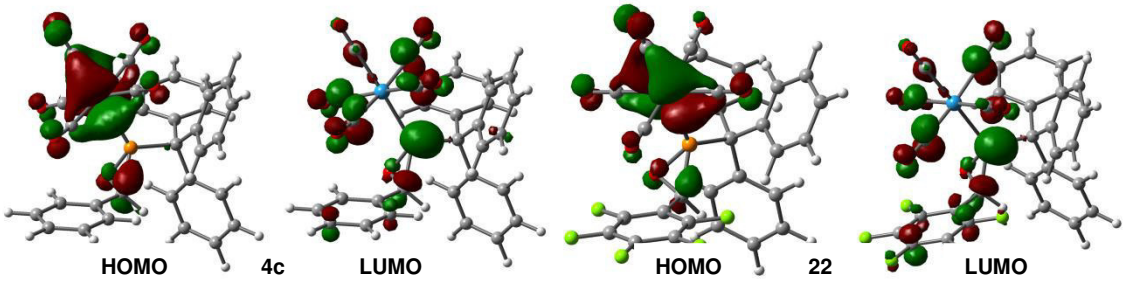

Figure 52. Frontier orbital plots of complexes **4c** and **22.**

Based on these preliminary theoretical results, reactions of *P*-CPh_3 substituted oxaphosphirane complexes having fluorinated and non-fluorinated complexes towards SET and multiple reductions using potassium graphite (KC_8) were investigated.

5.4.1 Reactivity towards KC_8

Firstly, the potential of using KC_8 as a reducing agent will be shortly described. Potassium graphite (KC_8) behaves, in some cases, similar or poorly compared to its homogeneous analogue sodium naphthalenide[134] but it has the advantage that it does not form any soluble by-products. It was realized that this advantage is particularly important in organometallic chemistry.[135,136] In addition KC_8 was chosen as reductant for the following specific 3 reasons: (1) it is a powerful reductant (the redox potential of K/K^+ is -2.92 eV). Thermodynamically, it is considered as the equivalent of potassium;[137] kinetically, it can form suspensions in common organic solvents so it has a greatly increased surface area compared to metallic potassium.[138] (2) The by-products of KC_8 reduction are graphite and potassium salts which are not soluble in organic solvents and can be readily removed by filtration. (3) It is possible to prepare high quality KC_8 by mixing a stoichiometric amount of potassium and graphite and milling the mixture at high temperature under an inert atmosphere.[135]

Oxaphosphirane complexes **4c** and **22** were firstly treated with 1 equivalent of KC_8 in a THF solution using a glovebox, and these solutions were stirred at room temperature for 14 days. Under these conditions, no reaction was observed in both cases. The amount of potassium graphite was then increased to 2 equivalents and after 8 hours stirring a $^{31}P\{^1H\}$ NMR measurement detected a reaction for both oxaphosphirane complexes **4c** and **22** (**Scheme 66**). Firstly, the reactivity of the non-fluorinated oxaphosphirane complex **4c** will be discussed.

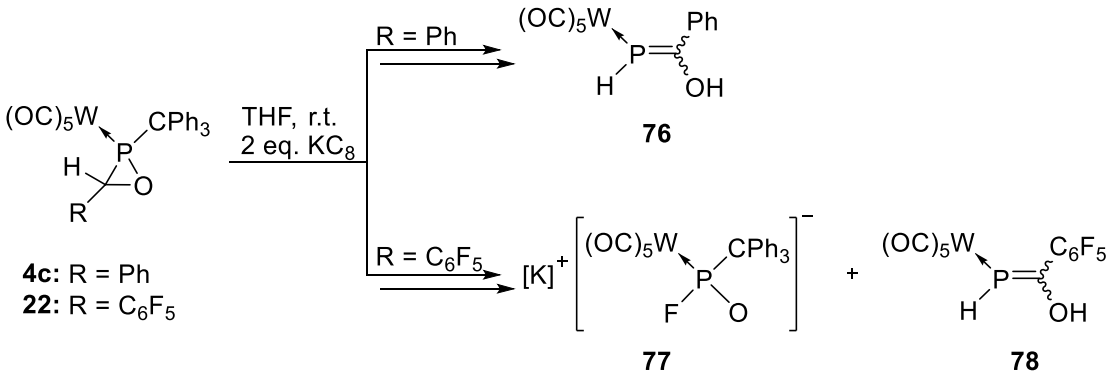

Scheme 66. Reaction of oxaphosphirane complexes **4c** and **22** with potassium graphite.

A first sample was taken after 2 days of stirring and a $^{31}P\{^1H\}$ NMR spectrum recorded (**Figure 53**). Two new phosphorus resonance signals appeared at lower field, both presenting a direct coupling to one hydrogen atom. The complete consumption of the

starting material was reached after about one week, leading to a deep red solution with a black precipitate, presumably corresponding to the graphite, and presenting a main product with a $^{31}P\{^{1}H\}$ NMR resonance at 91.5 ppm.

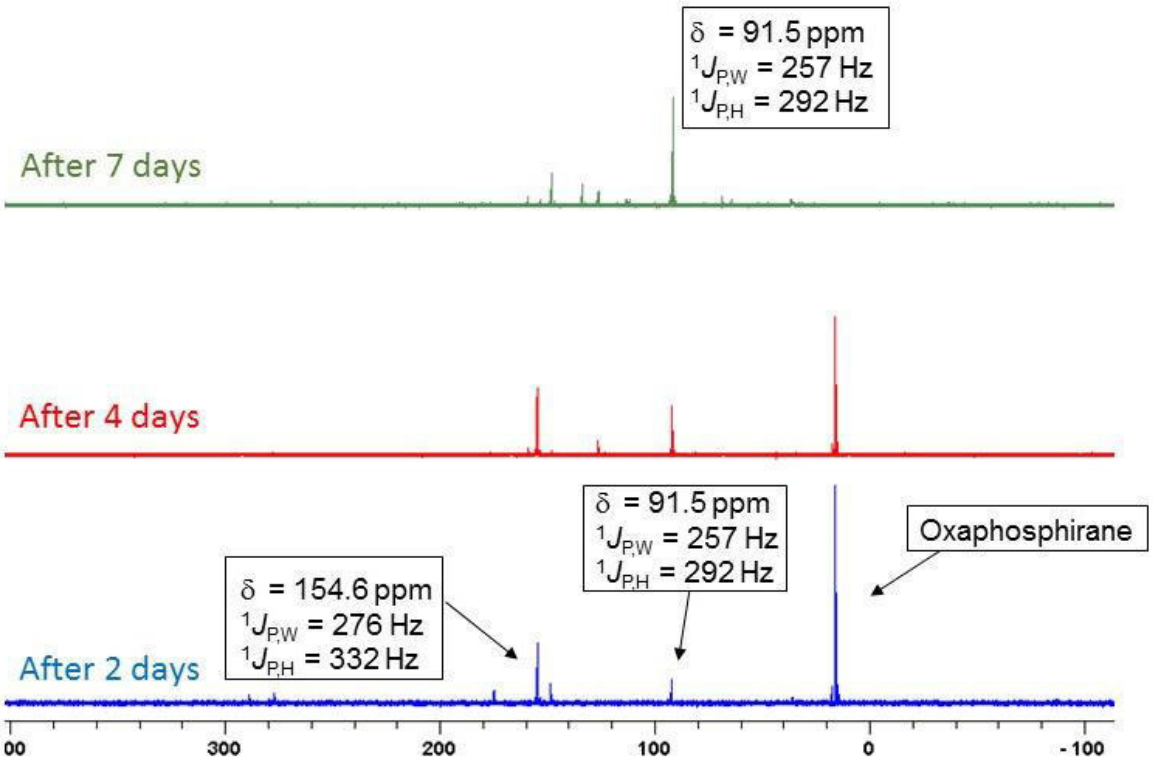

Figure 53. $^{31}P\{^{1}H\}$ NMR spectroscopic monitoring of the reaction of **4c** with potassium graphite.

After the separation of the precipitate (via filtration), a multinuclear NMR analysis was performed (**Figure 54**). In the ^{1}H NMR spectrum, apart from the aromatic protons (green in **Figure 54**) corresponding to the trityl moiety and the phenyl group attached to the carbon atom of the oxaphosphirane, three new resonances were detected. As in the phosphorus NMR already observed, the directly bound proton appears at 8.5 ppm (blue in **Figure 54**) presenting a coupling to the phosphorus nucleus of 292 Hz. Another proton at 2.8 ppm (yellow in **Figure 54**), which is long-range coupled to the phosphorus nucleus (**Table 31**) and at 5.5 ppm (black in **Figure 54**) a new resonance, assigned to Ph_3CH was found. This indicated that the P-bound triphenylmethyl was cleaved off. As the triphenylmethyl radical is known to be stable insolution under inert atmosphere and at room temperature,[50] the detection of this radical should be possible.

Table 31. Selected $^{31}P\{^{1}H\}$ and ^{1}H NMR resonances [ppm], $^{1}J_{P,W}$ and $^{n}J_{P,H}$ [Hz] of complex **76** in THF-d8.

$^{31}P\{^{1}H\}$	$^{1}J_{P,W}$	^{1}H	$^{n}J_{P,H}$
91.5	257.3	8.5	292.1
		7.6 - 6.8	-
		5.5	-
		2.8	13.1

A proposal for the outcome of this reaction in given in **Figure 54** together with the proton NMR analysis.

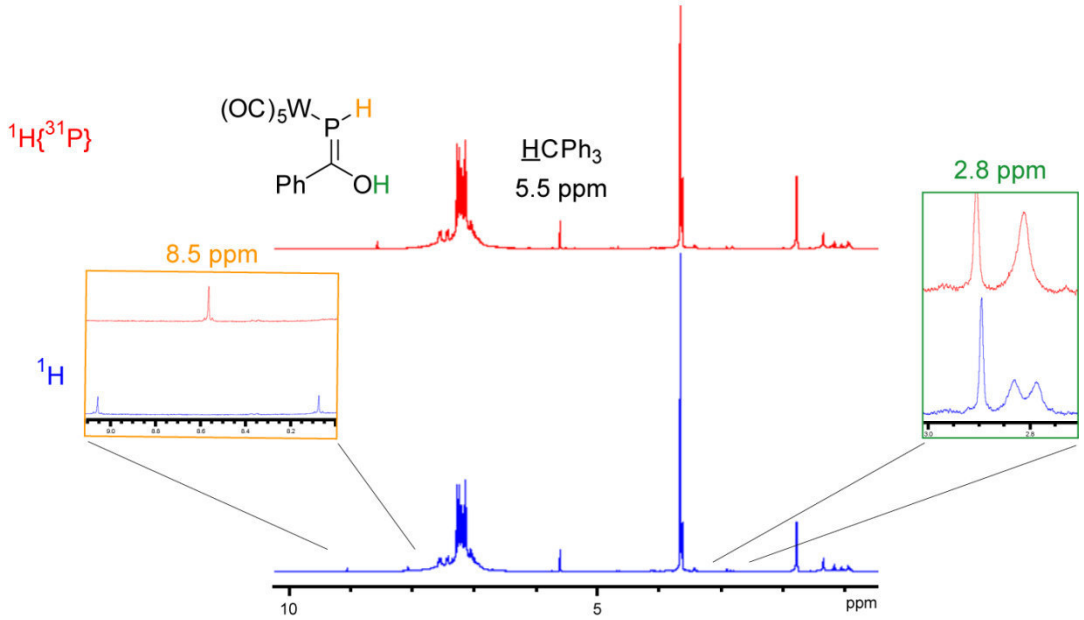

Figure 54. Analysis of the ^{1}H NMR spectrum and proposal for the product of the reaction of **4c** with KC_8, the phosphaalkene complex **76**.

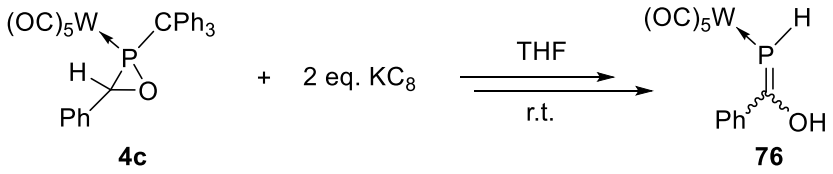

Scheme 67. Reaction of **4c** with 2 eq. of KC_8 to give **76**.

To detect the presence of radical species, EPR measurements were performed in collaboration with the research group of Schiemann, Bonn. First measurements by Matsuoka revealed the presence of an organic radical, but to confirm that this radical corresponded to triphenylmethyl, several experiments were necessary to find the optimal conditions. Finally, the trityl radical was confirmed as the proton splitting is in good agreement with data from the literature (**Figure 55**).

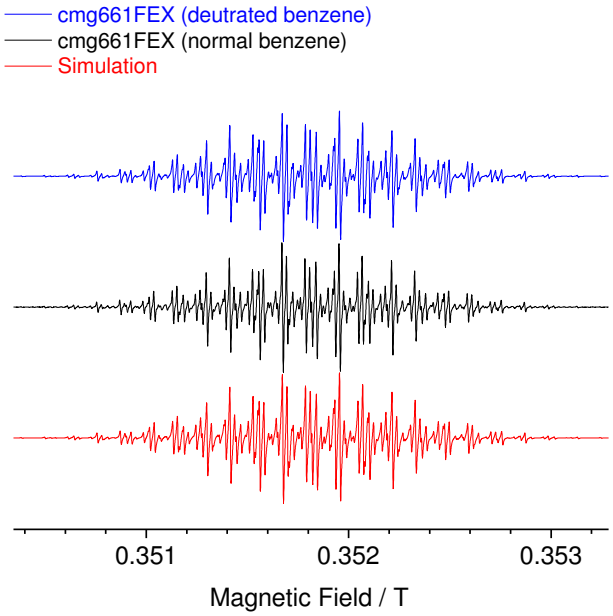

Figure 55. High-resolution EPR of cmg661FEX in deuterated benzene (blue) and benzene (black). Red lines show the spectral simulation.

The magnitude and number of the splitting depend on the spin density at protons and the number of protons. As shown in **Figure 56**, there exist the six *ortho*-, six *meta*-, and three *para*-protons in the triphenylmethyl radical. In the spectra simulation, three inequivalent protons were considered, each of which is composed of six, six and three equivalent protons, respectively. The number of protons is identical to that in the triphenylmethyl radical. The magnitude of the splitting due to each proton was determined by the spectral simulation, which is given in **Table 32**. Here, the magnitude is normally called 'hyperfine coupling constant (A).

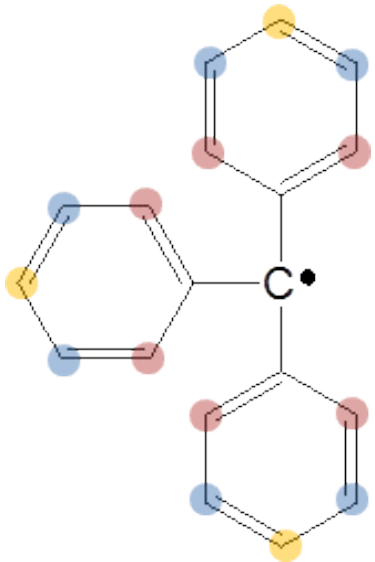

Figure 56. The number of *ortho*-, *meta*-, and *para*-protons in the triphenylmehyl radical, shown by red, blue, and yellow circles.

Table 32. Experimental and theoretical hyperfine coupling constants of protons in the triphenylmethyl radical.

	Hyperfine coupling constant, A [MHz]		
	Experimental	**Theoretical**	**Literature[139]**
Ortho	7.27	7.36	7.31
Meta	3.21	3.84	3.20
Para	7.92	8.14	8.01

The hyperfine coupling constants A were also calculated by density functional theory. The calculated constants are also shown in **Table 32**, which reasonably reproduce the experimental values.

The decay kinetics of EPR was measured twice as shown in **Figure 57**. The sample was purged with argon in an EPR tube sealed with a cap in Period A, where the EPR signal intensity was constant. The result indicates that the radical is stable under argon atmosphere. Immediately after the sample was exposed to air by opening the sealed tube, the signal intensity decayed with time (period B), meaning that the radical is unstable in air. As shown in literatures, triphenylmethyl radical reacts with oxygen to yield triphenylmethyl peroxide in solution. Combined with the spectral simulations, it can be concluded that the radicals observed here are assigned to the triphenylmethyl radical.

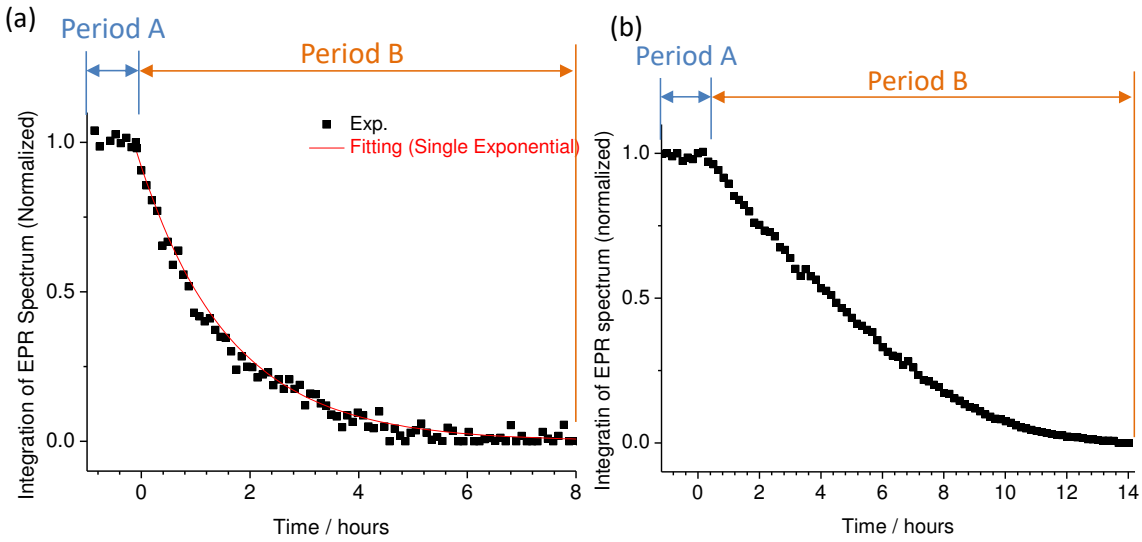

Figure 57. Decay kinetis of EPR signals measured on (a) Dec. 8 and (b) Dec. 14. The sample was purged with argon in an EPR tube sealed with a cap in eriod A, and the sample was exposed to air during the measurement by opening the sealed tube in period B.

Although the *exo* P-C bond cleavage reaction is relatively selective, the presence of triphenylmethyl and other by-products made isolation and characterization of the main product very complicated. To have more insights into a plausible mechanism that could explain the formation of the main product, theoretical calculations were done by Frontera on the reaction pathway of the SET reduction of the oxaphosphirane **4c** with KC_8. Firstly, the LUMO of compound **4c** was examined in order to know the effect of populating this orbital by one electron, and the initially formed anion radical undergoes a *P*–CPh_3 bond breaking, yielding the trityl radical and the intermediate **80** (**Scheme 68**). The latter can react via proton abstraction (from the solvent) or via proton shift to yield the complexes **81** and **82**, respectively. In case of **82**, again, proton abstraction (from the solvent) may yield the final product **76**; it couldn't be clarified why only one isomer was formed under these conditions.

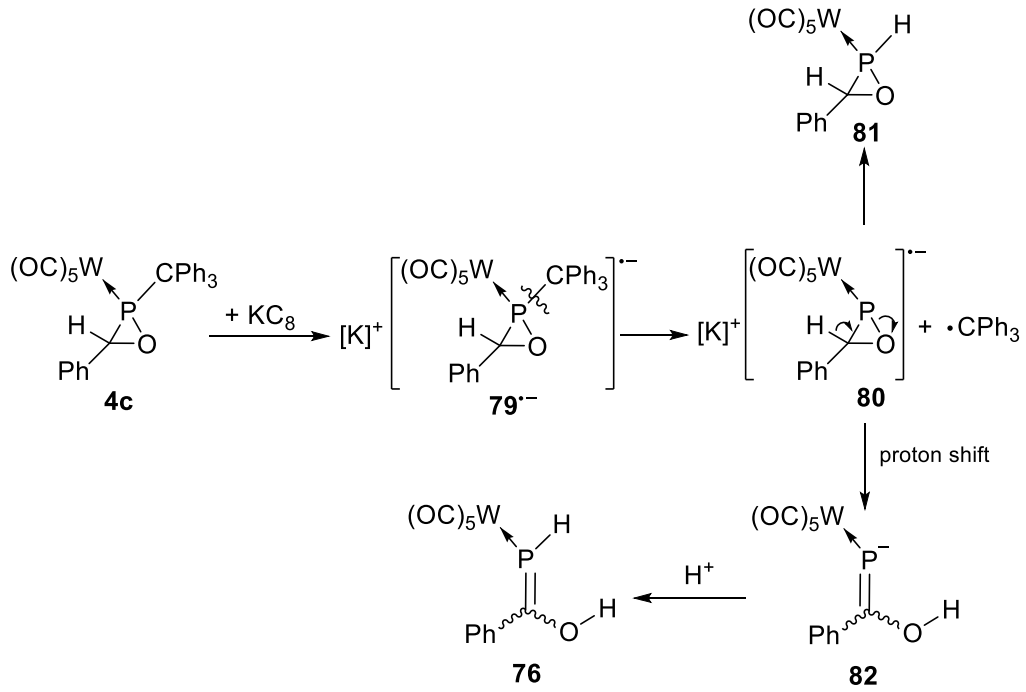

Scheme 68. Plausible mechanism for the reaction of oxaphosphirane **4c** upon addition of KC_8.

The optimized structures of complexes **80** and **82** and their relative energies (in THF) are shown in **Figure 58**.

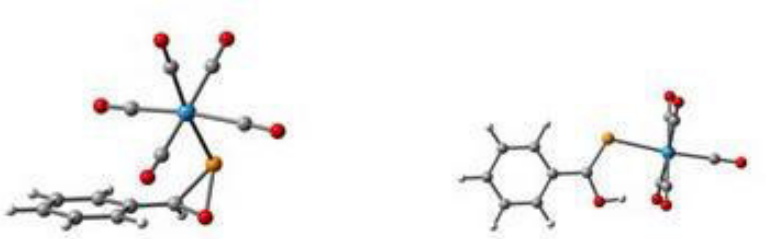

80 **82**

31.2 E_{rel} (kcal/mol) 27.8

Figure 58. Optimized geometries of the anionic compounds that can be derived from the mechanism shown in Scheme 1, the relative energies are given in kcal/mol.

To compare this outcome, reaction of the fluorinated oxaphosphirane complex **22** with potassium graphite was also investigated. The $^{31}P\{^{1}H\}$ NMR spectra of the reaction solutions showed a resonance at 92.9 ppm which may indicate a related phosphalkene complex, as proposed for the reaction of **4c,** but in this case it was not the major product. This signal is accompanied by a resonance at 152.0 ppm which presents a phosphorus nucleus with a direct coupling to a fluorine atom ($^{1}J_{P,F}$ = 1041.4 Hz). The NMR features are almost identical to that of **66**, thus being (most likely) potassium fluorophosphinite complex **77**. In total, it can be concluded that two reaction pathways are competing in the case of the 1:1 stoichiometry.

Table 33. Selected $^{31}P\{^{1}H\}$ and $^{19}F\{^{1}H\}$ NMR resonances [ppm], $^{1}J_{P,W}$, $^{1}J_{P,F}$ and $^{1}J_{P,H}$ [Hz] in THF-*d8*.

Compound	^{31}P-NMR	^{19}F-NMR	$^{1}J_{P,W}$	$^{1}J_{P,F}$	$^{1}J_{P,H}$
76	91.5	-	257.2	-	292.3
78/77	92.9/152.0	-/-33.0	319.7	1041.4	-
66	152.7	-33.0	319.8	1032.7	30.3

According to the theoretical study of Frontera, the fluorinated derivative **22** can follow the same mechanism as **4c** and give the corresponding analogue **78** (**Table 33**)**.** To check if a trityl radical is also present in this case, EPR measurements were performed and the result revealed the presence of small amounts of the trityl radical. As indicated in the literature, the concentration of triphenylmethyl radical in benzene solution is ~ 2% at room temperature. Since the radical concentration in benzene was 0.01 mM, the initial concentration of the radical was expected to be 0.5 mM, which is far below the concentration of the given sample. This may be due to the two competing pathways thus not giving stoichiometric amounts of the radical.

Since it is known from the literature that variations in the amounts of KC_8 can lead to different outcomes,[140] these reactions of complexes **4c** and **22** were repeated using an excess of potassium graphite (2-3 equivalents)**.**

In both cases the starting materials were consumed after 24 hours of stirring at room temperature in THF. $^{31}P\{^1H\}$-NMR measurements showed "empty" spectra for both oxaphosphirane complexes, *i.e.,* no signals were obtained. This could be, presumably, due to the presence of radicals located on or near the phosphorus atom. The reaction of **4c** led to a dark red solution with black precipitate which was also observed for **22,** but in this case together with a dark brown solution; the graphite was easily separated from the reaction mixtures via filtration. ^1H and ^{13}C- NMR spectroscopic measurements of both reactions revealed only the resonances corresponding to the triphenylmethane group. Therefore, EPR measurements were performed to detect presence of radicals, which was successful in case of the trityl radical, but also small amounts of another non-carbon centered radical were detected. Brief exposure of both reaction solutions to air led to a rapidly vanishing color, thus turning into light yellow solutions. After this color change had occurred, a new NMR analysis was performed but still no resonances in the $^{31}P\{^1H\}$ NMR spectrum were observed. Further efforts to trap the radicals via reacting the colored solutions with TEMPO, anthracene or tetrachloro-*ortho*-benzoquinone were not successful.

To bring some more light to the reaction outcome, theoretical calculations were performed by Frontera at the BP86-D3/def2-TZVP level of theory, and preliminary results were used to discuss a plausible mechanism for the reduction of oxaphosphirane complexes **4c** and **22** using three equivalents of KC_8 (**Scheme 69**). This proposal is based on the assumption that $K_2[W(CO)_5]$ and $(Ph)_3C^{\cdot}$ species are formed at an early stage of the reaction. Compound **83** and its isomers and protonated derivatives **85-91** were computed in order to know (at least) their relative stabilities.

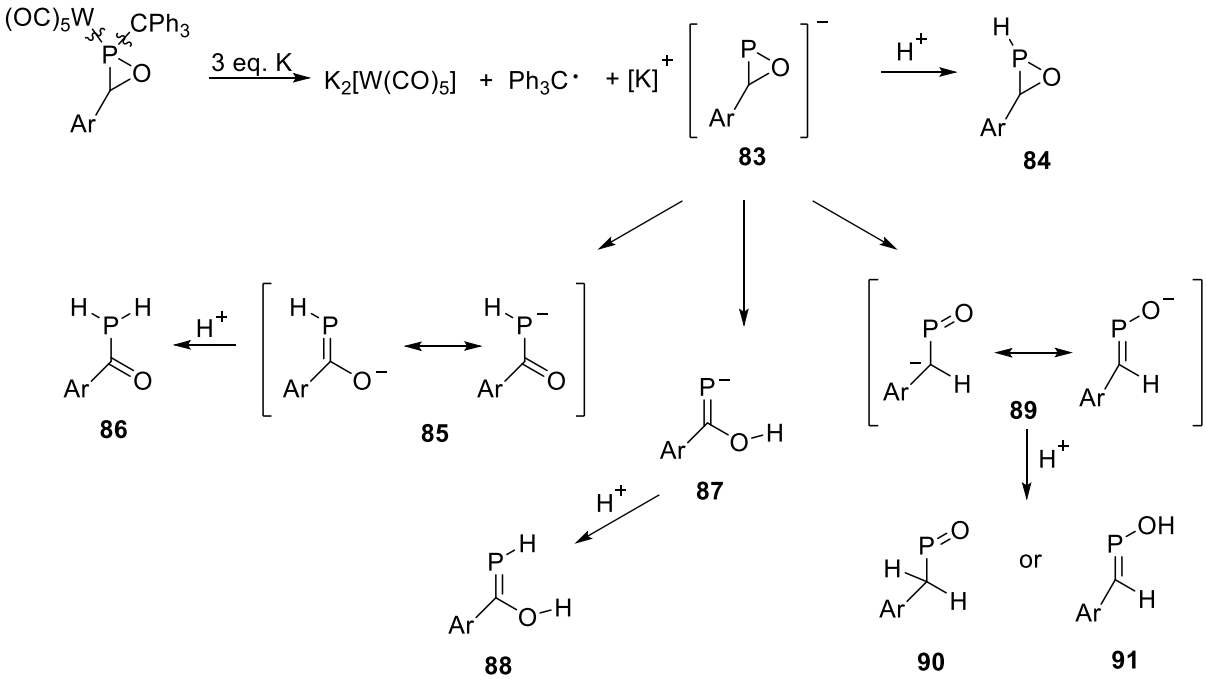

Scheme 69. Plausible theoretical mechanism for the formation of **85, 87, 89** anions for Ar = Ph and C_6F_5 and products derived via formal protonation.

The optimized compounds and relative energies (in THF) are shown in **Figure 59a** for Ar = Ph (**83**, **85**, **87** and **89**) and in **Figure 59b** for Ar = C_6F_5 (**83^F**, **85^F**, **87^F** and **89^F**). The cyclic intermediates (**83** and **83^F**) are highly energetic (due to the ring strain) and upon opening could yield different derivatives (**85**, **87** and **89**, **Scheme 69**). For both derivativess (phenyl or pentafluorophenyl) the most stable derivative is **89** in which the negative charge is delocalized between the O and C atoms. For Ar = Ph, the anionic product **85,** having the negative charge also delocalized, is only 4.6 kcal/mol higher in energy than **89**. Conversely, for Ar = C_6F_5 product **89^F** is much higher in energy than **85^F**, because the electron withdrawing C_6F_5 group is able to stabilize the negative charge in **89^F** by both inductive and resonance effects. Note that this behavior is not observed when the $W(CO)_5$ moiety is present. We have also evaluated the relative energies of all possible final products (upon protonation of the anions), which are shown in **Figure 60**. The most stable isomers correspond to the two possible protonated isomers of the anionic species **89** (denoted as **90** and **91**) for both series, that are almost isoenergetic. This behaviors is different if the $W(CO)_5$ moiety is present at phosphorus, since the most stable isomer is **90** instead of **91** for Ar = Ph.

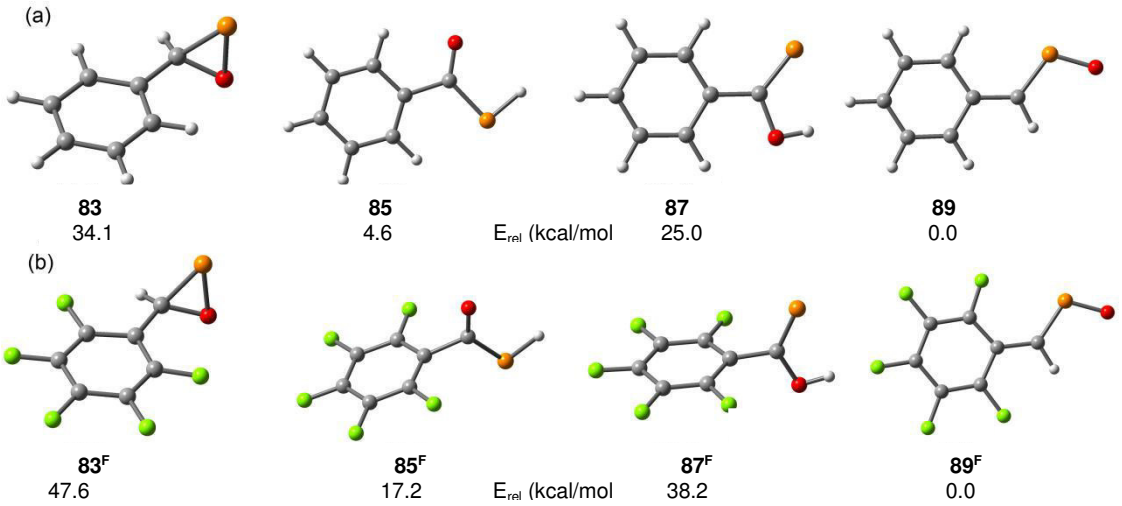

Figure 59. Optimized geometries of anionic compounds that can be derived from the mechanism shown in **Scheme 69** (color code: green (F), grey (C), orange (P), red (O) and white (H)); relative energies are given in kcal/mol.

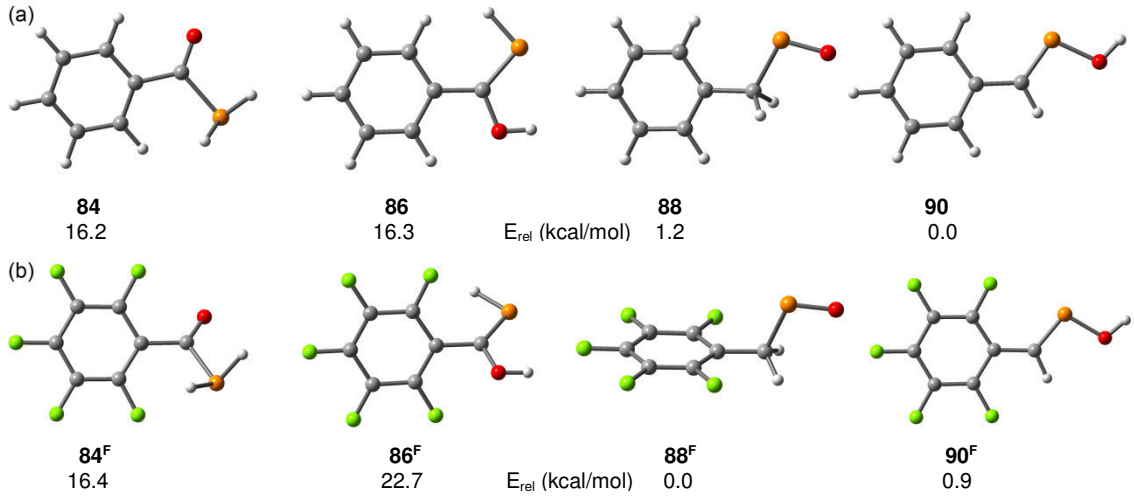

Figure 60. Optimized geometries of the protonated compounds that can be derived from the mechanism shown in **Scheme 69** (color code: green (F), grey (C), orange (P), red (O) and white (H)); The relative energies are given in kcal/mol.

5.4.2 Deoxygenation reactions of *P*-CPh_3 substituted oxaphosphirane complexes

The chemistry of free radicals is one of the most useful tools for the formation of C-C bonds in organic synthesis. This is due to the facile generation of radicals under mild conditions, the broad compatibility with several functional groups and solvents and the high selectivity towards different transformations.[141]

In this context, metals in a low oxidation state such as Sm^{II} species[142,143] and Ti^{III} species [142] play a key role. Especially titanium reagents, apart from being excellent reagents for single electron transfer (SET) reactions, present a low toxicity and a facile

and low cost production. As such, titanocene trichloride and Cp_2TiCl, characterized by Green in 1972[144] has demonstrated to be a high utility reagent with some interesting features.[144] First, it is easily generated by *in situ* reaction of Ti^{IV} derivatives such as Cp_2TiCl_2 with a reducing metal such as Mn,[145] Al,[146] Zn[146] or Mg,[147] as **Scheme 70** shows.[148]

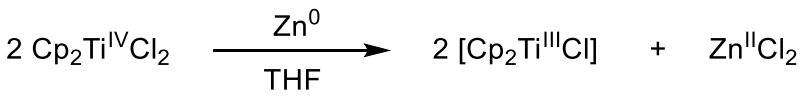

Scheme 70. *In situ* synthesis of a reactive Ti^{III} species using Zn (Cp = C_5H_5).[148]

Under specific conditions, this complex crystallizes as a trinuclear species, however experimental results suggest that such structures are only characteristic in the solid state.[145,147] Indeed, it has been demonstrated that in solution the complex presents an equilibrium between the monomer Cp_2TiCl and the dimer $(Cp_2TiCl)_2$.[149] Both species have unpaired electrons that confer the one-electron transfer character.

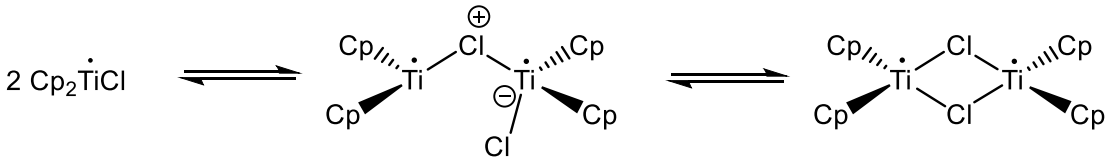

Scheme 71. Reversible equilibrium of $[Cp_2Ti^{III}Cl]$ XXX in solution.[149]

It has been demonstrated that titanocene^{III} easily and selectively allows the deoxygenation of epoxides. The process consists of two consecutive one electron transfers. After the coordination and *inner-sphere* one electron transfer, a homolytic C-O bond cleavage occurs. If the β-titanoxy radical formed is trapped by a second unit of titanocene^{III}, a deoxygenation process takes place and the corresponding alkene is generated.

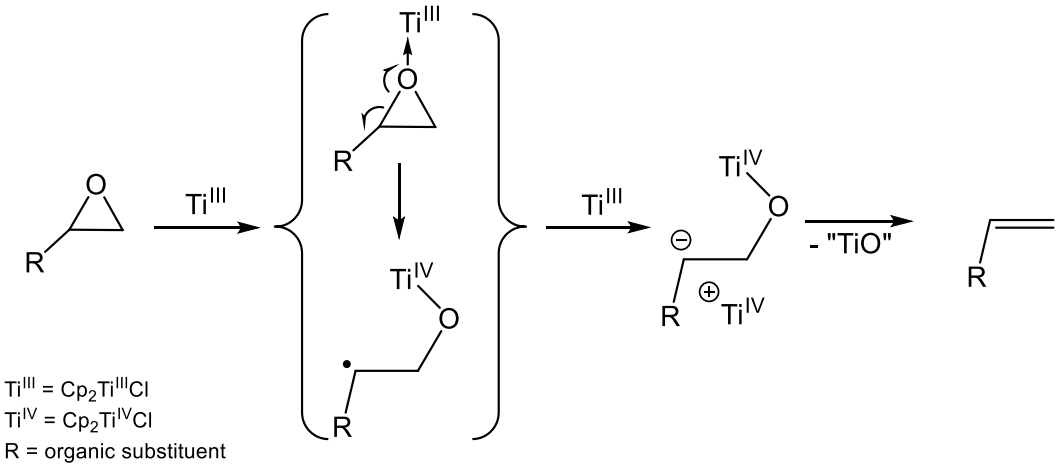

Scheme 72. Deoxygenation of epoxides with $Cp_2Ti^{III}Cl$.[150]

Another precursor for a Ti^{III} reagent, suitable for deoxygenation reactions, is cyclopentadienyltitanium(IV)trichloride ($CpTi^{IV}Cl_3$) which can be reduced with Zn and used *in situ* as mixture of $[CpTi^{III}Cl_2]$ and zinc dichloride.[151]

$$2\ CpTi^{IV}Cl_3 \xrightarrow[THF]{Zn^0} 2\ [CpTi^{III}Cl_2] + Zn^{II}Cl_2$$

Scheme 73. *In situ* preparation of $[CpTi^{III}Cl_2]$.[151]

In the introduction of this Thesis it was pointed out that phosphorus strongly resembles carbon and indeed, many phosphorus compounds undergo similar reactions as their carbon analogs. Recently, Albrecht *et al.* demonstrated for the first time that reactions of oxaphosphirane complexes with titanium(III) reagents successfully led to a diastereomeric mixture of the corresponding *E/Z* phosphalkene complexes via deoxygenation (**Scheme 74**); both isomers were formed in a ratio close to 1:1.[152] This has been demonstrated for oxaphosphirane complexes bearing different organic substituents at phosphorus (Cp* and $CH(SiMe_3)_2$). It is worthmentioning that these reactions are very sensitive towards sterically demanding C-substituents and/or Ti^{III} reagents; the system $CpTiCl_3$/Zn in THF showed higher selectivities. In case of *P*-CPh_3 substituted oxaphosphirane complexes introduction of functionalized groups at the ring carbon atom such as donor groups also make a difference and formation of *P,N*-chelate phosphaalkene complexes were observed by Klein, *i.e.* in case of 3-mono(2-pyridyl) substituted oxaphosphirane complexes.[153]

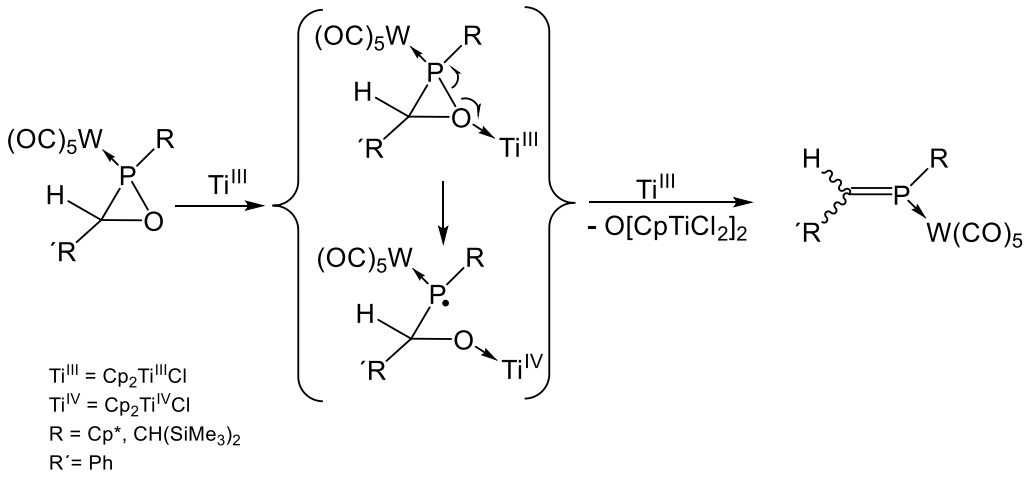

Scheme 74. SET-induced deoxygenation of $\sigma^3\lambda^3$-oxaphosphirane complexes.[152]

5.4.2.1 Reactivity of CPh3-P substituted oxaphosphirane complexes towards deoxygenation with TiIII reagents

In the following, the influence of electron-withdrawing groups at the carbon atom of the oxaphospirane ring in deoxygenation reactions with Ti^{III} SET reagents was studied. Firstly, oxaphosphirane complex **4c** was reacted with stoichiometric amounts of *in situ* generated solutions of $CpTiCl_3/Zn$ in THF as **Scheme 75** shows.

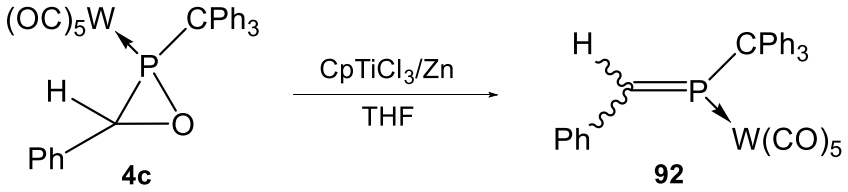

Scheme 75. Reaction of oxaphosphirane complex **4c** with the system $CpTiCl_3/Zn$.

The reaction of **4c** with the system $CpTiCl_3/Zn$ was performed inside the glovebox, at room temperature, and the mixture was stirred for 24 hours. After this time, a sample was taken and a $^{31}P\{^1H\}$ NMR spectrum was measured, showing only one phosphorus resonance, of the phosphaalkene complex **92**. The dark green mixture was filtered and subsequently controlled by new NMR measurements; it was observed that complex **92** slowly decomposed over time as depicted in **Figure 61**.

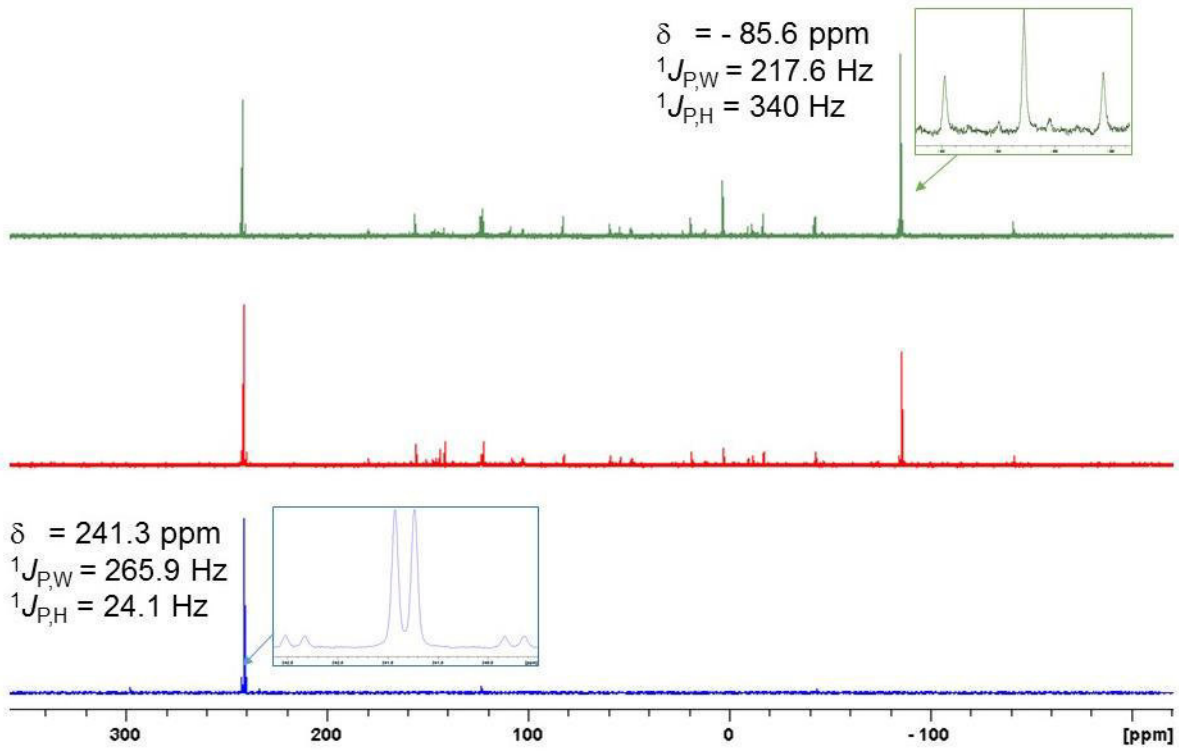

Figure 61. ^{31}P NMR monitoring of the reaction of **4c** with $CpTiCl_3$/Zn (Blue: measured 10 min. after filtration; red: 1 hour after filtration; green: 2 hours after filtration).

Complex **86** slowly decomposed in solution (r.t.) to give a main product at -85.6 ppm together with a direct coupling to two hydrogen atoms which, therefore, can be assigned to the corresponding Ph_3CPH_2 tungsten complex.[154] Complex **92** could be characterized by performing a multinuclear NMR spectral analysis right after consumption of **4c** was completed (20 h); selected NMR data are given in **Table 34**.

Table 34. Selected NMR data of **92** and its *P*-$CH(SiMe_3)_3$ substituted analogous complex (**B**); shifts in [ppm] and couplings in [Hz]

Compound	^{1}H NMR		^{13}C{^{1}H} NMR ($^nJ_{P,C}$)			
	C<u>H</u>P	$^2J_{P,H}$	<u>C</u>HP	<u>C</u>P	*cis*-CO	*trans*-CO
92	9.1	23.7	170.9 (35.6)	67.3 (br)	194.8 (9.0)	197.7 (33.4)
B*[152]	8.3	17.5	165.1 (39.0)	23.5 (19.6)	195.4 (9.7)	197.5 (29.7)

*Only the data of one isomer is given here.

Besides the ^{31}P{^{1}H} NMR resonance of **92**, the data of the ^{13}C{^{1}H} NMR spectrum supports the phosphaalkene structure, especially the signal at 170.9 ppm having a $^1J_{P,C}$ coupling constant of 35.6 Hz. The resonance of the C<u>H</u>=P proton was found at

9.1 ppm, thus having a very similar shift like in the case of the known P-$CH(SiMe_3)_2$ substituted complex complex **B** (**Table 34**).

Albrecht had obtained some evidence that the deoxygenation might follow an outer-sphere mechanism, but this hypothesis wasn't fully confirmed.[155] Therefore, the fluorinated oxaphosphirane derivatives **20**-**22** were also reacted with *in situ* generated solutions of $CpTiCl_3$/Zn in THF under the same conditions.

But for these three derivatives no reaction was observed, neither with $CpTiCl_3$/Zn nor with Cp_2TiCl_2/Zn. Several attempts to achieve a reaction were carried out by changing the typical reaction parameters such as stoichiometry, concentrations and temperature, but the fluorinated oxaphosphirane complexes always stayed intact. The conclusion is that the electron-withdrawing nature of the fluorinated substituents are leading to a less basic oxygen atom of the oxaphosphirane ring that is required to coordinate to the titanium center as strictly required by an inner-sphere mechanism.

6. Summary

The objective of this thesis was to synthesize different *P*-CPh_3 substituted oxaphosphirane complexes with a main focus on derivatives bearing fluorinated substituents at the ring carbon atom, as well as, the study of their reactivity towards strong σ-donors *i.e.* NHCs, ring-opening reactions with Brønsted acids, SET (single electron transfer) and multiple electron reductions.

Using reactions of Li/Cl phosphinindenoid complexes **3a-c** and different aldehydes (benzaldehyde, acetaldehyde and butyraldehyde) new oxaphosphirane complexes **4a,b**, **5** and **6** were synthesized in very good yields (**4a**: 88%; **4b**: 78%;**5**: 76%, **6**: 81%) and fully characterized including X-ray structures in most cases.

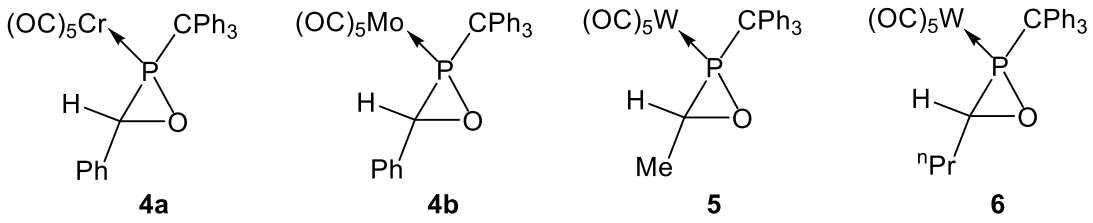

Scheme 76. Newly synthesized oxaphosphirane complexes **4a-c**, **5** and **6**.

Using a sterically more demanding ketoneinstead of an aldehyde, *i.e.* benzophenone, complexes **9** and **10** were formed, bearing P-ligands with fused ring systems (**Scheme 77**). The ligand structures of **9a-c** and **10a-c** were confirmed by NMR spectroscopy and X-ray diffraction studies.

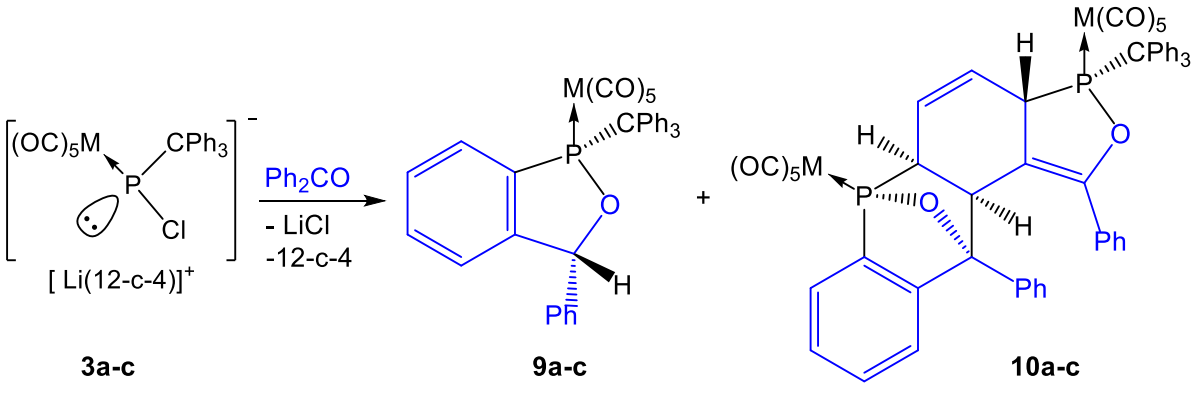

3a-c **9a-c** **10a-c**

a: M = Cr
b: M = Mo
c: M = W

Scheme 77. Reaction of Li/Cl phosphinidenoid complexes **3a-c** with benzophenone.

DFT studies showed that complexes **9a-c** were formed from a short-lived oxaphosphirane complex via P-C ring cleavage, followed by P-C (phenyl) cyclization

and either pericyclic or (most likely) water catalyzed (concerted or stepwise) suprafacial [1,3]H shift. The novel pentacyclic structure type **10a-c** may arise from a phospha-Diels-Alder reaction between two reactive intermediates, one of which being a 2-phosphafurane complex transiently formed via a phospha-ene elimination of $HCPh_3$.

To study in greater depth the electronic situation of the strained heterocyclic P-ligand, several *C*-fluorinated oxaphosphirane complexes were synthesized and isolated in very good yields (**20**: 74%; **21**: 81%; **22**: 87%; **23**: 82%; **24**: 88%; **27**: 91%; **41**: 92%; **Scheme 78**); only **31** decomposed in solution due to an unknown instability.

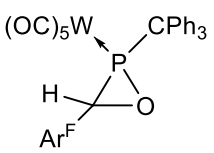

20: Ar^F = 2,6-difluorophenyl

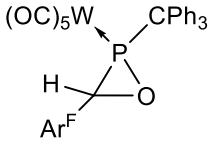

21: Ar^F = 2,4,6-trifluorophenyl

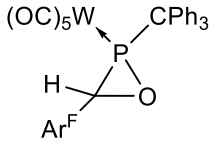

22: Ar^F = perfluorophenyl

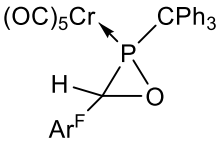

23: Ar^F = perfluorophenyl

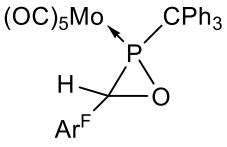

24: Ar^F = perfluorophenyl

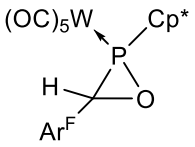

27: Ar^F = perfluorophenyl

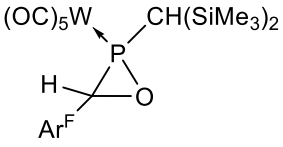

31: Ar^F = perfluorophenyl

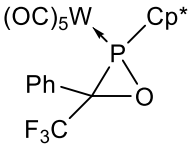

41

Scheme 78. Synthesis of fluorinated oxaphosphirane complexes **20-24**, **27**, **31** and **41**.

In the solid state structures of the new oxaphosphirane tungsten complexes **4c**, **20-22** CO···π arene contacts between the oxygen atom of one carbonyl ligand to the arene ring plane were identified. Unexpectedly, the *C*-phenyl substituted oxaphosphirane complex **4c** shows the shortest CO···π distance (2.981 Å), being similar to the one observed for the pentafluorophenyl derivative **22** (2.983 Å; **Figure 62**). By means of theoretical calculations, the affinity of the M–CO moiety for both “electron rich” and electron deficient rings was rationalized as follows: the interaction can be understood as a π–π interaction in which the negative part of the CO group interacts dominantly in **22** with the π-acidic arene, whereas the interactions of the positive part of the CO

group is dominant in **4c** in case of a (more) π-basic arene; additional packing effects were also discussed.

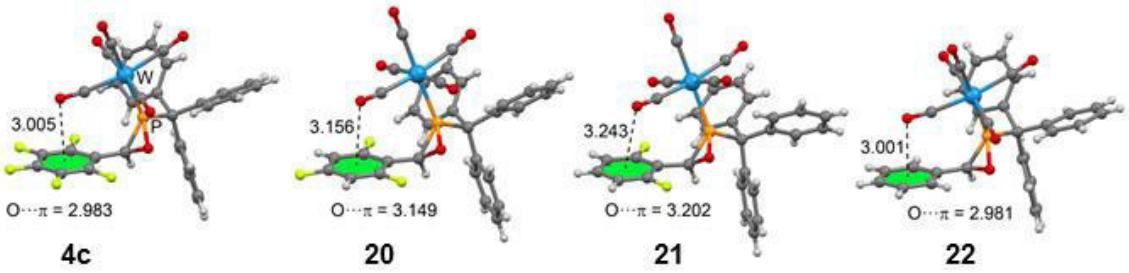

Figure 62. X-ray structures of **4c**[53] and **20-22** showing the intramolecular interaction (distances in Å).

The reactions of Li/Cl phosphinidenoid complexes (**3c**, **26** and **30**) towards fluorinated ketones revealed an unprecedented ambiguous reactivity. For the *P*-trityl (**3c**) and *P*-Cp* derivatives (**26**) a SET pathway involving a transient phosphanyl complex / hexafluoroacetonyl radical pair was disclosed. The reaction pathway starts with a noncovalent π-hole complex between the phosphinidenoid complex anion and hexafluoroacetone which is followed by an E1cBI elimination of fluoride promoted by the Li(12-crown-4) cation. In case of the *P*–$CH(SiMe_3)_2$ substituted derivative **30** the reaction course is strongly influenced by a noncovalent O···Si interaction present after the initial P-C bond forming step – not involving a radical pair according to DFT calculations – which is followed by several rearrangements and terminated by hydrolysis of a phosphaalkene complex to give the 1,2-bifunctional diol-type product **35**. All compounds were fully characterized and their structure confirmed by X-ray crystallography.

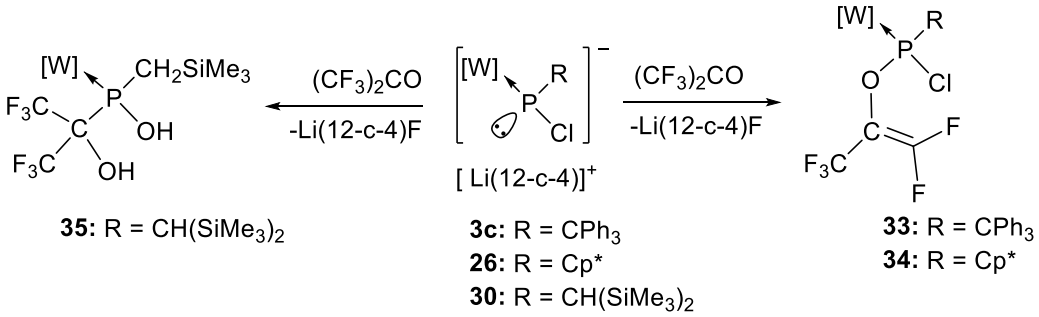

35: R = $CH(SiMe_3)_2$

3c: R = CPh_3
26: R = Cp*
30: R = $CH(SiMe_3)_2$

33: R = CPh_3
34: R = Cp*

Scheme 79. Reaction of phosphinidenoid complexes **3c, 29** and **30** with hexafluoro-acetone.

The reaction of the related *P*-Cp*-substituted oxaphosphirane complex **27** with aldehydes in *ortho*-dichlorobenzol under refluxing conditions led stereoselectively to

O,P,C-cage complexes **46** and **47** (**Scheme 80**). Theoretical calculations enable to propose a reaction pathway for the cage formation with the C-O bond cleavage in complex **27** as initial and rate determining step.

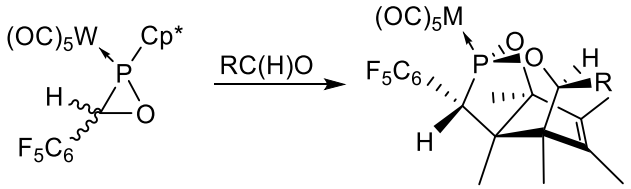

27

46: R = Ph
47: R = C_6F_5

Scheme 80. Synthesis of fluorinated O,P,C-cage complexes **46** and **46^F**.

Furthermore, the diverse reactivity of fluorinated oxaphosphirane complexes was investigated. In case of the thermal reaction of **22** (toluene, 100°C), decomplexation, involving loss of the pentacarbonyltungsten moiety and P-P bond formation, yielded the final product **45**. The addition of a Brønsted acid to the more electron-deficient derivative **22** in the presence of aldehydes with different electronic character led to ring expansion reactions but, in contrast to previous results using a *C*-phenyl substituted oxaphosphirane complex, the reaction of **22** with the system triflic acid/NEt_3 required significantly higher temperatures. Nevertheless the targeted 1,3,4-dioxaphospholane complexes **53-55** were isolated in good yields (**53**: 70%; **54**: 80%; **55**: 84%); the latter represent first examples of fluorinated 1,3,4-dioxaphospholane complexes (**Scheme 81**).

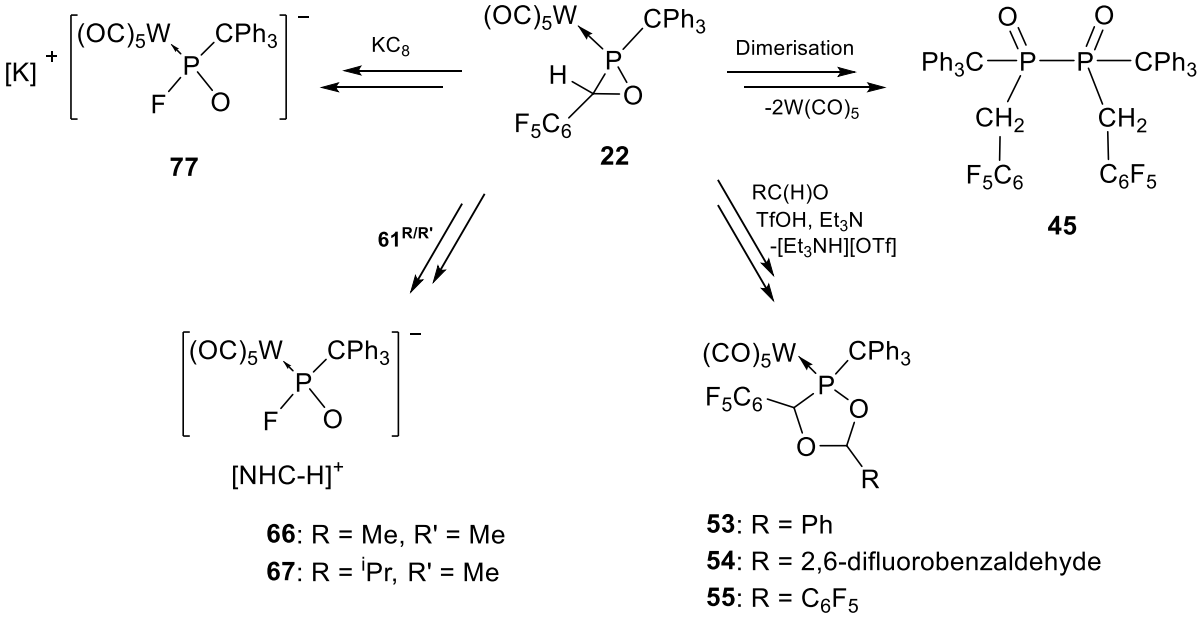

77

22

45

[NHC-H]+

66: R = Me, R' = Me
67: R = ^{i}Pr, R' = Me

53: R = Ph
54: R = 2,6-difluorobenzaldehyde
55: R = C_6F_5

Scheme 81. Versatile reactions of **22**.

Complex **22** was also used to study its reactivity towards strong and basic nucleophiles. Therefore, two N-heterocyclic carbenes (NHCs; **61**$^{R/R'}$) of different steric demand at the nitrogen atoms (R = Me, ^{i}Pr) were employed, leading to the formation of imidazolium fluorophosphinite complexes **66**, **67** (**Scheme 78**); preliminary theoretical results were used to discuss a plausible reaction mechanism. Interestingly, reduction of **22** with an excess of KC_8 (3 eq.) gave the corresponding potassium fluorophosphinite complex **77**.

In contrast, the KC_8 reduction of **4c** using a 2:1 stoichiometry led to the exo P−C_{trityl} bond cleavage. The corresponding triphenylmethyl radical was confirmed by EPR spectroscopy, and the end-on phosphaalkene complex **76** was identified and characterized (**Scheme 82**).

The reactivity of **4c** in SET reduction reactions using $CpTiCl_3$/Zn was also studied. Here, the formation of the *end*-on phosphaalkene complex 92 was observed (**Scheme 82**). In contrast, the fluorinated oxaphosphirane derivatives **20**-**22** did not show any reaction, which strongly points to the effect of the electron-withdrawing nature of the perfluorinated phenyl substituent, thus resulting in a lower nucleophilicity/donicity of the oxygen atom of the oxaphosphirane ring towards the Ti center that was previously proposed as the necessary initial step.

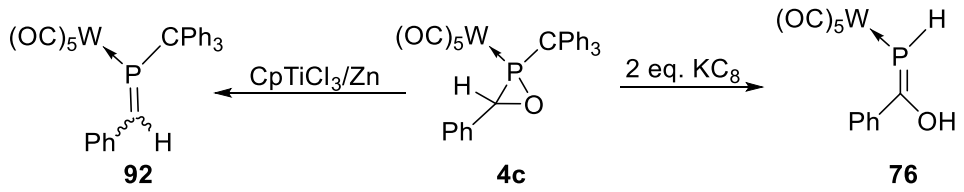

Scheme 82. Reactions of oxaphosphirane complex **4c** with KC_8 and $CpTiCl_3$/Zn.

7. Experimental Part

7.1 Preparative methods

All operations were carried out under an atmosphere of deoxygenated and dried Argon employing a BTS catalyst (Merck) heated at 100-110°C, phosphorus pentoxide and silica gel using either, standard Schlenk techniques and conventional glassware or Glovebox techniques.

The use of Schlenk techniques required flame-dried glassware to remove adsorbed water. Prior to coming into an inert atmosphere, vessels were further dried by *purge-and-refill* — the vessels were subjected to a high vacuum to remove gases and water, and then refilled with inert gas. This cycle was usually repeated three times.

All solvents were dried according to standard procedures using sodium wire/benzophenone or CaH_2 and stored in brown bottles over sodium wire or molecular sieves under inert gas atmosphere.[156]

Most products were purified by low temperature column chromatography using columns equipped with an integrated cooling and vacuum mantel cooled with ethanol via a connected cryostat (information on column dimensions, temperature, solid phase and eluents will be provided for each compound).

7.2 Measuring methods and instruments

7.2.1 Melting point determination:

The melting points were determined with a Büchi (530) capillary apparatus.

7.2.2 Elementary analysis:

Elemental analyses were performed using an elementary vario EL analytical gas chromatograph.

7.2.3 Mass spectrometry:

Electron ionization (EI) mass spectra were recorded on the following spectrometers of the company Thermo Finnigan: Typs MAT 90, MAT 95 XL (70eV). ESI spectra (positive mode) and ESI tandem mass spectra were recorded on a Bruker APEX IV Fourier transform ion cyclotron resonance (FT-ICR) mass spectrometer equipped with an Apollo ESI source (selected data given).

7.2.4 NMR spectroscopy:

NMR spectra were recorded at 25°C on a Bruker Advance DMX 300 spectrometer (^{1}H: 300.1 MHz, ^{13}C: 75.0 MHz, ^{19}F: 300.1 MHz, ^{29}Si: 59.6 MHz and ^{31}P: 121.5 MHz) or on a Bruker DPX 400 (^{1}H: 400.1 MHz, ^{7}Li: 155.5 MHz, ^{13}C: 100.6 MHz, ^{19}F: 300.1 MHz, ^{29}Si: 79.5 MHz, ^{31}P: 161.9 MHz) using $CDCl_3$, THF-d^8 or C_6D_6 as solvents; shifts are given relative to external tetramethylsilane (^{1}H, ^{13}C, ^{29}Si), trichlorofluoromethane (^{19}F) and 85% H_3PO_4 (^{31}P).

7.2.5 IR-Spectroscopy:

The IR-spectra were measured either with a Nicolet 380 spectrometer. Solid as KBr pellets, with Nujol as film between two KBr slides, or with a SMART ITR ATR-Unity (Thermo Scientific) with diamond crystal. A selection of the measured bands and intensities will be given. The intensities will be characterized with the following abreviations: s = strong, m = medium, w = weak, sh = shoulder.

7.2.6 Single-crystal structure analysis:

Crystal structures were recorded at 123(2) K (Mo Kα-radiation (λ = 0.71073 Å) on a Nonius Kappa CCD diffractometer or on a STOE IPDS-2T diffractometer. The structures were resolved by Patterson-methods and refined by full-matrix least squares on F2 (SHELXL-97).[157] All non-hydrogens were refined anisotropically. Hydrogen atoms were included isotropically using the riding model on the bound atoms; in some (denoted) cases hydrogen atoms were located in the Fourier difference electron density. Absorption corrections were carried out analytically or semi-empirically from equivalents. Additionally, the analysis of the X-ray data as well as the graphic representations were done using Diamond 3.0 software.

7.3 Chemicals

The following chemicals were commercially available and in most cases, purified before using:

- Acetaldehyde **Acros**
- Aluminiumoxid Merck 90 neutral (70-230 mesh ASTM) **Merck**
- Benzaldehyde **KMF**
- Benzophenone **Aldrich**

• Butyraldehyde	**Aldrich**
• Chromium hexacarbonyl	**Aldrich or Merck**
• 12-crown-4	**Acros**
• Diisopropylamine	**Aldrich**
• 2,6-difluorobenzaldehyde	**Aldrich**
• Diphenylacetylene	**Alfa-Aesar**
• [Dichlorobis(cyclopentadienyl)titan(IV)]	**Acros**
• Hexafluoroacetone	**ABCR**
• 3-hydroxy-2-butanone	**Aldrich**
• Hydrochloric acid	**Acros**
• Methyltriflat	**Aldrich**
• Molybdenum hexacarbonyl	**ABCR**
• N,N´-dimethylthiourea	**Acros**
• *n*-Butyllithium (1.6 M in hexane)	**Aldrich or Acros**
• 2,3,4,5,6-pentafluorobenzaldehyde	**Aldrich**
• Perfluorobenzophenone	**Aldrich**
• Silicagel Merck 60 (0.063-0.2 mm, pH = 6.5-7.5	**Merck**
• Sodiumhydride	**Alfa-Aesar**
• *t*-Butyllithium (1.6 M in hexane; 1.7 M in *n*-pentane)	**Aldrich or Acros**
• [Trichlorocyclopentadienyltitan(IV)]	**Acros**
• 2,4,6-trifluorobenzaldehyde	**Aldrich**
• Triethylamine	**Grüssing**
• 2,2,2-trifluoroacetophenone	**Aldrich**
• Trifluoromethane sulfonicic acid	**Aldrich**
• Trimethylamine-*N*-oxid·2H_2O	**Alfa-Aesar**
• Tungsten hexacarbonyl	**Aldrich**

The compounds listed hereafter were synthesized following the steps detailed in the corresponding literature:

- Acetonitrile(pentacarbonyle)chromium(0)[158]
- Acetonitrile(pentacarbonyle)molybdenum(0)[158]
- Acetonitrile(pentacarbonyle)tungsten(0)[158]
- [Bis(trimethylsilyl)methyl]dichlorophosphane[159]
- Dichloro(1,2,3,4,5-pentamethylcyclopenta-2,4-dien-1-yl)phosphane[97]
- Dichloro(triphenylmethyl)phosphane[154]
- {Pentacarbonyl[dichloro(triphenylmethyl)phosphane-κP]tungsten(0)}[53]
- {Pentacarbonyl[dichloro(1,2,3,4,5-pentamethylcyclopenta-2,4-dien-1-yl)phosphane-κP]tungsten(0)}[160]
- {Pentacarbonyl[dichloro{bis(trimethylsilyl)methyl}phosphane-κP]tungsten(0)}[68,103]
- Sodiumnaphthalenide[161]
- 1,3,4,5-Tetramethylimidazol-2-ylidene[128]
- 1,3-Diisopropyl-4,5-dimethylimidazol-2-ylidene[128]

7.4 Description of experiments and analytic data

7.4.1 General procedure for the synthesis of phosphinidenoid complexes 3a,b

The corresponding metal complex [(Ph_3CPCl_2)M($CO)_5$] (**a**: M = Cr, **b**: M = Mo) was dissolved in THF-*d8* (5 mL) and 1.0 eq. of 12-crown-4 was added. The solution was cooled to -80°C, 1.2 eq. of ^{t}BuLi [1.7 M in *n*-pentane] were added dropwise and the solution was stirred for 5 minutes. After that, the solution was transferred into a cooled (-90°C) NMR tube via a double-ended needle and was measured first at -80°C and the Li/Cl phosphinidenoid complex was then characterized by NMR methods at -60°C.

7.4.1.1 Synthesis of [Lithium(12-crown-4)][Pentacarbonyl(triphenyl-methyl-chlorophosphanido-κ*P*)chromium(0)] (3a)

3a: [(Ph_3CPCl_2)Cr($CO)_5$]: 250 mg (0.47 mmol); 12-crown-4: 75 µL (0,47 mmol), ^{t}BuLi: (0.33 mL, 0.56 mmol)

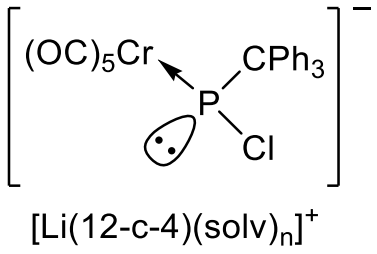

^{1}H NMR (THF-*d*8, -60°C, in ppm): δ = 3.74 (s, 16H, 12-c-4), 6.9 - 7.5 (m, 15H, CPh_3)

^{13}C{^{1}H} NMR (THF-*d*8, in ppm): δ = 66.9 (d, $^1J_{C,P}$ = 22.8 Hz, CP), 68.3 (s, 12-c-4), 125.1 (s, *para*-Ph), 125.5 (d, $^5J_{C,P}$ = 1.3 Hz, *para*-Ph), 125.9 (s, *para*-Ph), 127.1 (s, *meta*-Ph), 127.5 (s, *meta*-Ph), 128.0 (s, *meta*-Ph), 130.2 (d, $^3J_{C,P}$ = 15.7 Hz, *ortho*-Ph), 131.1 (s, *ortho*-Ph), 131.7 (d, $^3J_{C,P}$ = 5.7 Hz, *ortho*-Ph), 144.1 (d, $^2J_{C,P}$ = 16.3 Hz, *ipso*-Ph), 144.3 (d, $^2J_{C,P}$ = 4.2 Hz, *ipso*-Ph) 146.1 (s, *ipso*-Ph), 220.6 (d, $^2J_{C,P}$ = 6.9 Hz, *cis*-CO), 221.6 (d, $^2J_{C,P}$ = 20.1 Hz, *trans*-CO)

^{31}P{^{1}H} NMR (THF-*d8*, in ppm): δ = 310.4. This signal displayed a shoulder on the high-field side (ratio ca. 3:1) that corresponds to the ^{37}Cl isotopomer of **3a**.

7.4.1.2 Synthesis of [Lithium(12-crown-4)][Pentacarbonyl(triphenyl-methyl-chlorophosphanido-κ*P*)molybdenum(0)] (3b)

3b: $[(Ph_3CPCl_2)Mo(CO)_5]$: 250 mg (0.37 mmol); 12-crown-4: 70 µL (0,47 mmol), ^tBuLi: (0.33 mL, 0.44 mmol).

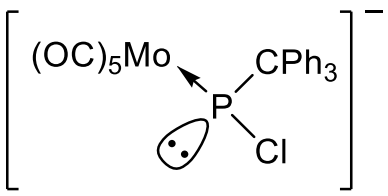

$[Li(12\text{-}c\text{-}4)(solv)_n]^+$

^{1}H NMR (THF-*d8*, -60°C, in ppm): δ = 3.79 (s, 16H, 12-c-4), 7.0 - 7.66 (m, 15H, CPh_3)

^{13}C{^{1}H} NMR (THF-*d*8, -60°C, in ppm): δ = 66.3 (s, 12-c-4), 67.1 (d, $^1J_{C,P}$ = 22.1 Hz, CP), 123.5 (s, *para*-Ph), 123.7 (s, *para*-Ph), 124.7 (d, $^5J_{C,P}$ = 1.35 Hz, *para*-Ph), 125.5 (s, *meta*-Ph), 125.9 (s, *meta*-Ph), 126.8 (s, *meta*-Ph), 128.2 (d, $^3J_{C,P}$ = 17.8 Hz, *ortho*-Ph), 130.4 (s, *ortho*-Ph), 130.9 (d, $^3J_{C,P}$ = 9.7 Hz, *ortho*-Ph), 147.2 (d, $^2J_{C,P}$ = 22.6 Hz, *ipso*-Ph), 148.9 (s, *ipso*-Ph), 149.2 (d, $^2J_{C,P}$ = 9.0 Hz, *ipso*-Ph), 208.8 (d, $^2J_{C,P}$ = 8.0 Hz, *cis*-CO), 216.2 (d, $^2J_{C,P}$ = 24 Hz, *trans*-CO)

^{31}P{^{1}H} NMR (THF-*d8*, -60°C, in ppm): δ = 280.4 (major). This signal displayed a shoulder on the high-field side (ratio ca. 3:1) that corresponds to the ^{37}Cl isotopomer of **3b**.

7.4.2 General procedure for the synthesis of oxaphosphirane complexes 4a,b

To the freshly synthesized Li/Cl phosphinidenoid complexes **3a-c**, 12-crown-4 (1.0 eq) and ^tBuLi (1.7 M in *n*-hexane, 1.2 eq) in THF (7 mL), the corresponding aldehyde (1.2 eq) was added at -78°C leading to the formation of a white precipitate. The reaction mixture was warmed up to −15°C in a cooling bath (ca. 2 h) and volatiles were evaporated *in vacuo (ca. 0.01 bar)*. The product was extracted with *n*-pentane (40 mL) and filtered. After evaporation of the solvent *in vacuo*, the residue was washed with *n*-pentane (3 × 1 mL) at −50°C, dried and thus obtained as white solid.

7.4.2.1 Synthesis of {Pentacarbonyl[(2-triphenylmethyl-3-phenyl)-1,2-oxaphosphiran-κ*P*]chromium(0)} (4a)

2a: 300 mg, 0.48 mmol; 12-crown-4: 95 µL, 0.48 mmol; ^{t}BuLi (1.7 M in *n*-hexane): 0.34 mL, 0.58 mmol; benzaldehyde: 70 µL, 0.58 mmol

Molecular formula: $C_{31}H_{21}CrO_6P$

Molecular weight: 572.05 g/mol

Melting point: 121°C

Yield: 264 mg (0.46 mmol, 88 %)

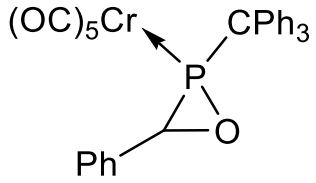

^{1}H NMR ($CDCl_3$, in ppm): δ = 3.9 (1H, d, $^{2}J_{H,P}$ = 2.2 Hz, CHP), 7.0 - 7.2 (m, 15H, CPh_3), 7.4 - 7.6 (m, 5H, Ph)

^{13}C{^{1}H} NMR ($CDCl_3$, in ppm): δ = 59.1 (d, $^{1}J_{C,P}$ = 20.6 Hz, PCO), 67.5 (d, $^{1}J_{C,P}$ = 14.1 Hz, $PCPh_3$), 125.4 (d, $J_{C,P}$ = 3.3 Hz, Ph), 127.7 (d, $J_{C,P}$ = 2.6 Hz, Ph), 129.1 (d, $J_{C,P}$ = 1.7 Hz, Ph), 129.7 (s, Ph), 133.2 (d, $J_{C,P}$ = 11 Hz, Ph), 138.5 (d, $^{2}J_{C,P}$ = 6.3 Hz, ipso-Ph), 211.6 (d, $^{2}J_{C,P}$ = 14.5 Hz, *cis*-CO), 214.3 (d, $^{2}J_{C,P}$ = 3.7 Hz, *trans*-CO)

^{31}P{^{1}H} NMR ($CDCl_3$, in ppm): δ = 58.7

MS selected data *m/z* (%): 572.0 $[M]^{+\bullet}$, 432.1 (30) $[M\text{-}5CO]^{+}$, 326.0 (15) $[M\text{-}5CO\text{-}C_7H_6O]^{+}$, 243.1 (100) $[CPh_3]^{+}$

IR (neat, ν(CO), in cm^{-1}): ν = 2069, 1996, 1959 (s);

Elemental analysis: C [%] H [%]

Calculated:	65.04	3.70
Found:	65.93	3.85

7.4.2.2 Synthesis of {Pentacarbonyl[(2-triphenylmethyl-3-phenyl)-1,2-oxaphosphiran-κ*P*]molybdenum(0)} (4b)

2b: 300 mg, 0.52 mmol; 12-crown-4: 84 µL, 0.52 mmol; ^{t}BuLi (1.7 M in *n*-hexane): 0.39 mL, 0.62 mmol); benzaldehyde: 64 µL, 0.62 mmol

Molecular formula: $C_{31}H_{21}MoO_6P$

Molecular weight: 618.01 g/mol

Melting point: 98°C

Yield: 234 mg (0.38 mmol, 78 %)

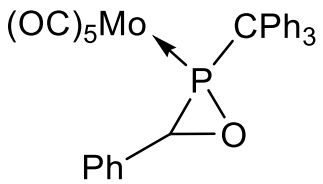

^{1}H NMR ($CDCl_3$, in ppm) δ = 3.6 (d, 1H, $^{2}J_{H,P}$ = 5.6 Hz, HP), 7.0 - 7.2 (m, 15H, CPh_3), 7.4 - 7.6 (m, 5H, Ph)

^{13}C{^{1}H} NMR ($CDCl_3$, in ppm): δ = 51.2 (d, $^{1}J_{C,P}$ = 20.2 Hz, PCO), 66.2 (d, $^{1}J_{C,P}$ = 13.7 Hz, $PCPh_3$), 127.2 (d, $J_{C,P}$ = 3.3 Hz, Ph), 128.4 (d, $J_{C,P}$ = 2.6 Hz, Ph), 129.0 (d, $J_{C,P}$ = 1.7 Hz, Ph), 129.1 (s, Ph), 139.2 (d, $J_{C,P}$ = 11 Hz, Ph), 139.6 (d, $^{2}J_{C,P}$ = 6.3 Hz, Ph), 202.3 (d, $^{2}J_{C,P}$ = 126.3 Hz, *cis*-CO), 208 (d, $^{2}J_{C,P}$ = 49 Hz, *trans*-CO)

^{31}P{^{1}H} NMR ($CDCl_3$, in ppm): δ = 33.4

MS (selected data *m/z* (%)): 618.0 $[M]^{+\bullet}$, 478.0 (20) $[M\text{-}5CO]^{+}$, 372 (5) $[M\text{-}5CO\ \text{-}C_7H_6O]^{+}$, 243.1 (100) $[CPh_3]^{+}$

IR (neat, ν(CO), in cm^{-1}): ν = 2077, 1996, 1968 (s)

Elemental analysis: C [%] H [%]

Calculated:	60.70	3.43
Found:	61.11	3.65

7.4.2.3 Synthesis of {Pentacarbonyl[(2-triphenylmethyl-3-propyl)-1,2-oxaphosphiran-κ*P*]tungsten(0)} (6)

2c: 200 mg, 0.30 mmol; 12-crown-4: 39 µL, 0.24 mmol, ^{t}BuLi (1.7 M in *n*-hexane): 0.25 mL, 0.36 mmol; butyraldehyde: 32 µL, 0.36 mmol

The pale white residue was purified by low temperature column chromatography Al_2O_3, -20°C, h = 2 cm, ø = 1 cm, petroleum ether (150 mL); petroleum ether/dichloromethane 10:1 (150 mL).

Molecular formula: $C_{28}H_{23}O_6PW$
Molecular weight: 616.39 g/mol
Melting point: 110°C
Yield: 161 mg (0.24 mmol, 81 %)

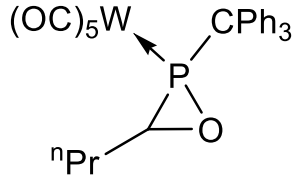

^{1}H NMR ($CDCl_3$, in ppm): δ = 0.84 (t, 3H, $^{3}J_{H,H}$= 7.3 Hz, CH_3), 1.31 - 1.53 (m, 2H, CH_2), 1.62 - 1.84 (m, 2H, CH_2), 2.75 (t, 1H, CH), 7.12 - 7.45 (m, 15H, CPh_3)

^{13}C{^{1}H} NMR ($CDCl_3$, in ppm): δ = 12.7 (s, CH_3), 18.6 (d, $^{3}J_{P,C}$ = 4.7 Hz, CH_2), 30.9 (d, $^{2}J_{P,C}$ = 2.8 Hz, PCO), 50.3 (d, $^{1}J_{P,C}$ = 27.5 Hz, PCO) 65.7 (d, $^{1}J_{C,P}$ = 7.3 Hz, $PCPh_3$), 126.5 (d, $J_{C,P}$ = 1.9 Hz, *m*-Ph), 127.6 (d, $J_{C,P}$ = 0.8 Hz,

p-Ph), 129.7 (d, $J_{C,P}$ = 7.2 Hz, *o*-Ph), 138.9 (d, $J_{C,P}$ = 2.3 Hz, *i*-Ph), 193.9 (d, $^{2}J_{C,P}$ = 8.1 Hz, *cis*-CO), 195.3 (d, $^{2}J_{C,P}$ = 39.1 Hz, *trans*-CO)

$^{31}P\{^{1}H\}$ NMR ($CDCl_3$, in ppm): δ = 8.7 ($^{1}J_{W,P}$ = 303 Hz, $^{2}J_{P,H}$ = 28.2 Hz, $^{3}J_{P,H}$ = 9.5 Hz);

MS selected data *m/z* (%): 670.1 $[M]^{+\bullet}$, 346.1 (10) $[M\text{-}5CO]^{+}$, 372 (5) $[M\text{-}5CO\text{ -}C_4H_8O]^{+\bullet}$, 243.1 (100) $[CPh_3]^{+}$

IR (neat, ν(CO), in cm^{-1}): ν = 2075, 1993, 1969 (s, CO)

Elemental analysis: C [%] H [%]

Calculated:	50.17	3.46
Found:	50.82	3.71

7.4.3 General procedure for the synthesis of complexes 9a-c, accompanied by the corresponding compounds 10a-c

To the freshly synthesized Li/Cl phosphinidenoid complex **3a-c**, 12-crown-4 (1.0 eq) and ^{t}BuLi (1.7 M in *n*-hexane, 1.2 eq) in 7 mL of THF, benzophenone (0.69 M in THF) was added at −78°C leading to the formation of a white precipitate. The reaction mixture was warmed to ambient temperature (4h of stirring) until complete consumption of the corresponding phosphinidenoid complex and volatiles were evaporated *in vacuo (ca. 0.01 bar)*. The product **9a** could not be obtained in pure form due to decomposition during purification but, as well as **9b,** could be identified from the reaction mixture *via* NMR spectroscopy. **9c** was extracted with *n*-pentane (40 mL), and filtered. After evaporation of the solvent in vacuo, washing with *n*-pentane (3 × 1 mL) at −50°C, drying, the corresponding metal complex was obtained as a white solid. All attempts to separate **10a,b** from **9a,b** were unsuccessful. However, the full NMR characterization of **9a-c** could be achieved as well as the $^{31}P\{^{1}H\}$ NMR resonances of **10a-c** by identification and assignment of the corresponding resonances out of the mixture of **9a-c** and **10a-c**.

7.4.3.1 Synthesis of {Pentacarbonyl[(2-triphenylmethyl-5-phenyl-benz[c])-1,2-oxaphospholane-κ*P*]chromium(0)} (9a)

9a: 300 mg, 0.48 mmol; 12-crown-4: 95 µL, 0.48 mmol; ^{t}BuLi: 0.34 mL, 0.58 mmol; benzophenone: 1.4 mL, 0.58 mmol

Molecular formula: $C_{37}CrH_{25}O_6P$

Molecular weight: 648.08 g/mol

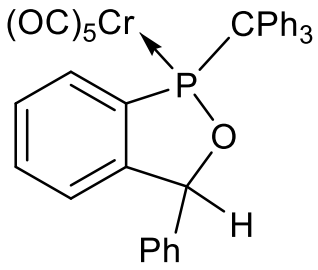

^{1}H NMR (THF-*d8*, in ppm): δ = 5.64 (s, 1H, HCPh$_3$); 6.27 (br. s, 1H, POC(H)Ph), 6.51 (d, $^{3}J_{H,H}$ = 8.11 Hz, 1H, Ar-H), 7.08 (d, $^{3}J_{H,H}$ = 7.40 Hz, 1H, CPh$_3$-H), 7.15 (d, $^{3}J_{H,H}$ = 6.70 Hz, 2H, Ar-H), 7,22 - 7,39 (m, 3H, Ph-H, CPh$_3$-H), 7,47 - 7,56 (m, 6H, CPh$_3$-H), 7,63 - 7,73 (m, 3H, CPh$_3$ -H, Ph-H), 7,81 - 7,83 (m, 3H, Ph-H, CPh$_3$-H), 7.84 - 7.89 (m, 2H, Ar-H)

^{13}C{^{1}H} NMR (THF-*d8*, in ppm): δ = 69.5 (d, $^{2/3}J_{P,C}$ = 2.5 Hz, POC(H)Ph), 86.3 (d, $^{1}J_{P,C}$ = 8.9 Hz, Ph$_3$C), 125.5 (s, C-Ph), 125.7 (d, $J_{P,C}$ = 10.5 Hz, Ar-C), 126.1 (s, *para*-Ph), 126.3 (d, JP,C = 10.5 Hz, *ortho*-Ph), 127.6 (s, *meta*-Ph), 127.7 (s, para-Ph), 128.0 (d, $^{1}J_{P,C}$ = 14.2 Hz, C-Ph), 128.8 (s, *ortho*-Ph), 129.2 (s, *meta*-Ph), 131.5 (s, *ortho*-Ph), 137.4 (s, C-Ph), 139.3 (d, $J_{P,C}$ = 22.9 Hz, *ipso*-Ph), 142.7 - 143.2 (m, Ph-C), 143.7 (s, *ipso*-Ph), 143.9 (s, *ipso*-Ph), 146,9 (s, Ph-C), 199.2 (dsat, $^{2}J_{P,C}$ = 9.6 Hz, $^{1}J_{W,C}$ = 132.0 Hz, *cis*-CO), 204.3 (d, $^{2}J_{P,C}$ = 32.9 Hz, *trans*-CO)

^{31}P{^{1}H} NMR (CDCl$_3$, in ppm): δ = 190.3

7.4.3.2 Synthesis of {Pentacarbonyl[(2-triphenylmethyl-5-phenyl-benz[c])-1,2-oxaphospholane-κ*P*]molybdenum(0)} (9b)

9b: 300 mg, 0.48 mmol; 12-crown-4: 97 µL, 0.48 mmol; ^{t}BuLi: 0.36 mL, 0.58 mmol; benzophenone: 1.4 mL, 0.58 mmol

Molecular formula: $C_{37}H_{25}MoO_6P$

Molecular weight: 694.04 g/mol

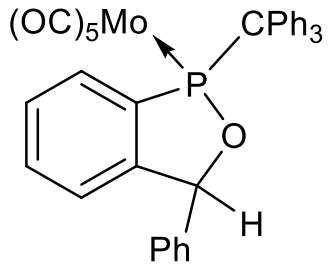

^{1}H NMR (THF-*d8*, in ppm): δ = 5.64 (s, 1H, HCPh$_3$), 6.35 (br. s, 1H, POC(H)Ph), 6.58 (d, $^{3}J_{H,H}$ = 8.11 Hz, 1H, Ar-H), 7.23 (d, $^{3}J_{H,H}$ = 7.80 Hz, 1H, CPh$_3$-H), 7.18 (d, $^{3}J_{H,H}$ = 6.52 Hz, 2H, Ar-H), 7,22 - 7,45 (m, 3H, Ph-H, CPh$_3$-H), 7,47 - 7,56 (m, 6H, CPh$_3$-H), 7,68 - 7,83 (m, 3H, CPh$_3$ -H, Ph-H), 7,81 - 7,83 (m, 3H, Ph-H, CPh$_3$-H), 7.84 - 7.89 (m, 2H, Ar-H)

^{13}C{^{1}H} NMR (THF-*d8*, in ppm): δ = 70.1 (d, $^{2/3}J_{P,C}$= 2.1 Hz, POC(H)Ph), 86.3 (d, $^{1}J_{P,C}$ = 8.5 Hz, Ph$_3$C), 123.1 (s, C-Ph), 123.7 (d, $J_{P,C}$ = 8.5 Hz, Ar-C), 125.3 (s, *para*-Ph), 125.8 (d, $J_{P,C}$ = 10.5 Hz, *ortho*-Ph), 126.2 (s, *meta*-Ph), 126.7 (s, para-Ph), 128.2 (d, $^{1}J_{P,C}$= 12.2 Hz, C-Ph), 128.8 (s, *ortho*-Ph), 129.7 (s, *meta*-Ph), 131.5 (s, *ortho*-Ph), 136.0 (s, C-Ph), 138.8 (d, $J_{P,C}$ = 20.2 Hz, *ipso*-Ph), 140.1 - 142.6 (m, Ph-C), 143.2 (s, *ipso*-Ph), 143.8 (s, *ipso*-Ph), 145.1 (s, Ph-C), 19.8 (dsat, $^{2}J_{P,C}$ = 6.6 Hz, $^{1}J_{W,C}$ = 132.0 Hz, *cis*-CO), 202.3 (d, $^{2}J_{P,C}$ = 32.9 Hz, *trans*-CO)

^{31}P{^{1}H} NMR (CDCl$_3$, in ppm): δ = 167.4

7.4.3.3 Synthesis of {Pentacarbonyl[(2-triphenylmethyl-5-phenyl-benz[c])-1,2-oxaphospholane-κ*P*]tungsten(0)} (9c).

9c: 300 mg, 0.43 mmol; 12-crown-4: 69 µL, 0.43 mmol; ^{t}BuLi: 0.25 mL, 0.50 mmol; benzophenone: 1.22 mL, 0.50 mmol; white solid.

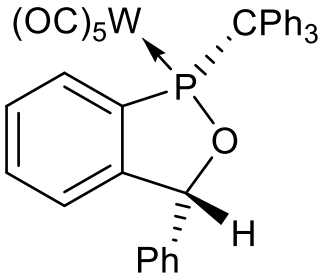

Molecular formula: $C_{37}H_{25}O_6PW$

Molecular weight: 780.09 g/mol

^{1}H NMR (THF-*d8*, in ppm): δ = 5.58 (s, 1H, HCPh$_3$), 6.50 (br. s, 1H, POC(H)Ph), 7.15 (d, $^{3}J_{H,H}$ = 6.70 Hz, 1H, Ar-H), 6.67 (d, $^{3}J_{H,H}$ = 8.18 Hz, 2H, Trt-H), 7.02 (t, $^{3}J_{H,H}$ = 8.80 Hz, 1H, Ar-H), 7,10 - 7,37 (m, 6H, Ph-H, Trt-H), 7,43 - 7,62 (m, 6H, Trt-H), 7,63 - 7,73 (m, 3H, TrtH, Ph-H), 7,77 - 7,85 (m, 3H, Ph-H, Trt-H), 7.91 (d, $^{3}J_{H,H}$ = 6.93 Hz, 2H, Ar-H)

^{13}C{^{1}H} NMR (THF-*d8*, in ppm): δ = 68.6 (d, $^{2/3}J_{P,C}$= 2.1 Hz, POC(H)Ph), 86.3 (d, $^{1}J_{P,C}$ = 8.7 Hz, Ph$_3$C), 123.0 (d, $J_{P,C}$ = 7.4 Hz, Ar-C), 126.3 (s, *para*-Ph), 126.5 (d, $J_{P,C}$ = 10.0 Hz, *ortho*-Ph), 127.3 (s, *meta*-Ph), 128,2 (s, *para*-Ph), 129,5 (s, *ortho*-Ph), 130,0 (s, *meta*-Ph), 132,4 (s, *ortho*-Ph), 137,6 (s, C-Ph), 139,2 - 140.0 (m, Ph-C), 141,1 (d, $J_{P,C}$ = 22.9 Hz, *ipso*-Ph), 143,2 (d, $J_{P,C}$ = 11.6 Hz, *ipso*-Ph), 143.9 (s, *ipso*-Ph), 146,9 (s, Ph-C), 196.5 (dsat, $^{2}J_{P,C}$ = 7.1 Hz, $^{1}J_{W,C}$ = 134.0 Hz, cis-CO), 199,5 (d, $^{2}J_{P,C}$ = 30,9 Hz, *trans*-CO)

^{31}P{^{1}H} NMR (CDCl$_3$, in ppm): δ = 145.1 ($^{1}J_{P,W}$ = 277.5 Hz)

MS (selected data *m/z* (%)): 780.1 $[M]^{+\bullet}$, 537.0 (3) $[M\text{-}CPh_3]^{+}$, 509.0 (1) $[M\text{-}CPh_3\text{ -CO}]^{+}$, 425.1 (20) $[M\text{-}CPh_3\text{-CO-3CO}]^{+}$, 397.1 (40) $[M\text{-}CPh_3\text{-CO-3CO-CO}]^{+}$, 243.2 (100) $[CPh_3]^{+}$

IR (neat, ν(CO), in cm^{-1}): ν = 2076, 1958, 1937 (s, CO)

Elemental analysis: C [%] H [%]

Calculated:	56.94	3.23
Found:	57.28	3.82

7.4.3.4 Structure data of complexes {7,12-Bispentacarbonyl[2,12-epoxy-7-triphenylmethyl-2,5-diphenyl-tetracyclo[4.3.0^{1,13}.0^{3,11}.0^{4,8}]-6,7,12-oxadiphosphahexadec-4,9,13,15,17-pentaen–κ*P*]metal(0)} (10a-c)

10a: metal = chromium; ratio of complex **9a**: complex **10a** = 5:1

Molecular formula: $C_{55}H_{34}Cr_2O_{12}P_2$
Molecular weight: 1052.03 g/mol
$^{31}P\{^1H\}$ NMR (THF-*d8*, in ppm): δ = 165.6 ($^5J_{P7,P12}$ = 3.8 Hz, P12), 210.5 ($^5J_{P7,P12}$ = 3.8 Hz, P7)

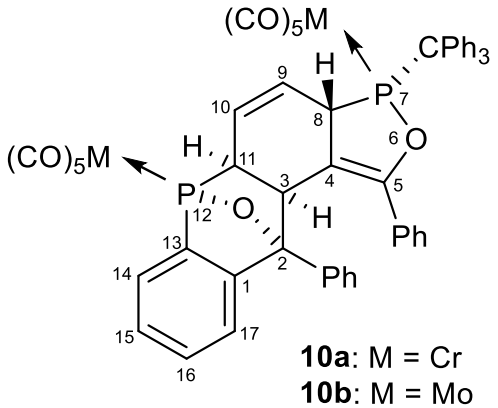

10a: M = Cr
10b: M = Mo
10c: M = W

10b: metal = molybdenum; ratio of complex **9b**: complex **10b** = 5:3

Molecular formula: $C_{55}H_{34}Mo_2O_{12}P_2$
Molecular weight: 1143.96 g/mol

^1H NMR (THF-*d8*, in ppm): δ = 1.81 (br. s, 1H, CH), 3.62 (br. s, 2H, CH), 5.64 (s, 1H, $HCPh_3$), 6.64 (m_c, 1H, CH-sp^2), 7.14 (m_c, 1H, CH-sp^2), 7.22 - 7.24 (m, 4H, Ph-H), 7.27 - 7.32 (m, 6H, Ph-H), 7.42 - 7.47 (m, 4H, Ph-H); 7.53 - 7.58 (m, 6H, CPh_3-H); 7.63 - 7.68 (m, 3H, CPh_3-H); 7.84 - 7.89 (m, 6H, CPh_3 -H)

$^{13}C\{^1H\}$ NMR (THF-*d8*, in ppm): δ = 56.4 (br. s, C2), 86.7 (d, $^1J_{P,C}$ = 9.0 Hz, CPh_3), 125.6 (s, Ar-C), 126.7 (s, *para*-Ph), 127.6 (br. s, *ortho*-Ph), 128.9 (s, *meta*-Ph), 129.2 (s, *para*-Ph), 131.5 (s, *ortho*-Ph), 137.4 (s, *meta*-Ph), 143.7 (s, *ipso*-Ph), 204.2 (dsat, $^2J_{P,C}$ = 8.4 Hz, cis-CO), 221.4 (d, $^2J_{P,C}$ = 54,3 Hz, *trans*-CO) other signals could not be assigned

$^{31}P\{^1H\}$ NMR ($CDCl_3$, in ppm): δ = 138.2 ($^5J_{P7,P12}$ = 3.8 Hz, P12), 186.3 ($^5J_{P7,P12}$ = 3.8 Hz, P7)

10c: metal = tungsten; ratio of complex **9c**: complex **10c** = 5:1

Molecular formula: $C_{55}H_{34}O_{12}P_2W_2$
Molecular weight: 1316.05 g/mol
$^{31}P\{^1H\}$ NMR (THF-*d8*, in ppm): δ = 112.3 ($^5J_{P7,P12}$ = 3.8 Hz, P12), 164.4 ($^5J_{P7,P12}$ = 3.8 Hz, P7)

7.4.4 General procedure for the synthesis of complexes 20-22.

500 mg (0.75 mmol) of [(CPh_3PCl_2)W(CO)$_5$] were dissolved in THF (10 mL) and 120 µL (1.0 eq.) of 12-crown-4 were added. The solution was cooled to -80°C and ^{t}BuLi (1.2 eq., 1.7 M in *n*-pentane) was given drop wise. Subsequently, the corresponding fluorinated aldehyde (1.2 eq.) was added. The suspension was stirred for 2 h while gently warming to -20°C. All volatiles were removed in *vacuo* (*ca.* 0.01 bar) and the residue extracted with 3 x 15 mL of *n*-pentane. After removing of all volatiles *in vacuo (ca. 0.01 bar)*, the obtained light yellow solid was purified by washing with *n*-pentane at -30°C.

7.4.4.1 Synthesis of {Pentacarbonyl[2-triphenylmethyl-3-(2,6-difluoro phenyl)-1,2-oxaphosphiran-κ*P*]tungsten(0)} (20)

2,6-difluorobenzaldehyde: 370 mg, 0.90 mmol

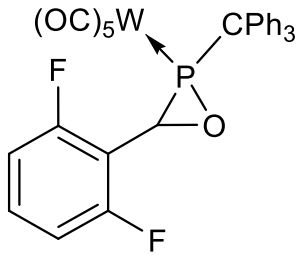

Molecular formula: $C_{31}H_{19}F_2O_6PW$

Molecular weight: 740.29 g/mol

Melting point: 110°C

Yield: 370 mg (0.50 mmol, 74%)

^{1}H NMR ($CDCl_3$, in ppm): δ = 4.95 (1H, s, CHP), 6.9 (1H, t, $^3J_{H,H}$ = 8.5 Hz, *p*-Ar^F), 7.1 - 7.5 (15H, m, 3Ph), 7.6 - 7.7 (2H, dt, H-Ar^F)

^{13}C{^{1}H} NMR ($CDCl_3$, in ppm): δ = 54.0 (d, $^1J_{C,P}$ = 25.6 Hz, PCO), 67.3 (d, $^1J_{C,P}$ = 6.7 Hz, P-CPh_3), 126.3 (s, *p*-Ph), 127.9 (d, $^1J_{C,F}$ = 1.85 Hz, *p*-Ar^F), 128.3 (d, $^3J_{C,P}$ = 5.2 Hz, *m*-Ar^F), 128.7 (s, *m*-Ph), 129.5 (s, *o*-Ph), 130.9 (d, $J_{C,P}$ = 7.3 Hz, *o*-Ph), 139.5 (d, $J_{C,P}$ = 2.4 Hz, *ipso*-Ar^F), 143.9 (s, *ipso*-Ph), 193.8 (d, $^2J_{C,P}$ = 8.1 Hz, *cis*-CO), 195.9 (d, $^2J_{C,P}$ = 41.7 Hz, *trans*-CO)

^{31}P{^{1}H} NMR ($CDCl_3$, in ppm): δ = 8.9 ($^1J_{W,P}$ = 314 Hz)

^{19}F{^{1}H} NMR ($CDCl_3$, in ppm): δ = -120.2

MS (selected data *m/z* (%)): 740.1 $[M]^{+\bullet}$, 598.1 (20) $[M\text{-}C_7H_5F_2O]^+$; 570.0 (20) $[M\text{-}C_7HF_5O\text{-}CO]^+$; 514.0 (20) $[M\text{-}C_7HF_5O\text{-}2CO\text{-}CO]^+$, (100) $[CPh_3]^+$

IR (ATR, ν(CO), in cm^{-1}): ν = 1920 (w), 1984 (m), 2076 (s)

Elemental analysis: C [%] H [%]

Calculated:	50.29	2.34
Found:	51.13	3.01

7.4.4.2 Synthesis of {Pentacarbonyl[2-triphenylmethyl-3-(2,4,6-trifluoro-phenyl)-1,2-oxaphosphiran-κ*P*]tungsten(0)} (21)

2,4,6-trifluorobenzaldehyde: 405 mg, 0.90 mmol

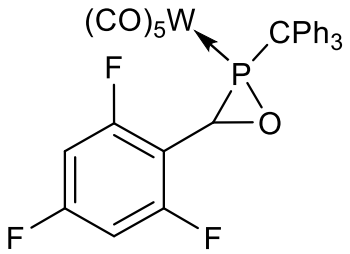

Molecular formula: $C_{31}H_{18}F_3O_6PW$

Molecular weight: 758.27 g/mol

Melting point: 110°C

Yield: 405 mg (0.53 mmol, 81%)

^{1}H NMR ($CDCl_3$, in ppm): δ = 5.75 (1H, s, CHP), 7.1 − 7.5 (15H, m, 3Ph), 7.6 - 7.7 (2H, dt, H-Ar^F)

^{13}C{^{1}H} NMR ($CDCl_3$, in ppm): δ = 53.4 (d, $^1J_{C,P}$ = 25.7 Hz, PCO), 67.4 (d, $^1J_{C,P}$ = 6.3 Hz, P-CPh_3), 126.3 (s, *p*-Ph), 127.9 (d, $^1J_{C,F}$ = 1.85 Hz, *p*-Ar^F), 128.3 (s, *m*-Ph), 128.8 (s, *m*-Ar^F), 129.5 (s, *o*-Ph), 130.9 (d, $J_{C,P}$ = 7.5 Hz, *o*-Ar^F), 139.4 (d, $J_{C,P}$ = 2.5 Hz, *ipso*-Ar^F), 143.9 (s, *ipso*-Ph), 193.9 (d, $^2J_{C,P}$ = 7.9 Hz, *cis*-CO), 195.6 (d, $^2J_{C,P}$ = 41.6 Hz, *trans*-CO)

^{31}P{^{1}H} NMR ($CDCl_3$, in ppm): δ = 8.5 ($^1J_{W,P}$ = 316 Hz)

^{19}F{^{1}H} NMR ($CDCl_3$, in ppm): δ = -131.3 (*o*-F), -146.2 (*p*-F);

MS (selected data, *m/z* (%)): 758.1 $[M]^{+\bullet}$, 598.1 (20) $[M\text{-}C_7H_4F_3O]^+$, 570.0 (20) $[M\text{-}C_7HF_5O\text{-}CO]^+$, 514.0 (20) $[M\text{-}C_7HF_5O\text{-}2CO\text{-}CO]^+$, (100) $[CPh_3]^+$

IR (ATR, ν(CO), in cm^{-1}): ν = 1932 (s), 1952 (m), 1995 (m), 2077 (s)

Elemental analysis: C [%] H [%]

Calculated:	49.10	2.39
Found:	50.66	3.22

7.4.4.3 Synthesis of {Pentacarbonyl[(2-triphenylmethyl-3-pentafluoro-phenyl)-1,2-oxaphosphiran-κ*P*]tungsten(0)} (22)

2,3,4,5,6-pentafluorobenzaldehyde: 112 μL, 0.90 mmol

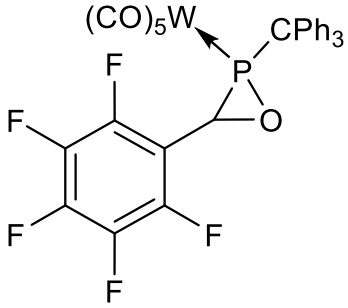

Molecular formula: $C_{31}H_{16}F_5O_6PW$

Molecular weight: 794.01 g/mol

Melting point: 98°C

Yield: 435 mg (0.55 mmol, 87%)

^{1}H NMR ($CDCl_3$, in ppm): δ = 7.06 − 7.72 (15H, m, 3Ph), CHP (hidden by the trityl signals)

^{13}C{^{1}H} NMR ($CDCl_3$, in ppm): δ = 53.3 (d, $^1J_{C,P}$ = 24.7 Hz, PCO), 67.6 (d, $^1J_{C,P}$ = 6.6 Hz, P-CPh_3),128.1 (d, $J_{C,P}$ = 1.8 Hz, Ph), 128.3 (s, Ph), 128.9 (s, Ph), 129.4 (d, $J_{C,P}$ = 11 Hz, Ar^F), 130.8 (d, $J_{C,P}$ = 7.7 Hz, Ar^F), 139.1 (d, $^3J_{C,P}$ = 2.4 Hz, Ar^F), 193.7 (d, $^2J_{C,P}$ = 8.1 Hz, *cis*-CO), 195.1 (d, $^2J_{C,P}$ = 41.8 Hz, *trans*-CO)

^{31}P{^{1}H} NMR ($CDCl_3$, in ppm): δ = 7.5 ($^1J_{W,P}$ = 320 Hz)

^{19}F{^{1}H} NMR ($CDCl_3$, in ppm): δ = -139.5 (*p*-F), -153.2 (*m*-F), -161.4 (*o*-F);

MS (selected data, *m/z* (%)): 794.1 $[M]^{+\bullet}$, 598.1 (20) $[M\text{-}C_7HF_5O]^+$, 542.0 (2) $[M\text{-}C_7HF_5O\text{-}2CO]^+$, 514.0 (3) $[M\text{-}C_7HF_5O\text{-}2CO\text{-}CO]^+$, (100) $[CPh_3]^+$

IR (ATR, ν(CO), in cm^{-1}): ν = 1936 (s), 1956 (b), 1967 (b), 1994 (s), 2077 (s)

Elemental analysis: C [%] H [%]

Calculated:	46.88	2.03
Found:	47.79	3.11

7.4.5 General procedure for the synthesis of complexes 23, 24, 27

To the freshly synthesized Li/Cl phosphinidenoid complex **3a-c**, 12-crown-4 (1.0 eq) and ^{t}BuLi (1.2 eq) in 12 mL of THF, pentafluorobenzaldehyde (1.2 eq) was added at -78°C leading to the formation of a white precipitate. The reaction mixture was warmed up to −15°C in a cooling bath (ca. 2 h), and volatiles were evaporated *in vacuo (ca. 0.01 bar)*. The product was extracted with Et_2O (3 x 20 mL) and filtered. The solvents were then removed in *vacuo* (*ca.* 0.01 bar) and the pale white residue was purified by low temperature column chromatography.

7.4.5.1 Synthesis of {Pentacarbonyl[(2-triphenylmethyl-3-pentafluoro-phenyl)-1,2-oxaphosphiran-κ*P*]chromium(0)} (23)

3a: 1.00 g, 1.86 mmol; 12-crown-4: 0.3 mL, 1.86 mmol; ^{t}BuLi (1.7 M in *n*-hexane) 1.32 mL, 2.24 mmol; pentafluorobenzaldehyde: 0.6 mL, 2.24 mmol

Column chromatography: Al_2O_3, -20°C, h = 4 cm, ø = 5 cm, petroleum ether (300 mL); petroleum ether/diethyl ether 1:1 (300 mL)

Molecular formula: $C_{31}H_{16}CrF_5O_6P$
Molecular weight: 662.00 g/mol
Melting point: 115°C
Yield: 820 mg (1.23 mmol, 82 %)

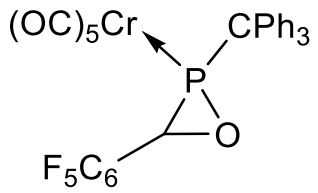

^{1}H NMR ($CDCl_3$, in ppm) δ = 3.93 (1H, s, CHP), 7.12 − 7.62 (15H, m, 3Ph)

^{13}C{^{1}H} NMR ($CDCl_3$, in ppm): δ = 51.1 (d, $^{1}J_{C,P}$ = 21.8 Hz, PCO), 68.8 (d, $^{1}J_{C,P}$ = 13.6 Hz, P-CPh_3), 125.2 (m, Ar^F), 127.1 (d, $^{1}J_{C,P}$ = 1.81 Hz, *p*-Ph), 127.3 (m, Ar^F), 127.9 (s, *m*-Ph), 128.4 (s, Ar^F), 129.6 (d, $J_{C,P}$ = 7.1 Hz, *o*-Ph), 138.0 (d, $J_{C,P}$ = 2.72 Hz, *ipso*-Ar^F), 212.2 (d, $^{2}J_{C,P}$ = 14.1 Hz, *cis*-CO), 216.9 (s, *trans*-CO)

^{31}P{^{1}H} NMR ($CDCl_3$, in ppm): δ = 54.6

^{19}F{^{1}H} NMR ($CDCl_3$, in ppm): δ = -138.3 (*p*-F), -156.1 (*m*-F), -162.3 (*o*-F);

MS (selected data *m/z* (%)): 661.9 $[M]^{+\bullet}$, 597.9 $[M\text{-}3CO]^+$, 549.9 $[M\text{-}3CO\text{-}CO]^+$, 521.9 $[M\text{-}3CO\text{-}CO\text{-}CO]^+$, 326.0 $[M\text{-}3CO\text{-}CO\text{-}CO\text{-}C_7HF_5O]^+$, 274.0 $[M\text{-}3CO\text{-}CO\ \text{-}CO\text{-}C_7HF_5O\text{-}Cr]^+$, 243.1 $[M\text{-}3CO\text{-}CO\text{-}CO\text{-}C_7HF_5O\text{-}Cr\text{-}P]^+$

IR (neat, ν(CO), in cm^{-1}): ν = 2070, 1993, 1963(s, CO), 1941(sh), 1932(br)

Elemental analysis: C [%] H [%]

Calculated: 56.21 2.43

Found: 55.94 3.06

7.4.5.2 Synthesis of {Pentacarbonyl[(2-triphenylmethyl-3-pentafluoro phenyl)-1,2-oxa-phosphiran-κ*P*]-molybdenum(0)} (24)

3b: 300 mg, 0.52 mmol; 12-crown-4: 66 µL, 0.48 mmol; ^{t}BuLi (1.6 M in *n*-hexane): 0.39 mL, 0.58 mmol; pentafluorobenzaldehyde: 77 µL, 0.58 mmol

Column chromatography: Al_2O_3, -20°C, h = 2 cm, ø = 1 cm, petroleum ether (100 mL); petroleum ether/diethyl ether 1:1 (300 mL).

Molecular formula: $C_{31}H_{16}F_5MoO_6P$
Molecular weight: 706.35 g/mol
Melting point: 92°C
Yield: 263 mg (0.37 mmol, 88 %)

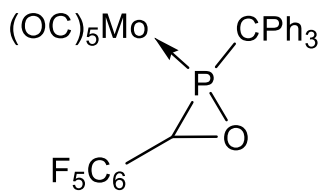

^{1}H NMR ($CDCl_3$, in ppm) δ = 3.78 (s, 1H, CHP), 7.03 - 7.52 (m, 15H, CPh_3)

^{13}C{^{1}H} NMR ($CDCl_3$, in ppm): δ = 52.3 (d, $^{1}J_{C,P}$ = 20.2 Hz, PCO), 66.3 (d, $^{1}J_{C,P}$ = 13.6 Hz, $PCPh_3$), 125.3 (s, Ar^F), 128.1 (d, $^{1}J_{C,P}$ = 1.82 Hz, *m*-Ph), 127.3 (s, Ar^F), 127.8 (s, *p*-Ph), 128.4 (s, Ar^F), 129.7 (d, $J_{C,P}$ = 7.31 Hz, *o*-Ph), 139.2 (d, $J_{C,P}$ = 3.09 Hz, *ipso*-Ph), 202.7 (d, $^{2}J_{C,P}$ = 9.9 Hz, *cis*-CO), 205.5 (d, $^{2}J_{C,P}$ = 42.3 Hz, *trans*-CO)

^{31}P{^{1}H} NMR ($CDCl_3$, in ppm): δ = 27.9

^{19}F{^{1}H} NMR ($CDCl_3$, in ppm): δ = -136.1 (*p*-F), -151.4 (*m*-F), -161.6 (*o*-F);

MS (selected data *m/z* (%)): 707.9 $[M]^{+\bullet}$, 511.9 $[M\text{-}C_7HF_5O]^{+}$, 274.1 $[M\text{-}C_7HF_5O\text{ -}Mo(CO)_5]^{+}$, 243.1 $[M\text{-}C_7HF_5O\text{-}Mo(CO)_5\text{-}P]^{+}$

IR (neat, ν(CO), in cm^{-1}): ν = 2078, 1996, 1968(s, CO), 1959(sh), 1937(br)

Elemental analysis: C [%] H [%]

Calculated: 52.71 2.28

Found: 52.51 2.53.

7.4.5.3 Synthesis of {Pentacarbonyl [(2-pentamethylcyclopentadienyl-3 -pentafluorophenyl)-1,2-oxaphosphiran-κ*P*]-tungsten(0)} (27)

28: 600 mg, 1.07 mmol; 12-crown-4: 0.15 mL, 1.07 mmol; ^{t}BuLi (1.6 M in *n*-hexane): 1.33 mL, 2.14 mmol; pentafluorobenzaldehyde: 0.25 mL, 2.14 mmol

Column chromatography: Al_2O_3, -20°C, h = 2 cm, ø = 1 cm, petroleum ether (100 mL); petroleum ether/diethyl ether 1:1 (300 mL).

Molecular formula: $C_{22}H_{16}F_5O_6PW$
Molecular weight: 686.17 g/mol
Melting point: 129°C
Yield: 547 mg (0.69 mmol, 91%)

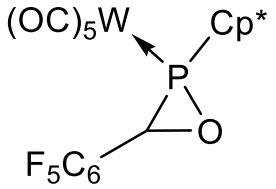

^{1}H NMR ($CDCl_3$, in ppm): δ = 1.11 (3H, d, $^{3}J_{P,H}$= 12.2 Hz, Cp*-C^{1}-CH_3), 1.79 (6H, m_c, Cp*-CH_3), 1.9 (3H, s, Cp*-CH_3), 1.97 (3H, s, Cp*-CH_3), 4.4 (1H, s, POC-H)

^{13}C{^{1}H} NMR ($CDCl_3$, in ppm): δ = 9.6 (t, $J_{P,C}$ = 2.8 Hz, Cp*-CH_3), 10.4 (d, $J_{P,C}$ = 2.03 Hz, Cp*-CH_3), 10.6 (d, $J_{P,C}$ = 1.2 Hz, Cp*-CH_3), 10.99 (d, $J_{P,C}$ = 2.2 Hz, Cp*-CH_3), 12.5 (d, $J_{P,C}$ = 5.8 Hz, Cp*-C^{1}-CH_3), 49.1 (d, $J_{P,C}$ = 17.8 Hz, P-CH-Ar^{F}), 62.8 (d, $J_{P,C}$ = 9.6 Hz, Cp*-C^{1}), 109 (m, *ipso*-Ar^{F}), 132.5 (d, $J_{P,C}$ = 6.9 Hz-Cp*), 135.2 (m, Ar^{F}), 136.1 (d, $J_{P,C}$ = 2.1 Hz-Cp*), 138.5 (m, *o*-Ar^{F}), 142.1 (d, $J_{P,C}$ = 6.3 Hz, Cp*), 144 (d, $J_{P,C}$ = 8 Hz, Cp*), 146, (m, *m*-Ar^{F}), 192 (d, $J_{P,C}$ = 8.2 Hz, $J_{W,C}$ = 125.7 Hz, *cis*-CO), 193, (d, $^{2}J_{P,C}$ = 39 Hz, *trans*-CO)

^{19}F{^{1}H} NMR ($CDCl_3$, in ppm): δ = -139.6 (*p*-F), -153.1 (*m*-F), -162.0 (*o*-F);

^{31}P{^{1}H} NMR ($CDCl_3$, in ppm): δ = 26.4

MS (selected data *m/z* (%)): 686.9 $[M]^{+\bullet}$, 490.1 $[M\text{-}C_7HF_5O]^{+}$, 323.9 $[M\text{-}C_7HF_5O\text{ -}W(CO)_5]^{+}$

Elemental analysis: C [%] H [%]

Calculated:	38.31	2.35
Found:	38.46	2.62

7.4.6 Synthesis of {Pentacarbonyl-[triphenylmethyl-(1,1,3,3,3-pentafluoro prop-1-en-2-oxyl)chlorophosphane-κ*P*]-tungsten(0)} (33)

500 mg (0.75 mmol) of $[W(CO)_5(CPh_3PCl_2)]$ were dissolved in THF (10 mL) and 120 µL (1.0 eq.) of 12-crown-4 were added. The solution was then cooled to -100°C and 1.2 eq. of ^{t}BuLi (1.7 M in *n*-pentane) were added dropwise. Afterwards hexafluoroacetone was bubbled through the solution for a few seconds until the color changed from orange to green. Subsequently, the solvent was removed in *vacuo* (*ca.* 0.01 bar) at low temperature (-20°C) and the residue extracted with 45 mL of *n*-pentane. All volatiles were removed *in vacuo* (ca. 0.01 bar), the residue was purified by washing with *n*-pentane at -30°C and the resulting product isolated was light yellow solid.

Molecular formula: $C_{27}H_{15}ClF_5O_6PW$

Molecular weight: 780.66 g/mol

Melting point: 110°C (decomp.)

Yield: 460 mg (0.50 mmol, 92 %)

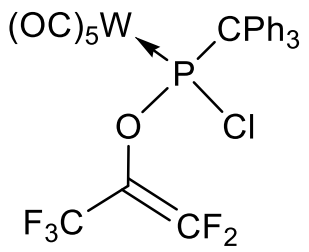

^{1}H NMR ($CDCl_3$, in ppm): δ = 7.1 − 7.5 (m, 15H, 3Ph)

^{13}C{^{1}H} NMR ($CDCl_3$, in ppm): δ = 73.9 (d, $^1J_{C,P}$ = 9.1 Hz, P-<u>C</u>Ph$_3$), 107.5 (br m, CF_3<u>C</u>CF_2), 119.3 (q m, $^1J_{C,F}$ = 274 Hz, CF_3), 125.9 (s, *p*-Ph), 127.3 (d, $^4J_{C,P}$ = 1.5 Hz, *m*-Ph), 127.7 (d, $^4J_{C,P}$ = 1.6 Hz, *m*-Ph), 127.8 (d, $^3J_{C,P}$ = 3.1 Hz, *o*-Ph), 127.9 (s, *p*-Ph), 128.1 (d, $^4J_{C,P}$ = 1.2 Hz, *m*-Ph), 128.3 (d, $^3J_{C,P}$ = 3.2 Hz, *o*-Ph), 128.5 (d, $^4J_{C,P}$ = 1.8 Hz, *m*-Ph), 129.1 (s, *p*-Ph), 130.6 (d, $^3J_{C,P}$ = 7.7 Hz, *o*-Ph), 131.1 (d, $^3J_{C,P}$ = 8.3 Hz, *o*-Ph), 138.4 (d, $^2J_{C,P}$ = 4.5 Hz, *ipso*-Ph), 139.9 (d, $^2J_{C,P}$ = 7.1 Hz, *ipso*-Ph), 140.4 (d, $^2J_{C,P}$ = 13.6 Hz, *ipso*-Ph), 155.7 (pt m, $^1J_{C,F}$ = 297 Hz, CF_2), 194.0 (ddsat, $^2J_{C,P}$ = 7.1 Hz, $J_{C,F}$ < 1 Hz, $J_{C,W}$ = 127.5 Hz, *cis*-CO), 195.7 (d, $^2J_{C,P}$ = 45.4 Hz, *trans*-CO)

^{19}F NMR ($CDCl_3$, in ppm): δ = -63.2 (d m, 3F, $J_{F,F}$ = 23 Hz, -CF_3), -77.2 (d m, 1F, $J_{F,F}$ = 23 Hz, C=CF), -92.5 (pquint m, 1F, $J_{F,F}$ = 23 Hz, C=CF)

^{31}P{^{1}H} NMR ($CDCl_3$, ppm): δ = 200.6 (t_{sat}, $^1J_{W,P}$ = 336.5 Hz; $^4J_{P,F}$ = 6.0 Hz)

MS (selected data *m/z* (%)): 780 $[M]^{+\bullet}$, 640.0 (30) $[M\text{-}5CO]^+$, 455.9 (20) $[M\text{-}5CO\ \text{-}W]^+$; 309.1 (30) $[M\text{-}5CO\text{-}W\text{-}C_3F_5O]^+$; 243.1 (100) $[CPh_3]^+$

IR (ATR, ν(CO), in cm^{-1}): ν = 2084, 2017, 2003, 1958, 1941, (s, CO)

Elemental analysis: C [%] H [%]

Calculated: 41.54 1.94

Found: 41.27 2.26

7.4.7 Synthesis of {Pentacarbonyl[Pentamethylcyclopentadienyl-(1,1,3,3,3 -pentafluoroprop-1-en-2-oxyl)-chlorophosphane-κ*P*]-tungsten(0)} (34)

500 mg (0.89 mmol) of $[W(CO)_5(Cp^*PCl_2)]$ were dissolved in THF (10 mL) and 176 µL (1.0 eq.) of 12-crown-4 were added. The solution was then cooled to -100°C and 1.2 eq. of ^tBuLi (1.7 M in *n*-pentane) were added dropwise. Afterwards, hexafluoroacetone was bubbled through the solution for a few seconds until the color changed from dark yellow to green. Subsequently, the solvent was removed in *vacuo* (*ca.* 0.01 bar) at low temperature (-20°C) and the residue extracted with 45 mL of *n*-pentane. All volatiles were removed *in vacuo* (ca. 0.01 bar), the residue was purified by washing with *n*-pentane at -30°C and the resulting product isolated was light yellow solid.

Molecular formula: $C_{18}H_{15}ClF_5O_6PW$

Molecular weight: 672.97 g/mol

Melting point: 126°C

Yield: 460 mg (0.53 mmol, 91 %)

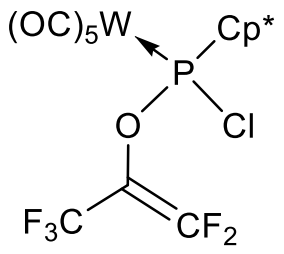

^{1}H NMR ($CDCl_3$, in ppm): δ = 1.43 (d, 3H, $^3J_{P,H}$ = 14.1 Hz, Cp*-C^1-CH_3), 1.77 (d, 6H, $J_{P,H}$ = 3.2 Hz, Cp*-CH_3), 1.87 (d, 6H, $J_{P,H}$ = 15.4 Hz Cp*-CH_3)

^{13}C{^{1}H} NMR ($CDCl_3$, in ppm): δ = 11.6 (d, $J_{C,P}$ = 3.7 Hz, Cp*-CH_3), 11.9 (d, $J_{C,P}$ = 1.9 Hz, Cp*-CH_3), 12.7 (br s, Cp*-CH_3), 13.6 (d, $J_{C,P}$ = 7.2 Hz, Cp*-CH_3), 69.2 (d, $^1J_{C,P}$ = 6.3 Hz, P-Cp*), 106.9 (br m, $CF_3\underline{C}CF_2$), 121.6 (qdd, $^1J_{C,F}$ = 269.7 Hz, CF_3), 135.2 (d, $J_{C,P}$ = 8.9 Hz, Cp*-ring-C), 135.6 ($J_{C,P}$ = 5.9 Hz, Cp*), 145.3 (d, $J_{C,P}$ = 9.1 Hz, Cp*-ring-C), 145.5 (d, $J_{C,P}$ = 9.1 Hz, Cp*-ring-C), 155.9 (ddq, $^1J_{C,F}$ = 298.8 Hz, CF_2), 194.5 (ddsat, $^2J_{C,P}$ = 7.6, $J_{C,F}$ = 1.9 Hz, $J_{C,W}$ = 128.3 Hz, *cis*-CO), 195.7 (d, $^2J_{C,P}$ = 42.9 Hz, *trans*-CO)

^{19}F NMR ($CDCl_3$, in ppm): δ = -65.3 (dd, 3F, $J_{F,F}$ = 20.6 Hz, CF_3), -76.6 (dq, 1F, $J_{F,F}$ = 52.3 Hz, C=CF), -88.9 (dq, 1F, $J_{F,F}$ = 59.2 Hz, C=CF)

$^{31}P\{^1H\}$ NMR ($CDCl_3$, in ppm): δ = 193.2 ppm (t_{sat}, $^1J_{W,P}$ = 344.4 Hz, $^4J_{P,F}$ = 7.2 Hz)

MS (selected data *m/z* (%)): 672 (100) $[M]^{+\bullet}$, 616.0 (30) $[M\text{-}2CO]^+$; 588.0 (70) $[M\text{-}2CO\text{-}CO]^+$; 532.0 (90) $[M\text{-}2CO\text{-}CO\text{-}2CO]^+$, 348.1 (10) $[M\text{-}2CO\text{-}CO\text{-}2CO\text{-}W]^+$; 201.1 (10) $[M\text{-}2CO\text{-}CO\text{-}2CO\text{-}W\text{-}C_3F_5O]^+$

IR (ATR, ν(CO), in cm^{-1}): ν = 2077 (s), 1998 (br), 1919 (s);

Elemental analysis: C [%] H [%]

Calculated:	32.15	2.25
Found:	32.41	2.83

7.4.8 Synthesis of {Pentacarbonyl[trimethylsilylmethyl-(1,1,1,3,3,3- hexafluoro-2-ol–propan-2-yl)-phosphanol-κ*P*]-tungsten(0)} (35)

500 mg (0.85 mmol) of $[W(CO)_5\{(Me_3Si)_2HCPCl_2\}]$ were dissolved in THF (10 mL) and 138 µL (1.0 eq.) of 12-crown-4 were added. The solution was cooled to -100°C and 1.2 eq. of ^{t}BuLi [1.7 M in *n*-pentane] were given dropwise. Afterwards, hexafluoroacetone was bubbled through the solution for a few seconds until the color changed from dark yellow to green. Subsequently, the solvent was removed *in vacuo* (*ca.* 0.01 bar) at low temperature (-20°C) and the residue extracted with 45 mL of *n*-pentane. In addition to the main product **35**, two phosphorus resonances with lower intensity were observed at 31.0 ppm (~20%, m_c) and 176.8 ppm (~10%, m_c). A separation of the product mixture was not possible, neither by recrystallisation nor by chromatography. Therefore, complex **35** could only be characterized from this solution by means of multinuclear NMR spectroscopy, but its molecular structure was confirmed by X-ray crystallography.

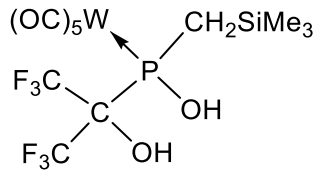

Molecular formula: $C_{12}H_{13}F_6O_7PsiW$

Molecular weight: 626.13 g/mol

^{1}H NMR ($CDCl_3$, in ppm): δ = 0.21 (s, 9H, $Si(CH_3)_3$), 3.3 (d, $^2J_{P,H}$ = 9.5 Hz, 2H, PCH2), 9.6 (d, $^2J_{P,H}$ = 36.5 Hz, 1H, P-OH), PC-OH, n.o.

$^{13}C\{^1H\}$ NMR ($CDCl_3$, in ppm): δ = 1.66 (d, $^3J_{C,P}$ = 6.6 Hz, $Si(CH_3)_3$), 49.3 (d, $^1J_{C,P}$ = 117.0 Hz, CH_2P), 122.4 (q m, $^1J_{C,F}$ = 287 Hz, CF_3), 123.7 (q m, $^1J_{C,F}$ = 285.0 Hz, CF_3), ($F_3C\underline{C}CF_3$, not found), 194.3 (d, $^2J_{C,P}$ = 9.3 Hz, *cis*-CO), 196.6 (d, $^2J_{C,P}$ = 35.2 Hz, *trans*-CO)

^{19}F NMR ($CDCl_3$, in ppm): δ = -67.1 (m_c, 3F, CF_3,), -67.5 (m_c, 3F, CF_3)

^{31}P{^{1}H} NMR ($CDCl_3$, in ppm): δ = 247.6 (m_{sat} ,$^1J_{W,P}$ = 277.8 Hz, $^2J_{P,H}$ = 36.5 Hz)

7.4.9 Synthesis of {Pentacarbonyl [(2-pentamethylcyclopentadienyl -3-phenyl-3-trifluoromethyl)-1,2-oxaphosphiran-κ*P*]-pentacarbonyl tungsten(0)} (41)

To the freshly synthesized Li/Cl phosphinidenoid complex **28** (500 mg, 0.89 mmol), 12-crown-4 (115 µL, 0.71 mmol) and ^{t}BuLi (1.6 M in *n*-hexane, 0.67 mL) in 7 mL of THF, 2,2,2-trifluoroacetophenone was added (160 µL, 1.1 mmol) at -78°C leading to the formation of a white precipitate. The reaction mixture was warmed up to −15°C in the cooling bath (ca. 2 h) and volatiles were evaporated *in vacuo (ca. 0.01 bar)*. The product was extracted with Et_2O (3 x 15 mL) and filtered. The solvents were then removed *in vacuo* (*ca.* 0.01 bar) and the pale white residue was purified by low temperature column chromatography Al_2O_3, -20°C, h = 2 cm, ø = 1 cm, petroleum ether (150 mL); petroleum ether/dichloromethane 10:1 (150 mL).

Molecular formula: $C_{23}H_{20}F_3O_6PW$

Molecular weight: 664.22 g/mol

Melting point: 129°C

Yield: 547 mg (0.69 mmol, 91%)

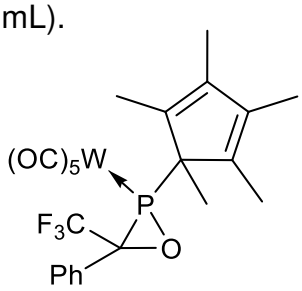

^{1}H NMR ($CDCl_3$, in ppm): δ = 0.16 (3H, d, $^3J_{P,H}$ = 11.3 Hz, Cp*-*i*-CH_3), 1.81 (6H, m_c, Cp*-CH_3), 1.9 (3H, s, Cp*-CH_3), 2.1 (3H, s, Cp*-CH_3), 7.4 - 7.5 (5H, m, Ph)

^{13}C{^{1}H} NMR ($CDCl_3$, in ppm): δ = 10.6 (2, $J_{P,C}$ = 2.4 Hz, Cp*-CH_3), 11.0 (d, $J_{P,C}$ = 1.2 Hz, Cp*-CH_3), 11.1 (m_c, Cp*-CH_3), 16.8 (d, $J_{P,C}$ = 6.1 Hz, Cp*-C^1-CH_3), 63.6 (dd, $J_{P,C}$ = 35.3 Hz, $J_{F,C}$ = 8.9 Hz, P-C-CF_3), 65.7 (d, $J_{P,C}$ = 13.9 Hz, Cp*-C^1), 122.3 (dd, $J_{P,C}$ = 6.9 Hz, $J_{F,C}$ = 273.6 Hz, P-C-CF_3),127.1 (s, Ph), 127.7 (s, Ph), 128.2 (s, Ph), 130.4 (d, $J_{P,C}$ = 0.6 Hz, *i*-Ph), 134.2 (d, $J_{P,C}$ = 10.5 Hz, Cp*), 138.3 (d, $J_{P,C}$ = 4.7 Hz, Cp*), 142.5 (d, $J_{P,C}$ = 7.7 Hz, Cp*), 143.8 (d, $J_{P,C}$ = 8.6 Hz, Cp*), 193.2 (m_c, $J_{C,W}$ = 136.9 Hz, *cis*-CO), 193.9 (d, $^2J_{P,C}$ = 40.2 Hz, *trans*-CO)

^{19}F NMR ($CDCl_3$, in ppm): δ = -64.8 (d, 3F, $^3J_{P,F}$ = 1.3 Hz, CF_3)

^{31}P{^{1}H} NMR ($CDCl_3$, in ppm): δ = 41.8 ($^1J_{W,P}$ = 311.9 Hz)

7.4.10 Synthesis of 1,2-(bistriphenylmethyl-bispentafluorobenzyl)-diphosphan-P,P'-dioxid) (45)

A solution of complex **22** (200 mg, 0.25 mmol) in toluene was stirred at 100 °C for 4 hours. All volatiles were removed *in vacuo* (ca. 0.01 bar) and a column chromatography was performed (Al_2O_3, -20°C, h = 2 cm, ø = 1 cm, petroleum ether (100 mL); petroleum ether/diethyl ether 1:1 (300 mL)).

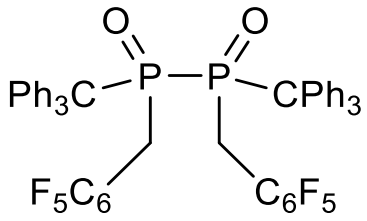

Molecular formula: $C_{52}H_{34}F_{10}O_2P_2$

Molecular weight: 942.77 g/mol

^{1}H NMR (THF-*d8*, in ppm): δ = 2.6 (2H, dd, $^3J_{P,H}$ = 282.8 Hz, $^3J_{H,H}$ = 10.6 Hz), 3.2 (2H, dd, $^3J_{P,H}$ = 282.8 Hz, $^3J_{H,H}$ = 10.6 Hz), .6.5 − 7.9 (15H, m, 3Ph)

^{13}C{^{1}H} NMR (THF-*d8*, in ppm): δ = 26.5 (d, $^1J_{C,P}$ = 34.2 Hz, CH_2), 66.0 (d, $^1J_{C,P}$ = 26.6 Hz, CPh_3), 127.5 (s, *p*-Ph), 128.2 (s, *m*-Ph), 129.5 (s, *o*-Ph), 134.6 (m, C_6F_5), 138.0 (m, C_6F_5), 140.2 (m, C_6F_5), 142.6 (m, C_6F_5), 144.0 (s, *i*-Ph), 145.9 (m, *i*-C_6F_5)

^{19}F{^{1}H} NMR ($CDCl_3$, in ppm): δ = -136.4 (major, *p*-F), -137.4 (minor, *p*-F), -157.1 (minor, *m*-F), -157.4 (major, *m*-F), -163.6 (minor, *o*-F), -164.1 (major, *p*-F).

^{31}P{^{1}H} NMR (THF-*d8*, in ppm): δ = 48.2 (minor, s), 50.4 (major, s)

7.4.11 General procedure for the synthesis of complexes 53-55

350 mg (0.45 mmol) of complex **1** were dissolved in CH_2Cl_2 (7 mL) and 90 μL (2 eq.) of TfOH were added. After that, 2 eq of the corresponding aldehyde were added and the solution was stirred under refluxing conditions for 2 h. The dark brown solution was cooled until room temperature and 2 eq. of Et_3N (140 μL) were added dropwise. The color of the solution turned into light yellow and the reaction mixture was stirred for 10 min. The solvents were removed in *vacuo* (*ca.* 0.01 bar) and the light yellow oily residue was purified by low temperature column chromatography Al_2O_3, -20°C, h = 2 cm, ø = 1 cm, petroleum ether (200 mL); petroleum ether/diethyl ether 4:1 (200 mL), resulting in a light yellow solid.

7.4.11.1 Synthesis of {Pentacarbonyl[(4-triphenylmethyl-2-phenyl -5-pentafluorophenyl)-1, 3,4-dioxaphospholane-κP]-tungsten(0)} (53)

Benzaldehyde: 91 µL (0.90 mmol)

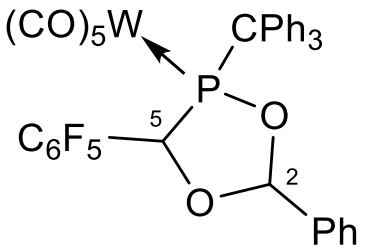

Molecular formula: $C_{38}H_{22}F_5O_7PW$

Molecular weight: 900.05 g/mol

Yield: 245 mg (0.28 mmol, 70 %)

^{1}H NMR (THF-*d8*, in ppm): δ = 5.8 (1H, d, $^3J_{P,H}$ = 4.2 Hz, C^5-H), 6.1 (1H, d, $^3J_{P,H}$ = 2.9 Hz, C^2-H), 6.6 − 7.3 (15H, m, 3Ph), 7.5 (5H, m, Ph)

^{13}C{^{1}H} NMR ($CDCl_3$, in ppm): δ = 68.1 (d, $^2J_{C,P}$ = 4.1 Hz C-Ph_3), 72.1 (d, $^3J_{C,P}$ = 3.8 Hz, $C^{2/5}$), 99.2 (br, $C^{5/2}$),126.5 (s, Ph) 126.9 (s, Ph), 127.2 (s, Ph), 127.8 (s, Ph), 128.3 (s, Ph), 128.5 (s, Ph), 130.2 (s, Ph), 131.0 (s, Ph), 132.6 (d, $^3J_{C,P}$ = 4.2 Hz, *i*-Ph), 133.6 (d, $^3J_{C,P}$ = 5.1 Hz, *i*-Ph), 139.5 (d, $^3J_{C,P}$ = 6.5 Hz, *i*-Ph), 141.4 (m, *i*- C_6F_5), 156.2 (m, *o*-C_6F_5), 161.1 (m, *m*-C_6F_5), 163.8 (m, *p*-C_6F_5), 195.1 (dSat, $^2J_{C,P}$ = 5.9 Hz, $^1J_{W,C}$ = 129.2 Hz, *cis*-CO), 197.1 (d, $^2J_{C,W}$ = 37.2 Hz, *trans*-CO)

^{19}F NMR ($CDCl_3$, in ppm): δ = -137.3 (d, $^3J_{F,F}$ = 17.0 Hz, *o*-C_6F_5), -145.8 (t, $^3J_{F,F}$ = 18.8 Hz, *p*-C_6F_5), -156.1 (t, $^3J_{F,F}$ = 15.6 Hz, *m*- C_6F_5)

^{31}P{^{1}H} NMR ($CDCl_3$, in ppm): δ = 137.0 ($^1J_{W,P}$ = 297.2 Hz)

MS (selected data *m/z* (%)): 900.0 $[M]^{+\bullet}$, 816.0 $[M\text{-}3CO]^+$, 710.0 $[M\text{-}3CO\text{-}C_7H_6O]^+$, 466.9 $[M\text{-}3CO\text{-}C_7H_6O\text{-}CPh_3]^+$

Elemental analysis: C [%] H [%]

Calculated:	50.69	2.46
Found:	49.71	2.89

7.4.11.2 Synthesis of {Pentacarbonyl[4-triphenylmethyl-2-(2,6-difluoro phenyl)-5-pentafluorophenyl]-1,3,4dioxaphospholane-κ*P*}-tungsten(0) (54)

Difluoro benzaldehyde: 85 mL (0.90 mmol)

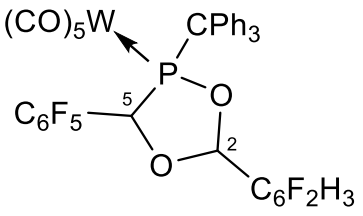

Molecular formula: $C_{38}H_{20}F_7O_7PW$

Molecular weight: 936.36 g/mol

Yield: 281 mg (0.30 mmol, 80 %)

^{1}H NMR (THF-*d8*, in ppm): δ = 6.6 (2H, m, C^2,C^5), 7.1−7.5 (15H, m, 3Ph), 7.6 (1H, br, H-Ar^F), 7.7 (1H, br, H-Ar^F), 7.8 (1H, br, H-Ar^F)

^{13}C{^{1}H} NMR ($CDCl_3$, in ppm): δ = 69.6 (d, $^2J_{C,P}$ = 3.2 Hz C-Ph_3), 76.3 (br, C^2), 100.9 (br, C^5), 127.9 (s, Ph), 128.3 (s, Ph), 128.5 (s, Ph), 128.6 (s, Ph), 129.4 (s, Ph), 131.4 (br, Ar^F-H), 131.7 (br, Ar^F-H), 132.5 (br, Ar^F-H), 137.9 (d, $^3J_{C,P}$ = 5.7 Hz, *i*-Ph), 139.6 (d, $^3J_{C,P}$ = 5.7 Hz, *i*-Ph), 141.2 (d, $^3J_{C,P}$ = 7.3 Hz, *i*-Ph), 143.9 (m, *i*-Ar^F), 146.2 (m, *i*-C_6F_5), 160.8 (m, *o*-C_6F_5), 163.0 (m, *m*-C_6F_5), 165.0 (m, *p*-C_6F_5), 195.6 (dSat, $^2J_{C,P}$ = 6.8 Hz, $^1J_{W,C}$ = 134.3 Hz, *cis*-CO), 197.4 (d, $^2J_{C,W}$ = 36.2 Hz, *trans*-CO)

^{19}F NMR ($CDCl_3$, in ppm): δ = -117.3 (s, Ar^F), -139.2 (d, $^3J_{F,F}$ = 15.5 Hz, *o*-C_6F_5), -148.8 (t, $^3J_{F,F}$ = 19.3 Hz, *p*-C_6F_5), -158.1 (t, $^3J_{F,F}$ = 15.8 Hz, *m*-C_6F_5)

^{31}P{^{1}H} NMR ($CDCl_3$, in ppm): δ = 137.6 ($^1J_{W,P}$ = 297.2 Hz)

MS (selected data *m/z* (%)): 936.0 $[M]^{+\bullet}$, 880.4 $[M\text{-}2CO]^+$, 612.1 $[M\text{-}2CO\text{-}3CO\text{-}W]^+$, 368.9 $[M\text{-}2CO\text{-}3CO\text{-}W\text{-}CPh_3]^+$

Elemental analysis: C [%] H [%]

Calculated:	48.74	2.15
Found:	49.83	2.98

7.4.11.3 Synthesis of {Pentacarbonyl[(4-triphenylmethyl-2,5–bispentafluoro phenyl)-1,3,4-dioxaphospholane-κ*P*]-tungsten(0)} (55)

Pentafluoro benzaldehyde: 110 μL (0.90 mmol)

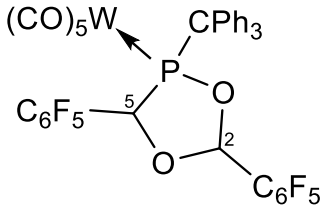

Molecular formula: $C_{38}H_{17}F_{10}O_7PW$

Molecular weight: 990.34 g/mol

Yield: 293 mg (0.30 mmol, 84 %)

^{1}H NMR (THF-*d8*, in ppm): δ = 6.4 (1H, d, $^3J_{P,H}$ = 4.9 Hz, C^5-H), 6.9 (1H, d, $^3J_{P,H}$ = 2.7 Hz, C^2-H), 7.2 − 7.8 (15H, m, 3Ph)

^{13}C{^{1}H} NMR ($CDCl_3$, in ppm): δ = 69.9 (br, C-Ph_3), 77.6 (d, $^1J_{C,P}$ = 2.6 Hz, C^2), 101.2 (d, $^3J_{C,P}$ = 8.3 Hz, C^5), 125.6 (d, $J_{C,P}$ = 3.8 Hz, Ph), 125.7 (s, Ph), 126.9 (s, Ph), 127.0 (s, Ph), 127.2 (s, Ph), 127.6 (d, $J_{C,P}$ = 5.7 Hz, *i*-Ph), 127.9 (s, Ph), 128.8 (d, $J_{C,P}$ = 5.6 Hz, *i*-Ph), 130.4 (br, *i*-Ar^F), 130.9 (br, *i*-Ar^F), 131.6 (br, Ar^F), 135.7 (m, Ar^F), 138.7 (m, Ar^F), 139.6 (m, Ar^F), 141.5 (m, Ar^F), 143.9 (m, Ar^F), 194.9 (dSat, $^2J_{C,P}$ = 7.2 Hz, $^1J_{W,C}$ = 132.3 Hz, *cis*-CO), 196.4 (d, $^2J_{C,W}$ = 34.9 Hz, *trans*-CO)

^{19}F NMR ($CDCl_3$, in ppm): δ = -136.3 (d, $^3J_{F,F}$ = 19.1 Hz, *o*-Ar^F), -140.7 (d, $^3J_{F,F}$ = 17.2 Hz, *o*-Ar^F), -153.8 (t, $^3J_{F,F}$ = 21.2 Hz, *p*-Ar^F), -154.4 (d, $^3J_{F,F}$ = 20.7 Hz, *p*-Ar^F), -162.4 (t, $^3J_{F,F}$ = 17.3 Hz, *m*-Ar^F), -163.3 (t, $^3J_{F,F}$ = 16.9 Hz, *m*-Ar^F)

^{31}P{^{1}H} NMR ($CDCl_3$, in ppm): δ = 162.9 ($^1J_{W,P}$ = 293.1 Hz)

MS (selected data *m/z* (%)): 990.0 $[M]^{+\bullet}$, 933.9 $[M\text{-}2CO]^+$, 666.2 $[M\text{-}2CO\text{-}3CO\text{-}W]^+$, 423.21 $[M\text{-}2CO\text{-}3CO\text{-}CPh_3]^+$

Elemental analysis: C [%] H [%]

Calculated:	46.09	1.73
Found:	46.57	2.01

7.4.12 Synthesis of {Pentacarbonyl[2-ethoxy-3-pentafluorophenyl-1,5,6,7,8-pentamethyl-bicyclo[3.3.0]4,2-oxaphosphaoct-6-en-κ*P*]-tungsten(0)} (60)

170 mg (0.25 mmol) of complex **27** were dissolved in CH_2Cl_2 (5 mL) and 45 μL (2 eq.) of TfOH were added. After 10 min. of stirring, an excess of ETOH was added and the solution was stirred at 0°C for 10 min. Then 2 eq. of Et_3N (70 μL) were added dropwise to the dark brown solution. The color of the solution turned into light yellow and the reaction mixture was stirred for other extra 10 min. The solvent was removed *in vacuo* (ca. 0.01 bar) and the light yellow oily residue was purified by low temperature column chromatography Al_2O_3, -20°C, h = 2 cm, ø = 1 cm, petroleum ether (200 mL); petroleum ether/diethyl ether 4:1 (200 mL), resulting in a white solid.

Molecular formula: $C_{24}H_{22}F_5O_7PW$

Molecular weight: 732.1 g/mol

Yield: 145 mg (0.30 mmol, 85 %)

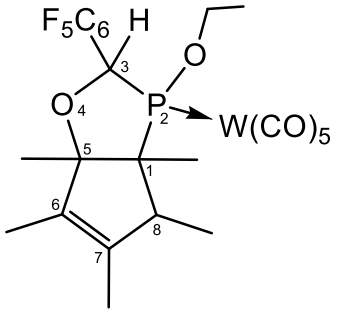

^{1}H NMR (THF-*d8*, in ppm): δ = 1.1 (3H, d, $^2J_{H,P}$ = 7.3 Hz, Cp*-CH_3), 1.12 (3H, m$_c$, Cp*-CH_3), 1.16 (3H, m$_c$, Cp*-CH_3), 1.30 (3H, s, *CH_3*CH_2O), 1.45 (3H, m$_c$, Cp*-CH_3), 1.6 (3H, m$_c$, Cp*-CH_3), 3.5 (2H, dm$_c$, CH_3*CH_2*O), 4,7 (1H, d, $^2J_{H,P}$ = 22.9 Hz, CH)

^{13}C{^{1}H} NMR ($CDCl_3$, in ppm): δ = 9.2 (s, CH_3), 12.5 (s. CH_3), 12.7 (s, CH_3), 15.2 (d, $J_{C,P}$ = 10.4 Hz, CH_3), 15.9 (d, $J_{C,P}$ = 7.1 Hz, CH_3), 21 (d, $J_{C,P}$ = 3 Hz, *CH_3*CH_2O), 58 (d, $J_{C,P}$ = 18.9 Hz, C^q), 66 (d, $J_{C,P}$ = 9.7 Hz, CH_3*CH_2*O), 79.4 (d, $J_{C,P}$ = 24 Hz, CHP), 98 (d, $J_{C,P}$ = 1.2 Hz, CH-Cp*), 109 (m, *ipso*-Ar^F), 133 (s, Cp*-C^q) 136 (m, C^q-Ar^F), 139 (m, C^q-Ar^F), 140 (s, Cp*- C^q), 143 (m, C^q-Ar^F), 147 (m, C^q-Ar^F), 195 (m, C^q-Ar^F), 196.1 (d, $^2J_{C,P}$ = 7.2 Hz, *cis*-CO), 196.7 (d, $^2J_{C,P}$ = 27 Hz, *trans*-CO)

^{19}F NMR ($CDCl_3$, in ppm): δ = -154.4 (d, $^3J_{F,F}$ = 20.7 Hz, *p*-Ar^F), -162.4 (t, $^3J_{F,F}$ = 17.3 Hz, *m*-Ar^F), -163.3 (t, $^3J_{F,F}$ = 16.9 Hz, *m*-Ar^F);

^{31}P{^{1}H} NMR ($CDCl_3$, in ppm): δ = 178.7 ($^1J_{W,P}$ = 275.4 Hz)

MS (selected data *m/z* (%)): 732.1 [M]$^{+\bullet}$, 536.1 [M-C_7HF_5O]$^+$, 452.1 [M-C_7HF_5O -3CO]$^+$, 212.1 [M-C_7HF_5O-3CO-W(CO)$_2$]$^+$, 136.1

$[M\text{-}C_7HF_5O\text{-}3CO\text{-}W(CO)_2 \quad -POCH_2CH_3]^+$, 121.1

$[M\text{-}C_7HF_5O\text{-}3CO\text{-}W(CO)_2\text{-}POCH_2CH_3\text{-}CH_3]^+$

Elemental analysis: C [%] H [%]

Calculated: 39.37 3.10

Found: 39.28 3.68

7.4.13 General procedure for the synthesis of 1,3,4,5-tetramethylimidazolium {Pentacarbonyl-[triphenylmethyl(fluoro) phosphanoxido-κP]tungsten(0)} (66) and 1,3-diisopropyl-4,5-dimethylimidazolium{pentacarbony-[triphenylmethyl(fluoro) phosphanoxido-κP]tungsten(0)} (67)

350 mg (0.45 mmol) of complex **22** were dissolved in THF (4 mL) and 1.2 eq. of the corresponding *N*-heterocyclic carbene (**61$^{Me/Me}$** and **61$^{iPr/Me}$**) were added. The solution was then stirred under refluxing conditions for about 15 min. The dark brown solution was characterized by multinuclear NMR analysis.

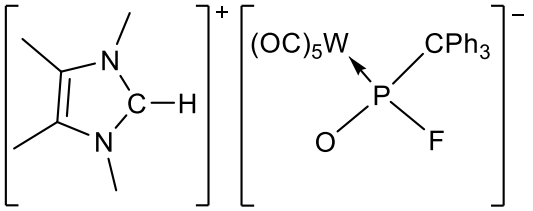

66: **61$^{Me/Me}$**: 67 mg, 0.54 mmol

Molecular formula: $C_{31}H_{28}FN_2O_6PW$

Molecular weight: 758.37 g/mol

^{1}H NMR (THF-*d8*, in ppm): δ = 2.3 (6H, s, CCH_3), 3.4 (6H, s, N-CH_3), 6.6 − 7.3 (15H, m, 3Ph), 10.6 (1H, br, C−H)

^{13}C{^{1}H} NMR (THF-*d8*, in ppm): δ = 7.52 (s, C-CH_3), 30.2 (br, N-CH_3), 56.7 (d, $^1J_{C,P}$ = 28.3 Hz, C-Ph_3), 125.4 (s, Me-C=C-Me),126.1 (s, *p*-Ph) 128.2 (d, $^4J_{C,P}$ = 1.32 Hz *m*-Ph), 129.5 (d, $^3J_{C,P}$ = 2.43 Hz, *o*-Ph, 144. 5 (d, $^2J_{C,P}$ = 4.20 Hz, *i*-Ph), 147.0 (s, C-H), 199.8 (d, $^2J_{C,P}$ = 10.8 Hz, *cis*-CO), *trans*-CO (not observed)

^{19}F NMR (THF-*d8*, in ppm): δ = -33.03 (d, $^1J_{P,F}$ = 1032.8 Hz, $^2J_{F,W}$ = 30.3 Hz)

^{31}P{^{1}H} NMR (THF-*d8*, in ppm): δ = 152.7 ($^1J_{W,P}$ = 319.8 Hz, $^1J_{P,F}$ = 1032.8 Hz)

67: **61**$^{iPr/Me}$: 97 mg, 0.54 mmol

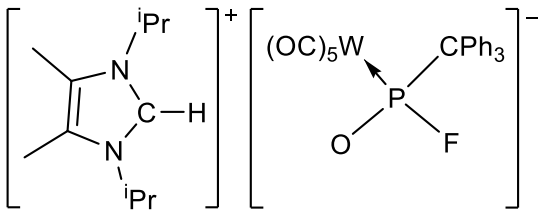

Molecular formula: $C_{35}H_{36}FN_2O_6PW$

Molecular weight: 814.48 g/mol

^{1}H NMR (THF-*d8*, in ppm): δ = 1.2 (12H, d, $^4J_{H,H}$ = 6.7 Hz, N-CH(C<u>H</u>$_3$)$_2$, 1.3 (6H, s, C-CH$_3$), 3.6 (2H, sept, $^3J_{H,H}$ = 6.3 Hz N-C<u>H</u>(CH$_3$)$_2$), 6.9 − 7.9 (15H, m, 3Ph), 10.6 (1H, br, C−H)

^{13}C{^{1}H} NMR (THF-*d8*, in ppm): δ = 7.5 (s, C-CH$_3$), 21.9 (N-CH(<u>C</u>H$_3$)$_2$), 50.5 (N-<u>C</u>H(CH$_3$)$_2$), 56.7 (d, $^1J_{C,P}$ = 28.3 Hz, C-Ph$_3$),125.2 (s, Me-C=C-Me), 126.1 (s, *p*-Ph), 128.2 (d, $^4J_{C,P}$ = 1.32 Hz *m*-Ph), 129.5 (d, $^3J_{C,P}$ = 2.43 Hz, *o*-Ph, 144. 5 (d, $^2J_{C,P}$ = 4.20 Hz, *i*-Ph), 148.3 (s, C-H), 199.8 (d, $^2J_{C,P}$ = 10.8 Hz, *cis*-CO), *trans*-CO (not observed)

^{19}F NMR (THF-*d8*, in ppm): δ = -33.03 (d, $^1J_{P,F}$ = 1032.8 Hz, $^2J_{F,W}$ = 30.3 Hz)

^{31}P{^{1}H} NMR (THF-*d8*, in ppm): δ = 152.7 ($^1J_{W,P}$ = 319.8 Hz, $^1J_{P,F}$ = 1032.8 Hz)

7.4.14 General procedure for the synthesis of Tetrabutylamonium {Pentacarbonyl[triphenylmethyl(fluoro)phosphanoxido-κP] tungsten(0)} (74) and Tetrabutylamonium{pentacarbonyl-[triphenylmethyl(fluoro)phosphanoxido-κP]chromium(0)} (75)

The complexes **25** and **26** were dissolved in THF (4 mL) and 1.2 eq. of TBAF (*n*butyl ammonium fluoride) were added. The solution was stirred under reflux conditions for about 15 min. The dark brown solution was characterized by multinuclear NMR analysis.

74: **22**: 360 mg, 0.45 mmol; TBAF: 0.54 mL, 0.54 mmol

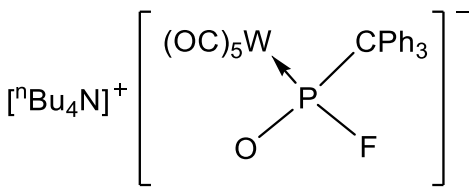

Molecular formula: $C_{40}H_{51}FNO_6PW$

Molecular weight: 875.66 g/mol

^{1}H NMR (THF-*d8*, in ppm): δ = 1.01 (12H, t, $^2J_{H,H}$ = 7.3 Hz, CH$_3$), 1.4 (8H, sept, C<u>H</u>$_2$-CH$_3$), 1.8 (8H, m$_c$, C<u>H</u>$_2$-CH$_2$-CH$_3$), 3.7 (8H, m$_c$, N-CH$_2$), 7.1 − 7.3 (15H, m, 3Ph)

$^{13}C\{^1H\}$ NMR (THF-*d8*, in ppm): δ = 13.1 (s, C-CH_3), 19.6 (s, $\underline{C}H_2$-CH_3), 23.7 (s, $\underline{C}H_2$-CH_3), 25.4 (s, $\underline{C}H_2$-CH_3), 28.80 (s, $\underline{C}H_2$-CH_2-CH_3), 53.8 (s, N-CH_2), 58.1 (s, N-CH_2), 59.5 (s, N-CH_2), 67.2 (d, $^1J_{C,P}$ = 8.3 Hz, C-Ph_3), 125.9 (s, *p*-Ph), 127.9 (s, *m*-Ph), 131.5 (d, $^3J_{C,P}$ = 5.4 Hz, *o*-Ph, 145. 8 (d, $^2J_{C,P}$ = 3.2 Hz, *i*-Ph), 199.3 (ddsat, $^2J_{C,P}$ = 10.8 Hz, $J_{C,F}$ = 1.2 Hz, $J_{C,W}$ = 123.5 Hz, *cis*-CO), *trans*-CO (dd, $^2J_{C,P}$ = 26.2 Hz, $J_{C,F}$ = 3.9 Hz)

^{19}F NMR (THF-*d8*, in ppm): δ = -32.5 (d, $^1J_{P,F}$ = 1042.9 Hz, $^2J_{F,W}$ = 31.4 Hz)

$^{31}P\{^1H\}$ NMR (THF-*d8*, in ppm): δ = 147.4 ($^1J_{W,P}$ = 317.8 Hz, $^1J_{P,F}$ = 1042.9 Hz)

75: **26**: 300 mg, 0.45 mmol; TBAF: 0.54 mL, 0.54 mmol

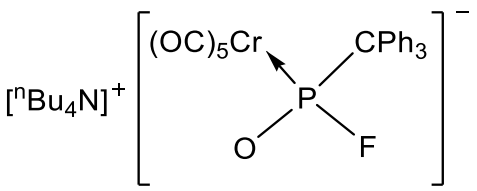

Molecular formula: $C_{40}H_{51}CrFNO_6P$
Molecular weight: 743.28 g/mol

^1H NMR (THF-*d8*, in ppm): δ = 0.8 (12H, t, $^2J_{H,H}$ = 7.3 Hz, CH_3), 1.2 (8H, sept, $C\underline{H}_2$-CH_3), 2.2 (8H, m_c, $C\underline{H}_2$-CH_2-CH_3), 3.2 (8H, m_c, N-$C\underline{H}_2$), 6.9 − 7.3 (15H, m, 3Ph)

$^{13}C\{^1H\}$ NMR (THF-*d8*, in ppm): δ = 12.6 (s, C-CH_3), 18.9 (s, $\underline{C}H_2$-CH_3), 21.2 (s, $\underline{C}H_2$-CH_3), 25.6 (s, $\underline{C}H_2$-CH_3), 26.5 (s, $\underline{C}H_2$-CH_2-CH_3), 52.2 (s, N-CH_2), 59.6 (s, N-CH_2), 60.5 (s, N-CH_2), 67.2 (d, $^1J_{C,P}$ = 8.3 Hz, C-Ph_3), 124.2 (s, *p*-Ph), 126.3 (s, *m*-Ph), 129.1 (d, $^3J_{C,P}$ = 5.2 Hz, *o*-Ph, 144.9 (d, $^2J_{C,P}$ = 4.5 Hz, *i*-Ph), 203.8 (dd, $^2J_{C,P}$ = 13.2 Hz, $J_{C,F}$ = 1.1 Hz, *cis*-CO), *trans*-CO (not observed)

^{19}F NMR (THF-*d8*, in ppm): δ = -26.7 (d, $^1J_{P,F}$ = 1062.6 Hz)

$^{31}P\{^1H\}$ NMR (THF-*d8*, in ppm): δ = 183.1 ($^1J_{P,F}$ = 1062.6 Hz)

7.4.15 Synthesis of {Pentacarbony-(1-Phenyl-1-hydroxy-2-phosphaalkene- κ*P*)tungsten(0)} (76)

A solution of the oxaphosphirane complex **4c** in THF-d^8 was treated with KC_8 (2.0 eq) After 24h of stirring, a multinuclear NMR analysis was performed.

Molecular formula: $C_{12}H_7O_6PW$

Molecular weight: 462.00 g/mol

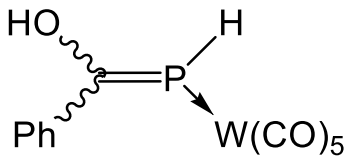

^{1}H NMR (THF-*d8*, in ppm): δ = 2.8 (1H, d, $^3J_{P,H}$ = 13.1 Hz, OH), 6.8 - 7.6 (5H, m, Ph), 8.6 (1H, d, $^1J_{P,H}$ = 292.1 Hz, PH)

^{13}C{^{1}H} NMR (THF-*d8*, in ppm): δ = 198.1 (d, $^2J_{C,P}$ = 35.2 Hz, C=P), 200.1(d, $^2J_{C,P}$ = 9.0 Hz, $^1J_{W,C}$ = 96.7 Hz, *cis*-CO), 203.1 (d, $^2J_{C,P}$ = 18.4 Hz, *trans*-CO);

^{31}P{^{1}H} NMR (THF-*d8*, in ppm): δ = 91.5 ($^1J_{P,H}$ = 292.1 Hz)

7.4.16 Synthesis of Potassium{pentacarbonyl[triphenylmethyl(fluoro) phosphanoxido-κP]tungsten(0)} (77)

Complex **22** in THF and 2 eq. of KC_8 (potassium graphite) were added. The solution was stirred at room temperature for . The dark brown solution was characterized by multinuclear NMR analysis.

22: 200 mg, 0.25 mmol; KC_8: 80 mg, 0.60 mmol

Molecular formula: $C_{24}H_{15}FKO_6PW$

Molecular weight: 672.29 g/mol

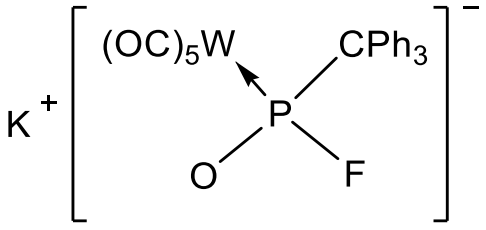

^{1}H NMR (THF-*d8*, in ppm): δ = 6.9 − 7.5 (15H, m, 3Ph)

^{13}C{^{1}H} NMR (THF-*d8*, in ppm): δ = 65.0 (d, $^1J_{C,P}$ = 8.7 Hz, C-Ph_3), 125.9 (s, *p*-Ph), 127.9 (s, *m*-Ph), 129.3 (s, *o*-Ph), 144.1 (s, *i*-Ph), 202.7 (dsat, $^2J_{C,P}$ = 12.3 Hz, $J_{C,F}$ and $^1J_{C,W}$ = not observed, *cis*-CO), 205.7 (d, $^2J_{C,P}$ = 25.3 Hz, $J_{C,F}$ = not observed)

^{19}F NMR (THF-*d8*, in ppm): δ = -33.0 (d, $^1J_{P,F}$ = 1041.7 Hz)

^{31}P{^{1}H} NMR (THF-*d8*, in ppm): δ = 150.9 ($^1J_{W,P}$ = 320.6 Hz, $^1J_{P,F}$ = 1041.7 Hz)

7.4.17 Synthesis of {Pentacarbonyl[1-phenyl-2-triphenylmethyl)-2-phospha-alkene-κ*P*]-tungsten(0)} (92)

A solution of the oxaphosphirane complex **4c** in THF-d^8 was treated with $TiCpCl_3$ (1.0 eq) and Zn powder (1.0 eq). After 24h of stirring, a multinuclear NMR analysis was performed.

Molecular formula: $C_{31}H_{21}O_5PW$

Molecular weight: 688.32 g/mol

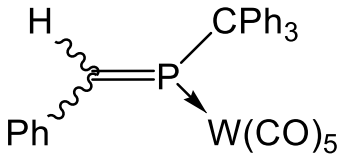

^{1}H NMR (THF-*d8*, in ppm): δ = 7.0 - 7.4 (15H, m, 3Ph), 7.6-7.7 (5H, m, Ph), 9.1 (1H, d, $^3J_{P,H}$ = 23.7 Hz, HC=P)

^{13}C{^{1}H} NMR (THF-*d8*, in ppm): δ = 67.1 (br, P-<u>C</u>Ph_3), 125.9 (s, *p*-Ph), 127.9 (s,CPh_3), 128.3 (s, Ph), 129.2 (s, CPh_3), 131.1 (s, Ph), 131.6 (d, $J_{C,P}$ = 6.6 Hz, *C*Ph_3), 142.2 (s, *i*-Ph), 144.1 (s, *i*-CPh_3), 170.9 (d, $^2J_{C,P}$ = 35.6 Hz, C=P), 194.8 (d, $^2J_{C,P}$ = 9.1 Hz, *cis*-CO), 197.7 (d, $^2J_{C,P}$ = 34.6 Hz, *trans*-CO);

^{31}P{^{1}H} NMR (THF-*d8*, in ppm): δ = 241.4 ($^2J_{P,H}$ = 23.7 Hz)

8. References and notes

[1] F. Krafft, *Angew. Chem. Int. Ed.* **1969**, *8*, 660–671.

[2] K. B. Dillon, J. F. Nixon, F. Mathey, *Phosphorus:. The carbon copy*, John Wiley, New York, Chichester, **1998**.

[3] J. P. Majoral, *New Aspects in Phosphorus Chemistry V*, Springer, **2005**.

[4] P. W. Atkins, *Shriver & Atkins' inorganic chemistry*, Oxford University Press, Oxford, **2010**.

[5] "New Aspects in Phosphorus Chemistry V", Springer, **2005**.

[6] S. Lacombe, D. Gonbeau, J. L. Cabioch, B. Pellerin, J. M. Denis, G. Pfister-Guillouzo, *J. Am. Chem. Soc.* **1988**, *110*, 6964–6967.

[7] A. Meriem, J.-P. Majoral, M. Revel, J. Navech, *Tetrahedron Lett.* **1983**, *24*, 1975–1978.

[8] R. de Vaumas, A. Marinetti, F. Mathey, *J. Organomet. Chem.* **1991**, *413*, 411–417.

[9] R. Steudel, *The chemistry of inorganic ring systems*, Elsevier, Amsterdam, **1992**.

[10] G. Grüttner, M. Wiernik, *Ber. Dtsch. Chem. Ges.* **1915**, *48*, 1759–1764.

[11] W.B. McCormack, *Chem. Abstr.* **1955**, 7602.

[12] R. K. Bansal (Ed.) *Topics in Heterocyclic Chemistry*, Springer Berlin Heidelberg, Berlin, Heidelberg, **2010**.

[13] S. Duraffour, R. Snoeck, M. Krecmerova, J. van den Oord, R. de Vos, A. Holy, J.-M. Crance, D. Garin, E. de Clercq, G. Andrei, *Antimicrob. Agents Chemother.* **2007**, *51*, 4410–4419.

[14] D.-Q. Shi, A. Feras, Y. Liu, *Phosphorus, Sulfur, Silicon Relat. Elem.* **2006**, *181*, 2663–2673.

[15] K. Moedritzer, R. E. Miller, *J. Org. Chem.* **1982**, *47*, 1530–1534.

[16] M. Epstein, S. A. Buckler, *Tetrahedron* **1962**, *18*, 1231–1242.

[17] J. M. L. Hillman, S. M. Roberts, *J. Chem. Soc., Perkin Trans. 1* **1997**, 3601–3608.

[18] S. G. Ruf, J. Dietz, M. Regitz, *Tetrahedron* **2000**, *56*, 6259–6267.

[19] C. Müller, R. Bartsch, A. Fischer, P. G. Jones, R. Schmutzler, *Chem. Ber.* **1995**, *128*.

[20] D. M. Perreault, E. V. Anslyn, *Angew. Chem. Int. Ed.* **1997**, *36*, 432–450.

[21] V. Gray, *Energy & Environment* **2007**, *18*, 433–440.

[22] T. R. Hull, B. K. Kandola, *Fire retardancy of polymers*. *New strategies and mechanisms / edited by T. Richard Hull, Baljinder K. Kandola*, Royal Society of Chemistry, Cambridge, **2009**.

[23] B. A. Howell, J. Uzibor, *J Vinyl Addit Technol* **2006**, *12*, 192–197.

[24] M. T. Boisdon, J. Barrans, *J. Chem. Soc., Chem. Commun.* **1988**, 615-617.

[25] M. Bode, M. Nieger, R. Streubel, *Organometallics* **2007**, *26*, 245–246.

[26] G. Wittig, U. Schöllkopf, *Chem. Ber.* **1954**, *87*, 1318–1330.

[27] H. Pommer, P. C. Thieme in *Topics in Current Chemistry*, *Vol. 109* (Eds.: F. L. Boschke, M. J. S. Dewar, J. D. Dunitz, K. Hafner, E. Heilbronner, S. Itô, J.-M. Lehn, K. Niedenzu, K. N. Raymond, C. W. Rees et al.), Springer Berlin Heidelberg, Berlin, Heidelberg, **1983**.

[28] a) T. Kawashima, K. Kato, R. Okazaki, *Angew. Chem.* **1993**, *105*, 941–942; b) Mazhar-ul-Haque, C. N. Caughlan, F. Ramirez, J. F. Pilot, C. P. Smith, *J. Am. Chem. Soc.* **1971**, *93*, 5229–5235; c) M. Hamaguchi, Y. Iyama, E. Mochizuki, T. Oshima, *Tetrahedron Lett.* **2005**, *46*, 8949–8952.

[29] A. W. Kyri, V. Nesterov, G. Schnakenburg, R. Streubel, *Angew. Chem. Int. Ed.* **2014**, *53*.

[30] B. Kaboudin, H. Haghighat, T. Yokomatsu, *Synlett* **2016**, 27, 1537-1540.

[31] A. Weissberger, E. C. Taylor, *Chem. Heterocycl. Compd.*, John Wiley & Sons, Inc, Hoboken, NJ, USA, **1977**.

[32] a) *Ullmann's Encyclopedia of Industrial Chemistry*, Wiley-VCH Verlag GmbH & Co. KGaA, Weinheim, Germany, **2000**; b) A. L. Branen, *Food additives*, M. Dekker, New York, **2002**.

[33] a) A. Vila, R. A. Mosquera, *Chem. Phys.* **2003**, *287*, 125–135; b) M. S. Gordon, *J. Am. Chem. Soc.* **1980**, *102*, 7419–7422.

[34] Hassner, Alfred. Ed, *Small ring heterocycles. Pt3, Oxiranes, arene oxides, oxaziridines, dioxetanes, thietanes, thietes, thiazetes, and others*, Wiley, New York, **1985**.

[35] O. Krahe, F. Neese, R. Streubel, *Chemistry* **2009**, *15*, 2594–2601.

[36] M. Regitz, O. J. Scherer, *Multiple bonds and low coordination in phosphorus chemistry*, Georg Thieme Verlag, Stuttgart, **1990**.
[37] A. Espinosa Ferao, R. Streubel, *to be publised*.
[38] F. U. Seifert, G.-V. Röschenthaler, *Z. Naturforsch. B* **1993**, *48*, 1089-1093.
[39] E. Niecke, D. Gudat, W. W. Schoeller, P. Rademacher, *J. Chem. Soc., Chem. Commun.* **1985**, 1050-1051.
[40] S. Bauer, A. Marinetti, L. Ricard, F. Mathey, *Angew. Chem.* **1990**, *102*, 1188–1189.
[41] S. Bauer, A. Marinetti, L. Ricard, F. Mathey, *Angew. Chem. Int. Ed.* **1990**, *29*, 1166–1167.
[42] Marc Schröder, *Dissertation*, **1999**.
[43] R. Streubel, A. Kusenberg, J. Jeske, P. G. Jones, *Angew. Chem. Int. Ed.* **1995**, *33*, 2427–2428.
[44] R. Streubel, H. Wilkens, A. Ostrowski, C. Neumann, F. Ruthe, P. G. Jones, *Angew. Chem. Int. Ed.* **1997**, *36*, 1492–1494.
[45] R. Streubel, M. Bode, J. Marinas Pérez, G. Schnakenburg, J. Daniels, M. Nieger, P. G. Jones, *Z. Anorg. Allg. Chem.* **2009**, *635*, 1163–1171.
[46] A. Ozbolat, G. von Frantzius, J. M. Perez, M. Nieger, R. Streubel, *Angew. Chem. Int. Ed.* **2007**, *46*, 9327–9330.
[47] R. Streubel, M. Klein, G. Schnakenburg, *Organometallics* **2012**, *31*, 4711–4715.
[48] M. Klein, G. Schnakenburg, A. Espinosa Ferao, R. Streubel, *Dalton Trans.* **2016**, *45*, 2085–2094.
[49] J. M. Pérez, M. Klein, A. W. Kyri, G. Schnakenburg, R. Streubel, *Organometallics* **2011**, *30*, 5636–5640.
[50] M. Gomberg, *J. Am. Chem. Soc.* **1900**, *22*, 757–771.
[51] V. Plack, J. R. Goerlich, A. Fischer, R. Schmutzler, *Z. Anorg. Allg. Chem.* **1999**, *625*, 1979–1984.
[52] V. Plack, R. Schmutzler, *Phosphorus, Sulfur, Silicon Relat. Elem* **1999**, *144*, 273–276.
[53] V. Nesterov, G. Schnakenburg, A. Espinosa, R. Streubel, *Inorg. Chem.* **2012**, *51*, 12343–12349.
[54] S. Grimme, A. Hansen, *Angew. Chem.* **2015**, *127*, 12483–12488.
[55] A. Ozbolat, A. A. Khan, G. von Frantzius, M. Nieger, R. Streubel, *Angew. Chem. Int. Ed.* **2007**, *46*, 2104–2107.
[56] C. M. García, A. E. Ferao, G. Schnakenburg, R. Streubel, *Dalton Trans.* **2016**, *45*, 2378–2385.
[57] V. Plack, J. R. Goerlich, R. Schmutzler, *Z. Naturforsch. B* **1998**, *53*, 1265-1266.
[58] V. Plack, J. R. Goerlich, R. Schmutzler, *Z. Anorg. Allg. Chem.* **1998**, *624*, 1940–1942.
[59] A. Espinosa, R. Streubel, *Chemistry* **2012**, *18*, 13405–13411.
[60] V. Plack, P. Sakhaii, M. Freytag, P. G. Jones, R. Schmutzler, *J. Fluorine Chem.* **2000**, *101*, 125–130.
[61] V. Plack, R. Schmutzler, *Phosphorus, Sulfur, Silicon Relat. Elem.* **1999**, *144*, 273–276.
[62] V. Nesterov, G. Schnakenburg, A. Espinosa, R. Streubel, *Inorg. Chem.* **2012**, *51*, 12343–12349.
[63] C. Albrecht, M. Bode, J. M. Pérez, J. Daniels, G. Schnakenburg, R. Streubel, *Dalton Trans.* **2011**, *40*, 2654–2665.
[64] L. Hirsivaara **2001**, *364*.
[65] R. Streubel, H. Wilkens, P. G. Jones, *Chem. Eur. J.* **2000**, *6,* 3997-4000.
[66] E. Wiberg, N. Wiberg, *Lehrbuch der anorganischen Chemie*, Walter de Gruyter, Berlin, **1995**.
[67] A. F. Gushwa, Y. Belabassi, J.-L. Montchamp, A. F. Richards, *J. Chem. Crystallogr.* **2009**, *39*, 337–347.
[68] Aysel Özbolat-Schön. *Dissertation, University of Bonn*, **2011**.
[69] A. Ostrowski, *Untersuchungen zur thermischen Zersetzung von Arylsubstituierten 2H-Azaphosphiren-Wolframkomplexen in Lösung*, Papierflieger, Clausthal-Zellerfeld, **1997**.
[70] J. Marinas Pérez, Dissertation, University of Bonn, 2010.
[71] P. K. Majhi, *private communication*, **2016**.
[72] a) A. D. Becke, *J. Chem. Phys.* **1993**, *98*, 5648-5652; b) Lee, Yang, Parr, *Physical review. B, Condensed matter* **1988**, *37*, 785–789.

[73] F. Weigend, R. Ahlrichs, *Phys. Chem. Chem. Phys.* **2005**, *7*, 3297-3305.
[74] M. Klein, G. Schnakenburg, A. Espinosa Ferao, R. Streubel, *Dalton Trans.* **2016**, *45*, 2085–2094.
[75] R. Streubel, C. Murcia-García, G. Schnakenburg, A. Espinosa Ferao, *Organometallics* **2015**, *34*, 2676–2682.
[76] a) R. Hoffmann, R. B. Woodward, *Science* **1970**, *167*, 825–831; b) S. Sharma, T. Rajale, D. K. Unruh, D. M. Birney, *J. Org. Chem.* **2015**, *80*, 11734–11743.
[77] a) C. J. Wu, L. E. Fried, L. H. Yang, N. Goldman, S. Bastea, *Nature Chem.* **2009**, *1*, 57–62; b) Z. Zhang, Y. Du, N. G. Petrik, G. A. Kimmel, I. Lyubinetsky, Z. Dohnálek, *J. Phys. Chem. C* **2009**, *113*, 1908–1916.
[78] a) A. Schäfer, H. Horn, R. Ahlrichs, *J. Chem. Phys.* **1992**, *97*, 2571; b) A. Schäfer, C. Huber, R. Ahlrichs, *J. Chem. Phys.* **1994**, *100*, 5829.
[79] V. Mouriès, F. Mercier, L. Ricard, F. Mathey, *Eur. J. Org. Chem.* **1998**, *1998*, 2683–2687.
[80] a) R. Appel, S. Korte, M. Halstenberg, F. Knoch, *Chem. Ber.* **1982**, *115*, 3610–3617; b) T. Möller, P. Wonneberger, M. B. Sárosi, P. Coburger, E. Hey-Hawkins, *Dalton Trans.* **2016**, *45*, 1904–1917.
[81] C. M. Garcia, A. E. Ferao, G. Schnakenburg, R. Streubel, *Dalton Trans.* **2016**, *45*, 2378–2385.
[82] M. Klein, G. Schnakenburg, A. Espinosa Ferao, R. Streubel, *Dalton Trans.* **2016**, *45*, 2085–2094.
[83] C. Murcia-García, A. Bauzá, A. Frontera, R. Streubel, *CrystEngComm* **2015**, *17*, 6736–6743.
[84] C. Murcia-García, A. Bauzá, G. Schnakenburg, A. Frontera, R. Streubel, *CrystEngComm* **2015**, *17*, 1769–1772.
[85] F. A. Cotton, *Advanced inorganic chemistry*, Wiley, New York, Chichester, **1999**.
[86] M. Bode, G. Schnakenburg, P. G. Jones, R. Streubel, *Organometallics* **2008**, *27*, 2664–2667.
[87] F. A. Cotton, C. S. Kraihanzel, *J. Am. Chem. Soc.* **1962**, *84*, 4432–4438.
[88] a) L. M. Salonen, M. Ellermann, F. Diederich, *Angew. Chem. Int. Ed.* **2011**, *50*, 4808–4842; b) K. Müller-Dethlefs, P. Hobza, *Chem. Rev.* **2000**, *100*, 143–168.
[89] a) M. Egli, S. Sarkhel, *Acc. Chem. Res.* **2007**, *40*, 197–205; b) T. J. Mooibroek, P. Gamez, J. Reedijk, *CrystEngComm* **2008**, *10*, 1501-1515.
[90] a) J. Zukerman-Schpector, I. Haiduc, E. R. Tiekink, *Chem. Commun.* **2011**, *47*, 12682-12684; b) E. R. T. Tiekink, J. Zukerman-Schpector, *The Importance of Pi-Interactions in Crystal Engineering*, John Wiley & Sons, Ltd, Chichester, UK, **2012**.
[91] R. Ahlrichs, M. Bär, M. Häser, H. Horn, C. Kölmel, *Chem. Phys. Lett.* **1989**, *162*, 165–169.
[92] S. Grimme, J. Antony, S. Ehrlich, H. Krieg, *J. Chem. Phys.* **2010**, *132*, 154104-154123.
[93] S. F. Boys, F. Bernardi, *Mol. Phys.* **2006**, *19*, 553–566.
[94] R. F. W. Bader, *Chem. Rev.* **1991**, *91*, 893–928.
[95] For the rest of the complexes see appendix.
[96] H. Wilkens, A. Ostrowski, J. Jeske, F. Ruthe, P. G. Jones, R. Streubel, *Organometallics* **1999**, *18*, 5627–5642.
[97] P. Jutzi, H. Saleske, D. Nadler, *J. Organomet. Chem.* **1976**, *118*, C8-C10.
[98] C. Murcia García, A. Bauzá, G. Schnakenburg, A. Frontera, R. Streubel, *Ang. Chem. Int. Ed.* **2016**, Submitted.
[99] A. Bauzá, T. J. Mooibroek, A. Frontera, *ChemPhysChem* **2015**, *16*, 2496–2517.
[100] M. Lukeman, J. C. Scaiano, *J. Am. Chem. Soc.* **2005**, *127*, 7698–7699.
[101] A. Bauzá, T. J. Mooibroek, A. Frontera, *Angew. Chem. Int. Ed.* **2013**, *52*, 12317–12321.
[102] F. P. Sargent, M. G. Bailey, *Can. J. Chem.* **1971**, *49*, 2350–2352.
[103] J. Marinas Pérez *Dissertation,* University of Bonn, **2010**.
[104] M. Klein, *Dissertation,* University of Bonn, **2015**.
[105] C. Albrecht. *Dissertation,* University of Bonn, **2013**.
[106] M. Bode, J. Daniels, R. Streubel, *Organometallics* **2009**, *28*, 4636–4638.
[107] X. Fang, Y. Ou, *Jingxi Huagong* **2007**, *24*, 401–403.

[108] Y. Ma, A.-L. Cheng, E.-Q. Gao, *Crystal Growth & Design* **2010**, *10*, 2832–2834.
[109] L. D. Quin, *A Guide to Organophosphorus Chemistry*, Wiley, **2000**.
[110] J. M. Villalba Franco, A. Espinosa Ferao, G. Schnakenburg, R. Streubel, *Chem. Commun.* **2013**, *49*, 9648–9650.
[111] A. Espinosa, R. Streubel, *Chemistry (Weinheim an der Bergstrasse, Germany)* **2012**, *18*, 13405–13411.
[112] a) A. Espinosa, C. Gomez, R. Streubel, *Inorg. Chem.* **2012**, *51*, 7250–7256; b) A. Espinosa, R. Streubel, *Chemistry* **2011**, *17*, 3166–3178; c) A. Espinosa, E. de las Heras, R. Streubel, *Inorg. Chem.* **2014**, *53*, 6132–6140.
[113] K. B. Wiberg, *Tetrahedron* **1968**, *24*, 1083–1096.
[114] P.-O. Löwdin, *J. Chem. Phys.* **1950**, *18*, 365-375.
[115] a) I. Mayer, *Chemical Physics Letters* **1983**, *97*, 270–274; b) I. Mayer, *Int. J. Quantum Chem.* **1984**, *26*, 151–154; c) A. J. Bridgeman, G. Cavigliasso, L. R. Ireland, J. Rothery, *J. Chem. Soc., Dalton Trans.* **2001**, 2095–2108.
[116] a) R. F. W. Bader, *Chem. Rev.* **1991**, *91*, 893–928; b) R. F. W. Bader, *J. Phys. Chem. A* **1998**, *102*, 7314–7323.
[117] a) C. Albrecht, E. Schneider, M. Engeser, G. Schnakenburg, A. Espinosa, R. Streubel, *Dalton Trans.* **2013**, *42*, 8897-8906; b) A. Bauzá, R. Streubel, A. Frontera, *Chem. Phys. Lett.* **2014**, *597*, 40–44.
[118] a) A. E. Reed, F. Weinhold, *J. Chem. Phys.* **1983**, *78*, 4066–4073; b) A. E. Reed, R. B. Weinstock, F. Weinhold, *J. Chem. Phys.* **1985**, *83*, 735-746.
[119] a) J. Contreras-García, E. R. Johnson, S. Keinan, R. Chaudret, J.-P. Piquemal, D. N. Beratan, W. Yang, *J. Chem. Theory Comput.* **2011**, *7*, 625–632; b) J. Contreras-García, E. R. Johnson, S. Keinan, R. Chaudret, J.-P. Piquemal, D. N. Beratan, W. Yang, *J. Chem. Theory Comput.* **2011**, *7*, 625–632.
[120] M. Bode, M. Nieger, R. Streubel, *Organometallics* **2007**, *26*, 245–246.
[121] J. M. Pérez, H. Helten, G. Schnakenburg, R. Streubel, *Chem. Asian J.* **2011**, *6*, 1539–1545.
[122] C. Albrecht, M. Bode, J. M. Pérez, J. Daniels, G. Schnakenburg, R. Streubel, *Dalton Trans.* **2011**, *40*, 2654-2665.
[123] R. Hoffmann, G. D. Zeiss, G. W. van Dine, *J. Am. Chem. Soc.* **1968**, *90*, 1485–1499.
[124] F. E. Hahn, M. C. Jahnke, *Angew. Chem. Int. Ed.* **2008**, *47*, 3122–3172.
[125] A. J. Arduengo, R. L. Harlow, M. Kline, *J. Am. Chem. Soc.* **1991**, *113*, 361–363.
[126] L. Duan, V. Nesterov, J. W. Runyon, G. Schnakenburg, A. J. Arduengo III, R. Streubel, *Aust. J. Chem.* **2011**, *64*, 1583-1586.
[127] M. Klein, G. Schnakenburg, A. Espinosa Ferao, N. Tokitoh, R. Streubel, *Eur. J. Inorg. Chem.* **2016**, *2016*, 685–690.
[128] N. Kuhn, T. Kratz, *Synthesis* **1993**, *1993*, 561–562.
[129] A. J. Arduengo, H. V. R. Dias, R. L. Harlow, M. Kline, *J. Am. Chem. Soc.* **1992**, *114*, 5530–5534.
[130] V. Nesterov, L. Duan, G. Schnakenburg, R. Streubel, *Eur. J. Inorg. Chem.* **2011**, *2011*, 567–572.
[131] S. Ando, T. Matsuura, *Magn. Reson. Chem.* **1995**, *33*, 639–645.
[132] V. Nesterov, Z.-W. Qu, G. Schnakenburg, S. Grimme, R. Streubel, *Chem. Commun.* **2014**, *50*, 12508–12511.
[133] C. Murcia García, T. Sasamori, G. Schnakenburg, R. Streubel, *to be published* **2016**.
[134] S. Jie, P. L. Diaconescu, *Organometallics* **2010**, *29*, 1222–1230.
[135] J. A. Plumley, J. D. Evanseck, J. *Phys. Chem. A* **2009**, *113*, 5985–5992.
[136] N. Meyer, P. W. Roesky, S. Bambirra, A. Meetsma, B. Hessen, K. Saliu, J. Takats, *Organometallics* **2013**, *32*, 3427-3427.
[137] a) N. Meyer, P. W. Roesky, S. Bambirra, A. Meetsma, B. Hessen, K. Saliu, J. Takats, *Organometallics* **2008**, *27*, 1501–1505; b) L. N. Bochkarev, T. A. Zheleznova, A. V. Safronova, M.

S. Drozdov, S. F. Zhil'tsov, L. N. Zakharov, G. K. Fukin, S. Y. Khorshev, *Russ. Chem. Bull.* **1998**, *47*, 165–168.
[138] J. L. Atwood, W. E. Hunter, R. D. Rogers, J. Holton, J. McMeeking, R. Pearce, M. F. Lappert, *J. Chem. Soc., Chem. Commun.* **1978**, 140-142.
[139] I. C. Lewis, L. S. Singer, *Org. Magn. Reson.* **1984**, *22*, 761–763.
[140] a) S.-P. Chia, H.-X. Yeong, C.-W. So, *Inorg. Chem.* **2012**, *51*, 1002–1010; b) S.-P. Chia, R. Ganguly, Y. Li, C.-W. So, *Organometallics* **2012**, *31*, 6415–6419; c) Y. Li, Y.-C. Chan, Y. Li, I. Purushothaman, S. De, P. Parameswaran, C.-W. So, *Inorg. Chem.* **2016**, *55*, 9091–9098.
[141] P. Renaud, M. P. Sibi, *Radicals in organic synthesis*, Wiley-VCH, Weinheim, Chichester, **2001**.
[142] G. A. Molander, C. R. Harris, *Chem. Rev.* **1996**, *96*, 307–338.
[143] A. Gansäuer, H. Bluhm, *Chem. Rev.* **2000**, *100*, 2771–2788.
[144] M. L. H. Green, C. R. Lucas, *J. Chem. Soc., Dalton Trans.* **1972**, 1000–1003.
[145] D. G. Sekutowski, G. D. Stucky, *Inorg. Chem.* **1975**, *14*, 2192–2199.
[146] R. Coutts, P. C. Wailes, R. L. Martin, *J. Organomet. Chem.* **1973**, *47*, 375–382.
[147] D. W. Stephan, *Organometallics* **1992**, *11*, 996–999.
[148] T. V. RajanBabu, W. A. Nugent, *J. Am. Chem. Soc.* **1989**, *111*, 4525–4527.
[149] K. Daasbjerg, H. Svith, S. Grimme, M. Gerenkamp, C. Mück-Lichtenfeld, A. Gansäuer, A. Barchuk, F. Keller, *Angew. Chem. Int. Ed.* **2006**, *45*, 2041–2044.
[150] T. V. RajanBabu, W. A. Nugent, M. S. Beattie, *J. Am. Chem. Soc.* **1990**, *112*, 6408–6409.
[151] M. Kilner, G. Parkin, *J. Organomet. Chem.* **1986**, *302*, 181–191.
[152] C. Albrecht, L. Shi, J. M. Perez, M. van Gastel, S. Schwieger, F. Neese, R. Streubel, *Chemistry* **2012**, *18*, 9780–9783.
[153] M. Klein, C. Albrecht, G. Schnakenburg, R. Streubel, *Organometallics* **2013**, *32*, 4938–4943.
[154] V. Plack, J. R. Goerlich, A. Fischer, H. Thönnessen, P. G. Jones, R. Schmutzler, *Z. Anorg. Allg. Chem.* **1995**, *621*, 1080–1092.
[155] C. Albrecht, K. Cummins, R. Streubel, *Unpublished results*.
[156] W. L. F. Armarego, D. D. Perrin, *(Eds.) PURIFICATION OF LABORATORY CHEMICALS // Purification of laboratory chemicals, Butterworth-Heinemann, Oxford,* **1997**.
[157] a) G. M. Sheldrick, *Acta Crystallogr Sect. A: Found. Crystallogr* **1990**, *46*, 467–473; b) O. V. Dolomanov, L. J. Bourhis, R. J. Gildea, J. A. K. Howard, H. Puschmann, *J Appl. Crystallogr.* **2009**, *42*, 339–341.
[158] U. Koelle, *J. Organomet. Chem.* **1977**, *133*, 53–58.
[159] M. J. S. Gynane, A. Hudson, M. F. Lappert, P. P. Power, H. Goldwhite, *J. Chem. Soc., Dalton Trans.* **1980**, 2428–2433.
[160] M. Bode, *Dissertation,* University of Bonn, **2009**.
[161] N. G. Connelly, W. E. Geiger, *Chem. Rev.* **1996**, *96*, 877–910.

9. Appendix

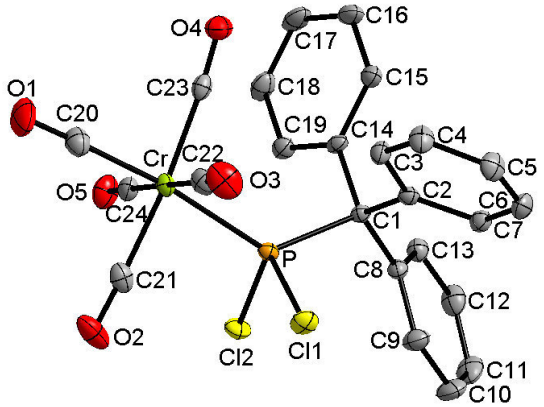

Table 1 Crystal data and structure refinement for 2a.

Identification code	GSTR496
Empirical formula	$C_{24}H_{15}Cl_2CrO_5P$
Formula weight	537.23
Temperature/K	150.0
Crystal system	monoclinic
Space group	$P2_1/n$
a/Å	9.2598(6)
b/Å	26.3413(17)
c/Å	9.5537(6)
α/°	90
β/°	90.001(2)
γ/°	90
Volume/Å^3	2330.3(3)
Z	4
ρ_{calc}g/cm^3	1.531
μ/mm^{-1}	0.823
F(000)	1088.0
Crystal size/mm^3	0.24 × 0.23 × 0.18
Tmin; Tmax	0.6459; 0.7459
Radiation	MoKα (λ = 0.71073)
2Θ range for data collection/°	4.536 to 55.998°
Completeness to theta	1.000
Index ranges	-12 ≤ h ≤ 12, -34 ≤ k ≤ 34, -12 ≤ l ≤ 12
Reflections collected	83902
Independent reflections	5625 [R_{int} = 0.0485, R_{sigma} = 0.0206]
Data/restraints/parameters	5625/0/298
Goodness-of-fit on F^2	1.046
Final R indexes [I>=2σ (I)]	R_1 = 0.0299, wR_2 = 0.0663
Final R indexes [all data]	R_1 = 0.0369, wR_2 = 0.0688
Largest diff. peak/hole / e Å^{-3}	0.35/-0.44

Table 2 Bond Lengths for 2a.

Atom	Atom	Length/Å	Atom	Atom	Length/Å
Cr	P	2.3327(5)	C2	C7	1.390(2)
Cr	C20	1.8774(18)	C3	C4	1.383(2)
Cr	C21	1.8965(18)	C4	C5	1.385(2)
Cr	C22	1.9107(18)	C5	C6	1.381(2)
Cr	C23	1.9258(17)	C6	C7	1.393(2)
Cr	C24	1.9048(17)	C8	C9	1.399(2)
Cl1	P	2.0534(5)	C8	C13	1.390(2)
Cl2	P	2.0592(5)	C9	C10	1.385(2)
P	C1	1.9557(15)	C10	C11	1.382(3)
O1	C20	1.144(2)	C11	C12	1.379(3)
O2	C21	1.138(2)	C12	C13	1.398(2)
O3	C22	1.137(2)	C14	C15	1.393(2)
O4	C23	1.133(2)	C14	C19	1.397(2)
O5	C24	1.135(2)	C15	C16	1.392(2)
C1	C2	1.536(2)	C16	C17	1.383(3)
C1	C8	1.541(2)	C17	C18	1.383(3)
C1	C14	1.5386(19)	C18	C19	1.391(2)
C2	C3	1.402(2)			

Table 3 Bond Angles for 2a.

Atom	Atom	Atom	Angle/˚	Atom	Atom	Atom	Angle/˚
C20	Cr	P	173.44(6)	C7	C2	C1	122.11(14)
C20	Cr	C21	87.33(8)	C7	C2	C3	117.81(14)
C20	Cr	C22	90.03(8)	C4	C3	C2	121.20(15)
C20	Cr	C23	87.72(7)	C3	C4	C5	120.23(16)
C20	Cr	C24	90.17(7)	C6	C5	C4	119.34(15)
C21	Cr	P	86.13(5)	C5	C6	C7	120.53(15)
C21	Cr	C22	90.14(7)	C2	C7	C6	120.78(15)
C21	Cr	C23	174.97(7)	C9	C8	C1	121.01(14)
C21	Cr	C24	89.59(7)	C13	C8	C1	121.26(13)
C22	Cr	P	90.50(5)	C13	C8	C9	117.66(15)
C22	Cr	C23	90.73(7)	C10	C9	C8	121.20(17)
C23	Cr	P	98.81(5)	C11	C10	C9	120.52(17)
C24	Cr	P	89.27(5)	C12	C11	C10	119.19(16)
C24	Cr	C22	179.66(8)	C11	C12	C13	120.51(17)
C24	Cr	C23	89.56(7)	C8	C13	C12	120.91(16)
Cl1	P	Cr	111.54(2)	C15	C14	C1	121.80(14)
Cl1	P	Cl2	98.54(2)	C15	C14	C19	118.09(14)
Cl2	P	Cr	109.85(2)	C19	C14	C1	120.04(13)
C1	P	Cr	127.91(5)	C16	C15	C14	120.53(16)
C1	P	Cl1	102.52(5)	C17	C16	C15	120.78(16)
C1	P	Cl2	102.36(5)	C16	C17	C18	119.32(15)
C2	C1	P	105.33(10)	C17	C18	C19	120.16(16)

C2	C1	C8	111.87(12)	C18	C19	C14	121.11(15)
C2	C1	C14	112.12(12)	O1	C20	Cr	178.35(18)
C8	C1	P	112.08(10)	O2	C21	Cr	177.63(16)
C14	C1	P	104.11(10)	O3	C22	Cr	178.80(16)
C14	C1	C8	110.96(12)	O4	C23	Cr	175.08(14)
C3	C2	C1	120.09(13)	O5	C24	Cr	179.42(17)

Table 4 Torsion Angles for 2a.

A	B	C	D	Angle/˚	A	B	C	D	Angle/˚
P	C1	C2	C3	-50.74(16)	C7	C2	C3	C4	-3.6(2)
P	C1	C2	C7	129.22(13)	C8	C1	C2	C3	-172.75(14)
P	C1	C8	C9	-56.95(17)	C8	C1	C2	C7	7.21(19)
P	C1	C8	C13	126.23(13)	C8	C1	C14	C15	-111.62(16)
P	C1	C14	C15	127.63(13)	C8	C1	C14	C19	65.08(18)
P	C1	C14	C19	-55.67(15)	C8	C9	C10	C11	0.8(3)
C1	C2	C3	C4	176.33(15)	C9	C8	C13	C12	1.3(2)
C1	C2	C7	C6	-177.81(14)	C9	C10	C11	C12	0.4(3)
C1	C8	C9	C10	-178.53(16)	C10	C11	C12	C13	-0.7(3)
C1	C8	C13	C12	178.21(14)	C11	C12	C13	C8	-0.2(3)
C1	C14	C15	C16	178.03(15)	C13	C8	C9	C10	-1.6(3)
C1	C14	C19	C18	-178.17(14)	C14	C1	C2	C3	61.86(18)
C2	C1	C8	C9	61.10(19)	C14	C1	C2	C7	-118.18(15)
C2	C1	C8	C13	-115.71(15)	C14	C1	C8	C9	-172.87(14)
C2	C1	C14	C15	14.3(2)	C14	C1	C8	C13	10.3(2)
C2	C1	C14	C19	-169.03(13)	C14	C15	C16	C17	-0.4(3)
C2	C3	C4	C5	2.1(3)	C15	C14	C19	C18	-1.3(2)
C3	C2	C7	C6	2.1(2)	C15	C16	C17	C18	-0.5(3)
C3	C4	C5	C6	0.9(3)	C16	C17	C18	C19	0.4(3)
C4	C5	C6	C7	-2.4(3)	C17	C18	C19	C14	0.5(3)
C5	C6	C7	C2	0.8(2)	C19	C14	C15	C16	1.3(2)

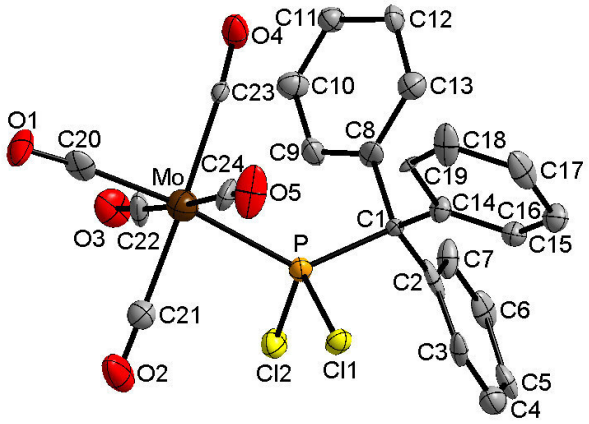

Table 1 Crystal data and structure refinement for 2b.

Identification code	GSTR408
Empirical formula	$C_{24}H_{15}O_5PCl_2Mo$
Formula weight	581.17
Temperature/K	100
Crystal system	monoclinic
Space group	$P2_1/c$
a/Å	7.663(4)
b/Å	9.482(3)
c/Å	32.804(13)
α/°	90
β/°	94.65(3)
γ/°	90
Volume/Å^3	2375.6(17)
Z	4
ρ_{calc}g/cm^3	1.625
μ/mm^{-1}	0.878
F(000)	1160.0
Crystal size/mm^3	0.2 × 0.08 × 0.05
Tmin; Tmax	0.4534; 0.7460
Radiation	MoKα (λ = 0.71073)
2Θ range for data collection/°	4.472 to 52°
Completeness to theta	0.814
Index ranges	-5 ≤ h ≤ 8, -11 ≤ k ≤ 11, -40 ≤ l ≤ 40
Reflections collected	7789
Independent reflections	3805 [R_{int} = 0.2205, R_{sigma} = 0.3536]
Data/restraints/parameters	3805/66/298
Goodness-of-fit on F^2	0.981
Final R indexes [I>=2σ (I)]	R_1 = 0.1220, wR_2 = 0.2500
Final R indexes [all data]	R_1 = 0.2574, wR_2 = 0.3345
Largest diff. peak/hole / e Å^{-3}	0.84/-1.66

Table 2 Bond Lengths for 2b.

Atom	Atom	Length/Å	Atom	Atom	Length/Å
Mo	P	2.489(5)	C2	C7	1.37(2)
Mo	C20	2.05(2)	C3	C4	1.39(3)
Mo	C21	2.09(2)	C4	C5	1.40(2)
Mo	C22	2.13(2)	C5	C6	1.39(3)
Mo	C23	2.15(2)	C6	C7	1.42(3)
Mo	C24	2.11(2)	C8	C9	1.37(2)
Cl1	P	2.049(6)	C8	C13	1.42(3)
Cl2	P	2.023(8)	C9	C10	1.41(3)
P	C1	1.938(16)	C10	C11	1.37(3)
O1	C20	1.14(2)	C11	C12	1.43(2)
O2	C21	1.13(3)	C12	C13	1.38(3)
O3	C22	1.10(2)	C14	C15	1.38(2)
O4	C23	1.11(2)	C14	C19	1.38(2)
O5	C24	1.12(2)	C15	C16	1.37(2)
C1	C2	1.48(3)	C16	C17	1.46(3)
C1	C8	1.54(3)	C17	C18	1.42(2)
C1	C14	1.55(2)	C18	C19	1.40(2)
C2	C3	1.38(3)			

Table 3 Bond Angles for 2b.

Atom	Atom	Atom	Angle/˚	Atom	Atom	Atom	Angle/˚
C20	Mo	P	173.2(6)	C7	C2	C1	121(2)
C20	Mo	C21	87.7(8)	C7	C2	C3	117(2)
C20	Mo	C22	89.7(7)	C2	C3	C4	122.0(19)
C20	Mo	C23	90.4(8)	C3	C4	C5	122(2)
C20	Mo	C24	89.9(7)	C6	C5	C4	116(2)
C21	Mo	P	85.5(6)	C5	C6	C7	122.2(19)
C21	Mo	C22	89.9(8)	C2	C7	C6	121(2)
C21	Mo	C23	177.6(7)	C9	C8	C1	122.4(19)
C21	Mo	C24	93.5(8)	C9	C8	C13	116.7(18)
C22	Mo	P	89.7(6)	C13	C8	C1	120.8(16)
C22	Mo	C23	88.6(8)	C8	C9	C10	123(2)
C23	Mo	P	96.4(5)	C11	C10	C9	118.8(18)
C24	Mo	P	91.1(6)	C10	C11	C12	121.0(19)
C24	Mo	C22	176.5(10)	C13	C12	C11	118(2)
C24	Mo	C23	87.9(8)	C12	C13	C8	123.0(18)
Cl1	P	Mo	109.6(2)	C15	C14	C1	123.2(16)
Cl2	P	Mo	109.2(2)	C19	C14	C1	120.0(14)
Cl2	P	Cl1	100.8(3)	C19	C14	C15	116.8(16)
C1	P	Mo	130.5(7)	C16	C15	C14	123.6(19)
C1	P	Cl1	101.6(5)	C15	C16	C17	119.3(17)
C1	P	Cl2	101.2(6)	C18	C17	C16	117.5(18)
C2	C1	P	112.1(14)	C19	C18	C17	118.7(19)

C2	C1	C8	110.6(15)	C14	C19	C18	124.0(16)
C2	C1	C14	114.3(13)	O1	C20	Mo	175(2)
C8	C1	P	104.6(10)	O2	C21	Mo	179(2)
C8	C1	C14	110.6(17)	O3	C22	Mo	175(2)
C14	C1	P	104.1(10)	O4	C23	Mo	175.7(16)
C3	C2	C1	121.1(17)	O5	C24	Mo	177(2)

Table 4 Torsion Angles for 2b.

A	B	C	D	Angle/˚	A	B	C	D	Angle/˚
P	C1	C2	C3	-62.8(19)	C7	C2	C3	C4	-5(3)
P	C1	C2	C7	119.5(17)	C8	C1	C2	C3	-179.1(16)
P	C1	C8	C9	-49(2)	C8	C1	C2	C7	3(2)
P	C1	C8	C13	134.1(17)	C8	C1	C14	C15	-120.1(19)
P	C1	C14	C15	128.1(17)	C8	C1	C14	C19	57(2)
P	C1	C14	C19	-55(2)	C8	C9	C10	C11	-2(3)
C1	C2	C3	C4	177.5(17)	C9	C8	C13	C12	1(3)
C1	C2	C7	C6	-178.5(17)	C9	C10	C11	C12	4(3)
C1	C8	C9	C10	-177.6(18)	C10	C11	C12	C13	-4(3)
C1	C8	C13	C12	178.3(18)	C11	C12	C13	C8	1(3)
C1	C14	C15	C16	179.4(18)	C13	C8	C9	C10	0(3)
C1	C14	C19	C18	-179.9(17)	C14	C1	C2	C3	55(2)
C2	C1	C8	C9	72(2)	C14	C1	C2	C7	-122.4(18)
C2	C1	C8	C13	-105(2)	C14	C1	C8	C9	-160.3(17)
C2	C1	C14	C15	5(3)	C14	C1	C8	C13	23(2)
C2	C1	C14	C19	-177.4(18)	C14	C15	C16	C17	-2(3)
C2	C3	C4	C5	3(3)	C15	C14	C19	C18	-3(3)
C3	C2	C7	C6	4(3)	C15	C16	C17	C18	3(3)
C3	C4	C5	C6	0(3)	C16	C17	C18	C19	-3(3)
C4	C5	C6	C7	-1(3)	C17	C18	C19	C14	3(3)
C5	C6	C7	C2	-1(3)	C19	C14	C15	C16	2(3)

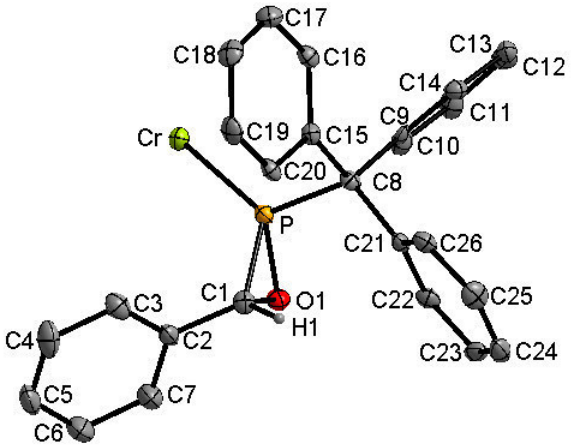

Table 1 Crystal data and structure refinement for 4a.

Identification code	GSTR243
Empirical formula	$C_{31}H_{21}CrO_6P$
Formula weight	572.45
Temperature/K	123(2)
Crystal system	orthorhombic
Space group	$P2_12_12_1$
a/Å	8.5858(5)
b/Å	19.6165(9)
c/Å	15.6007(10)
α/°	90
β/°	90
γ/°	90
Volume/Å^3	2627.5(3)
Z	4
ρ_{calc}g/cm^3	1.447
μ/mm^{-1}	0.541
F(000)	1176
Crystal size/mm^3	0.15 × 0.12 × 0.04
Tmin; Tmax	0.9787; 0.9232
Radiation	MoKα (λ = 0.71073)
2Θ range for data collection/°	2.90 to 28°
Completeness to theta	0.998
Index ranges	-11 ≤ h ≤ 11, -22 ≤ k ≤ 25, -20 ≤ l ≤ 20
Reflections collected	14343
Independent reflections	6334 [R_{int} = 0.0754]
Data/restraints/parameters	6334/4/356
Goodness-of-fit on F^2	0.623
Final R indexes [I>=2σ (I)]	R_1 = 0.0409, wR_2 = 0.0495
Final R indexes [all data]	R_1 = 0.0816, wR_2 = 0.0567
Largest diff. peak/hole / e Å^{-3}	0.622/-0.408

Table 2 Bond Lengths for 4a.

Atom	Atom	Length/Å	Atom	Atom	Length/Å
C(1)	C(2)	1.478(4)	C(1)	O(1)	1.485(3)
C(1)	P	1.785(3)	C(2)	C(7)	1.381(4)
C(2)	C(3)	1.387(4)	C(3)	C(4)	1.385(4)
C(4)	C(5)	1.366(4)	C(5)	C(6)	1.381(5)
C(6)	C(7)	1.384(4)	C(8)	C(21)	1.538(4)
C(8)	C(15)	1.538(4)	C(8)	C(9)	1.548(4)
C(8)	P	1.895(3)	C(9)	C(14)	1.380(4)
C(9)	C(10)	1.386(4)	C(10)	C(11)	1.384(4)
C(11)	C(12)	1.390(4)	C(12)	C(13)	1.370(4)
C(13)	C(14)	1.388(4)	C(15)	C(20)	1.398(4)
C(15)	C(16)	1.400(4)	C(16)	C(17)	1.389(4)
C(17)	C(18)	1.375(4)	C(18)	C(19)	1.391(4)
C(19)	C(20)	1.374(4)	C(21)	C(26)	1.395(4)
C(21)	C(22)	1.399(4)	C(22)	C(23)	1.379(4)
C(23)	C(24)	1.374(4)	C(24)	C(25)	1.376(4)
C(25)	C(26)	1.387(4)	C(27)	O(2)	1.141(4)
C(27)	Cr	1.895(3)	C(28)	O(3)	1.133(3)
C(28)	Cr	1.899(3)	C(29)	O(4)	1.152(3)
C(29)	Cr	1.861(3)	C(30)	O(5)	1.128(3)
C(30)	Cr	1.915(3)	C(31)	O(6)	1.129(4)
C(31)	Cr	1.919(3)	Cr	P	2.3328(9)
O(1)	P	1.663(2)			

Table 3 Bond Angles for 4a.

Atom	Atom	Atom	Angle/˚	Atom	Atom	Atom	Angle/˚
C(2)	C(1)	O(1)	117.6(2)	C(2)	C(1)	P	124.8(2)
O(1)	C(1)	P	60.30(13)	C(7)	C(2)	C(3)	119.2(3)
C(7)	C(2)	C(1)	120.1(3)	C(3)	C(2)	C(1)	120.6(3)
C(4)	C(3)	C(2)	120.1(3)	C(5)	C(4)	C(3)	120.1(3)
C(4)	C(5)	C(6)	120.5(3)	C(5)	C(6)	C(7)	119.5(3)
C(2)	C(7)	C(6)	120.6(3)	C(21)	C(8)	C(15)	113.9(2)
C(21)	C(8)	C(9)	104.5(2)	C(15)	C(8)	C(9)	114.3(2)
C(21)	C(8)	P	114.68(19)	C(15)	C(8)	P	97.98(19)
C(9)	C(8)	P	111.9(2)	C(14)	C(9)	C(10)	117.6(3)
C(14)	C(9)	C(8)	119.3(3)	C(10)	C(9)	C(8)	122.8(3)
C(11)	C(10)	C(9)	121.8(3)	C(10)	C(11)	C(12)	119.6(3)
C(13)	C(12)	C(11)	119.1(3)	C(12)	C(13)	C(14)	120.8(3)
C(9)	C(14)	C(13)	121.0(3)	C(20)	C(15)	C(16)	117.2(3)
C(20)	C(15)	C(8)	119.9(2)	C(16)	C(15)	C(8)	122.7(3)
C(17)	C(16)	C(15)	120.8(3)	C(18)	C(17)	C(16)	120.8(3)
C(17)	C(18)	C(19)	119.2(3)	C(20)	C(19)	C(18)	120.1(3)
C(19)	C(20)	C(15)	121.9(3)	C(26)	C(21)	C(22)	117.5(3)
C(26)	C(21)	C(8)	121.6(3)	C(22)	C(21)	C(8)	120.6(3)

C(23)	C(22)	C(21)	121.1(3)	C(24)	C(23)	C(22)	120.6(3)
C(23)	C(24)	C(25)	119.4(3)	C(24)	C(25)	C(26)	120.6(3)
C(25)	C(26)	C(21)	120.7(3)	O(2)	C(27)	Cr	178.0(3)
O(3)	C(28)	Cr	172.6(3)	O(4)	C(29)	Cr	177.5(3)
O(5)	C(30)	Cr	174.2(3)	O(6)	C(31)	Cr	177.8(3)
C(29)	Cr	C(27)	91.34(13)	C(29)	Cr	C(28)	85.75(12)
C(27)	Cr	C(28)	87.59(14)	C(29)	Cr	C(30)	88.35(13)
C(27)	Cr	C(30)	88.19(14)	C(28)	Cr	C(30)	172.66(14)
C(29)	Cr	C(31)	89.09(13)	C(27)	Cr	C(31)	179.33(15)
C(28)	Cr	C(31)	92.95(14)	C(30)	Cr	C(31)	91.31(14)
C(29)	Cr	P	175.21(10)	C(27)	Cr	P	90.46(9)
C(28)	Cr	P	89.89(9)	C(30)	Cr	P	96.14(9)
C(31)	Cr	P	89.15(9)	C(1)	O(1)	P	68.83(14)
O(1)	P	C(1)	50.88(11)	O(1)	P	C(8)	110.31(11)
C(1)	P	C(8)	104.35(14)	O(1)	P	Cr	117.33(8)
C(1)	P	Cr	125.73(11)	C(8)	P	Cr	125.40(9)

Table 4 Torsion Angles for 4a.

A	B	C	D	Angle/˚	A	B	C	D	Angle/˚
O(1)	C(1)	C(2)	C(7)	38.8(4)	P	C(1)	C(2)	C(7)	110.3(3)
O(1)	C(1)	C(2)	C(3)	-144.0(3)	P	C(1)	C(2)	C(3)	-72.5(4)
C(7)	C(2)	C(3)	C(4)	-0.4(4)	C(1)	C(2)	C(3)	C(4)	-177.7(3)
C(2)	C(3)	C(4)	C(5)	0.1(5)	C(3)	C(4)	C(5)	C(6)	0.2(5)
C(4)	C(5)	C(6)	C(7)	0.0(5)	C(3)	C(2)	C(7)	C(6)	0.6(5)
C(1)	C(2)	C(7)	C(6)	177.8(3)	C(5)	C(6)	C(7)	C(2)	-0.3(5)
C(21)	C(8)	C(9)	C(14)	-72.6(3)	C(15)	C(8)	C(9)	C(14)	52.6(4)
P	C(8)	C(9)	C(14)	162.8(2)	C(21)	C(8)	C(9)	C(10)	101.0(3)
C(15)	C(8)	C(9)	C(10)	-133.8(3)	P	C(8)	C(9)	C(10)	-23.7(3)
C(14)	C(9)	C(10)	C(11)	-2.3(4)	C(8)	C(9)	C(10)	C(11)	-176.0(3)
C(9)	C(10)	C(11)	C(12)	1.3(4)	C(10)	C(11)	C(12)	C(13)	0.4(4)
C(11)	C(12)	C(13)	C(14)	-1.1(4)	C(10)	C(9)	C(14)	C(13)	1.6(4)
C(8)	C(9)	C(14)	C(13)	175.5(3)	C(12)	C(13)	C(14)	C(9)	0.0(4)
C(21)	C(8)	C(15)	C(20)	-51.0(4)	C(9)	C(8)	C(15)	C(20)	-171.0(3)
P	C(8)	C(15)	C(20)	70.6(3)	C(21)	C(8)	C(15)	C(16)	134.0(3)
C(9)	C(8)	C(15)	C(16)	13.9(4)	P	C(8)	C(15)	C(16)	-104.5(3)
C(20)	C(15)	C(16)	C(17)	1.9(4)	C(8)	C(15)	C(16)	C(17)	177.1(3)
C(15)	C(16)	C(17)	C(18)	-1.5(5)	C(16)	C(17)	C(18)	C(19)	0.6(5)
C(17)	C(18)	C(19)	C(20)	-0.2(5)	C(18)	C(19)	C(20)	C(15)	0.6(5)
C(16)	C(15)	C(20)	C(19)	-1.4(4)	C(8)	C(15)	C(20)	C(19)	-176.8(3)
C(15)	C(8)	C(21)	C(26)	-18.0(4)	C(9)	C(8)	C(21)	C(26)	107.4(3)
P	C(8)	C(21)	C(26)	-129.8(3)	C(15)	C(8)	C(21)	C(22)	167.3(3)
C(9)	C(8)	C(21)	C(22)	-67.3(3)	P	C(8)	C(21)	C(22)	55.6(3)
C(26)	C(21)	C(22)	C(23)	1.4(5)	C(8)	C(21)	C(22)	C(23)	176.3(3)
C(21)	C(22)	C(23)	C(24)	-2.0(5)	C(22)	C(23)	C(24)	C(25)	0.8(5)
C(23)	C(24)	C(25)	C(26)	0.9(5)	C(24)	C(25)	C(26)	C(21)	-1.4(5)

C(22)	C(21)	C(26)	C(25)	0.3(5)
O(4)	C(29)	Cr	C(27)	116(6)
O(4)	C(29)	Cr	C(30)	-156(6)
O(4)	C(29)	Cr	P	4(7)
O(2)	C(27)	Cr	C(28)	94(9)
O(2)	C(27)	Cr	C(31)	-121(12)
O(3)	C(28)	Cr	C(29)	42(2)
O(3)	C(28)	Cr	C(30)	5(3)
O(3)	C(28)	Cr	P	-140(2)
O(5)	C(30)	Cr	C(27)	71(3)
O(5)	C(30)	Cr	C(31)	-110(3)
O(6)	C(31)	Cr	C(29)	24(7)
O(6)	C(31)	Cr	C(28)	-62(7)
O(6)	C(31)	Cr	P	-152(7)
C(1)	O(1)	P	C(8)	92.27(18)
C(2)	C(1)	P	O(1)	-104.7(3)
O(1)	C(1)	P	C(8)	-104.70(15)
O(1)	C(1)	P	Cr	98.28(14)
C(15)	C(8)	P	O(1)	-146.51(16)
C(21)	C(8)	P	C(1)	27.6(3)
C(9)	C(8)	P	C(1)	146.43(19)
C(15)	C(8)	P	Cr	63.8(2)
C(29)	Cr	P	O(1)	61.9(12)
C(28)	Cr	P	O(1)	37.34(13)
C(31)	Cr	P	O(1)	130.30(13)
C(27)	Cr	P	C(1)	-110.04(15)
C(30)	Cr	P	C(1)	161.73(16)
C(29)	Cr	P	C(8)	-150.3(11)
C(28)	Cr	P	C(8)	-174.80(16)
C(31)	Cr	P	C(8)	-81.84(15)
C(8)	C(21)	C(26)	C(25)	-174.5(3)
O(4)	C(29)	Cr	C(28)	29(6)
O(4)	C(29)	Cr	C(31)	-65(6)
O(2)	C(27)	Cr	C(29)	9(9)
O(2)	C(27)	Cr	C(30)	-80(9)
O(2)	C(27)	Cr	P	-176(100)
O(3)	C(28)	Cr	C(27)	-50(2)
O(3)	C(28)	Cr	C(31)	131(2)
O(5)	C(30)	Cr	C(29)	-21(3)
O(5)	C(30)	Cr	C(28)	16(4)
O(5)	C(30)	Cr	P	161(3)
O(6)	C(31)	Cr	C(27)	153(10)
O(6)	C(31)	Cr	C(30)	112(7)
C(2)	C(1)	O(1)	P	116.3(2)
C(1)	O(1)	P	Cr	-115.27(14)
C(2)	C(1)	P	C(8)	150.6(2)
C(2)	C(1)	P	Cr	-6.4(3)
C(21)	C(8)	P	O(1)	-25.5(2)
C(9)	C(8)	P	O(1)	93.3(2)
C(15)	C(8)	P	C(1)	-93.36(18)
C(21)	C(8)	P	Cr	-175.24(17)
C(9)	C(8)	P	Cr	-56.5(2)
C(27)	Cr	P	O(1)	-50.25(13)
C(30)	Cr	P	O(1)	-138.48(13)
C(29)	Cr	P	C(1)	2.1(12)
C(28)	Cr	P	C(1)	-22.45(16)
C(31)	Cr	P	C(1)	70.51(16)
C(27)	Cr	P	C(8)	97.61(15)
C(30)	Cr	P	C(8)	9.38(16)

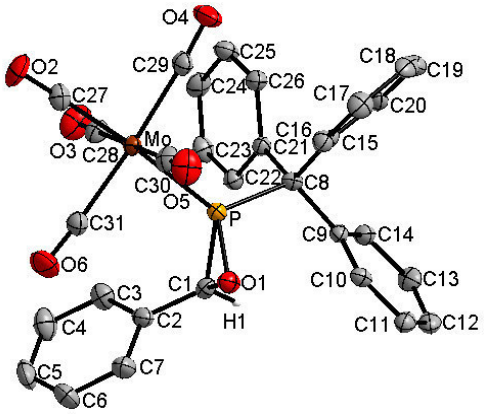

Table 1 Crystal data and structure refinement for 4b.

Identification code	GSTR273
Empirical formula	$C_{31}H_{21}O_6PMo$
Formula weight	616.39
Temperature/K	123(2)
Crystal system	orthorhombic
Space group	$P2_1/2_1/2_1$
a/Å	8.6515(3)
b/Å	15.6935(4)
c/Å	19.9770(8)
α/°	90
β/°	90
γ/°	90
Volume/Å^3	2712.32(16)
Z	4
ρ_{calc}g/cm^3	1.509
μ/mm^{-1}	0.586
F(000)	1248.0
Crystal size/mm^3	0.10 × 0.03 × 0.02
Tmin; Tmax	0.9437; 0.9884
Radiation	MoKα (λ = 0.71073)
2Θ range for data collection/°	2.88 to 28.00°
Completeness to theta	0.995
Index ranges	-11 ≤ h ≤ 11, -20 ≤ k ≤ 20, -26 ≤ l ≤ 21
Reflections collected	19516
Independent reflections	6550 [R_{int} = 0.0826]
Data/restraints/parameters	6550/0/356
Goodness-of-fit on F^2	0.840
Final R indexes [I>=2σ (I)]	R_1 = 0.0432, wR_2 = 0.0549
Final R indexes [all data]	R_1 = 0.0646, wR_2 = 0.0585
Largest diff. peak/hole / e Å^{-3}	0.592/-0.653

Table 2 Bond Lengths for 4b.

Atom	Atom	Length/Å	Atom	Atom	Length/Å
C1	C2	1.487(5)	C17	C18	1.375(6)
C1	P	1.7813	C18	C19	1.377(6)
C2	C3	1.385(6)	C19	C20	1.381(6)
C2	C7	1.386(5)	C21	C22	1.393(5)
C3	C4	1.368(6)	C21	C26	1.404(5)
C4	C5	1.379(6)	C22	C23	1.374(5)
C5	C6	1.388(6)	C23	C24	1.378(5)
C6	C7	1.369(6)	C24	C25	1.383(6)
C8	C15	1.534(5)	C25	C26	1.384(5)
C8	C21	1.553(5)	C27	O2	1.145(4)
C8	C9	1.556(5)	C27	Mo	1.996(4)
C8	P	1.892(4)	C28	O3	1.136(5)
C9	C14	1.372(6)	C28	Mo	2.052(4)
C9	C10	1.407(5)	C29	O4	1.145(4)
C10	C11	1.387(5)	C29	Mo	2.044(4)
C11	C12	1.357(6)	C30	O5	1.148(5)
C12	C13	1.381(5)	C30	Mo	2.024(5)
C13	C14	1.391(5)	C31	O6	1.141(5)
C15	C16	1.384(6)	C31	Mo	2.052(4)
C15	C20	1.403(5)	O1	P	1.668(2)
C16	C17	1.380(5)	P	Mo	2.4864(10)

Table 3 Bond Angles for 4b.

Atom	Atom	Atom	Angle/˚	Atom	Atom	Atom	Angle/˚
O1	C1	C2	117.6(3)	C22	C21	C8	120.6(3)
O1	C1	P	60.92(17)	C26	C21	C8	121.4(3)
C2	C1	P	123.8(3)	C23	C22	C21	121.6(4)
C3	C2	C7	118.6(4)	C22	C23	C24	120.6(4)
C3	C2	C1	121.0(3)	C23	C24	C25	118.7(4)
C7	C2	C1	120.4(4)	C24	C25	C26	121.5(3)
C4	C3	C2	120.9(4)	C25	C26	C21	119.9(4)
C3	C4	C5	120.0(4)	O2	C27	Mo	178.8(4)
C4	C5	C6	119.8(4)	O3	C28	Mo	177.9(4)
C7	C6	C5	119.7(5)	O4	C29	Mo	175.3(4)
C6	C7	C2	120.9(4)	O5	C30	Mo	179.0(4)
C15	C8	C21	114.7(3)	O6	C31	Mo	173.7(4)
C15	C8	C9	105.8(3)	C1	O1	P	68.93(16)
C21	C8	C9	112.8(3)	O1	P	C1	50.16(14)
C15	C8	P	112.4(3)	O1	P	C8	110.82(14)
C21	C8	P	97.6(2)	C1	P	C8	105.61(17)
C9	C8	P	113.8(2)	O1	P	Mo	117.36(11)
C14	C9	C10	118.1(3)	C1	P	Mo	125.28(14)
C14	C9	C8	122.0(3)	C8	P	Mo	124.80(10)

C10	C9	C8	119.5(3)	C27	Mo	C30	90.56(17)
C11	C10	C9	120.2(4)	C27	Mo	C29	88.67(15)
C12	C11	C10	120.7(4)	C30	Mo	C29	88.63(17)
C11	C12	C13	120.0(4)	C27	Mo	C31	85.72(15)
C12	C13	C14	119.9(4	C30	Mo	C31	87.20(17)
C9	C14	C13	121.1(4)	C29	Mo	C31	172.97(19)
C16	C15	C20	117.7(4)	C27	Mo	C28	89.55(15)
C16	C15	C8	123.3(4)	C30	Mo	C28	179.88(18)
C20	C15	C8	118.7(4)	C29	Mo	C28	91.42(16)
C17	C16	C15	121.2(4)	C31	Mo	C28	92.76(17)
C18	C17	C16	120.6(4)	C27	Mo	P	175.72(12)
C17	C18	C19	119.1(4)	C30	Mo	P	90.66(11)
C18	C19	C20	120.8(4)	C29	Mo	P	95.46(11)
C19	C20	C15	120.5(4)	C31	Mo	P	90.24(12)
C22	C21	C26	117.7(3)	C28	Mo	P	89.23(11)

Table 4 Torsion Angles for 4b.

A	B	C	D	Angle/°	A	B	C	D	Angle/°
O1	C1	C2	C3	144.0(3)	C8	C15	C16	C17	176.1(3)
P	C1	C2	C3	72.1(5)	C15	C16	C17	C18	1.5(6)
O1	C1	C2	C7	37.7(5)	C16	C17	C18	C19	0.1(6)
P	C1	C2	C7	109.6(4)	C17	C18	C19	C20	0.2(5)
C7	C2	C3	C4	0.3(6)	C18	C19	C20	C15	1.7(5)
C1	C2	C3	C4	178.6(4)	C16	C15	C20	C19	3.0(5)
C2	C3	C4	C5	0.8(7)	C8	C15	C20	C19	176.5(3)
C3	C4	C5	C6	0.8(7)	C15	C8	C21	C22	171.6(3)
C4	C5	C6	C7	0.2(7)	C9	C8	C21	C22	50.4(5)
C5	C6	C7	C2	0.4(7)	P	C8	C21	C22	69.5(4)
C3	C2	C7	C6	0.4(7)	C15	C8	C21	C26	14.4(5)
C1	C2	C7	C6	178.0(4)	C9	C8	C21	C26	135.7(4)
C15	C8	C9	C14	107.3(4)	P	C8	C21	C26	104.5(4)
C21	C8	C9	C14	18.9(5)	C26	C21	C22	C23	2.3(6)
P	C8	C9	C14	128.8(4)	C8	C21	C22	C23	176.5(4)
C15	C8	C9	C10	66.2(4)	C21	C22	C23	C24	1.5(6)
C21	C8	C9	C10	167.7(3)	C22	C23	C24	C25	1.2(6)
P	C8	C9	C10	57.7(4)	C23	C24	C25	C26	1.8(7)
C14	C9	C10	C11	2.6(6)	C24	C25	C26	C21	2.7(6)
C8	C9	C10	C11	176.3(3	C22	C21	C26	C25	2.9(6)
C9	C10	C11	C12	2.3(6)	C8	C21	C26	C25	177.0(4)
C10	C11	C12	C13	0.7(6)	C2	C1	O1	P	115.3(3
C11	C12	C13	C14	0.6(6)	C1	O1	P	C8	93.3(2)
C10	C9	C14	C13	1.4(6)	C1	O1	P	Mo	114.54(19)
C8	C9	C14	C13	174.9(4)	C2	C1	P	O1	105.4(4)
C12	C13	C14	C9	0.2(6)	O1	C1	P	C8	104.3(2)
C21	C8	C15	C16	132.1(4)	C2	C1	P	C8	150.2(3)

C9	C8	C15	C16	103.0(4)
P	C8	C15	C16	21.8(4)
C21	C8	C15	C20	54.8(4)
C9	C8	C15	C20	70.2(4)
P	C8	C15	C20	165.0(2)
C21	C8	P	C1	93.0(2)
C9	C8	P	C1	26.1(3)
C15	C8	P	Mo	56.0(3)
C21	C8	P	Mo	64.6(2)
C9	C8	P	Mo	176.3(2)
O2	C27	Mo	C30	109(19)
O2	C27	Mo	C29	162(19)
O2	C27	Mo	C31	22(19)
O2	C27	Mo	C28	71(19)
O5	C27	Mo	P	3(20)
O5	C30	Mo	C27	22(23)
O5	C30	Mo	C29	111(23)
O5	C30	Mo	C31	63(23)
O5	C30	Mo	C28	134(100)
O5	C30	Mo	P	154(23)
O4	C29	Mo	C27	16(5)
O4	C29	Mo	C30	75(5)
O4	C29	Mo	C31	21(6)
O4	C29	Mo	C28	106(5)
O4	C29	Mo	P	165(5)
O6	C31	Mo	C27	35(3)
O6	C31	Mo	C20	56(3)
C8	P	Mo	C28	82.22(19)
O1	C1	P	Mo	98.21(19)
C2	C1	P	Mo	7.2(4)
C15	C8	P	O1	93.6(2)
C21	C8	P	O1	145.7(2)
C9	C8	P	O1	26.6(3)
O6	C31	Mo	C29	2(4)
O6	C31	Mo	C28	124(3)
O6	C31	Mo	P	146(3)
O3	C28	Mo	C27	14(11)
O3	C28	Mo	C30	170(100)
O3	C28	Mo	C29	74(11)
O3	C28	Mo	C31	100(11)
O3	C28	Mo	P	170(11)
O1	P	Mo	C27	56.4(16)
C1	P	Mo	C27	2.4(17)
C8	P	Mo	C27	155.7(16)
O1	P	Mo	C30	50.07(17)
C1	P	Mo	C30	108.90(19)
C8	P	Mo	C30	97.82(19)
O1	P	Mo	C29	138.75(17)
C1	P	Mo	C29	162.4(2)
C8	P	Mo	C29	9.1(2)
O1	P	Mo	C31	37.13(17)
C1	P	Mo	C31	21.7(2)
C8	P	Mo	C31	174.98(19)
O1	P	Mo	C28	129.89(16)
C1	P	Mo	C28	71.06(19)

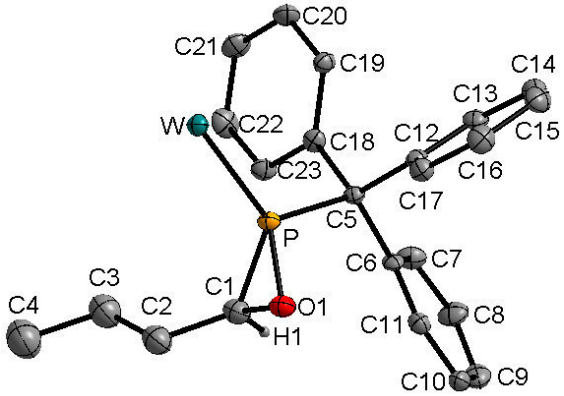

Table 1 Crystal data and structure refinement for 6.

Identification code	GSTR271
Empirical formula	$C_{28}H_{23}O_6PW$
Formula weight	670.28
Temperature/K	123(2)
Crystal system	orthorhombic
Space group	$P2_12_12_1$
a/Å	8.4672(2)
b/Å	15.6855(4)
c/Å	19.8873(4)
α/°	90
β/°	90
γ/°	90
Volume/Å^3	2641.28(11)
Z	4
ρ_{calc}g/cm^3	1.686
μ/mm^{-1}	4.474
F(000)	1312
Crystal size/mm^3	0.40 × 0.12 × 0.10
Tmin; Tmax	0.6632; 0.2677
Radiation	MoKα (λ = 0.71073)
2Θ range for data collection/°	2.60 to 28°
Completeness to theta	0.992
Index ranges	-9 ≤ h ≤ 11, -19 ≤ k ≤ 20, -26 ≤ l ≤ 25
Reflections collected	19378
Independent reflections	6229 [R_{int} = 0.0440]
Data/restraints/parameters	6229/74/327
Goodness-of-fit on F^2	1.009
Final R indexes [I>=2σ (I)]	R_1 = 0.0264, wR_2 = 0.0493
Final R indexes [all data]	R_1 = 0.0296, wR_2 = 0.0502
Largest diff. peak/hole / e Å^{-3}	1.496/-1.719

Table 2 Bond Lengths for 6.

Atom	Atom	Length/Å	Atom	Atom	Length/Å
C(1)	O(1)	1.482(5)	C(1)	C(2)	1.506(6)
C(1)	P	1.786(4)	C(2)	C(3)	1.505(6)
C(3)	C(4)	1.522(6)	C(5)	C(12)	1.533(5)
C(5)	C(18)	1.541(5)	C(5)	C(6)	1.546(5)
C(5)	P	1.902(4)	C(6)	C(11)	1.384(5)
C(6)	C(7)	1.399(5)	C(7)	C(8)	1.382(5)
C(8)	C(9)	1.384(6)	C(9)	C(10)	1.388(6)
C(10)	C(11)	1.383(5)	C(12)	C(13)	1.397(5)
C(12)	C(17)	1.404(5)	C(13)	C(14)	1.370(6)
C(14)	C(15)	1.400(5)	C(15)	C(16)	1.372(6)
C(16)	C(17)	1.393(6)	C(18)	C(19)	1.391(5)
C(18)	C(23)	1.394(6)	C(19)	C(20)	1.387(6)
C(20)	C(21)	1.392(7)	C(21)	C(22)	1.384(6)
C(22)	C(23)	1.385(6)	C(24)	O(2)	1.143(5)
C(24)	W	2.002(4)	C(25)	O(3)	1.141(5)
C(25)	W	2.047(4)	C(26)	O(4)	1.153(5)
C(26)	W	2.031(4)	C(27)	O(5)	1.149(5)
C(27)	W	2.024(4)	C(28)	O(6)	1.140(5)
C(28)	W	2.042(4)	W	P	2.4906(10)
O(1)	P	1.662(3)			

Table 3 Bond Angles for 6.

Atom	Atom	Atom	Angle/˚	Atom	Atom	Atom	Angle/˚
O(1)	C(1)	C(2)	115.6(3)	O(1)	C(1)	P	60.28(18)
C(2)	C(1)	P	124.0(3)	C(3)	C(2)	C(1)	112.1(3)
C(2)	C(3)	C(4)	113.5(4)	C(12)	C(5)	C(18)	114.9(3)
C(12)	C(5)	C(6)	105.0(3)	C(18)	C(5)	C(6)	112.9(3)
C(12)	C(5)	P	110.9(2)	C(18)	C(5)	P	98.5(2)
C(6)	C(5)	P	115.0(3)	C(11)	C(6)	C(7)	118.3(3)
C(11)	C(6)	C(5)	120.6(3)	C(7)	C(6)	C(5)	120.6(3)
C(8)	C(7)	C(6)	120.7(4)	C(7)	C(8)	C(9)	120.4(4)
C(8)	C(9)	C(10)	119.1(4)	C(11)	C(10)	C(9)	120.4(4)
C(10)	C(11)	C(6)	121.0(3)	C(13)	C(12)	C(17)	117.1(4)
C(13)	C(12)	C(5)	119.8(3)	C(17)	C(12)	C(5)	122.7(3)
C(14)	C(13)	C(12)	121.3(4)	C(13)	C(14)	C(15)	120.8(4)
C(16)	C(15)	C(14)	119.1(4)	C(15)	C(16)	C(17)	120.1(4)
C(16)	C(17)	C(12)	121.4(4)	C(19)	C(18)	C(23)	117.7(4)
C(19)	C(18)	C(5)	123.0(4)	C(23)	C(18)	C(5)	119.3(3)
C(20)	C(19)	C(18)	121.4(4)	C(19)	C(20)	C(21)	119.9(4)
C(22)	C(21)	C(20)	119.5(4)	C(21)	C(22)	C(23)	120.0(4)
C(22)	C(23)	C(18)	121.5(4)	O(2)	C(24)	W	178.4(4)
O(3)	C(25)	W	173.6(3)	O(4)	C(26)	W	179.0(4)
O(5)	C(27)	W	174.8(4)	O(6)	C(28)	W	176.9(4)

C(24)	W	C(27)	85.95(17)	C(24)	W	C(26)	91.93(18)
C(27)	W	C(26)	88.31(18)	C(24)	W	C(28)	88.39(17)
C(27)	W	C(28)	91.65(17)	C(26)	W	C(28)	179.67(18)
C(24)	W	C(25)	86.82(17)	C(27)	W	C(25)	171.53(16)
C(26)	W	C(25)	87.55(17)	C(28)	W	C(25)	92.54(17)
C(24)	W	P	178.85(14)	C(27)	W	P	93.01(12)
C(26)	W	P	88.51(12)	C(28)	W	P	91.17(12)
C(25)	W	P	94.26(11)	C(1)	O(1)	P	68.94(19)
O(1)	P	C(1)	50.77(16)	O(1)	P	C(5)	109.53(15)
C(1)	P	C(5)	106.87(18)	O(1)	P	W	118.63(10)
C(1)	P	W	128.11(14)	C(5)	P	W	121.87(12)

Table 4 Torsion Angles for 6.

A	B	C	D	Angle/˚	A	B	C	D	Angle/˚
O(1)	C(1)	C(2)	C(3)	153.8(4)	P	C(1)	C(2)	C(3)	83.6(5)
C(1)	C(2)	C(3)	C(4)	179.9(4)	C(12)	C(5)	C(6)	C(11)	66.2(4)
C(18)	C(5)	C(6)	C(11)	-167.8(4)	P	C(5)	C(6)	C(11)	-55.9(5)
C(12)	C(5)	C(6)	C(7)	-105.8(4)	C(18)	C(5)	C(6)	C(7)	20.2(5)
P	C(5)	C(6)	C(7)	132.1(4)	C(11)	C(6)	C(7)	C(8)	0.7(6)
C(5)	C(6)	C(7)	C(8)	172.8(4)	C(6)	C(7)	C(8)	C(9)	1.1(7)
C(7)	C(8)	C(9)	C(10)	-1.2(7)	C(8)	C(9)	C(10)	C(11)	-0.5(7)
C(9)	C(10)	C(11)	C(6)	2.3(6)	C(7)	C(6)	C(11)	C(10)	-2.4(6)
C(5)	C(6)	C(11)	C(10)	-174.6(4)	C(18)	C(5)	C(12)	C(13)	-54.6(5)
C(6)	C(5)	C(12)	C(13)	70.0(4)	P	C(5)	C(12)	C(13)	-165.2(3)
C(18)	C(5)	C(12)	C(17)	132.6(4)	C(6)	C(5)	C(12)	C(17)	-102.7(4)
P	C(5)	C(12)	C(17)	22.1(5)	C(17)	C(12)	C(13)	C(14)	-3.5(6)
C(5)	C(12)	C(13)	C(14)	-176.6(4)	C(12)	C(13)	C(14)	C(15)	2.0(6)
C(13)	C(14)	C(15)	C(16)	-0.7(6)	C(14)	C(15)	C(16)	C(17)	1.0(6)
C(15)	C(16)	C(17)	C(12)	-2.7(6)	C(13)	C(12)	C(17)	C(16)	3.9(6)
C(5)	C(12)	C(17)	C(16)	176.7(4)	C(12)	C(5)	C(18)	C(19)	-10.3(5)
C(6)	C(5)	C(18)	C(19)	-130.7(4)	P	C(5)	C(18)	C(19)	107.5(4)
C(12)	C(5)	C(18)	C(23)	171.9(3)	C(6)	C(5)	C(18)	C(23)	51.5(5)
P	C(5)	C(18)	C(23)	-70.3(4)	C(23)	C(18)	C(19)	C(20)	-1.1(6)
C(5)	C(18)	C(19)	C(20)	-179.0(4)	C(18)	C(19)	C(20)	C(21)	1.0(7)
C(19)	C(20)	C(21)	C(22)	-0.3(7)	C(20)	C(21)	C(22)	C(23)	-0.3(7)
C(21)	C(22)	C(23)	C(18)	0.1(6)	C(19)	C(18)	C(23)	C(22)	0.6(6)
C(5)	C(18)	C(23)	C(22)	178.5(4)	O(2)	C(24)	W	C(27)	-89(14)
O(2)	C(24)	W	C(26)	-177(100)	O(2)	C(24)	W	C(28)	3(14)
O(2)	C(24)	W	C(25)	96(14)	O(2)	C(24)	W	P	-64(17)
O(5)	C(27)	W	C(24)	-20(5)	O(5)	C(27)	W	C(26)	72(5)
O(5)	C(27)	W	C(28)	-108(5)	O(5)	C(27)	W	C(25)	11(5)
O(5)	C(27)	W	P	161(5)	O(4)	C(26)	W	C(24)	-122(24)
O(4)	C(26)	W	C(27)	152(24)	O(4)	C(26)	W	C(28)	71(47)
O(4)	C(26)	W	C(25)	-35(24)	O(4)	C(26)	W	P	59(24)
O(6)	C(28)	W	C(24)	6(7)	O(6)	C(28)	W	C(27)	91(7)

O(6)	C(28)	W	C(26)	173(100)
O(6)	C(28)	W	P	-175(7)
O(3)	C(25)	W	C(27)	-2(4)
O(3)	C(25)	W	C(28)	117(3)
C(2)	C(1)	O(1)	P	-116.1(4)
C(1)	O(1)	P	W	117.52(19)
O(1)	C(1)	P	C(5)	101.7(2)
O(1)	C(1)	P	W	-98.4(2)
C(12)	C(5)	P	O(1)	-85.6(3)
C(6)	C(5)	P	O(1)	33.3(3)
C(18)	C(5)	P	C(1)	99.9(3)
C(12)	C(5)	P	W	59.4(3)
C(6)	C(5)	P	W	178.3(2)
C(27)	W	P	O(1)	-48.47(17)
C(28)	W	P	O(1)	-140.18(17)
C(24)	W	P	C(1)	-12(6)
C(26)	W	P	C(1)	100.6(2)
C(25)	W	P	C(1)	-172.0(2)
C(27)	W	P	C(5)	169.56(19)
C(28)	W	P	C(5)	77.85(18)

O(6)	C(28)	W	C(25)	-81(7)
O(3)	C(25)	W	C(24)	29(3)
O(3)	C(25)	W	C(26)	-63(3)
O(3)	C(25)	W	P	-152(3)
C(1)	O(1)	P	C(5)	-96.2(2)
C(2)	C(1)	P	O(1)	102.5(4)
C(2)	C(1)	P	C(5)	-155.8(3)
C(2)	C(1)	P	W	4.1(4)
C(18)	C(5)	P	O(1)	153.5(2)
C(12)	C(5)	P	C(1)	-139.2(3)
C(6)	C(5)	P	C(1)	-20.3(3)
C(18)	C(5)	P	W	-61.5(3)
C(24)	W	P	O(1)	-73(6)
C(26)	W	P	O(1)	39.76(17)
C(25)	W	P	O(1)	127.19(17)
C(27)	W	P	C(1)	12.4(2)
C(28)	W	P	C(1)	-79.4(2)
C(24)	W	P	C(5)	145(6)
C(26)	W	P	C(5)	-102.22(19)
C(25)	W	P	C(5)	-14.78(19)

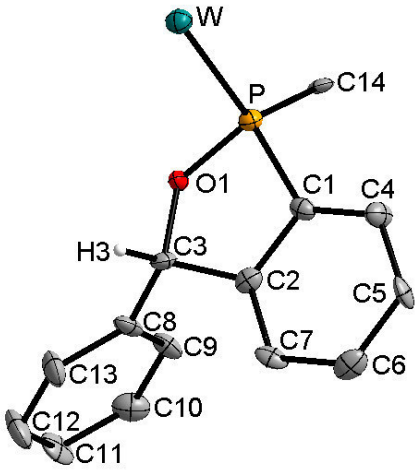

Table 1 Crystal data and structure refinement for 9c.

Identification code	GSTR361
Empirical formula	$C_{37}H_{25}O_6PW$
Formula weight	780.09
Temperature/K	123.15
Crystal system	triclinic
Space group	P-1
a/Å	9.4174(14)
b/Å	10.7473(14)
c/Å	17.631(2)
α/°	98.301(4)
β/°	94.830(4)
γ/°	112.865(4)
Volume/Å^3	1607.6(4)
Z	2
ρ_{calc}mg/mm^3	1.612
μ/mm^{-1}	3.688
F(000)	768.0
Crystal size/mm^3	0.06 × 0.04 × 0.03
Radiation	MoKα (λ = 0.71073)
2Θ range for data collection	5.46 to 50.5°
Index ranges	-11 ≤ h ≤ 11, -12 ≤ k ≤ 12, -21 ≤ l ≤ 19
Reflections collected	14721
Independent reflections	5711 [R_{int} = 0.0995, R_{sigma} = 0.1408]
Data/restraints/parameters	5711/18/406
Goodness-of-fit on F^2	0.962
Final R indexes [I>=2σ (I)]	R_1 = 0.0498, wR_2 = 0.0702
Final R indexes [all data]	R_1 = 0.0893, wR_2 = 0.0809
Largest diff. peak/hole / e Å^{-3}	1.27/-1.70

Table 2 Bond Lengths for 9c.

Atom	Atom	Length/Å	Atom	Atom	Length/Å
W	P	2.510(2)	C9	C10	1.377(10)
W	C33	2.012(9)	C10	C11	1.368(10)
W	C34	2.021(9)	C11	C12	1.355(10)
W	C35	2.030(9)	C12	C13	1.389(10)
W	C36	2.043(9)	C14	C15	1.544(10)
W	C37	2.027(9)	C14	C21	1.548(10)
P	O1	1.642(5)	C14	C27	1.533(10)
P	C1	1.801(7)	C15	C16	1.384(10)
P	C14	1.916(7)	C15	C20	1.374(9)
O1	C3	1.471(7)	C16	C17	1.388(10)
O2	C33	1.144(10)	C17	C18	1.378(10)
O3	C34	1.155(9)	C18	C19	1.360(10)
O4	C35	1.156(9)	C19	C20	1.406(10)
O5	C36	1.146(8)	C21	C22	1.387(10)
O6	C37	1.154(9)	C21	C26	1.389(10)
C1	C2	1.408(9)	C22	C23	1.368(10)
C1	C4	1.367(9)	C23	C24	1.375(11)
C2	C3	1.523(9)	C24	C25	1.394(11)
C2	C7	1.388(10)	C25	C26	1.380(10)
C3	C8	1.497(10)	C27	C28	1.398(9)
C4	C5	1.387(10)	C27	C32	1.406(10)
C5	C6	1.405(10)	C28	C29	1.394(11)
C6	C7	1.389(10)	C29	C30	1.361(11)
C8	C9	1.382(10)	C30	C31	1.393(10)
C8	C13	1.388(9)	C31	C32	1.370(10)

Table 3 Bond Angles for 9c.

Atom	Atom	Atom	Angle/˚	Atom	Atom	Atom	Angle/˚
C33	W	P	175.5(3)	C11	C10	C9	122.0(8)
C33	W	C34	87.0(3)	C12	C11	C10	118.9(8)
C33	W	C35	91.4(3)	C11	C12	C13	120.9(7)
C33	W	C36	89.1(3)	C8	C13	C12	120.0(8)
C33	W	C37	91.0(3)	C15	C14	P	106.4(5)
C34	W	P	97.1(2)	C15	C14	C21	110.4(6)
C34	W	C35	89.9(3)	C21	C14	P	106.3(4)
C34	W	C36	175.0(4)	C27	C14	P	110.1(5)
C34	W	C37	92.1(3)	C27	C14	C15	111.4(6)
C35	W	P	90.6(2)	C27	C14	C21	111.9(6)
C35	W	C36	87.2(3)	C16	C15	C14	120.2(7)
C36	W	P	86.9(2)	C20	C15	C14	120.8(7)
C37	W	P	86.9(2)	C20	C15	C16	118.9(7)
C37	W	C35	176.9(4)	C15	C16	C17	120.7(7)
C37	W	C36	91.0(3)	C18	C17	C16	119.9(8)

O1	P	W	109.80(19)
O1	P	C1	93.4(3)
O1	P	C14	102.4(3)
C1	P	W	112.9(2)
C1	P	C14	107.3(3)
C14	P	W	125.8(2)
C3	O1	P	112.7(4)
C2	C1	P	107.6(5)
C4	C1	P	131.8(6)
C4	C1	C2	120.6(7)
C1	C2	C3	114.0(6)
C7	C2	C1	120.0(7)
C7	C2	C3	125.8(7)
O1	C3	C2	104.4(5)
O1	C3	C8	109.5(5)
C8	C3	C2	117.7(6)
C1	C4	C5	119.9(7)
C4	C5	C6	119.9(7)
C7	C6	C5	120.3(7)
C2	C7	C6	119.2(7)
C9	C8	C3	122.5(7)
C9	C8	C13	119.0(7)
C13	C8	C3	118.4(7)
C10	C9	C8	119.2(7)
C19	C18	C17	120.0(8)
C18	C19	C20	120.2(7)
C15	C20	C19	120.2(7)
C22	C21	C14	120.9(7)
C22	C21	C26	116.1(7)
C26	C21	C14	123.0(7)
C23	C22	C21	123.2(8)
C22	C23	C24	119.6(8)
C23	C24	C25	119.4(8)
C26	C25	C24	119.5(8)
C25	C26	C21	122.2(8)
C28	C27	C14	122.1(7)
C28	C27	C32	115.9(7)
C32	C27	C14	121.9(6)
C29	C28	C27	121.6(8)
C30	C29	C28	121.1(8)
C29	C30	C31	118.6(8)
C32	C31	C30	120.6(8)
C31	C32	C27	122.2(7)
O2	C33	W	179.0(8)
O3	C34	W	174.7(8)
O4	C35	W	177.4(7)
O5	C36	W	177.6(7)
O6	C37	W	178.1(8)

Table 4 Torsion Angles for 9c.

A	B	C	D	Angle/˚
W	P	O1	C3	-90.2(4)
W	P	C1	C2	100.6(5)
W	P	C1	C4	-77.0(7)
W	P	C14	C15	-40.4(6)
W	P	C14	C21	77.3(5)
W	P	C14	C27	-161.3(4)
P	W	C33	O2	131(51)
P	W	C34	O3	-172(8)
P	W	C35	O4	-67(15)
P	W	C36	O5	131(17)
P	W	C37	O6	42(20)
P	O1	C3	C2	-29.7(6)
P	O1	C3	C8	-156.6(5)
P	C1	C2	C3	-3.1(7)
P	C1	C2	C7	-177.5(6)
P	C1	C4	C5	179.4(6)
P	C14	C15	C16	-43.9(8)
P	C14	C15	C20	138.3(6)
C15	C14	C21	C26	-119.7(8)
C15	C14	C27	C28	2.2(10)
C15	C14	C27	C32	177.2(6)
C15	C16	C17	C18	1.9(11)
C16	C15	C20	C19	2.1(11)
C16	C17	C18	C19	-0.6(12)
C17	C18	C19	C20	0.0(12)
C18	C19	C20	C15	-0.8(12)
C20	C15	C16	C17	-2.6(11)
C21	C14	C15	C16	-158.9(6)
C21	C14	C15	C20	23.3(10)
C21	C14	C27	C28	-121.9(7)
C21	C14	C27	C32	53.1(8)
C21	C22	C23	C24	-0.9(12)
C22	C21	C26	C25	0.8(11)
C22	C23	C24	C25	1.8(13)
C23	C24	C25	C26	-1.4(13)
C24	C25	C26	C21	0.0(12)

P	C14	C21	C22	-56.1(8)
P	C14	C21	C26	125.3(6)
P	C14	C27	C28	120.1(6)
P	C14	C27	C32	-65.0(8)
O1	P	C1	C2	-12.6(5)
O1	P	C1	C4	169.9(7)
O1	P	C14	C15	85.5(5)
O1	P	C14	C21	-156.9(5)
O1	P	C14	C27	-35.4(5)
O1	C3	C8	C9	52.1(9)
O1	C3	C8	C13	-128.3(7)
C1	P	O1	C3	25.6(5)
C1	P	C14	C15	-177.0(5)
C1	P	C14	C21	-59.3(6)
C1	P	C14	C27	62.1(6)
C1	C2	C3	O1	19.7(8)
C1	C2	C3	C8	141.3(6)
C1	C2	C7	C6	-3.6(11)
C1	C4	C5	C6	-1.4(11)
C2	C1	C4	C5	2.2(11)
C2	C3	C8	C9	-66.9(9)
C2	C3	C8	C13	112.7(8)
C3	C2	C7	C6	-177.3(6)
C3	C8	C9	C10	179.7(7)
C3	C8	C13	C12	179.3(7)
C4	C1	C2	C3	174.8(6)
C4	C1	C2	C7	0.3(11)
C4	C5	C6	C7	-2.0(11)
C5	C6	C7	C2	4.4(11)
C7	C2	C3	O1	-166.2(7)
C7	C2	C3	C8	-44.6(10)
C8	C9	C10	C11	0.7(12)
C9	C8	C13	C12	-1.1(12)
C9	C10	C11	C12	-0.5(12)
C10	C11	C12	C13	-0.5(13)
C11	C12	C13	C8	1.3(13)
C13	C8	C9	C10	0.1(11)
C14	P	O1	C3	134.1(5)
C14	P	C1	C2	-116.7(5)
C14	P	C1	C4	65.8(8)
C14	C15	C16	C17	179.5(7)
C14	C15	C20	C19	179.9(7)
C14	C21	C22	C23	-179.1(6)
C14	C21	C26	C25	179.6(7)
C14	C27	C28	C29	175.1(7)
C14	C27	C32	C31	-174.5(7)
C26	C21	C22	C23	-0.4(11)
C27	C14	C15	C16	76.1(8)
C27	C14	C15	C20	-101.7(8)
C27	C14	C21	C22	-176.3(6)
C27	C14	C21	C26	5.0(9)
C27	C28	C29	C30	-0.7(13)
C28	C27	C32	C31	0.7(11)
C28	C29	C30	C31	0.9(12)
C29	C30	C31	C32	-0.3(12)
C30	C31	C32	C27	-0.5(12)
C32	C27	C28	C29	-0.2(11)
C33	W	P	O1	34(3)
C33	W	P	C1	-69(3)
C33	W	P	C14	157(3)
C33	W	C34	O3	10(8)
C33	W	C35	O4	109(15)
C33	W	C36	O5	-51(17)
C33	W	C37	O6	-134(20)
C34	W	P	O1	-119.9(3)
C34	W	P	C1	137.4(3)
C34	W	P	C14	2.8(4)
C34	W	C33	O2	-74(52)
C34	W	C35	O4	-164(15)
C34	W	C36	O5	-14(20)
C34	W	C37	O6	139(20)
C35	W	P	O1	150.2(3)
C35	W	P	C1	47.4(3)
C35	W	P	C14	-87.2(3)
C35	W	C33	O2	15(52)
C35	W	C34	O3	-82(8)
C35	W	C36	O5	40(17)
C35	W	C37	O6	8(25)
C36	W	P	O1	63.0(3)
C36	W	P	C1	-39.7(3)
C36	W	P	C14	-174.3(4)
C36	W	C33	O2	103(52)
C36	W	C34	O3	-28(11)
C36	W	C35	O4	20(15)
C36	W	C37	O6	-45(20)
C37	W	P	O1	-28.1(3)
C37	W	P	C1	-130.9(3)
C37	W	P	C14	94.6(3)
C37	W	C33	O2	-166(52)
C37	W	C34	O3	101(8)
C37	W	C35	O4	-34(19)
C37	W	C36	O5	-142(17)

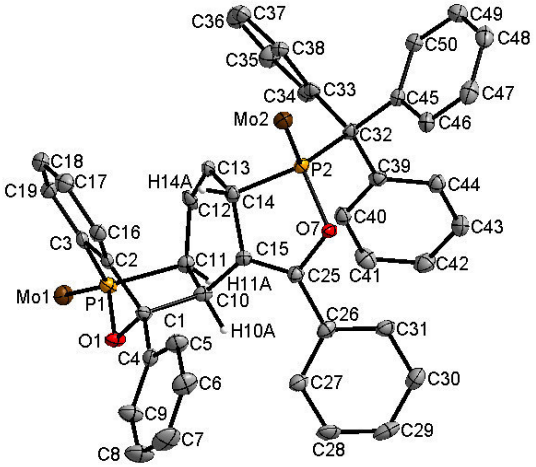

Table 1 Crystal data and structure refinement for 10b*THF.

Identification code	GSTR280
Empirical formula	$C_{59}H_{44}Mo_2O_{13}P_2$
Formula weight	1214.76
Temperature/K	123(2)
Crystal system	monoclinic
Space group	$P2_1/c$
a/Å	13.286(8)
b/Å	18.409(9)
c/Å	23.093(10)
α/°	90.00
β/°	103.99(4)
γ/°	90.00
Volume/Å^3	5481(5)
Z	4
ρ_{calc}g/cm^3	1.472
μ/mm^{-1}	0.580
F(000)	2464
Crystal size/mm^3	0.36 × 0.06 × 0.03
Tmin; Tmax	0.8183; 0.9828
Radiation	MoKα (λ = 0.71073)
2Θ range for data collection/°	2.94 to 28.00
Completeness to theta	0.999
Index ranges	-17 ≤ h ≤ 17, -24 ≤ k ≤ 23, -30 ≤ l ≤ 30
Reflections collected	51069
Independent reflections	13213 [R_{int} = 0.1524]
Data/restraints/parameters	13213/37/687
Goodness-of-fit on F^2	0.789
Final R indexes [I>=2σ (I)]	R_1 = 0.0492, wR_2 = 0.0858
Final R indexes [all data]	R_1 = 0.1109, wR_2 = 0.0985
Largest diff. peak/hole / e Å^{-3}	0.893/-1.233

Table 2 Bond Lengths for 10b*THF.

Atom	Atom	Length/Å	Atom	Atom	Length/Å
C1	O1	1.468(4)	C1	C4	1.502(6)
C1	C2	1.525(6)	C1	C10	1.602(5)
C2	C16	1.379(6)	C2	C3	1.392(6)
C3	C19	1.394(6)	C3	P1	1.797(4)
C4	C5	1.390(6)	C4	C9	1.392(6)
C5	C6	1.395(6)	C6	C7	1.380(7)
C7	C8	1.384(7)	C8	C9	1.377(7)
C10	C15	1.502(5)	C10	C11	1.545(6)
C11	C12	1.494(6)	C11	P1	1.890(4)
C12	C13	1.326(6)	C13	C14	1.502(5)
C14	C15	1.526(5)	C14	P2	1.889(4)
C15	C25	1.347(5)	C16	C17	1.400(6)
C17	C18	1.380(6)	C18	C19	1.380(6)
C20	O2	1.132(6)	C20	Mo1	2.038(5)
C21	O3	1.143(6)	C21	Mo1	2.049(5)
C22	O4	1.141(5)	C22	Mo1	2.046(5)
C23	O5	1.140(6)	C23	Mo1	2.045(5)
C24	O6	1.142(6)	C24	Mo1	2.064(5)
C25	O7	1.399(5)	C25	C26	1.484(6)
C26	C31	1.395(6)	C26	C27	1.403(5)
C27	C28	1.378(6)	C28	C29	1.370(7)
C29	C30	1.390(6)	C30	C31	1.385(6)
C32	C39	1.531(5)	C32	C33	1.539(5)
C32	C45	1.543(5)	C32	P2	1.960(4)
C33	C34	1.385(6)	C33	C38	1.390(6)
C34	C35	1.396(6)	C35	C36	1.387(7)
C36	C37	1.375(6)	C37	C38	1.396(6)
C39	C44	1.389(6)	C39	C40	1.407(5)
C40	C41	1.389(6)	C41	C42	1.382(6)
C42	C43	1.383(6)	C43	C44	1.391(6)
C45	C50	1.397(6)	C45	C46	1.400(6)
C46	C47	1.385(6)	C47	C48	1.399(6)
C48	C49	1.370(7)	C49	C50	1.399(6)
C51	O8	1.150(5)	C51	Mo2	1.988(5)
C52	O9	1.140(5)	C52	Mo2	2.047(5)
C53	O10	1.140(5)	C53	Mo2	2.065(5)
C54	O11	1.130(6)	C54	Mo2	2.067(5)
C55	O12	1.145(5)	C55	Mo2	2.036(5)
C56	C57	1.484(12)	C57	O13	1.400(8)
C58	O13	1.424(8)	C58	C59	1.461(10)
Mo1	P1	2.4258(15)	Mo2	P2	2.5259(18)
O1	P1	1.646(3)	O7	P2	1.654(3)

Table 3 Bond Angles for 10b*THF.

Atom	Atom	Atom	Angle/˚	Atom	Atom	Atom	Angle/˚
O1	C1	C4	109.0(3)	O1	C1	C2	103.6(3)
C4	C1	C2	117.8(3)	O1	C1	C10	100.2(3)
C4	C1	C10	114.4(3)	C2	C1	C10	109.8(3)
C16	C2	C3	120.0(4)	C16	C2	C1	129.4(4)
C3	C2	C1	110.5(3)	C2	C3	C19	121.2(4)
C2	C3	P1	105.7(3)	C19	C3	P1	132.9(3)
C5	C4	C9	117.8(4)	C5	C4	C1	120.3(4)
C9	C4	C1	121.9(4)	C4	C5	C6	121.7(4)
C7	C6	C5	119.3(4)	C6	C7	C8	119.4(4)
C9	C8	C7	121.1(4)	C8	C9	C4	120.7(4)
C15	C10	C11	112.1(3)	C15	C10	C1	117.9(3)
C11	C10	C1	105.5(3)	C12	C11	C10	116.5(3)
C12	C11	P1	108.7(3)	C10	C11	P1	102.4(2)
C13	C12	C11	124.3(4)	C12	C13	C14	122.9(4)
C13	C14	C15	112.7(3)	C13	C14	P2	119.9(3)
C15	C14	P2	103.0(3)	C25	C15	C10	126.9(4)
C25	C15	C14	113.5(3)	C10	C15	C14	118.5(3)
C2	C16	C17	118.8(4)	C18	C17	C16	120.9(4)
C19	C18	C17	120.7(4)	C18	C19	C3	118.4(4)
O2	C20	Mo1	179.5(6)	O3	C21	Mo1	177.2(4)
O4	C22	Mo1	177.8(4)	O5	C23	Mo1	178.1(4)
O6	C24	Mo1	176.4(5)	C15	C25	O7	116.2(4)
C15	C25	C26	130.5(4)	O7	C25	C26	112.9(3)
C31	C26	C27	119.0(4)	C31	C26	C25	118.1(4)
C27	C26	C25	122.8(4)	C28	C27	C26	119.9(4)
C29	C28	C27	120.8(4)	C28	C29	C30	120.0(4)
C31	C30	C29	119.9(4)	C30	C31	C26	120.2(4)
C39	C32	C33	113.2(3)	C39	C32	C45	110.4(3)
C33	C32	C45	110.3(3)	C39	C32	P2	110.3(3)
C33	C32	P2	106.0(3)	C45	C32	P2	106.4(3)
C34	C33	C38	117.9(4)	C34	C33	C32	122.6(4)
C38	C33	C32	119.6(4)	C33	C34	C35	121.2(4)
C36	C35	C34	119.9(4)	C37	C36	C35	119.5(4)
C36	C37	C38	120.2(4)	C33	C38	C37	121.1(4)
C44	C39	C40	117.5(4)	C44	C39	C32	122.5(3)
C40	C39	C32	120.0(3)	C41	C40	C39	121.6(4)
C42	C41	C40	119.4(4)	C41	C42	C43	120.2(4)
C42	C43	C44	120.1(4)	C39	C44	C43	121.2(4)
C50	C45	C46	118.2(4)	C50	C45	C32	121.4(4)
C46	C45	C32	120.3(3)	C47	C46	C45	120.8(4)
C46	C47	C48	120.4(4)	C49	C48	C47	119.2(4)
C48	C49	C50	120.9(4)	C45	C50	C49	120.5(4)
O8	C51	Mo2	176.9(5)	O9	C52	Mo2	178.5(4)
O10	C53	Mo2	176.7(4)	O11	C54	Mo2	177.7(4)

O12	C55	Mo2	175.2(4)	O13	C57	C56	110.4(7)
O13	C58	C59	110.6(7)	C20	Mo1	C23	90.1(2)
C20	Mo1	C22	91.4(2)	C23	Mo1	C22	89.57(19)
C20	Mo1	C21	90.3(2)	C23	Mo1	C21	179.3(2)
C22	Mo1	C21	91.02(18)	C20	Mo1	C24	92.5(2)
C23	Mo1	C24	92.4(2)	C22	Mo1	C24	175.62(18)
C21	Mo1	C24	87.0(2)	C20	Mo1	P1	177.19(16)
C23	Mo1	P1	87.51(13)	C22	Mo1	P1	87.08(13)
C21	Mo1	P1	92.14(14)	C24	Mo1	P1	89.11(14)
C51	Mo2	C55	86.7(2)	C51	Mo2	C52	89.1(2)
C55	Mo2	C52	90.0(2)	C51	Mo2	C53	88.33(19)
C55	Mo2	C53	174.91(18)	C52	Mo2	C53	90.94(18)
C51	Mo2	C54	89.2(2)	C55	Mo2	C54	88.7(2)
C52	Mo2	C54	177.96(19)	C53	Mo2	C54	90.13(18)
C51	Mo2	P2	173.66(14)	C55	Mo2	P2	87.61(14)
C52	Mo2	P2	88.17(13)	C53	Mo2	P2	97.42(13)
C54	Mo2	P2	93.42(13)	C1	O1	P1	102.6(2)
C25	O7	P2	113.7(2)	C57	O13	C58	115.6(6)
O1	P1	C3	91.49(17)	O1	P1	C11	92.50(16)
C3	P1	C11	95.13(18)	O1	P1	Mo1	122.33(10)
C3	P1	Mo1	124.95(14)	C11	P1	Mo1	121.89(13)
O7	P2	C14	93.15(16)	O7	P2	C32	102.64(16)
C14	P2	C32	111.90(17)	O7	P2	Mo2	110.79(11)
C14	P2	Mo2	110.02(13)	C32	P2	Mo2	123.72(12)

Table 4 Torsion Angles for 10b*THF.

A	B	C	D	Angle/˚	A	B	C	D	Angle/˚
O1	C1	C2	C16	151.5(4)	C4	C1	C2	C16	31.1(5)
C10	C1	C2	C16	-102.2(4)	O1	C1	C2	C3	-30.6(4)
C4	C1	C2	C3	-151.0(3)	C10	C1	C2	C3	75.7(4)
C16	C2	C3	C19	1.2(6)	C1	C2	C3	C19	-177.0(3)
C16	C2	C3	P1	176.8(3)	C1	C2	C3	P1	-1.4(4)
O1	C1	C4	C5	179.1(4)	C2	C1	C4	C5	-63.4(5)
C10	C1	C4	C5	67.8(5)	O1	C1	C4	C9	0.2(5)
C2	C1	C4	C9	117.7(4)	C10	C1	C4	C9	-111.0(4)
C9	C4	C5	C6	0.4(7)	C1	C4	C5	C6	-178.6(4)
C4	C5	C6	C7	0.9(7)	C5	C6	C7	C8	-1.1(7)
C6	C7	C8	C9	0.2(8)	C7	C8	C9	C4	1.1(8)
C5	C4	C9	C8	-1.3(7)	C1	C4	C9	C8	177.6(4)
O1	C1	C10	C15	173.1(3)	C4	C1	C10	C15	-70.4(4)
C2	C1	C10	C15	64.6(5)	O1	C1	C10	C11	47.0(3)
C4	C1	C10	C11	163.5(3)	C2	C1	C10	C11	-61.5(4)
C15	C10	C11	C12	-24.8(5)	C1	C10	C11	C12	104.9(4)
C15	C10	C11	P1	-143.3(3)	C1	C10	C11	P1	-13.6(3)
C10	C11	C12	C13	1.8(6)	P1	C11	C12	C13	116.8(4)

C11	C12	C13	C14	5.5(7)	C12	C13	C14	C15	11.0(6)
C12	C13	C14	P2	132.4(4)	C11	C10	C15	C25	-124.5(4)
C1	C10	C15	C25	112.7(5)	C11	C10	C15	C14	42.6(5)
C1	C10	C15	C14	-80.2(5)	C13	C14	C15	C25	132.7(4)
P2	C14	C15	C25	2.1(4)	C13	C14	C15	C10	-36.1(5)
P2	C14	C15	C10	-166.7(3)	C3	C2	C16	C17	-1.4(6)
C1	C2	C16	C17	176.3(4)	C2	C16	C17	C18	0.6(6)
C16	C17	C18	C19	0.4(6)	C17	C18	C19	C3	-0.7(6)
C2	C3	C19	C18	-0.1(6)	P1	C3	C19	C18	-174.3(3)
C10	C15	C25	O7	170.5(3)	C14	C15	C25	O7	2.8(5)
C10	C15	C25	C26	-2.4(7)	C14	C15	C25	C26	-170.1(4)
C15	C25	C26	C31	140.2(5)	O7	C25	C26	C31	-32.8(5)
C15	C25	C26	C27	-36.1(7)	O7	C25	C26	C27	150.9(4)
C31	C26	C27	C28	-3.3(6)	C25	C26	C27	C28	173.0(4)
C26	C27	C28	C29	2.0(7)	C27	C28	C29	C30	0.4(7)
C28	C29	C30	C31	-1.6(7)	C29	C30	C31	C26	0.3(7)
C27	C26	C31	C30	2.1(6)	C25	C26	C31	C30	-174.3(4)
C39	C32	C33	C34	-6.7(5)	C45	C32	C33	C34	117.5(4)
P2	C32	C33	C34	-127.7(3)	C39	C32	C33	C38	173.8(3)
C45	C32	C33	C38	-62.0(4)	P2	C32	C33	C38	52.8(4)
C38	C33	C34	C35	-3.6(6)	C32	C33	C34	C35	176.9(4)
C33	C34	C35	C36	0.2(7)	C34	C35	C36	C37	2.1(6)
C35	C36	C37	C38	-0.9(6)	C34	C33	C38	C37	4.8(6)
C32	C33	C38	C37	-175.7(3)	C36	C37	C38	C33	-2.6(6)
C33	C32	C39	C44	118.2(4)	C45	C32	C39	C44	-6.1(5)
P2	C32	C39	C44	-123.3(4)	C33	C32	C39	C40	-58.4(5)
C45	C32	C39	C40	177.3(4)	P2	C32	C39	C40	60.1(4)
C44	C39	C40	C41	1.8(6)	C32	C39	C40	C41	178.5(4)
C39	C40	C41	C42	-1.0(7)	C40	C41	C42	C43	-0.4(7)
C41	C42	C43	C44	0.9(7)	C40	C39	C44	C43	-1.3(6)
C32	C39	C44	C43	-177.9(4)	C42	C43	C44	C39	-0.1(7)
C39	C32	C45	C50	103.4(4)	C33	C32	C45	C50	-22.5(5)
P2	C32	C45	C50	-136.9(3)	C39	C32	C45	C46	-73.2(4)
C33	C32	C45	C46	160.9(4)	P2	C32	C45	C46	46.5(4)
C50	C45	C46	C47	2.4(6)	C32	C45	C46	C47	179.1(4)
C45	C46	C47	C48	-0.5(6)	C46	C47	C48	C49	-1.9(6)
C47	C48	C49	C50	2.4(7)	C46	C45	C50	C49	-1.9(6)
C32	C45	C50	C49	-178.6(4)	C48	C49	C50	C45	-0.5(6)
O2	C20	Mo1	C23	-176(100)	O2	C20	Mo1	C22	-87(81)
O2	C20	Mo1	C21	4(81)	O2	C20	Mo1	C24	91(81)
O2	C20	Mo1	P1	-144(79)	O5	C23	Mo1	C20	160(14)
O5	C23	Mo1	C22	69(14)	O5	C23	Mo1	C21	-78(22)
O5	C23	Mo1	C24	-107(14)	O5	C23	Mo1	P1	-18(14)
O4	C22	Mo1	C20	-160(11)	O4	C22	Mo1	C23	-70(11)
O4	C22	Mo1	C21	110(11)	O4	C22	Mo1	P1	18(11)
O4	C22	Mo1	C24	47(12)	O3	C21	Mo1	C23	-91(18)

O3	C21	Mo1	C20	30(9)
O3	C21	Mo1	C22	122(9)
O3	C21	Mo1	P1	-151(9)
O6	C24	Mo1	C23	134(7)
O6	C24	Mo1	C21	-45(7)
O8	C51	Mo2	C55	-58(10)
O8	C51	Mo2	C54	-147(10)
O12	C55	Mo2	C51	-10(6)
O12	C55	Mo2	C53	2(7)
O12	C55	Mo2	P2	173(6)
O9	C52	Mo2	C55	46(18)
O9	C52	Mo2	C54	-7(21)
O10	C53	Mo2	C51	-21(7)
O10	C53	Mo2	C52	68(7)
O10	C53	Mo2	P2	156(7)
O11	C54	Mo2	C55	-85(11)
O11	C54	Mo2	C53	90(11)
C4	C1	O1	P1	176.7(3)
C10	C1	O1	P1	-62.9(3)
C26	C25	O7	P2	167.0(3)
C59	C58	O13	C57	175.4(6)
C1	O1	P1	C11	49.2(3)
C2	C3	P1	O1	28.2(3)
C2	C3	P1	C11	-64.4(3)
C2	C3	P1	Mo1	160.4(2)
C12	C11	P1	O1	-143.1(3)
C12	C11	P1	C3	-51.4(3)
C12	C11	P1	Mo1	85.8(3)
C20	Mo1	P1	O1	-121(3)
C22	Mo1	P1	O1	-179.41(18)
C24	Mo1	P1	O1	2.73(19)
C23	Mo1	P1	C3	151.6(2)
C21	Mo1	P1	C3	-29.0(2)
C20	Mo1	P1	C11	-4(3)
C22	Mo1	P1	C11	-62.4(2)
C24	Mo1	P1	C11	119.8(2)
C25	O7	P2	C32	-106.4(3)
C13	C14	P2	O7	-131.1(3)
C13	C14	P2	C32	-26.1(4)
C13	C14	P2	Mo2	115.4(3)
C39	C32	P2	O7	24.8(3)
C45	C32	P2	O7	-94.9(3)
C33	C32	P2	C14	49.0(3)
C39	C32	P2	Mo2	150.7(2)
C45	C32	P2	Mo2	31.0(3)
C55	Mo2	P2	O7	-48.26(18)
O3	C21	Mo1	C24	-62(9)
O6	C24	Mo1	C20	-136(7)
O6	C24	Mo1	C22	17(9)
O6	C24	Mo1	P1	47(7)
O8	C51	Mo2	C52	32(10)
O8	C51	Mo2	C53	123(10)
O8	C51	Mo2	P2	-32(11)
O12	C55	Mo2	C52	-99(6)
O12	C55	Mo2	C54	80(6)
O9	C52	Mo2	C51	-40(18)
O9	C52	Mo2	C53	-129(18)
O9	C52	Mo2	P2	134(18)
O10	C53	Mo2	C55	-33(9)
O10	C53	Mo2	C54	-111(7)
O11	C54	Mo2	C51	1(11)
O11	C54	Mo2	C52	-32(14)
O11	C54	Mo2	P2	-173(100)
C2	C1	O1	P1	50.5(3)
C15	C25	O7	P2	-7.1(4)
C56	C57	O13	C58	179.0(6)
C1	O1	P1	C3	-46.0(2)
C1	O1	P1	Mo1	-179.99(18)
C19	C3	P1	O1	-156.9(4)
C19	C3	P1	C11	110.4(4)
C19	C3	P1	Mo1	-24.8(5)
C10	C11	P1	O1	-19.2(3)
C10	C11	P1	C3	72.5(3)
C10	C11	P1	Mo1	-150.35(19)
C23	Mo1	P1	O1	-89.71(19)
C21	Mo1	P1	O1	89.68(19)
C20	Mo1	P1	C3	120(3)
C22	Mo1	P1	C3	61.9(2)
C24	Mo1	P1	C3	-116.0(2)
C23	Mo1	P1	C11	27.3(2)
C21	Mo1	P1	C11	-153.3(2)
C25	O7	P2	C14	6.9(3)
C25	O7	P2	Mo2	119.7(2)
C15	C14	P2	O7	-5.0(3)
C15	C14	P2	C32	100.0(3)
C15	C14	P2	Mo2	-118.5(2)
C33	C32	P2	O7	147.7(2)
C39	C32	P2	C14	-73.9(3)
C45	C32	P2	C14	166.4(3)
C33	C32	P2	Mo2	-86.4(3)
C51	Mo2	P2	O7	-74.2(16)
C52	Mo2	P2	O7	-138.37(17)

C53	Mo2	P2	O7	130.92(16)	C54	Mo2	P2	O7	40.34(17)
C51	Mo2	P2	C14	27.4(16)	C55	Mo2	P2	C14	53.3(2)
C52	Mo2	P2	C14	-36.78(19)	C53	Mo2	P2	C14	-127.49(19)
C54	Mo2	P2	C14	141.93(19)	C51	Mo2	P2	C32	163.5(16)
C55	Mo2	P2	C32	-170.6(2)	C52	Mo2	P2	C32	99.3(2)
C53	Mo2	P2	C32	8.60(19)	C54	Mo2	P2	C32	-82.0(2)

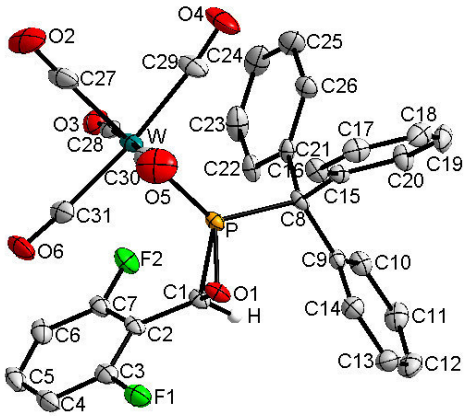

Table 1 Crystal data and structure refinement for 20*$CHCl_3$.

Identification code	GSTR305
Empirical formula	$C_{32}H_{20}Cl_3F_2O_6PW$
Formula weight	859.65
Temperature/K	123(2)
Crystal system	triclinic
Space group	P-1
a/Å	9.9709(8)
b/Å	10.8286(7)
c/Å	16.0930(15)
α/°	99.983(3)
β/°	98.899(3)
γ/°	109.619(2)
Volume/$Å^3$	1568.9(2)
Z	2
$\rho_{calc}g/cm^3$	1.820
μ/mm^{-1}	4.044
F(000)	836
Crystal size/mm^3	0.27 × 0.25 × 0.10
Tmin; Tmax	0.4081; 0.6879
Radiation	MoKα (λ = 0.71073)
2Θ range for data collection/°	2.64 to 27.00°
Completeness to theta	0.984
Index ranges	-12 ≤ h ≤ 11, -13 ≤ k ≤ 13, -20 ≤ l ≤ 20
Reflections collected	15563
Independent reflections	6741 [R_{int} = 0.0260]
Data/restraints/parameters	6741/0/443
Goodness-of-fit on F^2	1.058
Final R indexes [I>=2σ (I)]	R_1 = 0.0260, wR_2 = 0.0524
Final R indexes [all data]	R_1 = 0.0354, wR_2 = 0.0563
Largest diff. peak/hole / e $Å^{-3}$	1.517/-1.735

Table 2 Bond Lengths for 20*$CHCl_3$.

Atom	Atom	Length/Å	Atom	Atom	Length/Å
C1	O1	1.471(4)	C1	C2	1.492(4)
C1	P	1.793(3)	C2	C3	1.386(5)
C2	C7	1.389(5)	C3	F1	1.355(4)
C3	C4	1.379(5)	C4	C5	1.376(6)
C5	C6	1.389(5)	C6	C7	1.382(4)
C7	F2	1.356(4)	C8	C21	1.537(4)
C8	C15	1.543(4)	C8	C9	1.543(4)
C8	P	1.902(3)	C9	C10	1.392(5)
C9	C14	1.395(5)	C10	C11	1.402(5)
C11	C12	1.372(5)	C12	C13	1.394(5)
C13	C14	1.385(5)	C15	C16	1.379(5)
C15	C20	1.396(5)	C16	C17	1.399(4)
C17	C18	1.376(5)	C18	C19	1.390(5)
C19	C20	1.390(5)	C21	C26	1.394(4)
C21	C22	1.407(4)	C22	C23	1.389(5)
C23	C24	1.386(6)	C24	C25	1.377(5)
C25	C26	1.389(5)	C27	O2	1.125(5)
C27	W	2.025(4)	C28	O3	1.143(4)
C28	W	2.037(4)	C29	O4	1.130(4)
C29	W	2.059(4)	C30	O5	1.140(5)
C30	W	2.059(4)	C31	O6	1.139(4)
C31	W	2.041(4)	O1	P	1.663(2)
P	W	2.4783(8)	C32	Cl2	1.670(14)
C32	Cl1	1.749(7)	C32	Cl3	1.749(7)

Table 3 Bond Angles for 20*$CHCl_3$.

Atom	Atom	Atom	Angle/˚	Atom	Atom	Atom	Angle/˚
O1	C1	C2	116.3(3)	O1	C1	P	60.34(13)
C2	C1	P	124.6(2)	C3	C2	C7	115.2(3)
C3	C2	C1	123.8(3)	C7	C2	C1	120.7(3)
F1	C3	C4	118.3(3)	F1	C3	C2	118.5(3)
C4	C3	C2	123.2(3)	C5	C4	C3	119.0(3)
C4	C5	C6	120.9(3)	C7	C6	C5	117.6(3)
F2	C7	C6	118.2(3)	F2	C7	C2	117.6(3)
C6	C7	C2	124.1(3)	C21	C8	C15	113.5(2)
C21	C8	C9	113.4(3)	C15	C8	C9	105.6(2)
C21	C8	P	100.8(2)	C15	C8	P	111.5(2)
C9	C8	P	112.2(2)	C10	C9	C14	118.4(3)
C10	C9	C8	122.2(3)	C14	C9	C8	119.2(3)
C9	C10	C11	120.3(3)	C12	C11	C10	120.9(3)
C11	C12	C13	118.9(3)	C14	C13	C12	120.6(3)
C13	C14	C9	120.8(3)	C16	C15	C20	118.2(3)
C16	C15	C8	124.1(3)	C20	C15	C8	117.5(3)

C15	C16	C17	121.3(3)	C18	C17	C16	120.1(3)
C17	C18	C19	119.3(3)	C20	C19	C18	120.3(3)
C19	C20	C15	120.8(3)	C26	C21	C22	117.7(3)
C26	C21	C8	122.8(3)	C22	C21	C8	119.4(3)
C23	C22	C21	120.9(3)	C24	C23	C22	120.2(3)
C25	C24	C23	119.6(3)	C24	C25	C26	120.6(4)
C25	C26	C21	121.0(3)	O2	C27	W	177.3(3)
O3	C28	W	176.9(3)	O4	C29	W	173.5(3)
O5	C30	W	178.1(3)	O6	C31	W	176.1(3)
C1	O1	P	69.47(15)	O1	P	C1	50.19(13)
O1	P	C8	107.12(13)	C1	P	C8	105.44(14)
O1	P	W	119.63(9)	C1	P	W	125.55(11)
C8	P	W	125.30(10)	C27	W	C28	89.93(15)
C27	W	C31	88.30(14)	C28	W	C31	88.69(14)
C27	W	C29	85.04(15)	C28	W	C29	91.96(15)
C31	W	C29	173.31(14)	C27	W	C30	88.94(16)
C28	W	C30	177.35(15)	C31	W	C30	88.89(15)
C29	W	C30	90.32(15)	C27	W	P	178.75(13)
C28	W	P	88.89(9)	C31	W	P	92.08(9)
C29	W	P	94.59(10)	C30	W	P	92.26(11)
Cl2	C32	Cl1	105.9(6)	Cl2	C32	Cl3	120.0(6)
Cl1	C32	Cl3	110.5(4)				

Table 4 Torsion Angles for 20*$CHCl_3$.

A	B	C	D	Angle/˚	A	B	C	D	Angle/˚
O1	C1	C2	C3	-37.8(4)	P	C1	C2	C3	-108.5(3)
O1	C1	C2	C7	148.0(3)	P	C1	C2	C7	77.2(4)
C7	C2	C3	F1	178.9(3)	C1	C2	C3	F1	4.4(5)
C7	C2	C3	C4	-1.2(5)	C1	C2	C3	C4	-175.7(3)
F1	C3	C4	C5	-179.6(3)	C2	C3	C4	C5	0.5(5)
C3	C4	C5	C6	0.6(5)	C4	C5	C6	C7	-0.8(5)
C5	C6	C7	F2	179.0(3)	C5	C6	C7	C2	0.1(5)
C3	C2	C7	F2	-178.0(3)	C1	C2	C7	F2	-3.3(4)
C3	C2	C7	C6	0.9(5)	C1	C2	C7	C6	175.6(3)
C21	C8	C9	C10	4.4(4)	C15	C8	C9	C10	-120.5(3)
P	C8	C9	C10	117.9(3)	C21	C8	C9	C14	179.2(3)
C15	C8	C9	C14	54.3(4)	P	C8	C9	C14	-67.3(3)
C14	C9	C10	C11	2.4(5)	C8	C9	C10	C11	177.2(3)
C9	C10	C11	C12	-0.6(5)	C10	C11	C12	C13	-0.6(5)
C11	C12	C13	C14	-0.2(5)	C12	C13	C14	C9	2.0(5)
C10	C9	C14	C13	-3.1(5)	C8	C9	C14	C13	-178.1(3)
C21	C8	C15	C16	117.1(3)	C9	C8	C15	C16	-118.0(3)
P	C8	C15	C16	4.0(4)	C21	C8	C15	C20	-68.1(4)
C9	C8	C15	C20	56.8(4)	P	C8	C15	C20	178.9(2)
C20	C15	C16	C17	0.6(5)	C8	C15	C16	C17	175.4(3)

C15	C16	C17	C18	-1.1(5)
C17	C18	C19	C20	-0.6(5)
C16	C15	C20	C19	-0.1(5)
C15	C8	C21	C26	-3.0(4)
P	C8	C21	C26	116.3(3)
C9	C8	C21	C22	59.6(4)
C26	C21	C22	C23	0.9(5)
C21	C22	C23	C24	-0.9(5)
C23	C24	C25	C26	-0.3(6)
C22	C21	C26	C25	-0.6(5)
C2	C1	O1	P	-116.5(3)
C1	O1	P	W	113.37(15)
O1	C1	P	C8	99.63(17)
O1	C1	P	W	-101.28(15)
C21	C8	P	O1	158.80(17)
C9	C8	P	O1	37.8(2)
C15	C8	P	C1	-132.8(2)
C21	C8	P	W	-52.8(2)
C9	C8	P	W	-173.81(16)
O2	C27	W	C31	-153(9)
O2	C27	W	C30	118(9)
O3	C28	W	C27	-52(5)
O3	C28	W	C29	-137(5)
O3	C28	W	P	129(5)
O6	C31	W	C28	-94(5)
O6	C31	W	C30	85(5)
O4	C29	W	C27	9(3)
O4	C29	W	C31	4(4)
O4	C29	W	P	-172(3)
O5	C30	W	C28	-57(12)
O5	C30	W	C29	92(11)
O1	P	W	C27	-150(5)
C8	P	W	C27	65(5)
C1	P	W	C28	-71.07(17)
O1	P	W	C31	-42.51(14)
C8	P	W	C31	172.64(16)
C1	P	W	C29	-162.96(18)
O1	P	W	C30	46.46(14)
C8	P	W	C30	-98.39(16)
C16	C17	C18	C19	1.1(5)
C18	C19	C20	C15	0.0(5)
C8	C15	C20	C19	-175.2(3)
C9	C8	C21	C26	-123.5(3)
C15	C8	C21	C22	-179.9(3)
P	C8	C21	C22	-60.6(3)
C8	C21	C22	C23	177.9(3)
C22	C23	C24	C25	0.6(6)
C24	C25	C26	C21	0.3(6)
C8	C21	C26	C25	-177.5(3)
C1	O1	P	C8	-96.08(18)
C2	C1	P	O1	103.1(3)
C2	C1	P	C8	-157.2(3)
C2	C1	P	W	1.9(3)
C15	C8	P	O1	-80.4(2)
C21	C8	P	C1	106.4(2)
C9	C8	P	C1	-14.6(3)
C15	C8	P	W	68.0(2)
O2	C27	W	C28	-64(9)
O2	C27	W	C29	28(9)
O2	C27	W	P	-45(13)
O3	C28	W	C31	37(5)
O3	C28	W	C30	13(7)
O6	C31	W	C27	-4(5)
O6	C31	W	C29	2(6)
O6	C31	W	P	178(100)
O4	C29	W	C28	99(3)
O4	C29	W	C30	-80(3)
O5	C30	W	C27	7(11)
O5	C30	W	C31	-81(11)
O5	C30	W	P	-173(11)
C1	P	W	C27	-90(5)
O1	P	W	C28	-131.16(13)
C8	P	W	C28	84.00(15)
C1	P	W	C31	17.57(17)
O1	P	W	C29	136.96(14)
C8	P	W	C29	-7.88(17)
C1	P	W	C30	106.54(17)

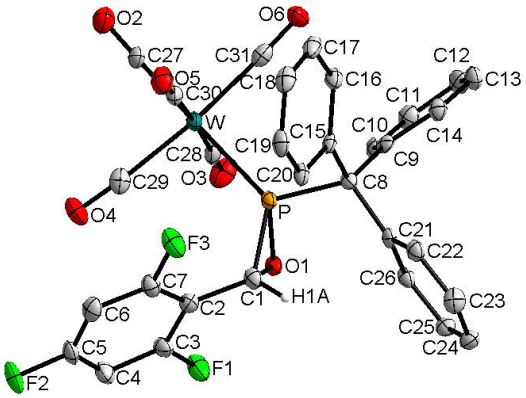

Table 1 Crystal data and structure refinement for 21.

Identification code	GSTR327
Empirical formula	$C_{31}H_{18}F_3O_6PW$
Formula weight	758.27
Temperature/K	123(2)
Crystal system	triclinic
Space group	P-1
a/Å	10.6618(3)
b/Å	16.0963(4)
c/Å	16.5683(5)
α/°	76.9465(16)
β/°	87.9808(16)
γ/°	86.8159(16)
Volume/Å^3	2764.88(13)
Z	4
ρ_{calc}g/cm^3	1.822
μ/mm^{-1}	4.301
F(000)	1472
Crystal size/mm^3	0.84 × 0.36 × 0.18
Tmin; Tmax	0.1228; 0.5115
Radiation	MoKα (λ = 0.71073)
2Θ range for data collection/°	2.56 to 26.00°
Completeness to theta	0.994
Index ranges	-12 ≤ h ≤ 13, -19 ≤ k ≤ 19, -18 ≤ l ≤ 20
Reflections collected	31025
Independent reflections	10799 [R_{int} = 0.0673]
Data/restraints/parameters	10799/7/757
Goodness-of-fit on F^2	1.005
Final R indexes [I>=2σ (I)]	R_1 = 0.0362, wR_2 = 0.0852
Final R indexes [all data]	R_1 = 0.0482, wR_2 = 0.0898
Largest diff. peak/hole / e Å^{-3}	1.991/-2.996

Table 2 Bond Lengths for 21.

Atom	Atom	Length/Å	Atom	Atom	Length/Å
C1	O1	1.479(5)	C1	C2	1.486(6)
C1	P1	1.786(5)	C2	C7	1.384(7)
C2	C3	1.390(6)	C3	F1	1.356(6)
C3	C4	1.381(7)	C4	C5	1.370(7)
C5	F2	1.352(5)	C5	C6	1.373(6)
C6	C7	1.377(6)	C7	F3	1.360(5)
C8	C21	1.539(7)	C8	C9	1.539(6)
C8	C15	1.546(6)	C8	P1	1.892(4)
C9	C10	1.379(6)	C9	C14	1.407(6)
C10	C11	1.394(6)	C11	C12	1.385(7)
C12	C13	1.379(7)	C13	C14	1.393(6)
C15	C16	1.395(6)	C15	C20	1.399(6)
C16	C17	1.396(7)	C17	C18	1.391(7)
C18	C19	1.378(7)	C19	C20	1.376(6)
C21	C22	1.399(7)	C21	C26	1.405(6)
C22	C23	1.381(7)	C23	C24	1.381(7)
C24	C25	1.389(7)	C25	C26	1.374(7)
C27	O2	1.158(6)	C27	W1	1.992(5)
C28	O3	1.138(6)	C28	W1	2.056(5)
C29	O4	1.137(6)	C29	W1	2.050(5)
C30	O5	1.132(6)	C30	W1	2.061(5)
C31	O6	1.143(6)	C31	W1	2.044(5)
O1	P1	1.663(3)	P1	W1	2.4656(13)

Table 3 Bond Angles for 21.

Atom	Atom	Atom	Angle/˚	Atom	Atom	Atom	Angle/˚
O1	C1	C2	116.1(4)	O1	C1	P1	60.4(2)
C2	C1	P1	122.7(4)	C7	C2	C3	114.4(4)
C7	C2	C1	122.3(4)	C3	C2	C1	123.2(4)
F1	C3	C4	117.7(4)	F1	C3	C2	118.2(4)
C4	C3	C2	124.0(5)	C5	C4	C3	116.9(4)
F2	C5	C4	117.9(4)	F2	C5	C6	118.7(4)
C4	C5	C6	123.4(4)	C5	C6	C7	116.3(4)
F3	C7	C6	118.0(4)	F3	C7	C2	117.0(4)
C6	C7	C2	125.0(4)	C21	C8	C9	105.4(4)
C21	C8	C15	114.1(4)	C9	C8	C15	115.3(3)
C21	C8	P1	113.8(3)	C9	C8	P1	109.7(3)
C15	C8	P1	98.6(3)	C10	C9	C14	118.4(4)
C10	C9	C8	122.6(4)	C14	C9	C8	118.7(4)
C9	C10	C11	121.2(4)	C12	C11	C10	120.0(4)
C13	C12	C11	119.7(4)	C12	C13	C14	120.5(4)
C13	C14	C9	120.2(4)	C16	C15	C20	117.9(4)
C16	C15	C8	123.0(4)	C20	C15	C8	118.9(4)

C15	C16	C17	120.3(5)	C18	C17	C16	120.8(5)
C19	C18	C17	118.8(4)	C20	C19	C18	120.8(5)
C19	C20	C15	121.4(4)	C22	C21	C26	117.0(4)
C22	C21	C8	124.2(4)	C26	C21	C8	118.5(4)
C23	C22	C21	121.2(4)	C22	C23	C24	120.9(5)
C23	C24	C25	118.6(5)	C26	C25	C24	120.8(4)
C25	C26	C21	121.4(4)	O2	C27	W1	179.3(4)
O3	C28	W1	178.2(4)	O4	C29	W1	175.8(5)
O5	C30	W1	178.1(4)	O6	C31	W1	176.2(4)
C1	O1	P1	69.0(2)	O1	P1	C8	108.58(19)
O1	P1	C1	50.62(17)	O1	P1	W1	117.36(13)
C1	P1	C8	106.6(2)	C8	P1	W1	123.18(15)
C1	P1	W1	127.83(17)	C27	W1	C29	87.57(19)
C27	W1	C31	86.59(19)	C27	W1	C28	90.45(19)
C31	W1	C29	174.2(2)	C29	W1	C28	87.69(18)
C31	W1	C28	92.12(19)	C31	W1	C30	90.82(18)
C27	W1	C30	92.10(19)	C28	W1	C30	176.22(17)
C29	W1	C30	89.62(18)	C31	W1	P1	91.94(14)
C27	W1	P1	175.87(14)	C28	W1	P1	85.75(14)
C29	W1	P1	93.87(15)	C30	W1	P1	91.78(14)

Table 4 Torsion Angles for 21.

A	B	C	D	Angle/˚	A	B	C	D	Angle/˚
O1	C1	C2	C7	-142.8(5)	P1	C1	C2	C7	-72.6(6)
O1	C1	C2	C3	40.8(7)	P1	C1	C2	C3	110.9(5)
C7	C2	C3	F1	-178.2(4)	C1	C2	C3	F1	-1.5(7)
C7	C2	C3	C4	0.2(8)	C1	C2	C3	C4	176.9(5)
F1	C3	C4	C5	178.4(5)	C2	C3	C4	C5	0.0(8)
C3	C4	C5	F2	-179.1(5)	C3	C4	C5	C6	-0.3(8)
F2	C5	C6	C7	179.1(4)	C4	C5	C6	C7	0.4(8)
C5	C6	C7	F3	179.9(4)	C5	C6	C7	C2	-0.2(8)
C3	C2	C7	F3	179.8(4)	C1	C2	C7	F3	3.1(7)
C3	C2	C7	C6	-0.1(8)	C1	C2	C7	C6	-176.8(5)
C21	C8	C9	C10	97.7(5)	C15	C8	C9	C10	-135.5(5)
P1	C8	C9	C10	-25.2(6)	C21	C8	C9	C14	-75.3(5)
C15	C8	C9	C14	51.5(6)	P1	C8	C9	C14	161.7(3)
C14	C9	C10	C11	-3.3(7)	C8	C9	C10	C11	-176.4(5)
C9	C10	C11	C12	1.0(8)	C10	C11	C12	C13	0.9(8)
C11	C12	C13	C14	-0.4(8)	C12	C13	C14	C9	-1.9(8)
C10	C9	C14	C13	3.7(7)	C8	C9	C14	C13	177.1(4)
C21	C8	C15	C16	133.5(4)	C9	C8	C15	C16	11.2(6)
P1	C8	C15	C16	-105.5(4)	C21	C8	C15	C20	-51.7(5)
C9	C8	C15	C20	-174.0(4)	P1	C8	C15	C20	69.3(5)
C20	C15	C16	C17	1.7(7)	C8	C15	C16	C17	176.6(4)
C15	C16	C17	C18	-0.3(8)	C16	C17	C18	C19	-0.5(8)

C17	C18	C19	C20	-0.2(8)
C16	C15	C20	C19	-2.5(7)
C9	C8	C21	C22	117.5(4)
P1	C8	C21	C22	-122.3(4)
C15	C8	C21	C26	176.0(4)
C26	C21	C22	C23	-1.5(6)
C21	C22	C23	C24	0.1(7)
C23	C24	C25	C26	-2.0(7)
C22	C21	C26	C25	1.2(6)
C2	C1	O1	P1	114.5(4)
C1	O1	P1	C8	96.6(3)
C2	C1	P1	O1	-103.7(4)
C2	C1	P1	C8	155.7(4)
C2	C1	P1	W1	-7.0(5)
C9	C8	P1	O1	85.5(3)
C21	C8	P1	C1	20.9(4)
C15	C8	P1	C1	-100.3(3)
C9	C8	P1	W1	-57.6(3)
O2	C27	W1	C31	35(33)
O2	C27	W1	C28	-57(33)
O2	C27	W1	P1	-34(34)
O6	C31	W1	C29	-16(8)
O6	C31	W1	C30	-110(7)
O4	C29	W1	C27	3(6)
O4	C29	W1	C28	-88(6)
O4	C29	W1	P1	-173(6)
O3	C28	W1	C31	120(14)
O3	C28	W1	C30	-21(15)
O5	C30	W1	C27	41(13)
O5	C30	W1	C29	-47(13)
O5	C30	W1	P1	-140(13)
C1	P1	W1	C27	-114.6(18)
O1	P1	W1	C31	-123.90(18)
C8	P1	W1	C31	16.2(2)
C1	P1	W1	C29	-4.4(2)
O1	P1	W1	C28	-31.92(18)
C8	P1	W1	C28	108.2(2)
C1	P1	W1	C30	85.4(2)

C18	C19	C20	C15	1.8(8)
C8	C15	C20	C19	-177.5(4)
C15	C8	C21	C22	-10.1(6)
C9	C8	C21	C26	-56.4(5)
P1	C8	C21	C26	63.8(5)
C8	C21	C22	C23	-175.5(4)
C22	C23	C24	C25	1.6(7)
C24	C25	C26	C21	0.6(6)
C8	C21	C26	C25	175.5(4)
C1	O1	P1	W1	-118.0(2)
O1	C1	P1	C8	-100.7(2)
O1	C1	P1	W1	96.6(2)
C21	C8	P1	O1	-32.4(4)
C15	C8	P1	O1	-153.6(3)
C9	C8	P1	C1	138.7(3)
C21	C8	P1	W1	-175.4(2)
C15	C8	P1	W1	63.4(3)
O2	C27	W1	C29	-145(33)
O2	C27	W1	C30	126(33)
O6	C31	W1	C27	-18(7)
O6	C31	W1	C28	72(7)
O6	C31	W1	P1	158(7)
O4	C29	W1	C31	1(7)
O4	C29	W1	C30	95(6)
O3	C28	W1	C27	-153(14)
O3	C28	W1	C29	-65(14)
O3	C28	W1	P1	29(14)
O5	C30	W1	C31	128(13)
O5	C30	W1	C28	-91(13)
O1	P1	W1	C27	-54.8(18)
C8	P1	W1	C27	85.3(18)
C1	P1	W1	C31	176.3(2)
O1	P1	W1	C29	55.47(18)
C8	P1	W1	C29	-164.4(2)
C1	P1	W1	C28	-91.7(2)
O1	P1	W1	C30	145.21(18)
C8	P1	W1	C30	-74.7(2)

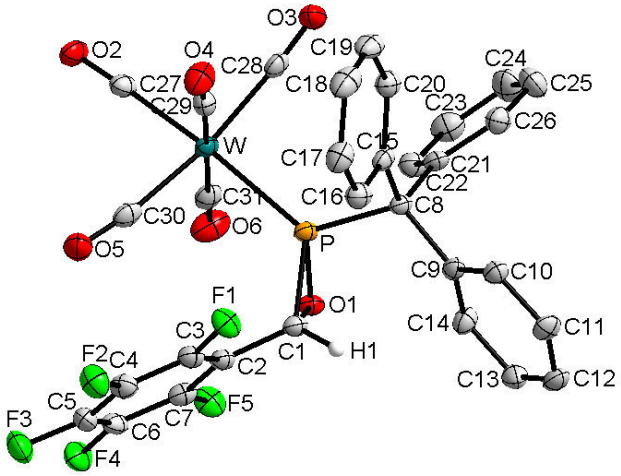

Table 1 Crystal data and structure refinement for 22.

Identification code	GSTR359
Empirical formula	$C_{31}H_{16}F_5O_6PW$
Formula weight	794.01
Temperature/K	123.15
Crystal system	monoclinic
Space group	C2/c
a/Å	36.0465(10)
b/Å	9.5603(3)
c/Å	16.5305(4)
α/°	90.00
β/°	93.8297(17)
γ/°	90.00
Volume/Å^3	5683.9(3)
Z	8
ρ_{calc}mg/mm^3	1.856
μ/mm^{-1}	4.198
F(000)	3072.0
Crystal size/mm^3	0.16 × 0.12 × 0.04
Radiation	MoKα (λ = 0.71073)
2Θ range for data collection	4.94 to 56°
Index ranges	-47 ≤ h ≤ 47, -12 ≤ k ≤ 12, -21 ≤ l ≤ 21
Reflections collected	50383
Independent reflections	6848 [R_{int} = 0.0952, R_{sigma} = 0.0556]
Data/restraints/parameters	6848/0/397
Goodness-of-fit on F^2	1.024
Final R indexes [I>=2σ (I)]	R_1 = 0.0378, wR_2 = 0.0857
Final R indexes [all data]	R_1 = 0.0581, wR_2 = 0.0931
Largest diff. peak/hole / e Å^{-3}	3.27/-2.47

Table 2 Bond Lengths for 22.

Atom	Atom	Length/Å	Atom	Atom	Length/Å
W	P	2.4630(11)	C4	C5	1.375(6)
W	C27	2.012(4)	C5	C6	1.380(6)
W	C28	2.054(5)	C6	C7	1.376(6)
W	C29	2.046(5)	C8	C9	1.553(5)
W	C30	2.034(5)	C8	C15	1.541(6)
W	C31	2.046(5)	C8	C21	1.551(5)
P	O1	1.669(3)	C9	C10	1.389(6)
P	C1	1.793(4)	C9	C14	1.393(6)
P	C8	1.881(4)	C10	C11	1.398(6)
F1	C3	1.345(5)	C11	C12	1.370(6)
F2	C4	1.347(5)	C12	C13	1.381(6)
F3	C5	1.333(5)	C13	C14	1.388(6)
F4	C6	1.337(5)	C15	C16	1.393(6)
F5	C7	1.343(5)	C15	C20	1.399(5)
O1	C1	1.460(5)	C16	C17	1.386(6)
O2	C27	1.143(5)	C17	C18	1.386(7)
O3	C28	1.140(5)	C18	C19	1.382(7)
O4	C29	1.142(5)	C19	C20	1.393(7)
O5	C30	1.152(5)	C21	C22	1.389(6)
O6	C31	1.137(5)	C21	C26	1.394(6)
C1	C2	1.491(6)	C22	C23	1.395(7)
C2	C3	1.384(6)	C23	C24	1.377(7)
C2	C7	1.390(6)	C24	C25	1.385(7)
C3	C4	1.373(6)	C25	C26	1.384(6)

Table 3 Bond Angles for 22.

Atom	Atom	Atom	Angle/˚	Atom	Atom	Atom	Angle/˚
C27	W	P	172.50(13)	C7	C6	C5	119.5(4)
C27	W	C28	89.46(16)	F5	C7	C2	120.1(4)
C27	W	C29	92.85(18)	F5	C7	C6	117.2(4)
C27	W	C30	83.92(16)	C6	C7	C2	122.8(4)
C27	W	C31	89.07(17)	C9	C8	P	115.2(3)
C28	W	P	93.06(12)	C15	C8	P	99.3(3)
C29	W	P	94.29(13)	C15	C8	C9	113.6(3)
C29	W	C28	87.96(18)	C15	C8	C21	114.3(3)
C30	W	P	94.29(12)	C21	C8	P	109.7(3)
C30	W	C28	170.86(17)	C21	C8	C9	105.0(3)
C30	W	C29	86.08(18)	C10	C9	C8	121.7(4)
C30	W	C31	91.39(17)	C10	C9	C14	118.1(4)
C31	W	P	83.69(12)	C14	C9	C8	119.9(4)
C31	W	C28	94.81(18)	C9	C10	C11	120.3(4)
C31	W	C29	176.65(17)	C12	C11	C10	120.8(4)
O1	P	W	115.76(11)	C11	C12	C13	119.5(4)

O1	P	C1	49.73(16)	C12	C13	C14	120.1(4)
O1	P	C8	108.25(16)	C13	C14	C9	121.2(4)
C1	P	W	125.42(15)	C16	C15	C8	118.7(3)
C1	P	C8	107.54(18)	C16	C15	C20	119.1(4)
C8	P	W	125.18(12)	C20	C15	C8	122.1(4)
C1	O1	P	69.58(19)	C17	C16	C15	120.8(4)
O1	C1	P	60.68(18)	C16	C17	C18	120.1(5)
O1	C1	C2	115.8(3)	C19	C18	C17	119.4(5)
C2	C1	P	122.5(3)	C18	C19	C20	121.3(4)
C3	C2	C1	120.2(4)	C19	C20	C15	119.3(4)
C3	C2	C7	115.7(4)	C22	C21	C8	122.8(4)
C7	C2	C1	124.1(4)	C22	C21	C26	118.3(4)
F1	C3	C2	118.9(4)	C26	C21	C8	118.7(4)
F1	C3	C4	118.3(4)	C21	C22	C23	121.0(4)
C4	C3	C2	122.8(4)	C24	C23	C22	120.1(4)
F2	C4	C3	120.6(4)	C23	C24	C25	119.3(4)
F2	C4	C5	119.5(4)	C26	C25	C24	120.9(5)
C3	C4	C5	119.9(4)	C25	C26	C21	120.4(4)
F3	C5	C4	120.3(4)	O2	C27	W	177.4(4)
F3	C5	C6	120.4(4)	O3	C28	W	175.9(4)
C4	C5	C6	119.3(4)	O4	C29	W	176.7(4)
F4	C6	C5	119.8(4)	O5	C30	W	172.7(4)
F4	C6	C7	120.7(4)	O6	C31	W	177.8(4)

Table 4 Torsion Angles for 22.

A	B	C	D	Angle/˚	A	B	C	D	Angle/˚
W	P	O1	C1	-115.8(2)	C9	C8	C21	C22	102.7(4)
W	P	C1	O1	95.5(2)	C9	C8	C21	C26	-71.7(4)
W	P	C1	C2	-8.0(4)	C9	C10	C11	C12	-0.3(7)
W	P	C8	C9	-179.6(2)	C10	C9	C14	C13	2.9(6)
W	P	C8	C15	58.7(3)	C10	C11	C12	C13	0.5(7)
W	P	C8	C21	-61.4(3)	C11	C12	C13	C14	0.9(7)
P	W	C27	O2	40(10)	C12	C13	C14	C9	-2.7(7)
P	W	C28	O3	-143(5)	C14	C9	C10	C11	-1.4(6)
P	W	C29	O4	-135(7)	C15	C8	C9	C10	-16.5(5)
P	W	C30	O5	160(3)	C15	C8	C9	C14	169.8(4)
P	W	C31	O6	17(11)	C15	C8	C21	C22	-132.2(4)
P	O1	C1	C2	114.4(3)	C15	C8	C21	C26	53.4(5)
P	C1	C2	C3	-85.6(5)	C15	C16	C17	C18	-0.2(7)
P	C1	C2	C7	93.8(5)	C16	C15	C20	C19	1.9(6)
P	C8	C9	C10	-130.2(4)	C16	C17	C18	C19	1.3(7)
P	C8	C9	C14	56.2(5)	C17	C18	C19	C20	-0.9(7)
P	C8	C15	C16	69.8(4)	C18	C19	C20	C15	-0.7(7)
P	C8	C15	C20	-106.2(4)	C20	C15	C16	C17	-1.4(6)
P	C8	C21	C22	-21.7(5)	C21	C8	C9	C10	109.0(4)

P	C8	C21	C26	164.0(3)	C21	C8	C9	C14	-64.6(5)
F1	C3	C4	F2	-0.3(6)	C21	C8	C15	C16	-173.5(4)
F1	C3	C4	C5	178.1(4)	C21	C8	C15	C20	10.4(6)
F2	C4	C5	F3	-0.4(6)	C21	C22	C23	C24	0.7(7)
F2	C4	C5	C6	179.3(4)	C22	C21	C26	C25	3.0(6)
F3	C5	C6	F4	-0.8(6)	C22	C23	C24	C25	0.8(8)
F3	C5	C6	C7	179.5(4)	C23	C24	C25	C26	-0.3(8)
F4	C6	C7	F5	-1.3(6)	C24	C25	C26	C21	-1.6(7)
F4	C6	C7	C2	179.6(4)	C26	C21	C22	C23	-2.5(6)
O1	P	C1	C2	-103.5(4)	C27	W	P	O1	-5.6(10)
O1	P	C8	C9	-37.2(3)	C27	W	P	C1	-63.0(10)
O1	P	C8	C15	-158.9(2)	C27	W	P	C8	134.4(10)
O1	P	C8	C21	81.0(3)	C27	W	C28	O3	44(5)
O1	C1	C2	C3	-155.9(4)	C27	W	C29	O4	42(7)
O1	C1	C2	C7	23.5(5)	C27	W	C30	O5	-27(3)
C1	P	C8	C9	15.3(3)	C27	W	C31	O6	-161(11)
C1	P	C8	C15	-106.5(3)	C28	W	P	O1	-115.05(18)
C1	P	C8	C21	133.4(3)	C28	W	P	C1	-172.5(2)
C1	C2	C3	F1	0.5(6)	C28	W	P	C8	24.9(2)
C1	C2	C3	C4	179.3(4)	C28	W	C27	O2	150(9)
C1	C2	C7	F5	2.4(6)	C28	W	C29	O4	132(7)
C1	C2	C7	C6	-178.6(4)	C28	W	C30	O5	17(4)
C2	C3	C4	F2	-179.1(4)	C28	W	C31	O6	110(11)
C2	C3	C4	C5	-0.8(6)	C29	W	P	O1	156.76(17)
C3	C2	C7	F5	-178.2(3)	C29	W	P	C1	99.3(2)
C3	C2	C7	C6	0.9(6)	C29	W	P	C8	-63.3(2)
C3	C4	C5	F3	-178.8(4)	C29	W	C27	O2	-122(9)
C3	C4	C5	C6	1.0(6)	C29	W	C28	O3	-49(5)
C4	C5	C6	F4	179.4(4)	C29	W	C30	O5	66(3)
C4	C5	C6	C7	-0.3(6)	C29	W	C31	O6	-36(13)
C5	C6	C7	F5	178.4(3)	C30	W	P	O1	70.39(18)
C5	C6	C7	C2	-0.7(6)	C30	W	P	C1	12.9(2)
C7	C2	C3	F1	-179.0(3)	C30	W	P	C8	-149.6(2)
C7	C2	C3	C4	-0.1(6)	C30	W	C27	O2	-37(9)
C8	P	O1	C1	97.8(2)	C30	W	C28	O3	0(6)
C8	P	C1	O1	-99.4(2)	C30	W	C29	O4	-41(7)
C8	P	C1	C2	157.1(3)	C30	W	C31	O6	-77(11)
C8	C9	C10	C11	-175.2(4)	C31	W	P	O1	-20.55(17)
C8	C9	C14	C13	176.8(4)	C31	W	P	C1	-78.0(2)
C8	C15	C16	C17	-177.6(4)	C31	W	P	C8	119.4(2)
C8	C15	C20	C19	177.9(4)	C31	W	C27	O2	55(9)
C8	C21	C22	C23	-176.9(4)	C31	W	C28	O3	133(5)
C8	C21	C26	C25	177.6(4)	C31	W	C29	O4	-82(8)
C9	C8	C15	C16	-53.1(5)	C31	W	C30	O5	-116(3)
C9	C8	C15	C20	130.9(4)					

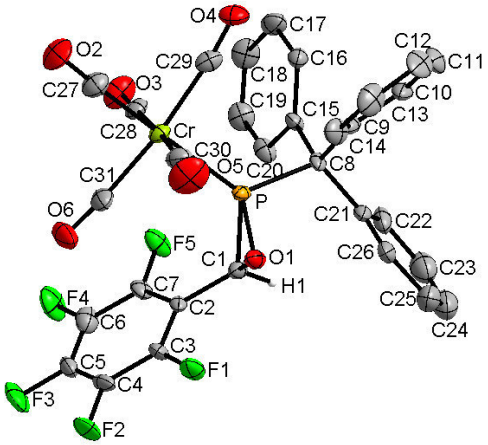

Table 1 Crystal data and structure refinement for 23*3CHCl$_3$.

Identification code	GSTR495
Empirical formula	$C_{34}H_{19}Cl_9CrF_5O_6P$
Formula weight	1020.51
Temperature/K	150.0
Crystal system	monoclinic
Space group	$P2_1/c$
a/Å	16.5199(17)
b/Å	14.4178(14)
c/Å	16.9989(17)
α/°	90
β/°	97.611(3)
γ/°	90
Volume/Å^3	4013.1(7)
Z	4
ρ_{calc}g/cm^3	1.689
μ/mm^{-1}	0.991
F(000)	2032.0
Crystal size/mm^3	0.14 × 0.07 × 0.06
Tmin; Tmax	0.5377; 0.7459
Radiation	MoKα (λ = 0.71073)
2Θ range for data collection/°	4.648 to 56°
Completeness to theta	0.999
Index ranges	-21 ≤ h ≤ 21, -19 ≤ k ≤ 19, -22 ≤ l ≤ 22
Reflections collected	98129
Independent reflections	9677 [R_{int} = 0.3950, R_{sigma} = 0.1760]
Data/restraints/parameters	9677/48/559
Goodness-of-fit on F^2	1.019
Final R indexes [I>=2σ (I)]	R_1 = 0.1211, wR_2 = 0.2922
Final R indexes [all data]	R_1 = 0.2437, wR_2 = 0.3687
Largest diff. peak/hole / e Å^{-3}	1.43/-1.49

Table 2 Bond Lengths for 23*3CHCl$_3$.

Atom	Atom	Length/Å	Atom	Atom	Length/Å
Cr	P	2.336(2)	C10	C11	1.368(12)
Cr	C27	1.883(9)	C11	C12	1.396(15)
Cr	C28	1.899(9)	C12	C13	1.364(15)
Cr	C29	1.905(9)	C13	C14	1.417(12)
Cr	C30	1.892(10)	C15	C16	1.394(11)
Cr	C31	1.915(10)	C15	C20	1.404(11)
P	O1	1.668(5)	C16	C17	1.391(12)
P	C1	1.790(8)	C17	C18	1.398(13)
P	C8	1.912(8)	C18	C19	1.369(13)
F1	C3	1.339(9)	C19	C20	1.378(12)
F2	C4	1.346(9)	C21	C22	1.408(13)
F3	C5	1.331(9)	C21	C26	1.392(13)
F4	C6	1.331(10)	C22	C23	1.392(14)
F5	C7	1.341(9)	C23	C24	1.338(16)
O1	C1	1.468(9)	C24	C25	1.339(15)
O2	C27	1.126(10)	C25	C26	1.416(13)
O3	C28	1.148(10)	Cl1	C32	1.72(2)
O4	C29	1.149(10)	Cl2	C32	1.807(17)
O5	C30	1.145(11)	Cl3	C32	1.70(3)
O6	C31	1.127(11)	Cl1S	C32	1.84(2)
C1	C2	1.504(10)	Cl2S	C32	1.660(15)
C2	C3	1.376(11)	Cl3S	C32	1.77(4)
C2	C7	1.396(11)	Cl2T	C32	2.07(4)
C3	C4	1.399(11)	Cl1T	C32	1.57(2)
C4	C5	1.369(12)	Cl3T	C32	1.727(19)
C5	C6	1.367(13)	Cl4	C33	1.77(2)
C6	C7	1.393(12)	Cl5	C33	1.75(2)
C8	C9	1.537(10)	Cl6	C33	1.60(2)
C8	C15	1.526(11)	Cl7	C34	1.71(2)
C8	C21	1.539(10)	Cl8	C34	1.74(2)
C9	C10	1.382(11)	Cl9	C34	1.75(2)
C9	C14	1.414(12)			

Table 3 Bond Angles for 23*3CHCl$_3$.

Atom	Atom	Atom	Angle/˚	Atom	Atom	Atom	Angle/˚
C27	Cr	P	177.9(3)	C15	C8	C21	114.9(6)
C27	Cr	C28	88.5(4)	C21	C8	P	112.6(5)
C27	Cr	C29	86.0(4)	C10	C9	C8	119.0(7)
C27	Cr	C30	89.8(4)	C10	C9	C14	118.3(7)
C27	Cr	C31	87.3(4)	C14	C9	C8	122.2(7)
C28	Cr	P	93.4(2)	C11	C10	C9	121.3(9)
C28	Cr	C29	89.9(4)	C10	C11	C12	120.9(9)

C28	Cr	C31	89.2(4)	C13	C12	C11	119.4(8)
C29	Cr	P	93.3(3)	C12	C13	C14	120.3(10)
C29	Cr	C31	173.2(3)	C9	C14	C13	119.6(9)
C30	Cr	P	88.2(3)	C16	C15	C8	123.6(7)
C30	Cr	C28	177.4(4)	C16	C15	C20	117.5(7)
C30	Cr	C29	92.0(4)	C20	C15	C8	118.8(7)
C30	Cr	C31	88.7(4)	C17	C16	C15	120.6(8)
C31	Cr	P	93.5(3)	C16	C17	C18	120.7(8)
O1	P	Cr	117.7(2)	C19	C18	C17	118.9(8)
O1	P	C1	50.1(3)	C18	C19	C20	120.9(8)
O1	P	C8	107.8(3)	C19	C20	C15	121.4(8)
C1	P	Cr	127.1(3)	C22	C21	C8	122.3(8)
C1	P	C8	104.9(3)	C26	C21	C8	119.3(8)
C8	P	Cr	125.2(2)	C26	C21	C22	118.3(8)
C1	O1	P	69.3(4)	C23	C22	C21	118.6(10)
O1	C1	P	60.6(3)	C24	C23	C22	122.2(11)
O1	C1	C2	115.6(6)	C23	C24	C25	120.8(10)
C2	C1	P	123.1(5)	C24	C25	C26	120.1(10)
C3	C2	C1	123.7(7)	C21	C26	C25	119.8(10)
C3	C2	C7	116.7(7)	O2	C27	Cr	177.5(9)
C7	C2	C1	119.6(7)	O3	C28	Cr	176.6(7)
F1	C3	C2	120.2(7)	O4	C29	Cr	174.3(7)
F1	C3	C4	118.5(7)	O5	C30	Cr	177.1(9)
C2	C3	C4	121.3(8)	O6	C31	Cr	174.5(7)
F2	C4	C3	118.9(8)	Cl1	C32	Cl2	107.7(11)
F2	C4	C5	120.7(8)	Cl3	C32	Cl1	111.1(11)
C5	C4	C3	120.4(7)	Cl3	C32	Cl2	115.2(10)
F3	C5	C4	119.5(8)	Cl2S	C32	Cl1S	108.3(11)
F3	C5	C6	120.5(8)	Cl2S	C32	Cl3S	111.5(14)
C6	C5	C4	120.0(8)	Cl3S	C32	Cl1S	110.6(14)
F4	C6	C5	121.0(8)	Cl1T	C32	Cl2T	100.1(17)
F4	C6	C7	119.9(8)	Cl1T	C32	Cl3T	122.9(11)
C5	C6	C7	119.1(8)	Cl3T	C32	Cl2T	86.6(16)
F5	C7	C2	119.3(7)	Cl5	C33	Cl4	109.4(12)
F5	C7	C6	118.2(7)	Cl6	C33	Cl4	117.6(13)
C6	C7	C2	122.4(8)	Cl6	C33	Cl5	112.5(11)
C9	C8	P	111.0(5)	Cl7	C34	Cl8	114.3(12)
C9	C8	C21	105.9(6)	Cl7	C34	Cl9	110.3(14)
C15	C8	P	99.0(5)	Cl8	C34	Cl9	110.6(12)
C15	C8	C9	113.6(6)				

Table 4 Torsion Angles for 23*3CHCl$_3$.

A	B	C	D	Angle/°	A	B	C	D	Angle/°
Cr	P	O1	C1	116.6(4)	C8	P	O1	C1	-94.8(4)
Cr	P	C1	O1	-97.4(4)	C8	P	C1	O1	101.0(4)
Cr	P	C1	C2	5.6(8)	C8	P	C1	C2	-156.0(6)
P	O1	C1	C2	-115.2(6)	C8	C9	C10	C11	-176.7(7)
P	C1	C2	C3	-107.8(8)	C8	C9	C14	C13	175.9(7)
P	C1	C2	C7	75.4(9)	C8	C15	C16	C17	-178.3(7)
P	C8	C9	C10	-169.8(6)	C8	C15	C20	C19	178.3(7)
P	C8	C9	C14	18.6(9)	C8	C21	C22	C23	179.4(8)
P	C8	C15	C16	112.4(7)	C8	C21	C26	C25	-178.5(7)
P	C8	C15	C20	-64.2(7)	C9	C8	C15	C16	-5.2(10)
P	C8	C21	C22	115.6(7)	C9	C8	C15	C20	178.1(7)
P	C8	C21	C26	-67.8(8)	C9	C8	C21	C22	-123.0(8)
F1	C3	C4	F2	0.8(11)	C9	C8	C21	C26	53.7(9)
F1	C3	C4	C5	-178.7(7)	C9	C10	C11	C12	2.2(13)
F2	C4	C5	F3	0.5(11)	C10	C9	C14	C13	4.3(12)
F2	C4	C5	C6	-179.9(7)	C10	C11	C12	C13	1.2(15)
F3	C5	C6	F4	0.6(12)	C11	C12	C13	C14	-1.6(15)
F3	C5	C6	C7	-179.5(7)	C12	C13	C14	C9	-1.1(14)
F4	C6	C7	F5	1.1(12)	C14	C9	C10	C11	-4.8(12)
F4	C6	C7	C2	178.5(7)	C15	C8	C9	C10	-59.4(9)
O1	P	C1	C2	103.0(8)	C15	C8	C9	C14	129.1(8)
O1	C1	C2	C3	-37.4(10)	C15	C8	C21	C22	3.2(10)
O1	C1	C2	C7	145.7(7)	C15	C8	C21	C26	179.9(7)
C1	C2	C3	F1	1.3(12)	C15	C16	C17	C18	0.6(12)
C1	C2	C3	C4	-177.8(7)	C16	C15	C20	C19	1.4(12)
C1	C2	C7	F5	-4.3(11)	C16	C17	C18	C19	0.7(13)
C1	C2	C7	C6	178.4(7)	C17	C18	C19	C20	-0.9(13)
C2	C3	C4	F2	179.9(7)	C18	C19	C20	C15	-0.2(13)
C2	C3	C4	C5	0.4(12)	C20	C15	C16	C17	-1.6(11)
C3	C2	C7	F5	178.6(7)	C21	C8	C9	C10	67.6(9)
C3	C2	C7	C6	1.3(11)	C21	C8	C9	C14	-103.9(8)
C3	C4	C5	F3	180.0(7)	C21	C8	C15	C16	-127.4(8)
C3	C4	C5	C6	-0.4(12)	C21	C8	C15	C20	56.0(9)
C4	C5	C6	F4	-179.0(8)	C21	C22	C23	C24	-2.3(14)
C4	C5	C6	C7	0.9(12)	C22	C21	C26	C25	-1.7(12)
C5	C6	C7	F5	-178.7(7)	C22	C23	C24	C25	0.6(16)
C5	C6	C7	C2	-1.3(12)	C23	C24	C25	C26	0.5(16)
C7	C2	C3	F1	178.2(7)	C24	C25	C26	C21	0.1(14)
C7	C2	C3	C4	-0.8(11)	C26	C21	C22	C23	2.7(12)

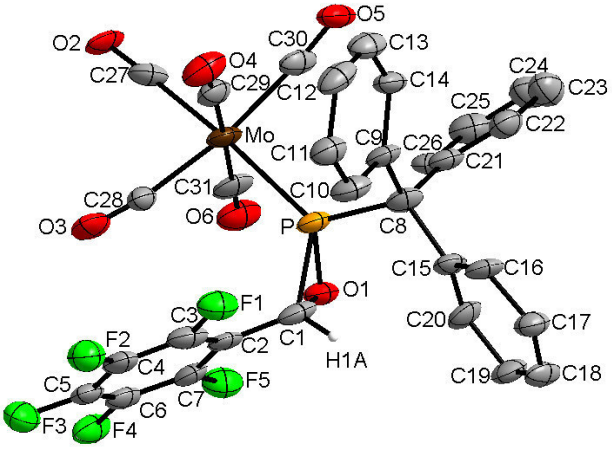

Table 1 Crystal data and structure refinement for 24.

Identification code	GSTR318
Empirical formula	$C_{31}H_{16}F_5MoO_6P$
Formula weight	706.35
Temperature/K	123(2)
Crystal system	monoclinic
Space group	C2/c
a/Å	36.147(5)
b/Å	9.5738(10)
c/Å	16.5371(15)
α/°	90
β/°	93.968(9)
γ/°	90
Volume/Å^3	5709.2(11)
Z	8
ρ_{calc}g/cm^3	1.644
μ/mm^{-1}	0.593
F(000)	2816
Crystal size/mm^3	0.25 × 0.20 × 0.02
Tmin; Tmax	0.8660; 0.9882
Radiation	MoKα (λ = 0.71073)
2Θ range for data collection/°	2.72 to 26.00°
Completeness to theta	0.998
Index ranges	-44 ≤ h ≤ 44, 0 ≤ k ≤ 11, 0 ≤ l ≤ 20
Reflections collected	5591
Independent reflections	5591 [R_{int} = 0.2665]
Data/restraints/parameters	5591/0/397
Goodness-of-fit on F^2	0.921
Final R indexes [I>=2σ (I)]	R_1 = 0.1005, wR_2 = 0.2358
Final R indexes [all data]	R_1 = 0.1413, wR_2 = 0.2473
Largest diff. peak/hole / e Å^{-3}	2.342/-3.015

Table 2 Bond Lengths for 24.

Atom	Atom	Length/Å	Atom	Atom	Length/Å
C1	O1	1.467(12)	C1	C2	1.476(14)
C1	P	1.804(10)	C2	C3	1.387(15)
C2	C7	1.410(13)	C3	F1	1.360(11)
C3	C4	1.371(15)	C4	F2	1.336(12)
C4	C5	1.393(15)	C5	F3	1.329(12)
C5	C6	1.360(15)	C6	F4	1.358(11)
C6	C7	1.364(14)	C7	F5	1.328(11)
C8	C21	1.529(14)	C8	C9	1.543(13)
C8	C15	1.548(11)	C8	P	1.889(10)
C9	C10	1.403(15)	C9	C14	1.408(12)
C10	C11	1.385(14)	C11	C12	1.413(15)
C12	C13	1.373(16)	C13	C14	1.404(15)
C15	C16	1.368(14)	C15	C20	1.390(13)
C16	C17	1.426(12)	C17	C18	1.363(14)
C18	C19	1.382(14)	C19	C20	1.400(12)
C21	C22	1.372(14)	C21	C26	1.394(14)
C22	C23	1.394(16)	C23	C24	1.352(16)
C24	C25	1.372(16)	C25	C26	1.429(15)
C27	O2	1.124(11)	C27	Mo	2.034(10)
C28	O3	1.148(12)	C28	Mo	2.031(11)
C29	O4	1.162(12)	C29	Mo	2.048(12)
C30	O5	1.162(12)	C30	Mo	2.050(11)
C31	O6	1.158(12)	C31	Mo	2.045(12)
Mo	P	2.467(2)	O1	P	1.684(6)

Table 3 Bond Angles for 24.

Atom	Atom	Atom	Angle/˚	Atom	Atom	Atom	Angle/˚
O1	C1	C2	117.1(8)	O1	C1	P	61.0(5)
C2	C1	P	122.1(6)	C3	C2	C7	114.9(9)
C3	C2	C1	122.4(9)	C7	C2	C1	122.8(9)
F1	C3	C4	117.4(10)	F1	C3	C2	118.1(10)
C4	C3	C2	124.5(10)	F2	C4	C3	121.3(10)
F2	C4	C5	119.7(10)	C3	C4	C5	119.0(11)
F3	C5	C6	123.1(9)	F3	C5	C4	119.3(10)
C6	C5	C4	117.6(10)	F4	C6	C5	117.8(9)
F4	C6	C7	118.6(10)	C5	C6	C7	123.6(10)
F5	C7	C6	119.4(9)	F5	C7	C2	120.2(9)
C6	C7	C2	120.4(10)	C21	C8	C9	114.3(8)
C21	C8	C15	106.0(8)	C9	C8	C15	113.0(8)
C21	C8	P	111.0(6)	C9	C8	P	98.5(6)
C15	C8	P	114.1(6)	C10	C9	C14	118.5(9)
C10	C9	C8	119.7(8)	C14	C9	C8	121.6(9)

C11	C10	C9	122.1(9)	C10	C11	C12	119.3(11)
C13	C12	C11	118.9(9)	C12	C13	C14	122.6(10)
C13	C14	C9	118.7(10)	C16	C15	C20	117.2(8)
C16	C15	C8	121.8(8)	C20	C15	C8	120.4(8)
C15	C16	C17	122.7(9)	C18	C17	C16	118.2(9)
C17	C18	C19	120.8(9)	C18	C19	C20	119.7(9)
C15	C20	C19	121.3(9)	C22	C21	C26	118.0(10)
C22	C21	C8	119.9(9)	C26	C21	C8	121.7(9)
C21	C22	C23	121.3(11)	C24	C23	C22	120.4(11)
C23	C24	C25	121.2(11)	C24	C25	C26	118.3(11)
C21	C26	C25	120.7(10)	O2	C27	Mo	177.2(8)
O3	C28	Mo	171.7(8)	O4	C29	Mo	176.3(9)
O5	C30	Mo	173.7(9)	O6	C31	Mo	178.8(8)
C28	Mo	C27	83.3(4)	C28	Mo	C31	90.8(4)
C27	Mo	C31	89.7(4)	C28	Mo	C29	86.6(4)
C27	Mo	C29	92.0(4)	C31	Mo	C29	176.7(4)
C28	Mo	C30	171.6(4)	C27	Mo	C30	89.9(4)
C31	Mo	C30	94.2(4)	C29	Mo	C30	88.7(4)
C28	Mo	P	94.6(3)	C27	Mo	P	173.0(3)
C31	Mo	P	83.6(3)	C29	Mo	P	94.5(3)
C30	Mo	P	92.7(3)	C1	O1	P	69.4(4)
O1	P	C1	49.6(4)	O1	P	C8	107.6(4)
C1	P	C8	108.2(4)	O1	P	Mo	115.3(2)
C1	P	Mo	125.0(4)	C8	P	Mo	125.4(3)

Table 4 Torsion Angles for 24.

A	B	C	D	Angle/˚	A	B	C	D	Angle/˚
O1	C1	C2	C3	-155.4(8)	P	C1	C2	C3	-84.3(10)
O1	C1	C2	C7	25.0(11)	P	C1	C2	C7	96.2(9)
C7	C2	C3	F1	-179.4(7)	C1	C2	C3	F1	1.0(12)
C7	C2	C3	C4	-0.8(13)	C1	C2	C3	C4	179.6(8)
F1	C3	C4	F2	-0.1(13)	C2	C3	C4	F2	-178.7(8)
F1	C3	C4	C5	178.4(8)	C2	C3	C4	C5	-0.2(14)
F2	C4	C5	F3	0.0(13)	C3	C4	C5	F3	-178.5(8)
F2	C4	C5	C6	178.7(8)	C3	C4	C5	C6	0.2(13)
F3	C5	C6	F4	-1.5(12)	C4	C5	C6	F4	179.8(8)
F3	C5	C6	C7	179.7(8)	C4	C5	C6	C7	1.0(13)
F4	C6	C7	F5	-0.5(12)	C5	C6	C7	F5	178.2(8)
F4	C6	C7	C2	179.0(7)	C5	C6	C7	C2	-2.2(13)
C3	C2	C7	F5	-178.4(7)	C1	C2	C7	F5	1.1(12)
C3	C2	C7	C6	2.0(12)	C1	C2	C7	C6	-178.5(8)
C21	C8	C9	C10	-173.9(9)	C15	C8	C9	C10	-52.5(12)
P	C8	C9	C10	68.4(9)	C21	C8	C9	C14	11.8(13)
C15	C8	C9	C14	133.2(9)	P	C8	C9	C14	-106.0(9)
C14	C9	C10	C11	-2.6(15)	C8	C9	C10	C11	-177.2(9)

C9	C10	C11	C12	0.6(15)	C10	C11	C12	C13	1.0(15)
C11	C12	C13	C14	-0.6(15)	C12	C13	C14	C9	-1.5(15)
C10	C9	C14	C13	3.0(14)	C8	C9	C14	C13	177.4(9)
C21	C8	C15	C16	107.2(11)	C9	C8	C15	C16	-18.8(14)
P	C8	C15	C16	-130.3(9)	C21	C8	C15	C20	-63.6(11)
C9	C8	C15	C20	170.5(9)	P	C8	C15	C20	58.9(11)
C20	C15	C16	C17	-2.4(16)	C8	C15	C16	C17	-173.4(9)
C15	C16	C17	C18	-0.6(16)	C16	C17	C18	C19	1.2(16)
C17	C18	C19	C20	1.2(17)	C16	C15	C20	C19	4.8(16)
C8	C15	C20	C19	176.0(9)	C18	C19	C20	C15	-4.3(17)
C9	C8	C21	C22	53.9(11)	C15	C8	C21	C22	-71.3(10)
P	C8	C21	C22	164.3(7)	C9	C8	C21	C26	-132.6(9)
C15	C8	C21	C26	102.2(10)	P	C8	C21	C26	-22.2(10)
C26	C21	C22	C23	3.7(14)	C8	C21	C22	C23	177.5(9)
C21	C22	C23	C24	-2.8(16)	C22	C23	C24	C25	1.0(17)
C23	C24	C25	C26	-0.3(16)	C22	C21	C26	C25	-3.0(13)
C8	C21	C26	C25	-176.6(8)	C24	C25	C26	C21	1.3(14)
O3	C28	Mo	C27	-34(6)	O3	C28	Mo	C31	-124(6)
O3	C28	Mo	C29	58(6)	O3	C28	Mo	C30	2(8)
O3	C28	Mo	P	152(6)	O2	C27	Mo	C28	-47(19)
O2	C27	Mo	C31	43(19)	O2	C27	Mo	C29	-134(19)
O2	C27	Mo	C30	138(19)	O2	C27	Mo	P	26(21)
O6	C31	Mo	C28	-86(51)	O6	C31	Mo	C27	-169(100)
O6	C31	Mo	C29	-48(55)	O6	C31	Mo	C30	101(51)
O6	C31	Mo	P	9(51)	O4	C29	Mo	C28	-27(13)
O4	C29	Mo	C27	56(13)	O4	C29	Mo	C31	-65(15)
O4	C29	Mo	C30	146(13)	O4	C29	Mo	P	-121(13)
O5	C30	Mo	C28	22(9)	O5	C30	Mo	C27	59(7)
O5	C30	Mo	C31	149(7)	O5	C30	Mo	C29	-33(7)
O5	C30	Mo	P	-128(7)	C2	C1	O1	P	113.5(7)
C1	O1	P	C8	99.3(6)	C1	O1	P	Mo	-115.5(5)
C2	C1	P	O1	-105.4(9)	O1	C1	P	C8	-97.9(5)
C2	C1	P	C8	156.6(8)	O1	C1	P	Mo	95.1(5)
C2	C1	P	Mo	-10.4(10)	C21	C8	P	O1	80.6(6)
C9	C8	P	O1	-159.1(5)	C15	C8	P	O1	-39.1(8)
C21	C8	P	C1	132.9(6)	C9	C8	P	C1	-106.8(6)
C15	C8	P	C1	13.2(8)	C21	C8	P	Mo	-60.1(7)
C9	C8	P	Mo	60.1(6)	C15	C8	P	Mo	-179.8(5)
C28	Mo	P	O1	70.7(4)	C27	Mo	P	O1	-2(2)
C31	Mo	P	O1	-19.6(4)	C29	Mo	P	O1	157.6(4)
C30	Mo	P	O1	-113.5(4)	C28	Mo	P	C1	13.7(5)
C27	Mo	P	C1	-59(2)	C31	Mo	P	C1	-76.6(5)
C29	Mo	P	C1	100.6(5)	C30	Mo	P	C1	-170.5(5)
C28	Mo	P	C8	-151.2(5)	C27	Mo	P	C8	136(2)
C31	Mo	P	C8	118.5(5)	C29	Mo	P	C8	-64.3(5)

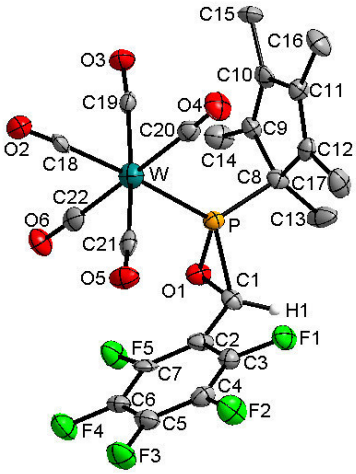

Table 1 Crystal data and structure refinement for 27.

Identification code	GSTR362
Empirical formula	$C_{22}H_{16}F_5O_6PW$
Formula weight	686.17
Temperature/K	123
Crystal system	monoclinic
Space group	Pn
a/Å	9.2418(4)
b/Å	9.8041(4)
c/Å	13.2530(6)
α/°	90.00
β/°	102.793(2)
γ/°	90.00
Volume/Å^3	1171.01(9)
Z	2
ρ_{calc}g/cm^3	1.946
μ/mm^{-1}	5.077
F(000)	660.0
Crystal size/mm^3	0.1 × 0.08 × 0.04
Radiation	MoKα (λ = 0.71073)
2Θ range for data collection/°	5.22 to 56
Index ranges	-12 ≤ h ≤ 12, -12 ≤ k ≤ 12, -12 ≤ l ≤ 17
Reflections collected	16798
Independent reflections	4844 [R_{int} = 0.0690, R_{sigma} = 0.0785]
Data/restraints/parameters	4844/2/321
Goodness-of-fit on F^2	1.020
Final R indexes [I>=2σ (I)]	R_1 = 0.0404, wR_2 = 0.0842
Final R indexes [all data]	R_1 = 0.0533, wR_2 = 0.0897
Largest diff. peak/hole / e Å^{-3}	3.26/-1.73

Table 2 Bond Lengths for 27.

Atom	Atom	Length/Å	Atom	Atom	Length/Å
W	P	2.467(2)	O6	C22	1.132(10)
W	C18	1.995(9)	C1	C2	1.473(12)
W	C19	2.053(8)	C2	C3	1.408(12)
W	C20	2.077(9)	C2	C7	1.358(12)
W	C21	2.032(9)	C3	C4	1.387(12)
W	C22	2.064(10)	C4	C5	1.375(13)
P	O1	1.668(6)	C5	C6	1.385(13)
P	C1	1.815(8)	C6	C7	1.383(11)
P	C8	1.852(9)	C8	C9	1.520(11)
F1	C3	1.344(10)	C8	C12	1.511(12)
F2	C4	1.341(10)	C8	C13	1.546(12)
F3	C5	1.327(10)	C9	C10	1.355(11)
F4	C6	1.349(11)	C9	C14	1.488(11)
F5	C7	1.351(9)	C10	C11	1.482(12)
O1	C1	1.454(10)	C10	C15	1.501(12)
O2	C18	1.148(10)	C11	C12	1.351(11)
O3	C19	1.146(10)	C11	C16	1.494(12)
O4	C20	1.118(10)	C12	C17	1.500(12)
O5	C21	1.145(10)			

Table 3 Bond Angles for 27.

Atom	Atom	Atom	Angle/˚	Atom	Atom	Atom	Angle/˚
C18	W	P	175.8(2)	C5	C4	C3	120.0(8)
C18	W	C19	88.3(3)	F3	C5	C4	120.5(8)
C18	W	C20	91.1(3)	F3	C5	C6	121.1(9)
C18	W	C21	85.6(3)	C4	C5	C6	118.3(8)
C18	W	C22	88.8(3)	F4	C6	C5	118.5(8)
C19	W	P	92.7(2)	F4	C6	C7	120.8(8)
C19	W	C20	90.2(3)	C7	C6	C5	120.7(9)
C19	W	C22	89.1(3)	F5	C7	C2	121.9(7)
C20	W	P	93.0(2)	F5	C7	C6	115.3(7)
C21	W	P	93.5(2)	C2	C7	C6	122.8(8)
C21	W	C19	173.7(3)	C9	C8	P	106.3(6)
C21	W	C20	88.3(3)	C9	C8	C13	112.3(7)
C21	W	C22	92.3(3)	C12	C8	P	104.9(5)
C22	W	P	87.2(2)	C12	C8	C9	104.2(6)
C22	W	C20	179.3(3)	C12	C8	C13	113.0(8)
O1	P	W	119.0(2)	C13	C8	P	115.1(6)
O1	P	C1	49.1(3)	C10	C9	C8	107.8(7)
O1	P	C8	105.6(3)	C10	C9	C14	129.1(8)
C1	P	W	124.7(3)	C14	C9	C8	123.1(7)
C1	P	C8	108.5(4)	C9	C10	C11	110.0(7)
C8	P	W	124.8(3)	C9	C10	C15	127.1(8)

C1	O1	P	70.7(4)	C11	C10	C15	122.8(8)
O1	C1	P	60.1(4)	C10	C11	C16	123.6(7)
O1	C1	C2	117.5(7)	C12	C11	C10	109.3(7)
C2	C1	P	121.3(6)	C12	C11	C16	127.1(8)
C3	C2	C1	117.4(8)	C11	C12	C8	108.7(7)
C7	C2	C1	126.6(8)	C11	C12	C17	128.6(8)
C7	C2	C3	116.0(8)	C17	C12	C8	122.7(7)
F1	C3	C2	118.8(7)	O2	C18	W	177.3(7)
F1	C3	C4	119.0(7)	O3	C19	W	174.6(7)
C4	C3	C2	122.3(8)	O4	C20	W	176.8(8)
F2	C4	C3	119.7(8)	O5	C21	W	173.7(7)
F2	C4	C5	120.4(8)	O6	C22	W	177.2(7)

Table 4 Torsion Angles for 27.

A	B	C	D	Angle/˚	A	B	C	D	Angle/˚
W	P	O1	C1	112.3(4)	C8	C9	C10	C15	-176.7(8)
W	P	C1	O1	-100.5(4)	C9	C8	C12	C11	0.4(9)
W	P	C1	C2	5.4(8)	C9	C8	C12	C17	179.3(8)
W	P	C8	C9	51.9(6)	C9	C10	C11	C12	0.0(10)
W	P	C8	C12	-58.2(6)	C9	C10	C11	C16	178.8(8)
W	P	C8	C13	176.9(5)	C10	C11	C12	C8	-0.2(10)
P	W	C18	O2	-41(18)	C10	C11	C12	C17	-179.0(9)
P	W	C19	O3	-175(8)	C12	C8	C9	C10	-0.4(9)
P	W	C20	O4	172(13)	C12	C8	C9	C14	-179.2(8)
P	W	C21	O5	-157(7)	C13	C8	C9	C10	122.3(8)
P	W	C22	O6	-178(100)	C13	C8	C9	C14	-56.5(11)
P	O1	C1	C2	-112.1(7)	C13	C8	C12	C11	-121.8(8)
P	C1	C2	C3	99.7(9)	C13	C8	C12	C17	57.0(11)
P	C1	C2	C7	-79.2(10)	C14	C9	C10	C11	179.0(9)
P	C8	C9	C10	-111.0(7)	C14	C9	C10	C15	2.0(15)
P	C8	C9	C14	70.2(9)	C15	C10	C11	C12	177.1(8)
P	C8	C12	C11	112.0(7)	C15	C10	C11	C16	-4.1(14)
P	C8	C12	C17	-69.1(9)	C16	C11	C12	C8	-179.0(9)
F1	C3	C4	F2	-1.4(12)	C16	C11	C12	C17	2.2(16)
F1	C3	C4	C5	178.7(8)	C18	W	P	O1	-4(3)
F2	C4	C5	F3	0.1(13)	C18	W	P	C1	54(3)
F2	C4	C5	C6	-179.1(8)	C18	W	P	C8	-144(3)
F3	C5	C6	F4	1.1(13)	C18	W	C19	O3	1(8)
F3	C5	C6	C7	-179.2(7)	C18	W	C20	O4	-7(13)
F4	C6	C7	F5	1.4(11)	C18	W	C21	O5	27(7)
F4	C6	C7	C2	179.8(8)	C18	W	C22	O6	1(16)
O1	P	C1	C2	105.9(8)	C19	W	P	O1	99.8(3)
O1	P	C8	C9	-92.1(5)	C19	W	P	C1	158.1(4)
O1	P	C8	C12	157.8(5)	C19	W	P	C8	-39.8(4)
O1	P	C8	C13	33.0(7)	C19	W	C18	O2	-145(15)

O1	C1	C2	C3	169.8(7)	C19	W	C20	O4	-96(13)
O1	C1	C2	C7	-9.2(12)	C19	W	C21	O5	13(9)
C1	P	C8	C9	-143.5(5)	C19	W	C22	O6	89(16)
C1	P	C8	C12	106.4(6)	C20	W	P	O1	-169.8(3)
C1	P	C8	C13	-18.5(8)	C20	W	P	C1	-111.6(4)
C1	C2	C3	F1	2.2(12)	C20	W	P	C8	50.5(4)
C1	C2	C3	C4	-177.4(8)	C20	W	C18	O2	124(15)
C1	C2	C7	F5	-3.6(13)	C20	W	C19	O3	92(8)
C1	C2	C7	C6	178.1(8)	C20	W	C21	O5	-64(7)
C2	C3	C4	F2	178.1(8)	C20	W	C22	O6	77(38)
C2	C3	C4	C5	-1.7(13)	C21	W	P	O1	-81.3(3)
C3	C2	C7	F5	177.4(8)	C21	W	P	C1	-23.1(4)
C3	C2	C7	C6	-0.9(12)	C21	W	P	C8	139.0(4)
C3	C4	C5	F3	-180.0(8)	C21	W	C18	O2	36(15)
C3	C4	C5	C6	0.8(13)	C21	W	C19	O3	16(10)
C4	C5	C6	F4	-179.7(8)	C21	W	C20	O4	78(13)
C4	C5	C6	C7	0.0(13)	C21	W	C22	O6	-85(16)
C5	C6	C7	F5	-178.3(8)	C22	W	P	O1	10.8(3)
C5	C6	C7	C2	0.1(13)	C22	W	P	C1	69.1(4)
C7	C2	C3	F1	-178.8(7)	C22	W	P	C8	-128.8(4)
C7	C2	C3	C4	1.7(13)	C22	W	C18	O2	-56(15)
C8	P	O1	C1	-101.2(5)	C22	W	C19	O3	-88(8)
C8	P	C1	O1	94.9(5)	C22	W	C20	O4	-83(36)
C8	P	C1	C2	-159.2(6)	C22	W	C21	O5	116(7)
C8	C9	C10	C11	0.3(10)					

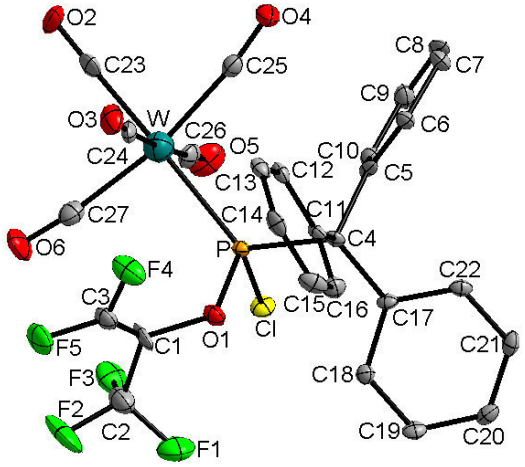

Table 1 Crystal data and structure refinement for 33.

Identification code	GSTR374
Empirical formula	$C_{27}H_{15}ClF_5O_6PW$
Formula weight	780.66
Temperature/K	100
Crystal system	monoclinic
Space group	$P2_1/c$
a/Å	15.3052(7)
b/Å	9.5908(4)
c/Å	37.3062(16)
α/°	90
β/°	101.829(2)
γ/°	90
Volume/Å^3	5359.9(4)
Z	8
ρ_{calc}g/cm^3	1.935
μ/mm^{-1}	4.546
F(000)	3008.0
Crystal size/mm^3	0.07 × 0.05 × 0.02
Tmin; Tmax	0.6136; 0.8498
Radiation	MoKα (λ = 0.71073)
2Θ range for data collection/°	3.144 to 51.998°
Completeness to theta	0.998
Index ranges	-9 ≤ h ≤ 18, -7 ≤ k ≤ 11, -46 ≤ l ≤ 43
Reflections collected	48898
Independent reflections	10691 [R_{int} = 0.0373, R_{sigma} = 0.0343]
Data/restraints/parameters	10691/48/743
Goodness-of-fit on F^2	1.106
Final R indexes [I>=2σ (I)]	R_1 = 0.0258, wR_2 = 0.0566
Final R indexes [all data]	R_1 = 0.0272, wR_2 = 0.0572
Largest diff. peak/hole / e Å^{-3}	1.83/-0.97

Table 2 Bond Lengths for 33.

Atom	Atom	Length/Å	Atom	Atom	Length/Å
W	P	2.4696(12)	W'	P'	2.4672(12)
W	C23	2.014(5)	W'	C23'	2.023(6)
W	C24	2.038(6)	W'	C24'	2.037(5)
W	C25	2.029(6)	W'	C25'	2.036(5)
W	C26	2.049(6)	W'	C26'	2.055(5)
W	C27	2.044(6)	W'	C27'	2.053(6)
Cl	P	2.0596(16)	Cl'	P'	2.0539(16)
P	O1	1.645(3)	P'	O1'	1.653(4)
P	C4	1.925(5)	P'	C4'	1.926(5)
F1	C2	1.339(6)	F1'	C2'	1.344(7)
F2	C2	1.316(6)	F2'	C2'	1.301(6)
F3	C2	1.327(6)	F3'	C2'	1.339(7)
F4	C3	1.291(6)	F4'	C3'	1.317(6)
F5	C3	1.317(6)	F5'	C3'	1.312(6)
O1	C1	1.392(5)	O1'	C1'	1.378(6)
O2	C23	1.140(6)	O2'	C23'	1.121(7)
O3	C24	1.155(7)	O3'	C24'	1.149(6)
O4	C25	1.155(6)	O4'	C25'	1.145(6)
O5	C26	1.143(6)	O5'	C26'	1.131(7)
O6	C27	1.143(6)	O6'	C27'	1.136(6)
C1	C2	1.501(7)	C1'	C2'	1.519(8)
C1	C3	1.304(7)	C1'	C3'	1.309(7)
C4	C5	1.540(6)	C4'	C5'	1.540(6)
C4	C11	1.536(6)	C4'	C11'	1.545(6)
C4	C17	1.542(6)	C4'	C17'	1.543(6)
C5	C6	1.391(6)	C5'	C6'	1.396(7)
C5	C10	1.404(6)	C5'	C10'	1.394(7)
C6	C7	1.384(7)	C6'	C7'	1.390(7)
C7	C8	1.375(8)	C7'	C8'	1.389(8)
C8	C9	1.387(7)	C8'	C9'	1.376(8)
C9	C10	1.383(7)	C9'	C10'	1.390(7)
C11	C12	1.398(6)	C11'	C12'	1.384(7)
C11	C16	1.412(7)	C11'	C16'	1.390(7)
C12	C13	1.389(7)	C12'	C13'	1.394(7)
C13	C14	1.387(7)	C13'	C14'	1.376(7)
C14	C15	1.385(7)	C14'	C15'	1.375(7)
C15	C16	1.377(7)	C15'	C16'	1.381(7)
C17	C18	1.402(7)	C17'	C18'	1.408(7)
C17	C22	1.394(7)	C17'	C22'	1.389(7)
C18	C19	1.397(7)	C18'	C19'	1.392(7)
C19	C20	1.376(8)	C19'	C20'	1.390(7)
C20	C21	1.385(8)	C20'	C21'	1.380(7)
C21	C22	1.388(7)	C21'	C22'	1.391(7)

Table 3 Bond Angles for 33.

Atom	Atom	Atom	Angle/˚	Atom	Atom	Atom	Angle/˚
C23	W	P	175.03(16)	C23'	W'	P'	177.25(18)
C23	W	C24	89.8(2)	C23'	W'	C24'	87.0(2)
C23	W	C25	85.9(2)	C23'	W'	C25'	83.9(2)
C23	W	C26	87.8(2)	C23'	W'	C26'	90.8(2)
C23	W	C27	86.9(2)	C23'	W'	C27'	85.4(2)
C24	W	P	86.54(15)	C24'	W'	P'	95.34(15)
C24	W	C26	175.7(2)	C24'	W'	C26'	176.9(2)
C24	W	C27	92.1(2)	C24'	W'	C27'	90.6(2)
C25	W	P	97.38(14)	C25'	W'	P'	97.54(14)
C25	W	C24	88.8(2)	C25'	W'	C24'	88.8(2)
C25	W	C26	87.5(2)	C25'	W'	C26'	88.7(2)
C25	W	C27	172.7(2)	C25'	W'	C27'	169.4(2)
C26	W	P	96.10(15)	C26'	W'	P'	86.93(15)
C27	W	P	89.91(15)	C27'	W'	P'	93.10(15)
C27	W	C26	91.3(2)	C27'	W'	C26'	91.4(2)
Cl	P	W	110.23(6)	Cl'	P'	W'	111.35(6)
O1	P	W	119.55(13)	O1'	P'	W'	119.83(13)
O1	P	Cl	99.74(13)	O1'	P'	Cl'	99.52(14)
O1	P	C4	94.83(18)	O1'	P'	C4'	95.22(18)
C4	P	W	126.08(15)	C4'	P'	W'	124.05(14)
C4	P	Cl	102.22(15)	C4'	P'	Cl'	102.94(15)
C1	O1	P	127.4(3)	C1'	O1'	P'	123.1(4)
O1	C1	C2	113.9(4)	O1'	C1'	C2'	115.5(4)
C3	C1	O1	118.3(5)	C3'	C1'	O1'	118.9(5)
C3	C1	C2	125.3(5)	C3'	C1'	C2'	122.3(5)
F1	C2	C1	111.3(4)	F1'	C2'	C1'	110.8(5)
F2	C2	F1	107.6(4)	F2'	C2'	F1'	108.0(5)
F2	C2	F3	107.6(4)	F2'	C2'	F3'	108.4(5)
F2	C2	C1	111.9(4)	F2'	C2'	C1'	114.0(5)
F3	C2	F1	106.1(4)	F3'	C2'	F1'	105.4(5)
F3	C2	C1	112.0(4)	F3'	C2'	C1'	109.9(5)
F4	C3	F5	111.2(4)	F5'	C3'	F4'	110.3(4)
F4	C3	C1	124.1(5)	C1'	C3'	F4'	123.0(5)
C1	C3	F5	124.6(5)	C1'	C3'	F5'	126.5(5)
C5	C4	P	107.7(3)	C5'	C4'	P'	106.7(3)
C5	C4	C17	111.5(4)	C5'	C4'	C11'	112.7(4)
C11	C4	P	113.4(3)	C5'	C4'	C17'	108.5(4)
C11	C4	C5	109.2(4)	C11'	C4'	P'	103.1(3)
C11	C4	C17	112.1(4)	C17'	C4'	P'	114.7(3)
C17	C4	P	102.8(3)	C17'	C4'	C11'	111.1(4)
C6	C5	C4	121.1(4)	C6'	C5'	C4'	121.2(4)
C6	C5	C10	118.1(4)	C10'	C5'	C4'	120.3(4)
C10	C5	C4	120.6(4)	C10'	C5'	C6'	118.1(4)
C7	C6	C5	120.8(5)	C7'	C6'	C5'	120.8(5)

C8	C7	C6	120.9(5)	C8'	C7'	C6'	120.1(5)
C7	C8	C9	119.1(5)	C9'	C8'	C7'	119.6(5)
C10	C9	C8	120.7(5)	C8'	C9'	C10'	120.4(5)
C9	C10	C5	120.4(5)	C9'	C10'	C5'	120.9(5)
C12	C11	C4	120.5(4)	C12'	C11'	C4'	120.1(4)
C12	C11	C16	116.6(4)	C12'	C11'	C16'	117.9(4)
C16	C11	C4	122.8(4)	C16'	C11'	C4'	122.0(4)
C13	C12	C11	121.7(5)	C11'	C12'	C13'	121.2(5)
C14	C13	C12	120.7(5)	C14'	C13'	C12'	120.1(5)
C15	C14	C13	118.4(5)	C15'	C14'	C13'	118.9(5)
C16	C15	C14	121.3(5)	C14'	C15'	C16'	121.3(5)
C15	C16	C11	121.3(5)	C15'	C16'	C11'	120.5(5)
C18	C17	C4	122.4(4)	C18'	C17'	C4'	122.6(4)
C22	C17	C4	119.6(4)	C22'	C17'	C4'	119.6(4)
C22	C17	C18	117.9(4)	C22'	C17'	C18'	117.5(4)
C19	C18	C17	120.8(5)	C19'	C18'	C17'	121.2(5)
C20	C19	C18	119.7(5)	C20'	C19'	C18'	119.7(5)
C19	C20	C21	120.6(5)	C21'	C20'	C19'	119.9(4)
C20	C21	C22	119.6(5)	C20'	C21'	C22'	120.1(5)
C21	C22	C17	121.4(5)	C17'	C22'	C21'	121.6(5)
O2	C23	W	179.5(5)	O2'	C23'	W'	178.8(5)
O3	C24	W	177.4(5)	O3'	C24'	W'	176.4(5)
O4	C25	W	173.3(4)	O4'	C25'	W'	172.4(4)
O5	C26	W	174.8(5)	O5'	C26'	W'	178.5(5)
O6	C27	W	176.1(5)	O6'	C27'	W'	173.9(5)

Table 4 Torsion Angles for 33.

A	B	C	D	Angle/˚	A	B	C	D	Angle/˚
W	P	O1	C1	-30.5(4)	W'	P'	O1'	C1'	31.2(4)
Cl	P	O1	C1	89.5(4)	Cl'	P'	O1'	C1'	-90.3(4)
P	O1	C1	C2	-94.8(5)	P'	O1'	C1'	C2'	95.5(5)
P	O1	C1	C3	102.0(5)	P'	O1'	C1'	C3'	-104.2(6)
P	C4	C5	C6	46.7(5)	P'	C4'	C5'	C6'	137.2(4)
P	C4	C5	C10	-138.8(4)	P'	C4'	C5'	C10'	-50.2(5)
P	C4	C11	C12	-140.4(4)	P'	C4'	C11'	C12'	-67.2(5)
P	C4	C11	C16	43.5(5)	P'	C4'	C11'	C16'	110.0(4)
P	C4	C17	C18	-112.7(4)	P'	C4'	C17'	C18'	-40.3(5)
P	C4	C17	C22	65.0(5)	P'	C4'	C17'	C22'	145.3(4)
O1	C1	C2	F1	-46.1(6)	O1'	C1'	C2'	F1'	37.5(7)
O1	C1	C2	F2	-166.6(4)	O1'	C1'	C2'	F2'	159.5(5)
O1	C1	C2	F3	72.5(6)	O1'	C1'	C2'	F3'	-78.6(6)
O1	C1	C3	F4	-10.6(8)	O1'	C1'	C3'	F4'	11.4(9)
O1	C1	C3	F5	171.9(4)	O1'	C1'	C3'	F5'	-174.5(5)
C2	C1	C3	F4	-171.7(5)	C2'	C1'	C3'	F4'	170.3(5)
C2	C1	C3	F5	10.8(9)	C2'	C1'	C3'	F5'	-15.6(10)

C3	C1	C2	F1	115.7(6)	C3'	C1'	C2'	F1'	-122.1(7)
C3	C1	C2	F2	-4.8(8)	C3'	C1'	C2'	F2'	0.0(9)
C3	C1	C2	F3	-125.7(6)	C3'	C1'	C2'	F3'	121.9(6)
C4	P	O1	C1	-167.2(4)	C4'	P'	O1'	C1'	165.6(4)
C4	C5	C6	C7	175.2(4)	C4'	C5'	C6'	C7'	174.6(4)
C4	C5	C10	C9	-175.4(4)	C4'	C5'	C10'	C9'	-175.5(4)
C4	C11	C12	C13	-178.0(4)	C4'	C11'	C12'	C13'	176.2(4)
C4	C11	C16	C15	178.6(4)	C4'	C11'	C16'	C15'	-175.5(5)
C4	C17	C18	C19	175.7(4)	C4'	C17'	C18'	C19'	-176.4(4)
C4	C17	C22	C21	-177.2(4)	C4'	C17'	C22'	C21'	176.2(4)
C5	C4	C11	C12	-20.3(6)	C5'	C4'	C11'	C12'	47.5(6)
C5	C4	C11	C16	163.6(4)	C5'	C4'	C11'	C16'	-135.3(5)
C5	C4	C17	C18	132.2(4)	C5'	C4'	C17'	C18'	-159.5(4)
C5	C4	C17	C22	-50.1(6)	C5'	C4'	C17'	C22'	26.1(6)
C5	C6	C7	C8	0.6(7)	C5'	C6'	C7'	C8'	0.2(7)
C6	C5	C10	C9	-0.7(7)	C6'	C5'	C10'	C9'	-2.7(7)
C6	C7	C8	C9	-1.7(8)	C6'	C7'	C8'	C9'	-1.4(7)
C7	C8	C9	C10	1.6(8)	C7'	C8'	C9'	C10'	0.6(8)
C8	C9	C10	C5	-0.4(7)	C8'	C9'	C10'	C5'	1.4(7)
C10	C5	C6	C7	0.6(7)	C10'	C5'	C6'	C7'	1.9(7)
C11	C4	C5	C6	-76.9(5)	C11'	C4'	C5'	C6'	24.8(6)
C11	C4	C5	C10	97.6(5)	C11'	C4'	C5'	C10'	-162.6(4)
C11	C4	C17	C18	9.4(6)	C11'	C4'	C17'	C18'	76.1(5)
C11	C4	C17	C22	-172.9(4)	C11'	C4'	C17'	C22'	-98.3(5)
C11	C12	C13	C14	0.8(7)	C11'	C12'	C13'	C14'	0.0(7)
C12	C11	C16	C15	2.3(7)	C12'	C11'	C16'	C15'	1.7(7)
C12	C13	C14	C15	-0.7(7)	C12'	C13'	C14'	C15'	0.6(7)
C13	C14	C15	C16	1.4(7)	C13'	C14'	C15'	C16'	0.0(8)
C14	C15	C16	C11	-2.3(8)	C14'	C15'	C16'	C11'	-1.2(8)
C16	C11	C12	C13	-1.6(7)	C16'	C11'	C12'	C13'	-1.2(7)
C17	C4	C5	C6	158.7(4)	C17'	C4'	C5'	C6'	-98.7(5)
C17	C4	C5	C10	-26.8(6)	C17'	C4'	C5'	C10'	73.9(5)
C17	C4	C11	C12	103.8(5)	C17'	C4'	C11'	C12'	169.5(4)
C17	C4	C11	C16	-72.4(5)	C17'	C4'	C11'	C16'	-13.3(6)
C17	C18	C19	C20	2.9(8)	C17'	C18'	C19'	C20'	1.3(7)
C18	C17	C22	C21	0.6(7)	C18'	C17'	C22'	C21'	1.6(7)
C18	C19	C20	C21	-2.2(8)	C18'	C19'	C20'	C21'	-0.3(7)
C19	C20	C21	C22	0.8(7)	C19'	C20'	C21'	C22'	-0.1(7)
C20	C21	C22	C17	0.0(7)	C20'	C21'	C22'	C17'	-0.6(7)
C22	C17	C18	C19	-2.1(7)	C22'	C17'	C18'	C19'	-1.9(7)

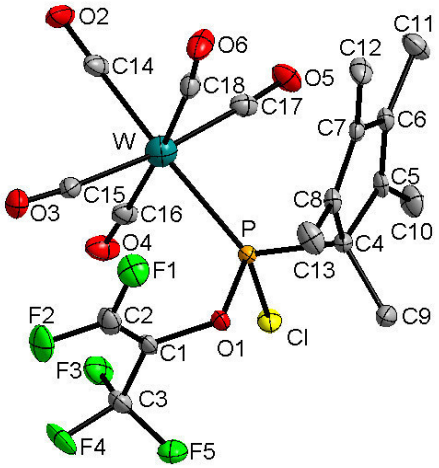

Table 1 Crystal data and structure refinement for 34.

Identification code	GSTR402
Empirical formula	$C_{18}H_{15}O_6F_5PClW$
Formula weight	672.97
Temperature/K	100
Crystal system	monoclinic
Space group	C2/c
a/Å	18.4900(10)
b/Å	14.6863(8)
c/Å	17.1298(10)
α/°	90
β/°	107.5984(15)
γ/°	90
Volume/Å^3	4433.9(4)
Z	8
ρ_{calc}g/cm^3	2.015
μ/mm^{-1}	5.477
F(000)	2576.0
Crystal size/mm^3	0.25 × 0.24 × 0.12
Tmin; Tmax	0.3086; 0.7460
Radiation	MoKα (λ = 0.71073)
2Θ range for data collection/°	6.084 to 55.994°
Completeness to theta	0.997
Index ranges	-21 ≤ h ≤ 24, -18 ≤ k ≤ 19, -22 ≤ l ≤ 22
Reflections collected	17104
Independent reflections	5353 [R_{int} = 0.0314, R_{sigma} = 0.0287]
Data/restraints/parameters	5353/0/294
Goodness-of-fit on F^2	1.031
Final R indexes [I>=2σ (I)]	R_1 = 0.0206, wR_2 = 0.0521
Final R indexes [all data]	R_1 = 0.0225, wR_2 = 0.0530
Largest diff. peak/hole / e Å^{-3}	1.93/-1.12

Table 2 Bond Lengths for 34.

Atom	Atom	Length/Å	Atom	Atom	Length/Å
W	P	2.4795(6)	O3	C15	1.138(3)
W	C14	2.016(3)	O4	C16	1.143(3)
W	C15	2.047(3)	O5	C17	1.137(3)
W	C16	2.056(3)	O6	C18	1.139(3)
W	C17	2.047(3)	C1	C2	1.310(4)
W	C18	2.051(3)	C1	C3	1.502(3)
Cl	P	2.0749(8)	C4	C5	1.520(3)
P	O1	1.6568(17)	C4	C8	1.522(3)
P	C4	1.862(2)	C4	C9	1.534(3)
F1	C2	1.315(3)	C5	C6	1.352(4)
F2	C2	1.312(3)	C5	C10	1.500(3)
F3	C3	1.343(3)	C6	C7	1.466(3)
F4	C3	1.331(3)	C6	C11	1.497(3)
F5	C3	1.325(3)	C7	C8	1.354(3)
O1	C1	1.377(3)	C7	C12	1.502(3)
O2	C14	1.146(3)	C8	C13	1.493(3)

Table 3 Bond Angles for 34.

Atom	Atom	Atom	Angle/˚	Atom	Atom	Atom	Angle/˚
C14	W	P	175.44(8)	F4	C3	F3	106.4(2)
C14	W	C15	86.65(11)	F4	C3	C1	111.7(2)
C14	W	C16	89.82(11)	F5	C3	F3	107.1(2)
C14	W	C17	86.54(11)	F5	C3	F4	107.9(2)
C14	W	C18	86.85(11)	F5	C3	C1	111.6(2)
C15	W	P	97.67(7)	C5	C4	P	105.64(15)
C15	W	C16	88.66(10)	C5	C4	C8	103.36(19)
C15	W	C18	88.94(10)	C5	C4	C9	114.9(2)
C16	W	P	88.81(7)	C8	C4	P	105.22(15)
C17	W	P	89.12(7)	C8	C4	C9	113.2(2)
C17	W	C15	173.15(10)	C9	C4	P	113.50(16)
C17	W	C16	90.64(10)	C6	C5	C4	108.5(2)
C17	W	C18	91.36(10)	C6	C5	C10	127.4(2)
C18	W	P	94.67(7)	C10	C5	C4	123.9(2)
C18	W	C16	176.01(10)	C5	C6	C7	109.7(2)
Cl	P	W	110.41(3)	C5	C6	C11	127.6(2)
O1	P	W	120.26(7)	C7	C6	C11	122.7(2)
O1	P	Cl	98.90(7)	C6	C7	C12	123.6(2)
O1	P	C4	96.64(9)	C8	C7	C6	110.1(2)
C4	P	W	125.25(7)	C8	C7	C12	126.1(2)
C4	P	Cl	100.94(8)	C7	C8	C4	108.1(2)
C1	O1	P	124.91(15)	C7	C8	C13	127.0(2)
O1	C1	C3	116.6(2)	C13	C8	C4	124.1(2)

C2	C1	O1	119.3(2)	O2	C14	W	179.1(2)
C2	C1	C3	123.9(2)	O3	C15	W	175.0(2)
F2	C2	F1	110.6(2)	O4	C16	W	178.1(2)
C1	C2	F1	123.8(2)	O5	C17	W	175.9(2)
C1	C2	F2	125.6(3)	O6	C18	W	173.4(2)
F3	C3	C1	111.7(2)				

Table 4 Torsion Angles for 34.

A	B	C	D	Angle/˚	A	B	C	D	Angle/˚
W	P	O1	C1	-29.7(2)	C2	C1	C3	F5	136.6(3)
W	P	C4	C5	47.84(18)	C3	C1	C2	F1	179.6(2)
W	P	C4	C8	-61.11(17)	C3	C1	C2	F2	0.0(4)
W	P	C4	C9	174.56(14)	C4	P	O1	C1	-167.47(19)
Cl	P	O1	C1	90.31(18)	C4	C5	C6	C7	-3.4(3)
Cl	P	C4	C5	-77.01(15)	C4	C5	C6	C11	177.7(2)
Cl	P	C4	C8	174.03(14)	C5	C4	C8	C7	-2.8(2)
Cl	P	C4	C9	49.70(18)	C5	C4	C8	C13	168.0(2)
P	O1	C1	C2	101.5(3)	C5	C6	C7	C8	1.6(3)
P	O1	C1	C3	-83.3(2)	C5	C6	C7	C12	-174.1(2)
P	C4	C5	C6	-106.51(18)	C6	C7	C8	C4	0.9(3)
P	C4	C5	C10	77.8(2)	C6	C7	C8	C13	-169.5(2)
P	C4	C8	C7	107.80(18)	C8	C4	C5	C6	3.8(2)
P	C4	C8	C13	-81.4(2)	C8	C4	C5	C10	-171.9(2)
O1	P	C4	C5	-177.45(15)	C9	C4	C5	C6	127.6(2)
O1	P	C4	C8	73.59(16)	C9	C4	C5	C10	-48.1(3)
O1	P	C4	C9	-50.73(19)	C9	C4	C8	C7	-127.7(2)
O1	C1	C2	F1	-5.5(4)	C9	C4	C8	C13	43.1(3)
O1	C1	C2	F2	174.9(2)	C10	C5	C6	C7	172.1(2)
O1	C1	C3	F3	81.5(3)	C10	C5	C6	C11	-6.8(4)
O1	C1	C3	F4	-159.4(2)	C11	C6	C7	C8	-179.5(2)
O1	C1	C3	F5	-38.4(3)	C11	C6	C7	C12	4.9(4)
C2	C1	C3	F3	-103.5(3)	C12	C7	C8	C4	176.5(2)
C2	C1	C3	F4	15.6(4)	C12	C7	C8	C13	6.0(4)

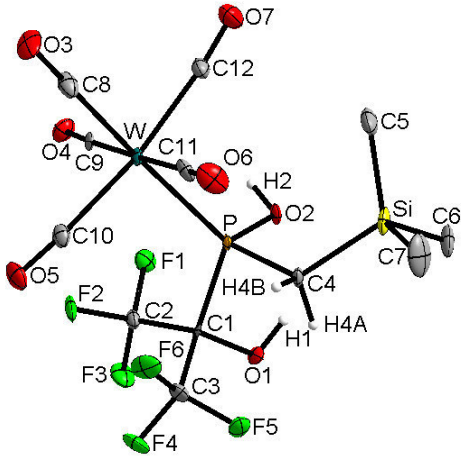

Table 1 Crystal data and structure refinement for 35.

Identification code	GSTR474
Empirical formula	$C_{12}H_{13}F_6O_7PSiW$
Formula weight	626.13
Temperature/K	100
Crystal system	monoclinic
Space group	C2/c
a/Å	18.3148(17)
b/Å	9.0555(8)
c/Å	24.691(2)
α/°	90
β/°	100.327(3)
γ/°	90
Volume/Å^3	4028.7(6)
Z	8
ρ_{calc}g/cm^3	2.065
μ/mm^{-1}	5.958
F(000)	2384.0
Crystal size/mm^3	0.24 × 0.18 × 0.16
Tmin; Tmax	0.1323; 0.7459
Radiation	MoKα (λ = 0.71073)
2Θ range for data collection/°	5.034 to 55.998°
Completeness to theta	0.999
Index ranges	-24 ≤ h ≤ 24, -11 ≤ k ≤ 11, -31 ≤ l ≤ 32
Reflections collected	52053
Independent reflections	4867 [R_{int} = 0.0692, R_{sigma} = 0.0327]
Data/restraints/parameters	4867/18/258
Goodness-of-fit on F^2	1.176
Final R indexes [I>=2σ (I)]	R_1 = 0.0353, wR_2 = 0.0774
Final R indexes [all data]	R_1 = 0.0384, wR_2 = 0.0786
Largest diff. peak/hole / e Å^{-3}	2.41/-2.07

Table 2 Bond Lengths for 35.

Atom	Atom	Length/Å	Atom	Atom	Length/Å
W	P	2.4761(12)	F2	C2	1.332(5)
W	C8	2.015(6)	F3	C2	1.333(6)
W	C9	2.031(5)	F4	C3	1.329(6)
W	C10	2.059(5)	F5	C3	1.334(6)
W	C11	2.049(5)	F6	C3	1.331(6)
W	C12	2.051(5)	O1	C1	1.416(5)
P	O2	1.625(3)	O3	C8	1.135(7)
P	C1	1.944(5)	O4	C9	1.143(6)
P	C4	1.794(5)	O5	C10	1.129(6)
Si	C4	1.907(5)	O6	C11	1.135(7)
Si	C5	1.849(6)	O7	C12	1.132(6)
Si	C6	1.848(5)	C1	C2	1.532(7)
Si	C7	1.862(6)	C1	C3	1.544(7)
F1	C2	1.346(6)			

Table 3 Bond Angles for 35.

Atom	Atom	Atom	Angle/°	Atom	Atom	Atom	Angle/°
C8	W	P	176.95(15)	C7	Si	C4	103.5(3)
C8	W	C9	90.6(2)	O1	C1	P	107.9(3)
C8	W	C10	87.5(2)	O1	C1	C2	106.3(4)
C8	W	C11	89.0(2)	O1	C1	C3	107.2(4)
C8	W	C12	85.8(2)	C2	C1	P	112.4(3)
C9	W	P	91.80(13)	C2	C1	C3	110.0(4)
C9	W	C10	89.24(19)	C3	C1	P	112.6(3)
C9	W	C11	179.00(19)	F1	C2	C1	109.9(4)
C9	W	C12	86.92(19)	F2	C2	F1	107.7(4)
C10	W	P	94.42(14)	F2	C2	F3	107.7(4)
C11	W	P	88.55(15)	F2	C2	C1	111.8(4)
C11	W	C10	91.7(2)	F3	C2	F1	106.6(4)
C11	W	C12	92.1(2)	F3	C2	C1	112.8(4)
C12	W	P	92.46(15)	F4	C3	F5	106.4(4)
C12	W	C10	172.2(2)	F4	C3	F6	107.7(4)
O2	P	W	117.49(13)	F4	C3	C1	112.8(4)
O2	P	C1	94.29(19)	F5	C3	C1	111.3(4)
O2	P	C4	99.5(2)	F6	C3	F5	107.3(5)
C1	P	W	121.71(14)	F6	C3	C1	111.1(4)
C4	P	W	119.08(17)	P	C4	Si	119.6(3)
C4	P	C1	99.8(2)	O3	C8	W	179.6(6)
C5	Si	C4	114.9(2)	O4	C9	W	177.5(4)
C5	Si	C7	110.2(3)	O5	C10	W	175.8(5)
C6	Si	C4	107.7(2)	O6	C11	W	179.5(5)
C6	Si	C5	108.8(3)	O7	C12	W	174.5(5)
C6	Si	C7	111.7(3)				

Table 4 Torsion Angles for 35.

A	B	C	D	Angle/˚	A	B	C	D	Angle/˚
W	P	C4	Si	-83.3(3)	O1	C1	C3	F5	36.3(6)
P	C1	C2	F1	46.9(5)	O1	C1	C3	F6	155.8(4)
P	C1	C2	F2	-72.7(4)	O2	P	C4	Si	45.7(3)
P	C1	C2	F3	165.7(3)	C1	P	C4	Si	141.8(3)
P	C1	C3	F4	158.3(4)	C2	C1	C3	F4	32.0(6)
P	C1	C3	F5	-82.2(5)	C2	C1	C3	F5	151.5(4)
P	C1	C3	F6	37.2(5)	C2	C1	C3	F6	-89.0(5)
O1	C1	C2	F1	-71.1(5)	C3	C1	C2	F1	173.2(4)
O1	C1	C2	F2	169.4(4)	C3	C1	C2	F2	53.7(5)
O1	C1	C2	F3	47.8(5)	C3	C1	C2	F3	-67.9(5)
O1	C1	C3	F4	-83.2(5)					

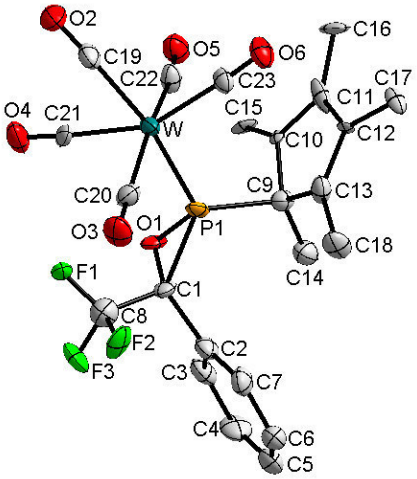

Table 1 Crystal data and structure refinement for 41.

Identification code	GSTR357
Empirical formula	$C_{23}H_{20}F_3O_6PW$
Formula weight	664.22
Temperature/K	100(2)
Crystal system	monoclinic
Space group	C2
a/Å	16.8338(11)
b/Å	13.1233(9)
c/Å	11.2064(7)
α/°	90
β/°	104.095(2)
γ/°	90
Volume/Å^3	2401.1(3)
Z	4
ρ_{calc}g/cm^3	1.837
μ/mm^{-1}	4.937
F(000)	1288
Crystal size/mm^3	0.24 × 0.18 × 0.04
Tmin; Tmax	0.3837; 0.8270
Radiation	MoKα (λ = 0.71073)
2Θ range for data collection/°	3.10 to 28.00°
Completeness to theta	0.997
Index ranges	-22 ≤ h ≤ 22, -16 ≤ k ≤ 17, -13 ≤ l ≤ 14
Reflections collected	9480
Independent reflections	5635 [R_{int} = 0.0362]
Data/restraints/parameters	5635/232/472
Goodness-of-fit on F^2	1.077
Final R indexes [I>=2σ (I)]	R_1 = 0.0293, wR_2 = 0.0716
Final R indexes [all data]	R_1 = 0.0351, wR_2 = 0.0758
Largest diff. peak/hole / e Å^{-3}	1.341/-1.361

Table 2 Bond Lengths for 41.

Atom	Atom	Length/Å	Atom	Atom	Length/Å
C19	O2	1.125(8)	C19	W	2.002(6)
C20	O3	1.146(8)	C20	W	1.995(6)
C21	O4	1.137(8)	C21	W	2.115(7)
C22	O5	1.118(9)	C22	W	1.998(8)
C23	O6	1.148(9)	C23	W	2.086(8)
O3	F1S	1.756(17)	W	P1S	2.475(7)
W	P1	2.517(7)	F3	C8	1.31(2)
F2	C8	1.389(10)	F1	C8	1.24(3)
P1	O1	1.671(18)	P1	C1	1.80(2)
P1	C9	1.91(3)	O1	C1	1.46(3)
C1	C8	1.503(10)	C1	C2	1.54(2)
C2	C3	1.3900	C2	C7	1.3900
C3	C4	1.3900	C4	C5	1.3900
C5	C6	1.3900	C6	C7	1.3900
C9	C10	1.47(3)	C9	C14	1.50(3)
C9	C13	1.54(4)	C10	C11	1.42(3)
C10	C15	1.43(3)	C11	C16	1.47(4)
C11	C12	1.49(4)	C12	C13	1.39(4)
C12	C17	1.44(3)	C13	C18	1.57(3)

Table 3 Bond Angles for 41.

Atom	Atom	Atom	Angle/˚	Atom	Atom	Atom	Angle/˚
O2	C19	W	176.6(5)	O3	C20	W	173.7(7)
O4	C21	W	176.2(6)	O5	C22	W	172.4(7)
O6	C23	W	176.3(7)	C20	O3	F1S	81.5(8)
C20	W	C22	163.4(3)	C20	W	C19	101.6(3)
C22	W	C19	90.4(3)	C20	W	C23	99.3(3)
C22	W	C23	92.2(3)	C19	W	C23	89.3(3)
C20	W	C21	95.1(3)	C22	W	C21	77.7(3)
C19	W	C21	71.5(2)	C23	W	C21	158.0(3)
C20	W	P1S	71.7(3)	C22	W	P1S	96.1(3)
C19	W	P1S	173.3(2)	C23	W	P1S	92.1(3)
C21	W	P1S	108.2(3)	C20	W	P1	89.6(3)
C22	W	P1	75.2(3)	C19	W	P1	156.2(2)
C23	W	P1	109.7(3)	C21	W	P1	86.8(2)
P1S	W	P1	27.14(7)	O1	P1	C1	49.5(10)
O1	P1	C9	105.1(10)	C1	P1	C9	113.8(10)
O1	P1	W	121.2(7)	C1	P1	W	122.8(8)
C9	P1	W	121.6(8)	C1	O1	P1	69.8(12)
O1	C1	C8	114.4(17)	O1	C1	C2	119.3(18)
C8	C1	C2	107(2)	O1	C1	P1	60.8(10)
C8	C1	P1	125.0(17)	C2	C1	P1	122.7(15)

C3	C2	C7	120.0	C3	C2	C1	115.2(14)
C7	C2	C1	124.5(14)	C2	C3	C4	120.0
C5	C4	C3	120.0	C4	C5	C6	120.0
C7	C6	C5	120.0	C6	C7	C2	120.0
F1	C8	F3	104.5(19)	F1	C8	F2	109.7(19)
F3	C8	F2	104.4(17)	F1	C8	C1	115.4(18)
F3	C8	C1	111(2)	F2	C8	C1	111(2)
C10	C9	C14	114(2)	C10	C9	C13	106(2)
C14	C9	C13	117(2)	C10	C9	P1	100.7(16)
C14	C9	P1	117.3(19)	C13	C9	P1	100.3(17)
C11	C10	C15	129(2)	C11	C10	C9	106.4(19)
C15	C10	C9	123.2(19)	C10	C11	C16	127(2)
C10	C11	C12	111(2)	C16	C11	C12	122(3)
C13	C12	C17	128(3)	C13	C12	C11	107(2)
C17	C12	C11	124(3)	C12	C13	C9	109(2)
C12	C13	C18	127(3)	C9	C13	C18	123(3)

Table 4 Torsion Angles for 41.

A	B	C	D	Angle/°	A	B	C	D	Angle/°
W	C20	O3	F1S	-175(5)	O3	C20	W	C22	160(5)
O3	C20	W	C19	-64(5)	O3	C20	W	C23	27(5)
O3	C20	W	C21	-136(5)	O3	C20	W	P1S	116(5)
O3	C20	W	P1	137(5)	O5	C22	W	C20	108(6)
O5	C22	W	C19	-29(6)	O5	C22	W	C23	-118(6)
O5	C22	W	C21	42(6)	O5	C22	W	P1S	149(6)
O5	C22	W	P1	132(6)	O2	C19	W	C20	-101(10)
O2	C19	W	C22	68(10)	O2	C19	W	C23	160(10)
O2	C19	W	C21	-9(10)	O2	C19	W	P1S	-98(10)
O2	C19	W	P1	16(10)	O6	C23	W	C20	-110(10)
O6	C23	W	C22	82(10)	O6	C23	W	C19	-8(10)
O6	C23	W	C21	21(11)	O6	C23	W	P1S	178(100)
O6	C23	W	P1	157(10)	O4	C21	W	C20	149(9)
O4	C21	W	C22	-46(9)	O4	C21	W	C19	48(9)
O4	C21	W	C23	18(9)	O4	C21	W	P1S	-139(9)
O4	C21	W	P1	-122(9)	C20	W	P1	O1	94.6(8)
C22	W	P1	O1	-78.7(8)	C19	W	P1	O1	-24.5(10)
C23	W	P1	O1	-165.7(8)	C21	W	P1	O1	-0.6(8)
P1S	W	P1	O1	142.0(11)	C20	W	P1	C1	35.5(10)
C22	W	P1	C1	-137.8(10)	C19	W	P1	C1	-83.5(11)
C23	W	P1	C1	135.2(10)	C21	W	P1	C1	-59.7(10)
P1S	W	P1	C1	82.9(12)	C20	W	P1	C9	-128.5(10)
C22	W	P1	C9	58.2(10)	C19	W	P1	C9	112.5(11)
C23	W	P1	C9	-28.7(10)	C21	W	P1	C9	136.4(10)
P1S	W	P1	C9	-81.1(11)	C9	P1	O1	C1	108.6(13)
W	P1	O1	C1	-108.4(11)	P1	O1	C1	C8	117.8(19)

P1	O1	C1	C2	-113.3(18)
W	P1	C1	O1	105.0(11)
C9	P1	C1	C8	169.3(19)
O1	P1	C1	C2	108(2)
W	P1	C1	C2	-147.2(15)
C8	C1	C2	C3	99.3(18)
O1	C1	C2	C7	152.8(15)
P1	C1	C2	C7	81(2)
C1	C2	C3	C4	-174.7(15)
C3	C4	C5	C6	0.0
C5	C6	C7	C2	0.0
C1	C2	C7	C6	174.2(17)
C2	C1	C8	F1	-172.7(18)
O1	C1	C8	F3	81(2)
P1	C1	C8	F3	151.2(19)
C2	C1	C8	F2	62(2)
O1	P1	C9	C10	87.6(15)
W	P1	C9	C10	-55.1(17)
C1	P1	C9	C14	15(2)
O1	P1	C9	C13	-164.0(15)
W	P1	C9	C13	53.2(19)
C13	C9	C10	C11	12(3)
C14	C9	C10	C15	51(3)
P1	C9	C10	C15	-76(2)
C9	C10	C11	C16	178(3)
C9	C10	C11	C12	-10(3)
C16	C11	C12	C13	177(3)
C16	C11	C12	C17	-14(4)
C11	C12	C13	C9	3(3)
C11	C12	C13	C18	175(3)
C14	C9	C13	C12	118(3)
C10	C9	C13	C18	179(2)
P1	C9	C13	C18	74(3)
C9	P1	C1	O1	-89.9(14)
O1	P1	C1	C8	-101(2)
W	P1	C1	C8	4(2)
C9	P1	C1	C2	18(2)
O1	C1	C2	C3	-33(2)
P1	C1	C2	C3	-105.0(17)
C8	C1	C2	C7	-75.1(19)
C7	C2	C3	C4	0.0
C2	C3	C4	C5	0.0
C4	C5	C6	C7	0.0
C3	C2	C7	C6	0.0
O1	C1	C8	F1	-38(3)
P1	C1	C8	F1	32(3)
C2	C1	C8	F3	-54(2)
O1	C1	C8	F2	-163.5(18)
P1	C1	C8	F2	-93(2)
C1	P1	C9	C10	139.6(15)
O1	P1	C9	C14	-37(2)
W	P1	C9	C14	-179.4(16)
C1	P1	C9	C13	-112.1(17)
C14	C9	C10	C11	-118(2)
P1	C9	C10	C11	115.7(18)
C13	C9	C10	C15	-180(2)
C15	C10	C11	C16	10(4)
C15	C10	C11	C12	-178(2)
C10	C11	C12	C13	4(3)
C10	C11	C12	C17	174(2)
C17	C12	C13	C9	-165(2)
C17	C12	C13	C18	6(5)
C10	C9	C13	C12	-9(3)
P1	C9	C13	C12	-114(2)
C14	C9	C13	C18	-53(4)

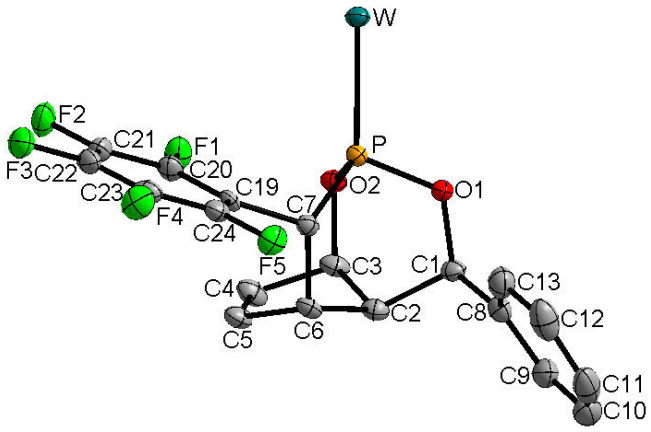

Table 1 Crystal data and structure refinement for 46.

Identification code	GSTR430
Empirical formula	$C_{29}H_{22}O_7F_5PW$
Formula weight	792.28
Temperature/K	100
Crystal system	monoclinic
Space group	$P2_1/n$
a/Å	10.5837(5)
b/Å	20.6735(9)
c/Å	13.4715(6)
α/°	90
β/°	95.6677(18)
γ/°	90
Volume/Å^3	2933.2(2)
Z	4
ρ_{calc}g/cm^3	1.794
μ/mm^{-1}	4.070
F(000)	1544.0
Crystal size/mm^3	0.18 × 0.16 × 0.12
Tmin; Tmax	0.5961; 0.7459
Radiation	MoKα (λ = 0.71073)
2Θ range for data collection/°	4.976 to 56°
Completeness to theta	0.997
Index ranges	-9 ≤ h ≤ 13, -27 ≤ k ≤ 27, -17 ≤ l ≤ 17
Reflections collected	57544
Independent reflections	7056 [R_{int} = 0.0425, R_{sigma} = 0.0262]
Data/restraints/parameters	7056/6/393
Goodness-of-fit on F^2	1.133
Final R indexes [I>=2σ (I)]	R_1 = 0.0239, wR_2 = 0.0425
Final R indexes [all data]	R_1 = 0.0366, wR_2 = 0.0482
Largest diff. peak/hole / e Å^{-3}	1.54/-0.72

Table 2 Bond Lengths for 46.

Atom	Atom	Length/Å	Atom	Atom	Length/Å
W	P	2.4345(7)	C2	C6	1.577(4)
W	C25	2.032(3)	C2	C14	1.538(4)
W	C26	2.052(3)	C3	C4	1.514(4)
W	C27	2.053(3)	C3	C15	1.511(4)
W	C28	2.037(3)	C4	C5	1.330(4)
W	C29	2.047(3)	C4	C16	1.497(4)
P	O1	1.613(2)	C5	C6	1.531(4)
P	O2	1.605(2)	C5	C17	1.511(4)
P	C7	1.855(3)	C6	C7	1.583(4)
F1	C20	1.352(3)	C6	C18	1.535(4)
F2	C21	1.343(3)	C7	C19	1.531(4)
F3	C22	1.344(3)	C8	C9	1.399(4)
F4	C23	1.341(3)	C8	C13	1.392(5)
F5	C24	1.350(3)	C9	C10	1.383(5)
O1	C1	1.459(3)	C10	C11	1.393(6)
O2	C3	1.504(3)	C11	C12	1.397(6)
O3	C25	1.143(4)	C12	C13	1.397(5)
O4	C26	1.144(4)	C19	C20	1.375(4)
O5	C27	1.142(4)	C19	C24	1.394(4)
O6	C28	1.147(3)	C20	C21	1.385(4)
O7	C29	1.143(4)	C21	C22	1.380(4)
C1	C2	1.563(4)	C22	C23	1.376(4)
C1	C8	1.521(4)	C23	C24	1.384(4)
C2	C3	1.568(4)			

Table 3 Bond Angles for 46.

Atom	Atom	Atom	Angle/˚	Atom	Atom	Atom	Angle/˚
C25	W	P	174.75(9)	C4	C5	C17	126.4(3)
C25	W	C26	89.95(12)	C17	C5	C6	122.1(3)
C25	W	C27	90.97(13)	C2	C6	C7	108.0(2)
C25	W	C28	90.93(12)	C5	C6	C2	100.4(2)
C25	W	C29	91.68(13)	C5	C6	C7	109.2(2)
C26	W	P	95.30(8)	C5	C6	C18	113.8(2)
C26	W	C27	93.17(12)	C18	C6	C2	115.4(2)
C27	W	P	88.61(8)	C18	C6	C7	109.4(2)
C28	W	P	83.82(8)	C6	C7	P	109.99(18)
C28	W	C26	179.06(12)	C19	C7	P	116.84(18)
C28	W	C27	86.50(11)	C19	C7	C6	115.0(2)
C28	W	C29	91.15(12)	C9	C8	C1	119.2(3)
C29	W	P	88.54(9)	C13	C8	C1	122.6(3)
C29	W	C26	89.14(13)	C13	C8	C9	118.2(3)
C29	W	C27	176.49(12)	C10	C9	C8	121.2(3)
O1	P	W	110.83(7)	C9	C10	C11	119.9(3)

O1	P	C7	96.76(11)
O2	P	W	113.83(8)
O2	P	O1	102.14(11)
O2	P	C7	105.19(11)
C7	P	W	124.73(9)
C1	O1	P	117.19(17)
C3	O2	P	117.09(16)
O1	C1	C2	111.6(2)
O1	C1	C8	107.9(2)
C8	C1	C2	116.3(2)
C1	C2	C3	111.0(2)
C1	C2	C6	117.1(2)
C3	C2	C6	100.1(2)
C14	C2	C1	108.7(2)
C14	C2	C3	109.2(2)
C14	C2	C6	110.3(2)
O2	C3	C2	109.5(2)
O2	C3	C4	106.2(2)
O2	C3	C15	104.7(2)
C4	C3	C2	102.4(2)
C15	C3	C2	117.0(3)
C15	C3	C4	116.6(3)
C5	C4	C3	110.1(3)
C5	C4	C16	129.2(3)
C16	C4	C3	120.6(3)
C4	C5	C6	111.5(3)
C10	C11	C12	120.1(3)
C11	C12	C13	119.1(4)
C8	C13	C12	121.5(3)
C20	C19	C7	125.2(2)
C20	C19	C24	115.9(3)
C24	C19	C7	118.9(2)
F1	C20	C19	120.8(3)
F1	C20	C21	116.6(3)
C19	C20	C21	122.7(3)
F2	C21	C20	120.7(3)
F2	C21	C22	119.5(3)
C22	C21	C20	119.8(3)
F3	C22	C21	119.9(3)
F3	C22	C23	120.7(3)
C23	C22	C21	119.5(3)
F4	C23	C22	120.3(3)
F4	C23	C24	120.4(3)
C22	C23	C24	119.3(3)
F5	C24	C19	120.3(3)
F5	C24	C23	116.9(3)
C23	C24	C19	122.8(3)
O3	C25	W	178.0(3)
O4	C26	W	178.1(3)
O5	C27	W	176.5(2)
O6	C28	W	178.6(3)
O7	C29	W	179.0(3)

Table 4 Torsion Angles for 46.

A	B	C	D	Angle/˚
W	P	O1	C1	-170.29(16)
W	P	O2	C3	177.70(16)
W	P	C7	C6	171.37(14)
W	P	C7	C19	37.8(2)
P	O1	C1	C2	-4.9(3)
P	O1	C1	C8	-133.9(2)
P	O2	C3	C2	-11.5(3)
P	O2	C3	C4	98.4(2)
P	O2	C3	C15	-137.7(2)
P	C7	C19	C20	47.1(3)
P	C7	C19	C24	-132.5(2)
F1	C20	C21	F2	1.2(4)
F1	C20	C21	C22	-178.4(3)
F2	C21	C22	F3	-0.2(4)
F2	C21	C22	C23	-179.8(3)
F3	C22	C23	F4	-1.0(4)
C4	C5	C6	C7	88.3(3)
C4	C5	C6	C18	-149.1(3)
C5	C6	C7	P	-88.1(2)
C5	C6	C7	C19	46.3(3)
C6	C2	C3	O2	76.1(2)
C6	C2	C3	C4	-36.3(3)
C6	C2	C3	C15	-165.1(2)
C6	C7	C19	C20	-84.1(3)
C6	C7	C19	C24	96.2(3)
C7	P	O1	C1	58.5(2)
C7	P	O2	C3	-42.4(2)
C7	C19	C20	F1	-2.1(4)
C7	C19	C20	C21	177.9(3)
C7	C19	C24	F5	1.3(4)
C7	C19	C24	C23	-178.4(3)
C8	C1	C2	C3	-177.6(2)

F3	C22	C23	C24	-180.0(3)	C8	C1	C2	C6	68.3(3)
F4	C23	C24	F5	0.7(4)	C8	C1	C2	C14	-57.5(3)
F4	C23	C24	C19	-179.6(3)	C8	C9	C10	C11	-1.7(5)
O1	P	O2	C3	58.2(2)	C9	C8	C13	C12	-2.9(5)
O1	P	C7	C6	-67.43(19)	C9	C10	C11	C12	-1.2(5)
O1	P	C7	C19	159.0(2)	C10	C11	C12	C13	2.0(5)
O1	C1	C2	C3	58.0(3)	C11	C12	C13	C8	0.1(5)
O1	C1	C2	C6	-56.1(3)	C13	C8	C9	C10	3.7(5)
O1	C1	C2	C14	178.1(2)	C14	C2	C3	O2	-168.1(2)
O1	C1	C8	C9	-153.3(3)	C14	C2	C3	C4	79.6(3)
O1	C1	C8	C13	24.2(4)	C14	C2	C3	C15	-49.2(3)
O2	P	O1	C1	-48.7(2)	C14	C2	C6	C5	-78.5(3)
O2	P	C7	C6	37.1(2)	C14	C2	C6	C7	167.1(2)
O2	P	C7	C19	-96.4(2)	C14	C2	C6	C18	44.3(3)
O2	C3	C4	C5	-91.9(3)	C15	C3	C4	C5	151.9(3)
O2	C3	C4	C16	84.8(3)	C15	C3	C4	C16	-31.3(4)
C1	C2	C3	O2	-48.3(3)	C16	C4	C5	C6	-174.7(3)
C1	C2	C3	C4	-160.7(2)	C16	C4	C5	C17	5.8(6)
C1	C2	C3	C15	70.5(3)	C17	C5	C6	C2	154.4(3)
C1	C2	C6	C5	156.4(2)	C17	C5	C6	C7	-92.2(3)
C1	C2	C6	C7	42.1(3)	C17	C5	C6	C18	30.4(4)
C1	C2	C6	C18	-80.7(3)	C18	C6	C7	P	146.7(2)
C1	C8	C9	C10	-178.7(3)	C18	C6	C7	C19	-78.9(3)
C1	C8	C13	C12	179.6(3)	C19	C20	C21	F2	-178.7(3)
C2	C1	C8	C9	80.5(3)	C19	C20	C21	C22	1.6(5)
C2	C1	C8	C13	-102.1(3)	C20	C19	C24	F5	-178.4(2)
C2	C3	C4	C5	22.9(3)	C20	C19	C24	C23	2.0(4)
C2	C3	C4	C16	-160.4(3)	C20	C21	C22	F3	179.5(3)
C2	C6	C7	P	20.3(3)	C20	C21	C22	C23	-0.1(5)
C2	C6	C7	C19	154.7(2)	C21	C22	C23	F4	178.6(3)
C3	C2	C6	C5	36.4(2)	C21	C22	C23	C24	-0.4(4)
C3	C2	C6	C7	-77.9(2)	C22	C23	C24	F5	179.8(3)
C3	C2	C6	C18	159.3(2)	C22	C23	C24	C19	-0.6(4)
C3	C4	C5	C6	1.6(4)	C24	C19	C20	F1	177.6(2)
C3	C4	C5	C17	-177.8(3)	C24	C19	C20	C21	-2.5(4)
C4	C5	C6	C2	-25.1(3)					

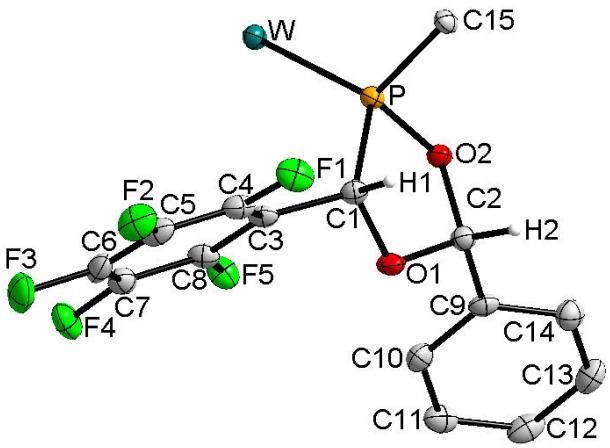

Table 1 Crystal data and structure refinement for 53.

Identification code	GSTR404
Empirical formula	$C_{38}H_{22}F_5O_7PW$
Formula weight	900.05
Temperature/K	100
Crystal system	monoclinic
Space group	$P2_1/n$
a/Å	16.1853(7)
b/Å	10.7821(5)
c/Å	20.0125(8)
α/°	90
β/°	108.6688(12)
γ/°	90
Volume/Å^3	3308.7(2)
Z	4
ρ_{calc}g/cm^3	1.808
μ/mm^{-1}	3.620
F(000)	1760.0
Crystal size/mm^3	0.11 × 0.06 × 0.05
Tmin; Tmax	0.5538; 0.7460
Radiation	MoKα (λ = 0.71073)
2Θ range for data collection/°	6.81 to 56°
Completeness to theta	0.995
Index ranges	-20 ≤ h ≤ 21, -11 ≤ k ≤ 14, -26 ≤ l ≤ 16
Reflections collected	18749
Independent reflections	7951 [R_{int} = 0.0235, R_{sigma} = 0.0325]
Data/restraints/parameters	7951/0/469
Goodness-of-fit on F^2	1.036
Final R indexes [I>=2σ (I)]	R_1 = 0.0259, wR_2 = 0.0536
Final R indexes [all data]	R_1 = 0.0333, wR_2 = 0.0558
Largest diff. peak/hole / e Å^{-3}	1.02/-0.61

Table 2 Bond Lengths for 53.

Atom	Atom	Length/Å	Atom	Atom	Length/Å
W	P	2.5230(7)	C7	C8	1.383(4)
W	C34	2.016(3)	C9	C10	1.386(4)
W	C35	2.043(3)	C9	C14	1.396(4)
W	C36	2.048(3)	C10	C11	1.378(4)
W	C37	2.043(3)	C11	C12	1.386(4)
W	C38	2.052(3)	C12	C13	1.383(4)
P	O2	1.632(2)	C13	C14	1.384(4)
P	C1	1.916(3)	C15	C16	1.545(4)
P	C15	1.949(3)	C15	C22	1.548(4)
F1	C4	1.338(3)	C15	C28	1.545(4)
F2	C5	1.340(3)	C16	C17	1.406(4)
F3	C6	1.341(3)	C16	C21	1.392(4)
F4	C7	1.340(3)	C17	C18	1.402(4)
F5	C8	1.338(3)	C18	C19	1.374(5)
O1	C1	1.426(3)	C19	C20	1.385(5)
O1	C2	1.404(3)	C20	C21	1.394(4)
O2	C2	1.474(3)	C22	C23	1.389(4)
O3	C34	1.140(4)	C22	C27	1.401(4)
O4	C35	1.143(4)	C23	C24	1.393(4)
O5	C36	1.140(3)	C24	C25	1.394(5)
O6	C37	1.141(4)	C25	C26	1.384(5)
O7	C38	1.139(3)	C26	C27	1.388(4)
C1	C3	1.510(4)	C28	C29	1.408(4)
C2	C9	1.493(4)	C28	C33	1.399(4)
C3	C4	1.390(4)	C29	C30	1.384(4)
C3	C8	1.384(4)	C30	C31	1.388(5)
C4	C5	1.381(4)	C31	C32	1.383(5)
C5	C6	1.376(4)	C32	C33	1.381(4)
C6	C7	1.372(5)			

Table 3 Bond Angles for 53.

Atom	Atom	Atom	Angle/˚	Atom	Atom	Atom	Angle/˚
C34	W	P	178.79(8)	F5	C8	C7	116.7(3)
C34	W	C35	86.50(12)	C7	C8	C3	122.6(3)
C34	W	C36	89.95(11)	C10	C9	C2	121.6(3)
C34	W	C37	89.19(12)	C10	C9	C14	119.5(3)
C34	W	C38	87.72(11)	C14	C9	C2	118.9(3)
C35	W	P	92.66(8)	C11	C10	C9	120.3(3)
C35	W	C36	95.88(11)	C10	C11	C12	120.0(3)
C35	W	C38	89.43(11)	C13	C12	C11	120.3(3)
C36	W	P	89.28(8)	C12	C13	C14	119.7(3)
C36	W	C38	174.06(11)	C13	C14	C9	120.2(3)
C37	W	P	91.63(8)	C16	C15	P	108.31(18)

C37	W	C35	175.25(11)	C16	C15	C22	111.2(2)
C37	W	C36	82.12(11)	C16	C15	C28	111.6(2)
C37	W	C38	92.38(12)	C22	C15	P	107.44(18)
C38	W	P	93.14(7)	C28	C15	P	108.42(17)
O2	P	W	109.80(8)	C28	C15	C22	109.8(2)
O2	P	C1	90.65(11)	C17	C16	C15	121.5(3)
O2	P	C15	104.82(11)	C21	C16	C15	121.4(3)
C1	P	W	123.45(9)	C21	C16	C17	117.1(3)
C1	P	C15	101.22(12)	C18	C17	C16	121.1(3)
C15	P	W	121.51(8)	C19	C18	C17	120.5(3)
C2	O1	C1	110.8(2)	C18	C19	C20	119.4(3)
C2	O2	P	113.52(16)	C19	C20	C21	120.4(3)
O1	C1	P	103.19(17)	C16	C21	C20	121.6(3)
O1	C1	C3	108.0(2)	C23	C22	C15	121.5(3)
C3	C1	P	120.03(18)	C23	C22	C27	117.4(3)
O1	C2	O2	106.1(2)	C27	C22	C15	121.2(3)
O1	C2	C9	110.1(2)	C22	C23	C24	122.0(3)
O2	C2	C9	110.0(2)	C23	C24	C25	119.6(3)
C4	C3	C1	119.9(3)	C26	C25	C24	119.2(3)
C8	C3	C1	123.9(3)	C25	C26	C27	120.7(3)
C8	C3	C4	115.9(3)	C26	C27	C22	121.1(3)
F1	C4	C3	119.5(3)	C29	C28	C15	120.1(2)
F1	C4	C5	117.7(3)	C33	C28	C15	122.1(2)
C5	C4	C3	122.8(3)	C33	C28	C29	117.6(3)
F2	C5	C4	120.5(3)	C30	C29	C28	120.7(3)
F2	C5	C6	120.4(3)	C29	C30	C31	120.5(3)
C6	C5	C4	119.1(3)	C32	C31	C30	119.4(3)
F3	C6	C5	119.9(3)	C33	C32	C31	120.4(3)
F3	C6	C7	119.9(3)	C32	C33	C28	121.4(3)
C7	C6	C5	120.2(3)	O3	C34	W	178.1(3)
F4	C7	C6	119.8(3)	O4	C35	W	176.2(2)
F4	C7	C8	120.8(3)	O5	C36	W	173.3(2)
C6	C7	C8	119.4(3)	O6	C37	W	175.2(3)
F5	C8	C3	120.7(2)	O7	C38	W	177.0(2)

Table 4 Torsion Angles for 53.

A	B	C	D	Angle/˚	A	B	C	D	Angle/˚
W	P	O2	C2	-136.15(15)	C8	C3	C4	F1	175.4(2)
P	O2	C2	O1	31.8(2)	C8	C3	C4	C5	-2.3(4)
P	O2	C2	C9	150.77(18)	C9	C10	C11	C12	-0.4(4)
P	C1	C3	C4	-114.5(3)	C10	C9	C14	C13	0.8(4)
P	C1	C3	C8	71.3(3)	C10	C11	C12	C13	0.3(4)
P	C15	C16	C17	-89.2(3)	C11	C12	C13	C14	0.3(5)
P	C15	C16	C21	88.8(3)	C12	C13	C14	C9	-0.8(4)
P	C15	C22	C23	-42.7(3)	C14	C9	C10	C11	-0.2(4)

P	C15	C22	C27	137.0(2)	C15	P	O2	C2	91.79(18)
P	C15	C28	C29	159.0(2)	C15	C16	C17	C18	177.9(3)
P	C15	C28	C33	-27.2(3)	C15	C16	C21	C20	-177.6(3)
F1	C4	C5	F2	1.1(4)	C15	C22	C23	C24	178.4(2)
F1	C4	C5	C6	-177.4(2)	C15	C22	C27	C26	-178.4(3)
F2	C5	C6	F3	1.2(4)	C15	C28	C29	C30	176.0(2)
F2	C5	C6	C7	-177.1(3)	C15	C28	C33	C32	-175.9(2)
F3	C6	C7	F4	-2.0(4)	C16	C15	C22	C23	75.6(3)
F3	C6	C7	C8	-179.5(2)	C16	C15	C22	C27	-104.6(3)
F4	C7	C8	F5	0.5(4)	C16	C15	C28	C29	39.7(3)
F4	C7	C8	C3	-178.4(2)	C16	C15	C28	C33	-146.5(2)
O1	C1	C3	C4	127.8(3)	C16	C17	C18	C19	0.0(5)
O1	C1	C3	C8	-46.4(3)	C17	C16	C21	C20	0.5(4)
O1	C2	C9	C10	28.4(3)	C17	C18	C19	C20	-0.1(5)
O1	C2	C9	C14	-150.8(2)	C18	C19	C20	C21	0.4(5)
O2	C2	C9	C10	-88.1(3)	C19	C20	C21	C16	-0.6(5)
O2	C2	C9	C14	92.7(3)	C21	C16	C17	C18	-0.2(4)
C1	P	O2	C2	-9.99(18)	C22	C15	C16	C17	153.0(3)
C1	O1	C2	O2	-43.2(3)	C22	C15	C16	C21	-29.0(4)
C1	O1	C2	C9	-162.1(2)	C22	C15	C28	C29	-84.0(3)
C1	C3	C4	F1	0.8(4)	C22	C15	C28	C33	89.8(3)
C1	C3	C4	C5	-177.0(3)	C22	C23	C24	C25	0.1(4)
C1	C3	C8	F5	-1.9(4)	C23	C22	C27	C26	1.4(4)
C1	C3	C8	C7	177.0(3)	C23	C24	C25	C26	1.2(4)
C2	O1	C1	P	34.8(2)	C24	C25	C26	C27	-1.2(4)
C2	O1	C1	C3	162.9(2)	C25	C26	C27	C22	-0.1(4)
C2	C9	C10	C11	-179.4(2)	C27	C22	C23	C24	-1.4(4)
C2	C9	C14	C13	-180.0(3)	C28	C15	C16	C17	30.1(4)
C3	C4	C5	F2	178.9(2)	C28	C15	C16	C21	-151.9(3)
C3	C4	C5	C6	0.4(4)	C28	C15	C22	C23	-160.4(2)
C4	C3	C8	F5	-176.3(2)	C28	C15	C22	C27	19.3(3)
C4	C3	C8	C7	2.6(4)	C28	C29	C30	C31	-0.8(4)
C4	C5	C6	F3	179.8(2)	C29	C28	C33	C32	-2.0(4)
C4	C5	C6	C7	1.5(4)	C29	C30	C31	C32	-0.4(4)
C5	C6	C7	F4	176.3(3)	C30	C31	C32	C33	0.3(4)
C5	C6	C7	C8	-1.2(4)	C31	C32	C33	C28	0.9(4)
C6	C7	C8	F5	178.1(2)	C33	C28	C29	C30	1.9(4)
C6	C7	C8	C3	-0.9(4)					

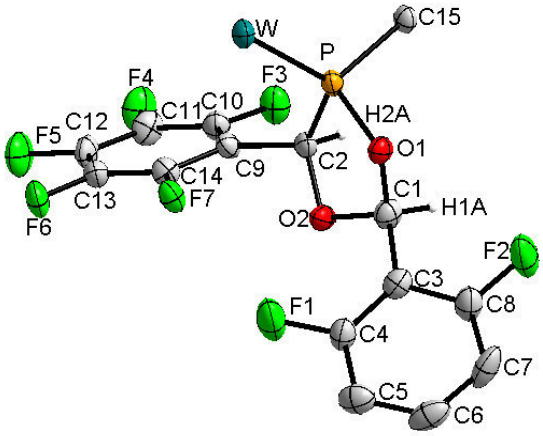

Table 1 Crystal data and structure refinement for 54.

Identification code	GSTR329
Empirical formula	$C_{38}H_{20}F_7O_7PW$
Formula weight	936.36
Temperature/K	123(2)
Crystal system	monoclinic
Space group	$P2_1/c$
a/Å	16.5400(6)
b/Å	10.6955(3)
c/Å	22.9543(8)
α/°	90
β/°	123.793(2)
γ/°	90
Volume/Å^3	3374.65(19)
Z	4
ρ_{calc}g/cm^3	1.843
μ/mm^{-1}	3.562
F(000)	1824
Crystal size/mm^3	0.18 × 0.14 × 0.04
Tmin; Tmax	0.5665; 0.8706
Radiation	MoKα (λ = 0.71073)
2Θ range for data collection/°	2.51 to 28.00°
Completeness to theta	0.993
Index ranges	-21 ≤ h ≤ 21, -14 ≤ k ≤ 14, -30 ≤ l ≤ 30
Reflections collected	44240
Independent reflections	8084 [R_{int} = 0.1087]
Data/restraints/parameters	8084/16/487
Goodness-of-fit on F^2	0.907
Final R indexes [I>=2σ (I)]	R_1 = 0.0405, wR_2 = 0.0740
Final R indexes [all data]	R_1 = 0.0936, wR_2 = 0.0853
Largest diff. peak/hole / e Å^{-3}	2.303/-2.261

Table 2 Bond Lengths for 54.

Atom	Atom	Length/Å	Atom	Atom	Length/Å
C1	O2	1.406(5)	C1	O1	1.454(6)
C1	C3	1.513(7)	C2	O2	1.437(5)
C2	C9	1.510(6)	C2	P	1.903(5)
C3	C8	1.379(7)	C3	C4	1.387(7)
C4	F1	1.352(5)	C4	C5	1.374(7)
C5	C6	1.375(8)	C6	C7	1.380(8)
C7	C8	1.375(7)	C8	F2	1.357(6)
C9	C10	1.373(7)	C9	C14	1.392(6)
C10	F3	1.356(5)	C10	C11	1.378(7)
C11	F4	1.349(5)	C11	C12	1.375(7)
C12	F5	1.349(5)	C12	C13	1.365(7)
C13	F6	1.346(5)	C13	C14	1.375(6)
C14	F7	1.338(5)	C15	C16	1.534(7)
C15	C28	1.548(7)	C15	C22	1.554(7)
C15	P	1.957(5)	C16	C21	1.385(7)
C16	C17	1.403(7)	C17	C18	1.374(7)
C18	C19	1.390(7)	C19	C20	1.370(7)
C20	C21	1.386(7)	C22	C27	1.384(7)
C22	C23	1.391(7)	C23	C24	1.384(7)
C24	C25	1.393(8)	C25	C26	1.355(8)
C26	C27	1.386(7)	C28	C29	1.397(7)
C28	C33	1.403(7)	C29	C30	1.393(7)
C30	C31	1.382(8)	C31	C32	1.381(8)
C32	C33	1.383(7)	C34	O3	1.150(6)
C34	W	2.003(6)	C35	O4	1.146(6)
C35	W	2.042(6)	C36	O5	1.154(6)
C36	W	2.031(5)	C37	O6	1.149(6)
C37	W	2.044(6)	C38	O7	1.156(6)
C38	W	2.029(6)	O1	P	1.639(3)
P	W	2.5271(14)			

Table 3 Bond Angles for 54.

Atom	Atom	Atom	Angle/˚	Atom	Atom	Atom	Angle/˚
O2	C1	O1	107.0(4)	O2	C1	C3	109.9(4)
O1	C1	C3	110.2(4)	O2	C2	C9	108.7(4)
O2	C2	P	103.2(3)	C9	C2	P	122.2(4)
C8	C3	C4	114.4(5)	C8	C3	C1	117.9(4)
C4	C3	C1	127.6(5)	F1	C4	C5	117.3(5)
F1	C4	C3	119.0(5)	C5	C4	C3	123.8(5)
C4	C5	C6	118.6(5)	C5	C6	C7	120.8(5)
C8	C7	C6	117.7(5)	F2	C8	C7	118.0(5)
F2	C8	C3	117.3(5)	C7	C8	C3	124.7(5)
C10	C9	C14	115.6(4)	C10	C9	C2	120.4(4)

C14	C9	C2	123.8(4)	F3	C10	C9	119.6(4)
F3	C10	C11	117.2(4)	C9	C10	C11	123.2(5)
F4	C11	C12	120.0(5)	F4	C11	C10	120.7(5)
C12	C11	C10	119.2(5)	F5	C12	C13	120.5(5)
F5	C12	C11	119.7(5)	C13	C12	C11	119.8(5)
F6	C13	C12	120.1(4)	F6	C13	C14	120.1(5)
C12	C13	C14	119.8(5)	F7	C14	C13	117.3(4)
F7	C14	C9	120.2(4)	C13	C14	C9	122.5(5)
C16	C15	C28	111.4(4)	C16	C15	C22	108.8(4)
C28	C15	C22	112.8(4)	C16	C15	P	108.6(3)
C28	C15	P	108.7(3)	C22	C15	P	106.3(3)
C21	C16	C17	116.5(5)	C21	C16	C15	122.3(4)
C17	C16	C15	121.2(4)	C18	C17	C16	122.0(5)
C17	C18	C19	120.3(5)	C20	C19	C18	118.5(5)
C19	C20	C21	121.0(5)	C16	C21	C20	121.6(5)
C27	C22	C23	117.1(5)	C27	C22	C15	121.8(4)
C23	C22	C15	121.0(4)	C24	C23	C22	121.0(5)
C23	C24	C25	120.3(5)	C26	C25	C24	119.4(5)
C25	C26	C27	120.1(5)	C22	C27	C26	122.1(5)
C29	C28	C33	117.0(5)	C29	C28	C15	122.5(4)
C33	C28	C15	120.4(5)	C30	C29	C28	121.0(5)
C31	C30	C29	121.2(6)	C32	C31	C30	118.2(5)
C31	C32	C33	121.3(5)	C32	C33	C28	121.3(5)
O3	C34	W	178.5(5)	O4	C35	W	176.0(5)
O5	C36	W	174.7(5)	O6	C37	W	177.9(5)
O7	C38	W	174.9(4)	C1	O1	P	112.8(3)
C1	O2	C2	108.2(3)	O1	P	C2	90.54(19)
O1	P	C15	105.83(19)	C2	P	C15	99.7(2)
O1	P	W	108.16(13)	C2	P	W	125.21(15)
C15	P	W	121.88(16)	C34	W	C38	87.2(2)
C34	W	C36	87.9(2)	C38	W	C36	174.5(2)
C34	W	C35	89.4(2)	C38	W	C35	93.8(2)
C36	W	C35	83.7(2)	C34	W	C37	88.4(2)
C38	W	C37	88.54(19)	C36	W	C37	93.77(19)
C35	W	C37	176.72(19)	C34	W	P	177.23(16)
C38	W	P	94.41(15)	C36	W	P	90.37(15)
C35	W	P	88.30(15)	C37	W	P	93.85(15)

Table 4 Torsion Angles for 54.

A	B	C	D	Angle/˚	A	B	C	D	Angle/˚
O2	C1	C3	C8	154.5(5)	O1	C1	C3	C8	-87.7(6)
O2	C1	C3	C4	-21.2(7)	O1	C1	C3	C4	96.6(6)
C8	C3	C4	F1	179.6(5)	C1	C3	C4	F1	-4.5(8)
C8	C3	C4	C5	-0.5(8)	C1	C3	C4	C5	175.3(5)
F1	C4	C5	C6	-179.5(5)	C3	C4	C5	C6	0.7(9)

C4	C5	C6	C7	0.5(9)
C6	C7	C8	F2	179.7(5)
C4	C3	C8	F2	-178.6(5)
C4	C3	C8	C7	-0.8(8)
O2	C2	C9	C10	-122.2(5)
O2	C2	C9	C14	52.1(6)
C14	C9	C10	F3	-175.3(4)
C14	C9	C10	C11	2.5(8)
F3	C10	C11	F4	-1.2(8)
F3	C10	C11	C12	177.4(5)
F4	C11	C12	F5	-1.3(8)
F4	C11	C12	C13	177.6(5)
F5	C12	C13	F6	0.4(8)
F5	C12	C13	C14	179.2(5)
F6	C13	C14	F7	0.8(7)
F6	C13	C14	C9	-179.3(5)
C10	C9	C14	F7	176.6(4)
C10	C9	C14	C13	-3.2(8)
C28	C15	C16	C21	103.2(5)
P	C15	C16	C21	-137.1(4)
C22	C15	C16	C17	158.3(4)
C21	C16	C17	C18	1.9(7)
C16	C17	C18	C19	-0.4(7)
C18	C19	C20	C21	1.8(8)
C15	C16	C21	C20	178.6(4)
C16	C15	C22	C27	-88.5(5)
P	C15	C22	C27	28.2(5)
C28	C15	C22	C23	-35.6(6)
C27	C22	C23	C24	-1.8(8)
C22	C23	C24	C25	0.7(8)
C24	C25	C26	C27	-0.3(9)
C15	C22	C27	C26	179.2(5)
C16	C15	C28	C29	-151.3(4)
P	C15	C28	C29	89.0(5)
C22	C15	C28	C33	154.3(4)
C33	C28	C29	C30	0.5(7)
C28	C29	C30	C31	-0.3(8)
C30	C31	C32	C33	-0.6(8)
C29	C28	C33	C32	-0.7(7)
O2	C1	O1	P	-33.0(4)
O1	C1	O2	C2	46.1(5)
C9	C2	O2	C1	-168.9(4)
C1	O1	P	C2	8.8(3)
C1	O1	P	W	136.4(3)
C9	C2	P	O1	138.7(4)
C9	C2	P	C15	-115.2(4)
C5	C6	C7	C8	-1.7(9)
C6	C7	C8	C3	1.9(9)
C1	C3	C8	F2	5.1(7)
C1	C3	C8	C7	-177.1(5)
P	C2	C9	C10	118.0(5)
P	C2	C9	C14	-67.7(6)
C2	C9	C10	F3	-0.6(7)
C2	C9	C10	C11	177.3(5)
C9	C10	C11	F4	-179.1(5)
C9	C10	C11	C12	-0.5(8)
C10	C11	C12	F5	-179.9(5)
C10	C11	C12	C13	-1.0(8)
C11	C12	C13	F6	-178.4(5)
C11	C12	C13	C14	0.3(8)
C12	C13	C14	F7	-177.9(4)
C12	C13	C14	C9	1.9(8)
C2	C9	C14	F7	2.0(8)
C2	C9	C14	C13	-177.8(5)
C22	C15	C16	C21	-21.8(6)
C28	C15	C16	C17	-76.8(5)
P	C15	C16	C17	43.0(5)
C15	C16	C17	C18	-178.2(4)
C17	C18	C19	C20	-1.4(8)
C17	C16	C21	C20	-1.4(7)
C19	C20	C21	C16	-0.4(8)
C28	C15	C22	C27	147.3(5)
C16	C15	C22	C23	88.5(5)
P	C15	C22	C23	-154.7(4)
C15	C22	C23	C24	-179.0(5)
C23	C24	C25	C26	0.5(9)
C23	C22	C27	C26	2.0(7)
C25	C26	C27	C22	-1.0(8)
C22	C15	C28	C29	-28.7(6)
C16	C15	C28	C33	31.7(6)
P	C15	C28	C33	-88.0(5)
C15	C28	C29	C30	-176.6(4)
C29	C30	C31	C32	0.3(8)
C31	C32	C33	C28	0.8(8)
C15	C28	C33	C32	176.4(4)
C3	C1	O1	P	-152.5(3)
C3	C1	O2	C2	165.8(4)
P	C2	O2	C1	-37.8(4)
C1	O1	P	C15	-91.5(3)
O2	C2	P	O1	16.3(3)
O2	C2	P	C15	122.5(3)
O2	C2	P	W	-96.5(3)

C9	C2	P	W	25.8(5)
C28	C15	P	O1	29.3(4)
C16	C15	P	C2	174.5(3)
C22	C15	P	C2	57.6(3)
C28	C15	P	W	153.2(3)
O3	C34	W	C38	-41(20)
O3	C34	W	C35	52(20)
O3	C34	W	P	85(20)
O7	C38	W	C36	-36(6)
O7	C38	W	C37	79(5)
O5	C36	W	C34	-51(5)
O5	C36	W	C35	39(5)
O5	C36	W	P	127(5)
O4	C35	W	C38	164(7)
O4	C35	W	C37	29(10)
O6	C37	W	C34	49(12)
O6	C37	W	C36	137(12)
O6	C37	W	P	-132(12)
C2	P	W	C34	109(3)
O1	P	W	C38	131.25(18)
C15	P	W	C38	8.4(2)
C2	P	W	C36	58.0(2)
O1	P	W	C35	37.59(19)
C15	P	W	C35	-85.2(2)
C2	P	W	C37	-35.8(2)
C16	C15	P	O1	-92.1(3)
C22	C15	P	O1	151.0(3)
C28	C15	P	C2	-64.1(4)
C16	C15	P	W	31.8(4)
C22	C15	P	W	-85.1(3)
O3	C34	W	C36	136(20)
O3	C34	W	C37	-130(20)
O7	C38	W	C34	-9(5)
O7	C38	W	C35	-98(5)
O7	C38	W	P	173(5)
O5	C36	W	C38	-24(6)
O5	C36	W	C37	-139(5)
O4	C35	W	C34	77(7)
O4	C35	W	C36	-11(7)
O4	C35	W	P	-102(7)
O6	C37	W	C38	-38(12)
O6	C37	W	C35	97(12)
O1	P	W	C34	5(3)
C15	P	W	C34	-118(3)
C2	P	W	C38	-124.6(2)
O1	P	W	C36	-46.12(18)
C15	P	W	C36	-168.9(2)
C2	P	W	C35	141.7(2)
O1	P	W	C37	-139.92(18)
C15	P	W	C37	97.3(2)

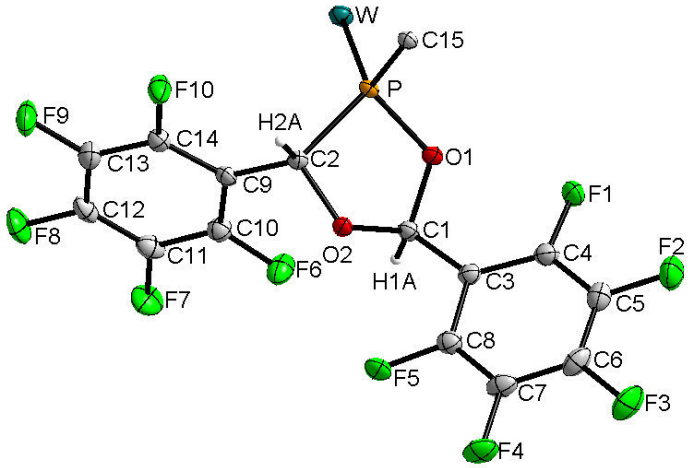

Table 1 Crystal data and structure refinement for 55.

Identification code	GSTR276
Empirical formula	$C_{38}H_{17}F_{10}O_7PW$
Formula weight	990.34
Temperature/K	100(2)
Crystal system	triclinic
Space group	P-1
a/Å	10.5469(4)
b/Å	12.5556(5)
c/Å	14.8775(5)
α/°	66.8310(10)
β/°	78.2940(10)
γ/°	80.5270(10)
Volume/Å^3	1765.68(11)
Z	2
ρ_{calc}mg/mm^3	1.863
m/mm^{-1}	3.421
F(000)	960
Crystal size/mm^3	0.30 × 0.10 × 0.05
Tmin; Tmax	0.4268; 0.8476
Radiation	MoKα (λ = 0.71073)
2Θ range for data collection	2.87 to 28.00°
Completeness to theta	0.985
Index ranges	-13 ≤ h ≤ 10, -16 ≤ k ≤ 16, -19 ≤ l ≤ 19
Reflections collected	41272
Independent reflections	8403 [R_{int} = 0.0360]
Data/restraints/parameters	8403/378/514
Goodness-of-fit on F^2	1.126
Final R indexes [I>=2σ (I)]	R_1 = 0.0303, wR_2 = 0.0729
Final R indexes [all data]	R_1 = 0.0367, wR_2 = 0.0766
Largest diff. peak/hole / e Å^{-3}	2.220/-1.406

Table 2 Bond Lengths for 55.

Atom	Atom	Length/Å	Atom	Atom	Length/Å
W	C34	2.025(4)	W	C35	2.044(4)
W	C36	2.047(4)	W	C37	2.055(4)
W	C38	2.063(4)	W	P	2.5090(8)
P	O1	1.639(2)	P	C2	1.890(3)
P	C15	1.944(3)	F1	C4	1.343(4)
F2	C5	1.339(4)	F3	C6	1.340(4)
F4	C7	1.339(4)	F5	C8	1.341(4)
F6	C10	1.346(4)	F7	C11	1.339(4)
F8	C12	1.339(4)	F9	C13	1.340(4)
F10	C14	1.348(4)	O1	C1	1.425(4)
O2	C1	1.421(4)	O2	C2	1.429(4)
O3	C34	1.132(5)	O4	C35	1.139(5)
O5	C36	1.134(5)	O6	C37	1.137(5)
O7	C38	1.130(5)	C1	C3	1.524(5)
C2	C9	1.518(5)	C3	C4	1.396(5)
C3	C8	1.402(5)	C4	C5	1.377(5)
C5	C6	1.377(6)	C6	C7	1.381(6)
C7	C8	1.378(5)	C9	C14	1.389(5)
C9	C10	1.391(5)	C10	C11	1.382(5)
C11	C12	1.373(5)	C12	C13	1.379(5)
C13	C14	1.379(5)	C15	C28	1.537(4)
C15	C16	1.549(5)	C15	C22	1.555(4)
C16	C21	1.394(5)	C16	C17	1.402(5)
C17	C18	1.382(5)	C18	C19	1.390(5)
C19	C20	1.379(5)	C20	C21	1.388(5)
C22	C27	1.399(5)	C22	C23	1.400(5)
C23	C24	1.392(5)	C24	C25	1.392(6)
C25	C26	1.378(6)	C26	C27	1.396(5)
C28	C33	1.396(5)	C28	C29	1.399(5)
C29	C30	1.384(5)	C30	C31	1.390(5)
C31	C32	1.380(5)	C32	C33	1.392(5)

Table 3 Bond Angles for 55.

Atom	Atom	Atom	Angle/˚	Atom	Atom	Atom	Angle/˚
C34	W	C35	86.91(15)	C34	W	C36	86.48(15)
C35	W	C36	88.93(16)	C34	W	C37	88.82(15)
C35	W	C37	175.34(14)	C36	W	C37	88.94(15)
C34	W	C38	86.89(15)	C35	W	C38	90.29(15)
C36	W	C38	173.36(14)	C37	W	C38	91.35(15)
C34	W	P	177.47(11)	C35	W	P	95.37(11)
C36	W	P	92.45(10)	C37	W	P	88.86(10)
C38	W	P	94.19(10)	O1	P	C2	91.38(13)

O1	P	C15	101.86(13)	C2	P	C15	103.58(14)
O1	P	W	111.68(9)	C2	P	W	120.01(10)
C15	P	W	122.65(10)	C1	O1	P	115.6(2)
C1	O2	C2	113.1(2)	O2	C1	O1	108.9(2)
O2	C1	C3	107.9(3)	O1	C1	C3	112.0(3)
O2	C2	C9	113.2(3)	O2	C2	P	103.8(2)
C9	C2	P	118.9(2)	C4	C3	C8	116.1(3)
C4	C3	C1	124.9(3)	C8	C3	C1	118.9(3)
F1	C4	C5	116.6(3)	F1	C4	C3	121.2(3)
C5	C4	C3	122.1(3)	F2	C5	C4	119.9(4)
F2	C5	C6	120.0(3)	C4	C5	C6	120.1(4)
F3	C6	C5	120.2(4)	F3	C6	C7	120.2(4)
C5	C6	C7	119.6(3)	F4	C7	C8	120.3(4)
F4	C7	C6	119.8(3)	C8	C7	C6	119.8(4)
F5	C8	C7	117.6(3)	F5	C8	C3	120.2(3)
C7	C8	C3	122.1(3)	C14	C9	C10	115.4(3)
C14	C9	C2	118.5(3)	C10	C9	C2	125.8(3)
F6	C10	C11	116.8(3)	F6	C10	C9	120.5(3)
C11	C10	C9	122.6(3)	F7	C11	C12	119.9(3)
F7	C11	C10	120.3(3)	C12	C11	C10	119.8(3)
F8	C12	C11	120.0(3)	F8	C12	C13	120.3(3)
C11	C12	C13	119.7(3)	F9	C13	C12	120.3(3)
F9	C13	C14	120.4(3)	C12	C13	C14	119.3(3)
F10	C14	C13	117.3(3)	F10	C14	C9	119.5(3)
C13	C14	C9	123.2(3)	C28	C15	C16	110.0(3)
C28	C15	C22	109.3(3)	C16	C15	C22	111.6(3)
C28	C15	P	110.5(2)	C16	C15	P	104.0(2)
C22	C15	P	111.3(2)	C21	C16	C17	117.7(3)
C21	C16	C15	121.9(3)	C17	C16	C15	120.3(3)
C18	C17	C16	121.4(3)	C17	C18	C19	119.8(3)
C20	C19	C18	119.5(3)	C19	C20	C21	120.7(3)
C20	C21	C16	120.7(3)	C27	C22	C23	117.2(3)
C27	C22	C15	122.2(3)	C23	C22	C15	120.5(3)
C24	C23	C22	121.4(3)	C23	C24	C25	120.5(4)
C26	C25	C24	118.7(3)	C25	C26	C27	121.0(4)
C26	C27	C22	121.1(4)	C33	C28	C29	117.4(3)
C33	C28	C15	123.3(3)	C29	C28	C15	118.9(3)
C30	C29	C28	121.3(3)	C29	C30	C31	120.4(3)
C32	C31	C30	119.3(3)	C31	C32	C33	120.3(3)
C32	C33	C28	121.3(3)	O3	C34	W	178.5(4)
O4	C35	W	176.3(3)	O5	C36	W	175.0(3)
O6	C37	W	177.3(3)	O7	C38	W	174.0(3)

Table 4 Torsion Angles for 55.

A	B	C	D	Angle/˚	A	B	C	D	Angle/˚
C34	W	P	O1	-12(3)	C35	W	P	O1	142.30(15)
C36	W	P	O1	53.15(15)	C37	W	P	O1	-35.74(14)
C38	W	P	O1	-127.01(14)	C34	W	P	C2	-117(3)
C35	W	P	C2	37.26(16)	C36	W	P	C2	-51.89(16)
C37	W	P	C2	-140.79(16)	C38	W	P	C2	127.94(16)
C34	W	P	C15	109(3)	C35	W	P	C15	-96.54(16)
C36	W	P	C15	174.31(16)	C37	W	P	C15	85.41(16)
C38	W	P	C15	-5.85(16)	C2	P	O1	C1	0.9(2)
C15	P	O1	C1	105.0(2)	W	P	O1	C1	-122.4(2)
C2	O2	C1	O1	28.6(3)	C2	O2	C1	C3	150.4(3)
P	O1	C1	O2	-16.3(3)	P	O1	C1	C3	-135.5(2)
C1	O2	C2	C9	103.7(3)	C1	O2	C2	P	-26.6(3)
O1	P	C2	O2	14.4(2)	C15	P	C2	O2	-88.2(2)
W	P	C2	O2	130.51(16)	O1	P	C2	C9	-112.5(3)
C15	P	C2	C9	145.0(2)	W	P	C2	C9	3.7(3)
O2	C1	C3	C4	-137.7(3)	O1	C1	C3	C4	-17.9(4)
O2	C1	C3	C8	46.9(4)	O1	C1	C3	C8	166.8(3)
C8	C3	C4	F1	174.5(3)	C1	C3	C4	F1	-1.0(5)
C8	C3	C4	C5	-3.9(5)	C1	C3	C4	C5	-179.4(3)
F1	C4	C5	F2	4.7(5)	C3	C4	C5	F2	-176.9(3)
F1	C4	C5	C6	-176.8(3)	C3	C4	C5	C6	1.6(5)
F2	C5	C6	F3	1.7(5)	C4	C5	C6	F3	179.8(3)
F2	C5	C6	C7	-180.0(3)	C4	C5	C6	C7	1.6(5)
F3	C6	C7	F4	-1.5(5)	C5	C6	C7	F4	176.8(3)
F3	C6	C7	C8	179.5(3)	C5	C6	C7	C8	-2.2(5)
F4	C7	C8	F5	-0.6(5)	C6	C7	C8	F5	178.3(3)
F4	C7	C8	C3	-179.2(3)	C6	C7	C8	C3	-0.3(5)
C4	C3	C8	F5	-175.3(3)	C1	C3	C8	F5	0.4(5)
C4	C3	C8	C7	3.2(5)	C1	C3	C8	C7	179.0(3)
O2	C2	C9	C14	138.5(3)	P	C2	C9	C14	-99.3(3)
O2	C2	C9	C10	-34.7(5)	P	C2	C9	C10	87.6(4)
C14	C9	C10	F6	-178.3(3)	C2	C9	C10	F6	-5.0(6)
C14	C9	C10	C11	-0.9(5)	C2	C9	C10	C11	172.5(3)
F6	C10	C11	F7	-1.4(5)	C9	C10	C11	F7	-178.9(3)
F6	C10	C11	C12	179.2(3)	C9	C10	C11	C12	1.6(6)
F7	C11	C12	F8	0.1(6)	C10	C11	C12	F8	179.5(3)
F7	C11	C12	C13	179.5(4)	C10	C11	C12	C13	-1.1(6)
F8	C12	C13	F9	-0.9(6)	C11	C12	C13	F9	179.7(4)
F8	C12	C13	C14	179.3(4)	C11	C12	C13	C14	-0.1(6)
F9	C13	C14	F10	2.9(6)	C12	C13	C14	F10	-177.3(3)
F9	C13	C14	C9	-178.9(3)	C12	C13	C14	C9	0.9(6)
C10	C9	C14	F10	177.8(3)	C2	C9	C14	F10	3.9(5)
C10	C9	C14	C13	-0.4(6)	C2	C9	C14	C13	-174.3(3)
O1	P	C15	C28	-158.9(2)	C2	P	C15	C28	64.5(2)

W	P	C15	C28	75.4(2)	O1	P	C15	C16	83.0(2)
C2	P	C15	C16	177.4(2)	W	P	C15	C16	-42.6(2)
O1	P	C15	C22	-37.3(2)	C2	P	C15	C22	57.1(2)
W	P	C15	C22	-162.91(18)	C28	C15	C16	C21	10.7(4)
C22	C15	C16	C21	-110.8(3)	P	C15	C16	C21	129.1(3)
C28	C15	C16	C17	-171.5(3)	C22	C15	C16	C17	67.0(4)
P	C15	C16	C17	-53.1(3)	C21	C16	C17	C18	2.1(5)
C15	C16	C17	C18	-175.7(3)	C16	C17	C18	C19	-0.4(5)
C17	C18	C19	C20	-1.7(5)	C18	C19	C20	C21	2.0(5)
C19	C20	C21	C16	-0.2(5)	C17	C16	C21	C20	-1.8(5)
C15	C16	C21	C20	176.0(3)	C28	C15	C22	C27	-128.1(3)
C16	C15	C22	C27	-6.2(4)	P	C15	C22	C27	109.5(3)
C28	C15	C22	C23	47.8(4)	C16	C15	C22	C23	169.7(3)
P	C15	C22	C23	-74.6(3)	C27	C22	C23	C24	-3.4(5)
C15	C22	C23	C24	-179.5(3)	C22	C23	C24	C25	1.9(5)
C23	C24	C25	C26	0.9(5)	C24	C25	C26	C27	-2.2(6)
C25	C26	C27	C22	0.6(6)	C23	C22	C27	C26	2.2(5)
C15	C22	C27	C26	178.2(3)	C16	C15	C28	C33	90.9(4)
C22	C15	C28	C33	-146.3(3)	P	C15	C28	C33	-23.4(4)
C16	C15	C28	C29	-83.0(4)	C22	C15	C28	C29	39.9(4)
P	C15	C28	C29	162.7(3)	C33	C28	C29	C30	-0.2(5)
C15	C28	C29	C30	174.0(3)	C28	C29	C30	C31	0.1(6)
C29	C30	C31	C32	0.6(6)	C30	C31	C32	C33	-1.2(6)
C31	C32	C33	C28	1.2(6)	C29	C28	C33	C32	-0.5(5)
C15	C28	C33	C32	-174.4(3)	C35	W	C34	O3	123(13)
C36	W	C34	O3	-148(13)	C37	W	C34	O3	-59(13)
C38	W	C34	O3	32(13)	P	W	C34	O3	-83(14)
C34	W	C35	O4	9(6)	C36	W	C35	O4	-77(6)
C37	W	C35	O4	-14(7)	C38	W	C35	O4	96(6)
P	W	C35	O4	-170(6)	C34	W	C36	O5	-9(4)
C35	W	C36	O5	78(4)	C37	W	C36	O5	-98(4)
C38	W	C36	O5	-5(5)	P	W	C36	O5	173(4)
C34	W	C37	O6	-36(8)	C35	W	C37	O6	-12(9)
C36	W	C37	O6	51(8)	C38	W	C37	O6	-123(8)
P	W	C37	O6	143(8)	C34	W	C38	O7	19(3)
C35	W	C38	O7	-68(3)	C36	W	C38	O7	16(4)
C37	W	C38	O7	108(3)	P	W	C38	O7	-163(3)

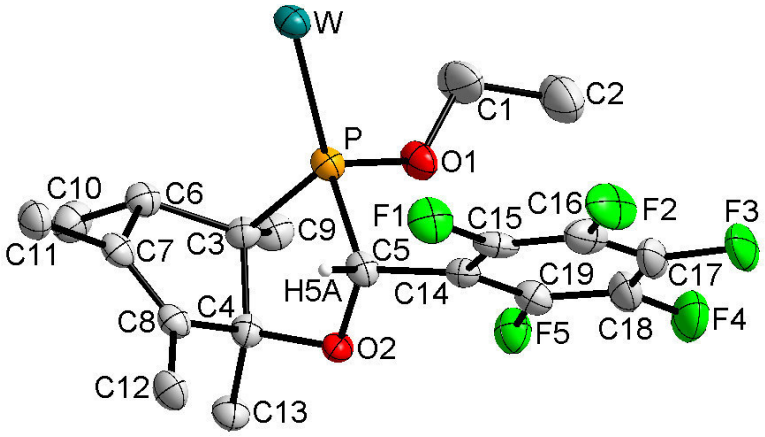

Table 1 Crystal data and structure refinement for 60.

Identification code	GSTR323
Empirical formula	$C_{24}H_{22}F_5O_7PW$
Formula weight	732.24
Temperature/K	123(2)
Crystal system	triclinic
Space group	P-1
a/Å	15.3955(4)
b/Å	17.2661(5)
c/Å	18.0841(5)
α/°	105.9080(15)
β/°	104.5500(16)
γ/°	113.2330(16)
Volume/Å^3	3881.1(2)
Z	6
ρ_{calc}g/cm^3	1.880
μ/mm^{-1}	4.605
F(000)	2136
Crystal size/mm^3	0.40 × 0.12 × 0.02
Tmin; Tmax	0.2603; 0.9135
Radiation	MoKα (λ = 0.71073)
2Θ range for data collection/°	1.95 to 28.00°
Completeness to theta	0.992
Index ranges	-20 ≤ h ≤ 20, -22 ≤ k ≤ 22, -23 ≤ l ≤ 23
Reflections collected	83764
Independent reflections	18559 [R_{int} = 0.0915]
Data/restraints/parameters	18559/5/1045
Goodness-of-fit on F^2	0.949
Final R indexes [I>=2σ (I)]	R_1 = 0.0374, wR_2 = 0.0659
Final R indexes [all data]	R_1 = 0.0767, wR_2 = 0.0742
Largest diff. peak/hole / e Å^{-3}	2.424/-1.722

Table 2 Bond Lengths for 60.

Atom	Atom	Length/Å	Atom	Atom	Length/Å
C1	O1	1.419(6)	C1	C2	1.491(8)
C3	C9	1.534(6)	C3	C6	1.547(6)
C3	C4	1.560(7)	C3	P1	1.885(5)
C4	O2	1.448(5)	C4	C13	1.504(7)
C4	C8	1.527(6)	C5	O2	1.416(5)
C5	C14	1.498(6)	C5	P1	1.882(5)
C6	C7	1.535(7)	C6	C10	1.538(7)
C7	C8	1.320(7)	C7	C11	1.515(6)
C8	C12	1.505(7)	C14	C19	1.407(6)
C14	C15	1.409(7)	C15	C16	1.346(7)
C15	F1	1.375(5)	C16	F2	1.343(6)
C16	C17	1.378(8)	C17	F3	1.336(6)
C17	C18	1.381(8)	C18	F4	1.342(6)
C18	C19	1.366(7)	C19	F5	1.338(6)
C20	O3	1.161(6)	C20	W1	1.999(6)
C21	O4	1.151(6)	C21	W1	2.034(6)
C22	O5	1.166(7)	C22	W1	2.019(6)
C23	O6	1.159(6)	C23	W1	2.026(6)
C24	O7	1.144(6)	C24	W1	2.046(6)
O1	P1	1.610(3)	P1	W1	2.5150(13)

Table 3 Bond Angles for 60.

Atom	Atom	Atom	Angle/˚	Atom	Atom	Atom	Angle/˚
O1	C1	C2	110.7(5)	C9	C3	C6	114.3(4)
C9	C3	C4	114.9(4)	C6	C3	C4	104.1(4)
C9	C3	P1	109.8(3)	C6	C3	P1	110.4(3)
C4	C3	P1	102.5(3)	O2	C4	C13	104.4(4)
O2	C4	C8	110.7(4)	C13	C4	C8	113.3(4)
O2	C4	C3	110.5(4)	C13	C4	C3	116.3(4)
C8	C4	C3	101.9(4)	O2	C5	C14	110.1(4)
O2	C5	P1	106.2(3)	C14	C5	P1	114.2(3)
C7	C6	C10	111.0(4)	C7	C6	C3	101.9(4)
C10	C6	C3	115.9(4)	C8	C7	C11	128.0(4)
C8	C7	C6	111.6(4)	C11	C7	C6	120.3(4)
C7	C8	C12	128.1(4)	C7	C8	C4	111.8(4)
C12	C8	C4	120.0(4)	C19	C14	C15	114.1(4)
C19	C14	C5	124.2(4)	C15	C14	C5	121.6(4)
C16	C15	F1	118.2(5)	C16	C15	C14	124.8(5)
F1	C15	C14	117.0(4)	F2	C16	C15	120.8(5)
F2	C16	C17	120.6(5)	C15	C16	C17	118.7(5)
F3	C17	C16	119.9(6)	F3	C17	C18	120.3(5)
C16	C17	C18	119.8(5)	F4	C18	C19	119.9(5)
F4	C18	C17	119.8(5)	C19	C18	C17	120.3(5)

F5	C19	C18	117.1(4)	F5	C19	C14	120.7(4)
C18	C19	C14	122.2(5)	O3	C20	W1	176.9(5)
O4	C21	W1	176.2(5)	O5	C22	W1	175.8(5)
O6	C23	W1	173.7(4)	O7	C24	W1	176.2(4)
C1	O1	P1	128.4(3)	C5	O2	C4	108.4(3)
O1	P1	C5	96.63(19)	O1	P1	C3	103.21(19)
C5	P1	C3	92.0(2)	O1	P1	W1	117.10(14)
C5	P1	W1	114.83(15)	C3	P1	W1	126.68(15)
C20	W1	C22	91.0(2)	C20	W1	C23	86.9(2)
C22	W1	C23	85.5(2)	C20	W1	C21	85.5(2)
C22	W1	C21	92.1(2)	C23	W1	C21	171.9(2)
C20	W1	C24	91.0(2)	C22	W1	C24	173.6(2)
C23	W1	C24	88.5(2)	C21	W1	C24	94.2(2)
C20	W1	P1	170.46(16)	C22	W1	P1	93.09(16)
C23	W1	P1	102.04(14)	C21	W1	P1	85.76(14)
C24	W1	P1	85.88(14)				

Table 4 Torsion Angles for 60.

A	B	C	D	Angle/˚	A	B	C	D	Angle/˚
C9	C3	C4	O2	88.9(5)	C6	C3	C4	O2	-145.3(4)
P1	C3	C4	O2	-30.2(4)	C9	C3	C4	C13	-29.8(6)
C6	C3	C4	C13	96.0(4)	P1	C3	C4	C13	-148.9(3)
C9	C3	C4	C8	-153.4(4)	C6	C3	C4	C8	-27.7(5)
P1	C3	C4	C8	87.5(3)	C9	C3	C6	C7	154.1(4)
C4	C3	C6	C7	27.9(5)	P1	C3	C6	C7	-81.5(4)
C9	C3	C6	C10	33.4(6)	C4	C3	C6	C10	-92.8(5)
P1	C3	C6	C10	157.8(4)	C10	C6	C7	C8	105.5(5)
C3	C6	C7	C8	-18.5(5)	C10	C6	C7	C11	-71.1(6)
C3	C6	C7	C11	164.9(4)	C11	C7	C8	C12	-0.7(9)
C6	C7	C8	C12	-176.9(5)	C11	C7	C8	C4	176.9(5)
C6	C7	C8	C4	0.6(6)	O2	C4	C8	C7	134.9(4)
C13	C4	C8	C7	-108.3(5)	C3	C4	C8	C7	17.4(5)
O2	C4	C8	C12	-47.3(6)	C13	C4	C8	C12	69.5(6)
C3	C4	C8	C12	-164.8(4)	O2	C5	C14	C19	42.8(6)
P1	C5	C14	C19	-76.5(5)	O2	C5	C14	C15	-141.6(4)
P1	C5	C14	C15	99.0(5)	C19	C14	C15	C16	3.9(7)
C5	C14	C15	C16	-172.0(5)	C19	C14	C15	F1	-179.3(4)
C5	C14	C15	F1	4.7(7)	F1	C15	C16	F2	1.4(7)
C14	C15	C16	F2	178.1(4)	F1	C15	C16	C17	-178.5(5)
C14	C15	C16	C17	-1.8(8)	F2	C16	C17	F3	-2.2(8)
C15	C16	C17	F3	177.7(5)	F2	C16	C17	C18	177.8(5)
C15	C16	C17	C18	-2.3(8)	F3	C17	C18	F4	2.5(8)
C16	C17	C18	F4	-177.6(5)	F3	C17	C18	C19	-176.0(5)
C16	C17	C18	C19	3.9(9)	F4	C18	C19	F5	1.6(7)
C17	C18	C19	F5	-179.9(5)	F4	C18	C19	C14	179.9(5)

C17	C18	C19	C14	-1.6(8)
C5	C14	C19	F5	-8.0(7)
C5	C14	C19	C18	173.7(5)
C14	C5	O2	C4	-166.9(4)
C13	C4	O2	C5	175.3(4)
C3	C4	O2	C5	49.6(4)
C1	O1	P1	C3	114.5(5)
O2	C5	P1	O1	-82.6(3)
O2	C5	P1	C3	21.0(3)
O2	C5	P1	W1	153.4(2)
C9	C3	P1	O1	-20.5(4)
C4	C3	P1	O1	102.2(3)
C6	C3	P1	C5	115.3(3)
C9	C3	P1	W1	118.8(3)
C4	C3	P1	W1	-118.5(2)
O3	C20	W1	C23	169(10)
O3	C20	W1	C24	80(10)
O5	C22	W1	C20	-64(7)
O5	C22	W1	C21	-150(7)
O5	C22	W1	P1	124(7)
O6	C23	W1	C22	-85(4)
O6	C23	W1	C24	97(4)
O4	C21	W1	C20	-18(7)
O4	C21	W1	C23	0(8)
O4	C21	W1	P1	165(7)
O7	C24	W1	C22	-6(8)
O7	C24	W1	C21	-173(7)
O1	P1	W1	C20	-73.2(10)
C3	P1	W1	C20	152.3(10)
C5	P1	W1	C22	154.4(2)
O1	P1	W1	C23	128.2(2)
C3	P1	W1	C23	-6.4(2)
C5	P1	W1	C21	62.6(2)
O1	P1	W1	C24	-144.2(2)
C3	P1	W1	C24	81.2(2)
C15	C14	C19	F5	176.1(4)
C15	C14	C19	C18	-2.2(7)
C2	C1	O1	P1	154.2(4)
P1	C5	O2	C4	-42.9(4)
C8	C4	O2	C5	-62.5(5)
C1	O1	P1	C5	-151.8(5)
C1	O1	P1	W1	-29.5(5)
C14	C5	P1	O1	38.9(4)
C14	C5	P1	C3	142.4(3)
C14	C5	P1	W1	-85.1(3)
C6	C3	P1	O1	-147.4(3)
C9	C3	P1	C5	-117.8(3)
C4	C3	P1	C5	4.9(3)
C6	C3	P1	W1	-8.1(4)
O3	C20	W1	C22	-106(10)
O3	C20	W1	C21	-14(10)
O3	C20	W1	P1	10(11)
O5	C22	W1	C23	22(7)
O5	C22	W1	C24	44(8)
O6	C23	W1	C20	6(4)
O6	C23	W1	C21	-12(5)
O6	C23	W1	P1	-178(4)
O4	C21	W1	C22	72(7)
O4	C21	W1	C24	-109(7)
O7	C24	W1	C20	102(7)
O7	C24	W1	C23	15(7)
O7	C24	W1	P1	-87(7)
C5	P1	W1	C20	39.1(10)
O1	P1	W1	C22	42.1(2)
C3	P1	W1	C22	-92.4(3)
C5	P1	W1	C23	-119.5(2)
O1	P1	W1	C21	-49.7(2)
C3	P1	W1	C21	175.7(2)
C5	P1	W1	C24	-31.9(2)

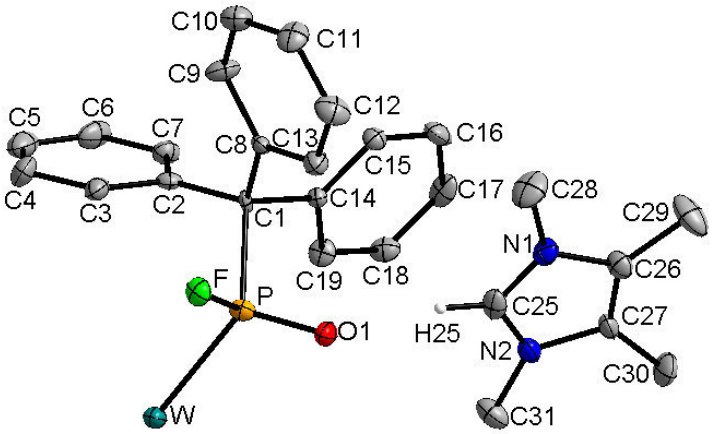

Table 1 Crystal data and structure refinement for 66.

Identification code	GSTR487
Empirical formula	$C_{31}H_{28}FN_2O_6PW$
Formula weight	758.37
Temperature/K	123
Crystal system	monoclinic
Space group	$P2_1/c$
a/Å	10.7296(9)
b/Å	9.0614(7)
c/Å	31.331(2)
α/°	90
β/°	91.689(3)
γ/°	90
Volume/Å^3	3044.8(4)
Z	4
ρ_{calc}g/cm^3	1.654
μ/mm^{-1}	3.898
F(000)	1496.0
Crystal size/mm^3	0.22 × 0.14 × 0.08
Tmin; Tmax	0.2932; 0.7461
Radiation	MoKα (λ = 0.71073)
2Θ range for data collection/°	4.54 to 56°
Completeness to theta	0.998
Index ranges	-14 ≤ h ≤ 14, -11 ≤ k ≤ 11, -41 ≤ l ≤ 41
Reflections collected	44254
Independent reflections	7328 [R_{int} = 0.1716, R_{sigma} = 0.0955]
Data/restraints/parameters	7328/24/383
Goodness-of-fit on F^2	1.260
Final R indexes [I>=2σ (I)]	R_1 = 0.0916, wR_2 = 0.1767
Final R indexes [all data]	R_1 = 0.1153, wR_2 = 0.1842
Largest diff. peak/hole / e Å^{-3}	2.75/-7.61

Table 2 Bond Lengths for 66.

Atom	Atom	Length/Å	Atom	Atom	Length/Å
W	P	2.544(3)	C6	C7	1.394(16)
W	C20	1.994(11)	C8	C9	1.404(14)
W	C21	2.015(10)	C8	C13	1.379(15)
W	C22	2.044(12)	C9	C10	1.383(16)
W	C23	2.032(12)	C10	C11	1.384(17)
W	C24	2.048(12)	C11	C12	1.398(17)
P	F	1.633(7)	C12	C13	1.389(16)
P	O1	1.492(8)	C14	C15	1.377(14)
P	C1	1.937(9)	C14	C19	1.374(14)
O2	C20	1.147(14)	C15	C16	1.397(16)
O3	C21	1.154(14)	C16	C17	1.412(17)
O4	C22	1.127(15)	C17	C18	1.395(17)
O5	C23	1.132(15)	C18	C19	1.415(15)
O6	C24	1.122(15)	N1	C25	1.315(15)
C1	C2	1.513(13)	N1	C26	1.397(14)
C1	C8	1.565(13)	N1	C28	1.454(15)
C1	C14	1.543(13)	N2	C25	1.308(15)
C2	C3	1.390(15)	N2	C27	1.388(14)
C2	C7	1.384(15)	N2	C31	1.465(14)
C3	C4	1.396(16)	C26	C27	1.353(16)
C4	C5	1.40(2)	C26	C29	1.477(16)
C5	C6	1.39(2)	C27	C30	1.485(16)

Table 3 Bond Angles for 66.

Atom	Atom	Atom	Angle/˚	Atom	Atom	Atom	Angle/˚
C20	W	P	171.6(3)	C9	C8	C1	119.9(9)
C20	W	C21	92.1(5)	C13	C8	C1	121.7(9)
C20	W	C22	90.3(5)	C13	C8	C9	118.2(10)
C20	W	C23	88.5(5)	C10	C9	C8	120.8(11)
C20	W	C24	89.6(5)	C9	C10	C11	119.9(11)
C21	W	P	91.0(3)	C10	C11	C12	120.0(11)
C21	W	C22	89.6(5)	C13	C12	C11	119.0(12)
C21	W	C23	179.0(5)	C8	C13	C12	121.8(11)
C21	W	C24	89.1(5)	C15	C14	C1	122.6(9)
C22	W	P	97.6(3)	C19	C14	C1	119.2(9)
C22	W	C24	178.7(5)	C19	C14	C15	118.2(10)
C23	W	P	88.5(3)	C14	C15	C16	123.0(10)
C23	W	C22	89.6(5)	C15	C16	C17	118.7(10)
C23	W	C24	91.7(5)	C18	C17	C16	118.7(10)
C24	W	P	82.6(3)	C17	C18	C19	120.3(10)
F	P	W	103.5(3)	C14	C19	C18	121.0(10)
F	P	C1	97.4(4)	O2	C20	W	178.6(11)
O1	P	W	115.9(3)	O3	C21	W	178.5(11)

O1	P	F	107.0(4)
O1	P	C1	106.8(4)
C1	P	W	123.4(3)
C2	C1	P	110.2(6)
C2	C1	C8	111.0(8)
C2	C1	C14	110.8(8)
C8	C1	P	108.5(6)
C14	C1	P	106.0(6)
C14	C1	C8	110.2(8)
C3	C2	C1	119.5(9)
C7	C2	C1	123.2(10)
C7	C2	C3	117.4(10)
C2	C3	C4	122.3(12)
C3	C4	C5	118.8(13)
C6	C5	C4	120.0(12)
C5	C6	C7	119.5(12)
C2	C7	C6	122.1(12)
O4	C22	W	175.7(11)
O5	C23	W	176.3(12)
O6	C24	W	175.3(12)
C25	N1	C26	108.5(9)
C25	N1	C28	127.0(11)
C26	N1	C28	124.5(10)
C25	N2	C27	107.9(9)
C25	N2	C31	127.4(10)
C27	N2	C31	124.7(10)
N2	C25	N1	110.3(10)
N1	C26	C29	122.3(11)
C27	C26	N1	105.6(10)
C27	C26	C29	132.1(11)
N2	C27	C30	121.3(10)
C26	C27	N2	107.8(10)
C26	C27	C30	130.9(11)

Table 4 Torsion Angles for 66.

A	B	C	D	Angle/°
P	C1	C2	C3	56.2(11)
P	C1	C2	C7	-124.5(9)
P	C1	C8	C9	-142.6(9)
P	C1	C8	C13	43.2(11)
P	C1	C14	C15	-131.1(9)
P	C1	C14	C19	52.1(10)
C1	C2	C3	C4	-179.4(10)
C1	C2	C7	C6	179.2(10)
C1	C8	C9	C10	-178.2(10)
C1	C8	C13	C12	176.1(10)
C1	C14	C15	C16	-178.2(10)
C1	C14	C19	C18	177.7(9)
C2	C1	C8	C9	-21.4(13)
C2	C1	C8	C13	164.3(9)
C2	C1	C14	C15	109.3(10)
C2	C1	C14	C19	-67.5(11)
C2	C3	C4	C5	0.1(17)
C3	C2	C7	C6	-1.4(15)
C3	C4	C5	C6	-1.2(18)
C4	C5	C6	C7	1.0(18)
C5	C6	C7	C2	0.4(17)
C7	C2	C3	C4	1.2(15)
C8	C1	C2	C3	-64.0(11)
C8	C1	C2	C7	115.3(10)
C8	C1	C14	C15	-13.9(13)
C10	C11	C12	C13	1.4(19)
C11	C12	C13	C8	-0.6(19)
C13	C8	C9	C10	-3.8(17)
C14	C1	C2	C3	173.2(9)
C14	C1	C2	C7	-7.5(13)
C14	C1	C8	C9	101.8(11)
C14	C1	C8	C13	-72.5(12)
C14	C15	C16	C17	1.1(18)
C15	C14	C19	C18	0.8(16)
C15	C16	C17	C18	-0.1(17)
C16	C17	C18	C19	-0.5(17)
C17	C18	C19	C14	0.1(17)
C19	C14	C15	C16	-1.4(16)
N1	C26	C27	N2	-0.4(12)
N1	C26	C27	C30	-177.3(12)
C25	N1	C26	C27	0.6(12)
C25	N1	C26	C29	179.5(12)
C25	N2	C27	C26	0.1(13)
C25	N2	C27	C30	177.3(10)
C26	N1	C25	N2	-0.6(13)
C27	N2	C25	N1	0.3(13)
C28	N1	C25	N2	178.6(11)
C28	N1	C26	C27	-178.6(11)
C28	N1	C26	C29	0.3(18)
C29	C26	C27	N2	-179.2(13)

C8	C1	C14	C19	169.3(9)	C29	C26	C27	C30	4(2)
C8	C9	C10	C11	4.7(19)	C31	N2	C25	N1	-177.2(10)
C9	C8	C13	C12	1.7(17)	C31	N2	C27	C26	177.6(10)
C9	C10	C11	C12	-3.5(19)	C31	N2	C27	C30	-5.2(17)

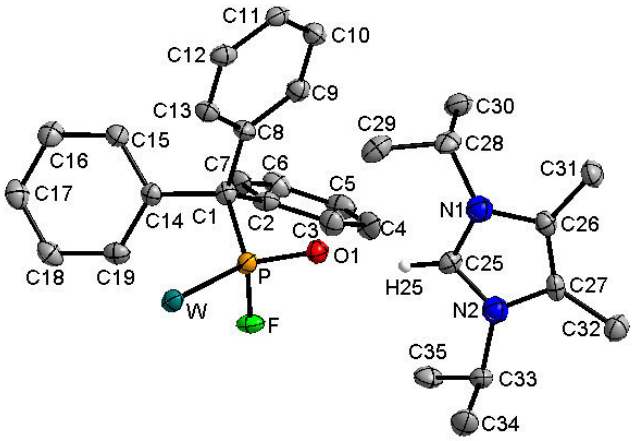

Table 1 Crystal data and structure refinement for 67.

Identification code	GSTR491
Empirical formula	$C_{35}H_{36}FN_2O_6PW$
Formula weight	814.48
Temperature/K	150
Crystal system	monoclinic
Space group	$P2_1/n$
a/Å	9.4393(6)
b/Å	18.6273(13)
c/Å	19.1677(13)
α/°	90
β/°	101.739(3)
γ/°	90
Volume/Å^3	3299.7(4)
Z	4
ρ_{calc}g/cm^3	1.639
μ/mm^{-1}	3.603
F(000)	1624.0
Crystal size/mm^3	0.12 × 0.11 × 0.1
Tmin; Tmax	0.6256; 0.7459
Radiation	MoKα (λ = 0.71073)
2Θ range for data collection/°	4.92 to 55.998°
Completeness to theta	0.997
Index ranges	-12 ≤ h ≤ 11, -24 ≤ k ≤ 24, -25 ≤ l ≤ 23
Reflections collected	50312
Independent reflections	7957 [R_{int} = 0.1211, R_{sigma} = 0.1085]
Data/restraints/parameters	7957/0/421
Goodness-of-fit on F^2	0.938
Final R indexes [I>=2σ (I)]	R_1 = 0.0527, wR_2 = 0.1077
Final R indexes [all data]	R_1 = 0.1052, wR_2 = 0.1252
Largest diff. peak/hole / e Å^{-3}	2.34/-3.57

Table 2 Bond Lengths for 67.

Atom	Atom	Length/Å	Atom	Atom	Length/Å
W	P	2.5362(17)	C8	C13	1.400(9)
W	C20	2.008(7)	C9	C10	1.395(9)
W	C21	2.042(8)	C10	C11	1.386(9)
W	C22	2.008(8)	C11	C12	1.388(9)
W	C23	2.053(8)	C12	C13	1.385(9)
W	C24	2.044(8)	C14	C15	1.391(9)
P	F	1.615(4)	C14	C19	1.394(8)
P	O1	1.505(4)	C15	C16	1.385(9)
P	C1	1.935(6)	C16	C17	1.397(9)
O2	C20	1.151(8)	C17	C18	1.382(10)
O3	C21	1.142(8)	C18	C19	1.387(9)
O4	C22	1.157(8)	N1	C25	1.341(8)
O5	C23	1.144(8)	N1	C26	1.396(8)
O6	C24	1.149(8)	N1	C28	1.497(8)
C1	C2	1.541(9)	N2	C25	1.328(8)
C1	C8	1.531(8)	N2	C27	1.384(7)
C1	C14	1.549(8)	N2	C33	1.493(8)
C2	C3	1.393(9)	C26	C27	1.360(9)
C2	C7	1.402(9)	C26	C31	1.490(8)
C3	C4	1.382(9)	C27	C32	1.489(9)
C4	C5	1.396(10)	C28	C29	1.486(9)
C5	C6	1.373(10)	C28	C30	1.543(10)
C6	C7	1.385(9)	C33	C34	1.524(9)
C8	C9	1.400(8)	C33	C35	1.504(9)

Table 3 Bond Angles for 67.

Atom	Atom	Atom	Angle/˚	Atom	Atom	Atom	Angle/˚
C20	W	P	169.8(2)	C10	C9	C8	121.2(6)
C20	W	C21	91.2(3)	C11	C10	C9	120.4(6)
C20	W	C22	88.6(3)	C10	C11	C12	118.7(6)
C20	W	C23	90.7(3)	C13	C12	C11	121.1(6)
C20	W	C24	90.4(3)	C12	C13	C8	121.0(6)
C21	W	P	88.08(19)	C15	C14	C1	120.6(5)
C21	W	C23	177.8(3)	C15	C14	C19	117.5(6)
C21	W	C24	89.9(3)	C19	C14	C1	121.8(6)
C22	W	P	81.22(19)	C16	C15	C14	122.3(6)
C22	W	C21	92.4(3)	C15	C16	C17	118.9(7)
C22	W	C23	88.7(3)	C18	C17	C16	119.9(6)
C22	W	C24	177.6(3)	C17	C18	C19	120.1(6)
C23	W	P	90.20(19)	C18	C19	C14	121.3(6)
C24	W	P	99.8(2)	O2	C20	W	176.0(6)
C24	W	C23	89.1(3)	O3	C21	W	178.4(6)
F	P	W	106.53(15)	O4	C22	W	177.5(6)

F	P	C1	97.7(2)
O1	P	W	113.01(19)
O1	P	F	105.7(2)
O1	P	C1	106.6(3)
C1	P	W	124.7(2)
C2	C1	P	110.6(4)
C2	C1	C14	110.5(5)
C8	C1	P	103.3(4)
C8	C1	C2	112.4(5)
C8	C1	C14	110.1(5)
C14	C1	P	109.7(4)
C3	C2	C1	122.2(6)
C3	C2	C7	117.0(6)
C7	C2	C1	120.5(6)
C4	C3	C2	121.9(7)
C3	C4	C5	119.7(7)
C6	C5	C4	119.4(7)
C5	C6	C7	120.5(7)
C6	C7	C2	121.3(7)
C9	C8	C1	122.8(6)
C13	C8	C1	119.7(6)
C13	C8	C9	117.5(6)
O5	C23	W	177.6(6)
O6	C24	W	176.5(6)
C25	N1	C26	108.6(5)
C25	N1	C28	125.3(5)
C26	N1	C28	125.7(5)
C25	N2	C27	110.0(5)
C25	N2	C33	124.2(5)
C27	N2	C33	125.8(5)
N2	C25	N1	108.0(5)
N1	C26	C31	121.8(6)
C27	C26	N1	107.0(5)
C27	C26	C31	131.2(6)
N2	C27	C32	122.8(6)
C26	C27	N2	106.3(6)
C26	C27	C32	130.8(6)
N1	C28	C30	106.4(5)
C29	C28	N1	111.4(5)
C29	C28	C30	112.3(6)
N2	C33	C34	109.0(5)
N2	C33	C35	111.2(5)
C35	C33	C34	113.1(5)

Table 4 Torsion Angles for 67.

A	B	C	D	Angle/˚
P	C1	C2	C3	38.2(7)
P	C1	C2	C7	-147.2(5)
P	C1	C8	C9	-110.9(6)
P	C1	C8	C13	68.1(6)
P	C1	C14	C15	-144.9(5)
P	C1	C14	C19	40.2(7)
C1	C2	C3	C4	175.7(6)
C1	C2	C7	C6	-175.2(6)
C1	C8	C9	C10	177.9(6)
C1	C8	C13	C12	-178.3(6)
C1	C14	C15	C16	-177.1(6)
C1	C14	C19	C18	178.3(6)
C2	C1	C8	C9	8.3(9)
C2	C1	C8	C13	-172.6(6)
C2	C1	C14	C15	92.8(7)
C2	C1	C14	C19	-82.0(7)
C2	C3	C4	C5	-0.6(11)
C3	C2	C7	C6	-0.3(10)
C3	C4	C5	C6	-0.4(10)
C4	C5	C6	C7	1.0(10)
C14	C1	C2	C7	-25.5(8)
C14	C1	C8	C9	132.0(6)
C14	C1	C8	C13	-48.9(8)
C14	C15	C16	C17	-0.3(10)
C15	C14	C19	C18	3.3(9)
C15	C16	C17	C18	1.5(10)
C16	C17	C18	C19	-0.3(10)
C17	C18	C19	C14	-2.2(10)
C19	C14	C15	C16	-2.0(10)
N1	C26	C27	N2	1.0(7)
N1	C26	C27	C32	178.1(6)
C25	N1	C26	C27	-1.3(7)
C25	N1	C26	C31	179.7(6)
C25	N1	C28	C29	35.9(9)
C25	N1	C28	C30	-86.8(7)
C25	N2	C27	C26	-0.3(7)
C25	N2	C27	C32	-177.7(6)
C25	N2	C33	C34	-92.0(7)
C25	N2	C33	C35	33.4(8)
C26	N1	C25	N2	1.1(7)

C5	C6	C7	C2	-0.6(10)		C26	N1	C28	C29	-152.4(6)
C7	C2	C3	C4	1.0(10)		C26	N1	C28	C30	84.8(7)
C8	C1	C2	C3	-76.6(8)		C27	N2	C25	N1	-0.5(7)
C8	C1	C2	C7	98.0(7)		C27	N2	C33	C34	85.9(7)
C8	C1	C14	C15	-32.0(8)		C27	N2	C33	C35	-148.7(6)
C8	C1	C14	C19	153.2(6)		C28	N1	C25	N2	174.0(6)
C8	C9	C10	C11	0.9(10)		C28	N1	C26	C27	-174.2(6)
C9	C8	C13	C12	0.8(10)		C28	N1	C26	C31	6.9(10)
C9	C10	C11	C12	-0.2(10)		C31	C26	C27	N2	179.8(7)
C10	C11	C12	C13	-0.3(10)		C31	C26	C27	C32	-3.1(13)
C11	C12	C13	C8	0.0(10)		C33	N2	C25	N1	177.7(5)
C13	C8	C9	C10	-1.2(10)		C33	N2	C27	C26	-178.5(6)
C14	C1	C2	C3	159.9(6)		C33	N2	C27	C32	4.1(10)

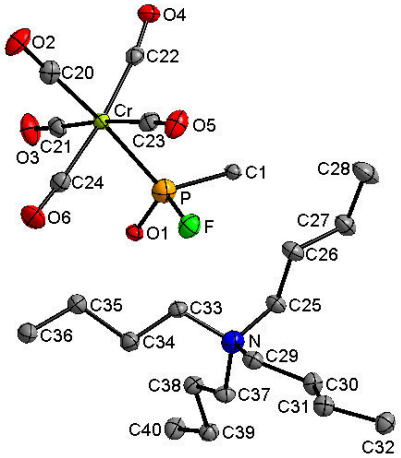

Table 1 Crystal data and structure refinement for 75.

Identification code	GSTR512
Empirical formula	$C_{43}H_{54}CrFNO_6P$
Formula weight	782.84
Temperature/K	100
Crystal system	monoclinic
Space group	$P2_1/n$
a/Å	11.4922(13)
b/Å	16.1502(19)
c/Å	22.301(2)
α/°	90
β/°	99.382(4)
γ/°	90
Volume/Å^3	4083.8(8)
Z	4
ρ_{calc}g/cm^3	1.273
μ/mm^{-1}	0.371
F(000)	1660.0
Crystal size/mm^3	0.21 × 0.18 × 0.06
Tmin; Tmax	0.4482; 0.7459
Radiation	MoKα (λ = 0.71073)
2Θ range for data collection/°	5.374 to 55.998°
Completeness to theta	0.998
Index ranges	-15 ≤ h ≤ 13, -21 ≤ k ≤ 21, -21 ≤ l ≤ 29
Reflections collected	62963
Independent reflections	9852 [R_{int} = 0.0537, R_{sigma} = 0.0383]
Data/restraints/parameters	9852/2/482
Goodness-of-fit on F^2	1.076
Final R indexes [I>=2σ (I)]	R_1 = 0.0418, wR_2 = 0.1103
Final R indexes [all data]	R_1 = 0.0656, wR_2 = 0.1300
Largest diff. peak/hole / e Å^{-3}	0.47/-0.64

Table 2 Bond Lengths for 75.

Atom	Atom	Length/Å	Atom	Atom	Length/Å
Cr	P	2.3974(6)	C12	C13	1.387(3)
Cr	C20	1.860(2)	C14	C15	1.399(3)
Cr	C21	1.889(2)	C14	C19	1.396(3)
Cr	C22	1.898(2)	C15	C16	1.390(3)
Cr	C23	1.907(2)	C16	C17	1.379(3)
Cr	C24	1.890(2)	C17	C18	1.386(3)
P	F	1.5712(14)	C18	C19	1.391(3)
P	O1	1.5325(14)	N	C25	1.524(2)
P	C1	1.9422(18)	N	C29	1.520(2)
O2	C20	1.148(3)	N	C33	1.518(2)
O3	C21	1.144(2)	N	C37	1.520(2)
O4	C22	1.148(2)	C25	C26	1.521(3)
O5	C23	1.143(2)	C26	C27	1.530(3)
O6	C24	1.147(2)	C27	C28	1.522(3)
C1	C2	1.538(2)	C29	C30	1.524(3)
C1	C8	1.537(2)	C30	C31	1.523(3)
C1	C14	1.539(2)	C31	C32	1.528(3)
C2	C3	1.396(3)	C33	C34	1.525(3)
C2	C7	1.390(2)	C34	C35	1.527(3)
C3	C4	1.386(3)	C35	C36	1.524(3)
C4	C5	1.383(3)	C37	C38	1.527(3)
C5	C6	1.386(3)	C38	C39	1.525(3)
C6	C7	1.388(3)	C39	C40	1.526(3)
C8	C9	1.399(3)	C41	C42	1.372(4)
C8	C13	1.399(3)	C41	C43[1]	1.383(4)
C9	C10	1.397(3)	C42	C43	1.382(4)
C10	C11	1.379(3)	C43	C41[1]	1.384(4)
C11	C12	1.388(3)			

[1]2-X, 1-Y, 1-Z

Table 3 Bond Angles for 75.

Atom	Atom	Atom	Angle/°	Atom	Atom	Atom	Angle/°
C20	Cr	P	174.69(6)	C11	C10	C9	120.54(19)
C20	Cr	C21	92.09(8)	C10	C11	C12	119.46(19)
C20	Cr	C22	86.24(9)	C13	C12	C11	120.3(2)
C20	Cr	C23	93.01(8)	C12	C13	C8	121.18(19)
C20	Cr	C24	88.54(9)	C15	C14	C1	121.47(16)
C21	Cr	P	88.64(6)	C19	C14	C1	120.60(16)
C21	Cr	C22	87.83(8)	C19	C14	C15	117.66(17)
C21	Cr	C23	174.48(9)	C16	C15	C14	121.42(18)
C21	Cr	C24	88.62(9)	C17	C16	C15	120.13(19)

C22	Cr	P	99.05(6)
C22	Cr	C23	94.59(9)
C23	Cr	P	86.08(6)
C24	Cr	P	86.23(6)
C24	Cr	C22	173.57(8)
C24	Cr	C23	89.42(9)
F	P	Cr	108.53(5)
F	P	C1	99.76(7)
O1	P	Cr	113.50(5)
O1	P	F	107.02(8)
O1	P	C1	103.65(7)
C1	P	Cr	122.72(6)
C2	C1	P	109.49(11)
C2	C1	C14	109.15(14)
C8	C1	P	108.06(11)
C8	C1	C2	110.08(14)
C8	C1	C14	110.67(14)
C14	C1	P	109.37(12)
C3	C2	C1	121.13(16)
C7	C2	C1	121.14(16)
C7	C2	C3	117.39(17)
C4	C3	C2	121.53(17)
C5	C4	C3	120.31(18)
C4	C5	C6	118.94(18)
C5	C6	C7	120.51(18)
C6	C7	C2	121.31(17)
C9	C8	C1	122.45(17)
C9	C8	C13	117.85(17)
C13	C8	C1	119.70(16)
C10	C9	C8	120.68(19)
C16	C17	C18	119.37(19)
C17	C18	C19	120.66(19)
C18	C19	C14	120.75(18)
O2	C20	Cr	179.08(19)
O3	C21	Cr	178.38(19)
O4	C22	Cr	171.96(16)
O5	C23	Cr	176.77(19)
O6	C24	Cr	176.33(18)
C29	N	C25	111.29(14)
C33	N	C25	108.61(14)
C33	N	C29	109.12(14)
C33	N	C37	111.23(14)
C37	N	C25	108.28(14)
C37	N	C29	108.33(14)
C26	C25	N	115.96(15)
C25	C26	C27	109.48(17)
C28	C27	C26	112.08(19)
N	C29	C30	116.24(15)
C31	C30	C29	109.12(15)
C30	C31	C32	112.52(16)
N	C33	C34	115.36(15)
C33	C34	C35	109.26(16)
C36	C35	C34	112.47(17)
N	C37	C38	115.41(15)
C39	C38	C37	109.53(15)
C38	C39	C40	112.11(16)
C42	C41	C43[1]	119.7(2)
C41	C42	C43	120.3(2)
C42	C43	C41[1]	119.9(2)

[1]2-X, 1-Y, 1-Z

Table 4 Torsion Angles for 75.

A	B	C	D	Angle/°	A	B	C	D	Angle/°
P	C1	C2	C3	45.6(2)	C14	C1	C2	C3	165.34(16)
P	C1	C2	C7	-141.21(15)	C14	C1	C2	C7	-21.5(2)
P	C1	C8	C9	-124.30(16)	C14	C1	C8	C9	115.97(18)
P	C1	C8	C13	56.78(18)	C14	C1	C8	C13	-62.9(2)
P	C1	C14	C15	-138.82(15)	C14	C15	C16	C17	-0.1(3)
P	C1	C14	C19	47.3(2)	C15	C14	C19	C18	0.3(3)
C1	C2	C3	C4	173.09(17)	C15	C16	C17	C18	-0.1(3)
C1	C2	C7	C6	-172.77(17)	C16	C17	C18	C19	0.3(3)
C1	C8	C9	C10	-179.90(16)	C17	C18	C19	C14	-0.5(3)
C1	C8	C13	C12	179.87(16)	C19	C14	C15	C16	0.0(3)
C1	C14	C15	C16	-174.05(18)	N	C25	C26	C27	167.17(16)

C1	C14	C19	C18	174.38(17)
C2	C1	C8	C9	-4.8(2)
C2	C1	C8	C13	176.31(15)
C2	C1	C14	C15	101.41(19)
C2	C1	C14	C19	-72.4(2)
C2	C3	C4	C5	-0.6(3)
C3	C2	C7	C6	0.6(3)
C3	C4	C5	C6	1.1(3)
C4	C5	C6	C7	-0.8(3)
C5	C6	C7	C2	-0.1(3)
C7	C2	C3	C4	-0.3(3)
C8	C1	C2	C3	-73.0(2)
C8	C1	C2	C7	100.13(19)
C8	C1	C14	C15	-19.9(2)
C8	C1	C14	C19	166.26(16)
C8	C9	C10	C11	0.4(3)
C9	C8	C13	C12	0.9(3)
C9	C10	C11	C12	0.3(3)
C10	C11	C12	C13	-0.4(3)
C11	C12	C13	C8	-0.2(3)
C13	C8	C9	C10	-1.0(3)
N	C29	C30	C31	-173.58(16)
N	C33	C34	C35	-179.02(15)
N	C37	C38	C39	157.14(15)
C25	N	C29	C30	-49.4(2)
C25	N	C33	C34	179.24(15)
C25	N	C37	C38	-70.62(19)
C25	C26	C27	C28	-178.56(18)
C29	N	C25	C26	-56.6(2)
C29	N	C33	C34	-59.3(2)
C29	N	C37	C38	168.57(15)
C29	C30	C31	C32	-172.40(16)
C33	N	C25	C26	63.6(2)
C33	N	C29	C30	-169.18(15)
C33	N	C37	C38	48.6(2)
C33	C34	C35	C36	-178.53(17)
C37	N	C25	C26	-175.52(16)
C37	N	C29	C30	69.58(19)
C37	N	C33	C34	60.2(2)
C37	C38	C39	C40	174.72(16)
C41	C42	C43	C41[1]	0.1(4)
C43[1]	C41	C42	C43	-0.2(4)

[1]2-X, 1-Y, 1-Z